19980311 168

DTIC QUALITY INSPECTED 4

DEPARTMENT OF THE AIR FORCE
AIR UNIVERSITY
AIR FORCE INSTITUTE OF TECHNOLOGY

Wright-Patterson Air Force Base, Ohio

AFIT/DS/ENP/97-10

MEASUREMENT OF ULTRAFAST CARRIER RECOMBINATION DYNAMICS IN MID-INFRARED SEMICONDUCTOR LASER MATERIAL

DISSERTATION

William T. Cooley, Captain, USAF

AFIT/DS/ENP/97-10

December 1997

Approved for public release; distribution unlimited

MEASUREMENT OF ULTRAFAST CARRIER RECOMBINATION

DYNAMICS IN MID-INFRARED SEMICONDUCTOR LASER MATERIAL

DISSERTATION

Presented to the Faculty of the Graduate School of Engineering

of the Air Force Institute of Technology

Air University

In Partial Fulfillment of the

Requirements for the Degree of

Doctor of Philosophy

William T. Cooley, B.S., M.S.

Captain, USAF

December 1997

2

MEASUREMENT OF ULTRAFAST CARRIER RECOMBINATION

DYNAMICS IN MID-INFRARED SEMICONDUCTOR LASER MATERIAL

William T. Cooley, B.S., M.S.
Captain, USAF

Approved:

_____   12/3/97

ROBERT L. HENGEHOLD
Professor of Physics and Head
Department of Engineering Physics
Chairman, Advisory Committee

_____   12/2/97

YUNG KEE YEO
Professor of Physics
Member, Advisory Committee

_____   12/2/97

JOHN P. LOEHR
Air Force Research Laboratory
Member, Advisory Committee

_____   12/2/97

VINCENT G. DOMINIC
Assistant Professor, Department of Electrical and Computer Engineering
University of Dayton
Member, Advisory Committee

_____   3 Dec 97

ALAN V. LAIR
Professor and Head, Department of Mathematics and Statistics
Deans Representative

Accepted:

_____

ROBERT A. CALICO, Jr.
Dean, Graduate School of Engineering

3

PREFACE

It's a long way from mechanical engineering to physics, but to be true to myself, I had to make the journey. This has been a long and arduous journey, one that I will be very happy to look back on, and thankful to have made.

Along the way I have been assisted by a multitude of people. First I thank my advisor, Dr. Robert L. Hengehold, for his enthusiasm and support of the upconversion experiment. I also thank Dr. George Turner for his patience while I wrestled with the upconversion experiment, his technical guidance which motivated this study, and the laser samples he provided. Dr. Thomas F. Boggess was the most helpful collaborator imaginable. Without his guidance in the field of ultrafast spectroscopy, I doubt that I would have seen upconverted photons. D.-J. (James) Jang, of the University of Iowa and a fellow doctoral student, was most helpful in making upconversion work in my laboratory. Dr. John P. Loehr was not only a key member of my committee, but a friend and supporter of my experimental effort. His understanding of Auger processes and semiconductor lasers contributed significantly to the analysis sections of this dissertation. Dr. Yung Kee Yeo and Dr. Vincent G. Domonic also contributed to this effort by serving on my committee, for which I am very grateful.

Building 194 in area B can be a lonely place. Greg Vansuch and I spent many hours in the lab wrestling with our individual research problems, and I am grateful for his company, friendship and sanity checks. In addition to keeping Greg and me company in Building 194, Rick Patton provided critical assistance on several occasions by repairing electronic equipment, for which I am grateful. My life-long friend, Larry Merkle, was not only a faithful lunch partner and connoisseur of peanut butter and jelly sandwiches, but also a superb programmer. I am grateful for his patience teaching me enough C programming language to be dangerous with GPIB and RS-232 instruments in the lab.

There are many others who contributed in large and small ways. Michael Falcon, of the Air Force Phillips Lab, provided funding to make this effort possible. I thank my classmates Monte Turner, for his assistance understanding nonlinear phenomena and the use of his laser, and Jack McCrae, for his assistance in attempting photoreflectance and modeling. I thank also Mike Marciniak for providing a basis to study mid-IR laser structures, and Professors Won Roh and David Weeks for their counsel and technical assistance with this challenging experiment and analysis.

Of all the individuals who assisted me on my journey, none contributed more than my traveling partner, my wife Janet. Her near-infinite patience with me while I trudged through the AFIT doctoral program made it possible for me to keep trudging. One year of my life was spent wrestling in the laboratory becoming an experimental physicist, and the frustration of failure took its toll on me. We have both made substantial sacrifices for this journey, and I know she is anxious as I, if not more so, to close this chapter of our lives. She has been my best and most constant supporter throughout, and I am blessed to have such a wonderful life companion.

Dedicated to my daughters, Kelly, Katherine, and Rachel.

William T. Cooley

ABSTRACT

Mid-infrared (mid-IR) semiconductor lasers have great promise for use in military applications such as IR countermeasures, remote detection of trace gases, and eye-safe illuminators. The principal barrier cited in the literature limiting mid-IR laser performance in terms of desired power levels and operating temperatures is non-radiative recombination mechanisms, in particular Auger recombination. Non-radiative recombination mechanisms require indirect measurement techniques, often on very short time scales. As a result, there are very few reports of experimental determination of recombination mechanisms and their associated rates in the literature.

This dissertation reports Shockley-Read-Hall, radiative, and Auger recombination rates in mid-infrared laser structures from time resolved photoluminescence (TRPL) using a nonlinear mixing technique known as frequency upconversion. The mid-IR lasers studied were actual InAsSb / InAlAsSb multiple-quantum-well (MQW) diode lasers emitting near 3.3 μm which have been previously characterized for laser performance. This effort extends the initial studies and reports on the carrier recombination dynamics.

TRPL data was taken for the peak intensity wavelength as determined by time integrated photoluminescence on three laser samples at a variety of temperatures. Extracting recombination coefficients from TRPL data is not straightforward, and has not been done prior to this effort for the narrow-spectral-band upconversion configuration used in this effort. A technique to analyze carrier dynamics based on sampling the occupation probability of discrete states in the sample is presented for the first time here in conjunction with the upconversion experiment.

Shockley-Read-Hall, radiative and Auger recombination rates at low temperature (77 K) were measured and found to be $A_{SRH} \approx 10 \times 10^{7} sec^{-1}$, $B_{rad} \approx 2 \times 10^{-10} cm^{3} sec^{-1}$ and $C_{Auger} < 10^{-29} cm^{6} s^{-1}$ respectively, for each sample measured. The measured

upconversion signal has a linear dependence on luminescence intensity, and because only one of the samples was a strong emitter at higher temperatures (150 K), recombination rates are reported on a single device. At higher temperatures (150 K), the recombination rates were measured to be $A_{SRH} \approx 40 \times 10^7 sec^{-1}$, $B_{rad} \approx 0.78 \times 10^{-10}$ $cm^3 sec^{-1}$ and $C_{Auger} <$ 7.0×10^{-28} $cm^6 s^{-1}$ respectively. The Auger coefficient reported here is significantly lower than previous reports on similar material from both theoretical and experimental investigations. This has significant implications for mid-IR laser research, in that Auger may not be the limiting problem.

TABLE OF CONTENTS

LIST OF FIGURES

LIST OF TABLES

1.Introduction

1.1. Motivation

Mid-infrared (mid-IR) semiconductor lasers have recently become increasingly attractive for a variety of commercial, Air Force, and other government agency applications. The Air Force is largely interested in mid-IR semiconductor lasers for infrared countermeasure applications. Because heat-seeking missiles are designed to lock on targets with a large mid-IR signature, a mid-IR laser may be able to deliver enough energy in the appropriate spectral region to spoof or even destroy the missile's detector system. Other practical advantages to mid-IR lasers are the atmosphere's transmission window between 2 μm and 5 μm and their relative "eye safety." Beyond 1.5 μm, the lens of the human eye absorbs light, preventing damage to the retina at the eye's image plane. Some possible commercial applications for mid-IR lasers include laser radar, remote sensing of trace gases (Choi, 1996), molecular spectroscopy, and laser medicine.

III-V semiconductor materials are currently an attractive alternative among the available options for generation of mid-IR photons, due to the availability of high quality film growth and the collective knowledge base acquired in these materials over the past three decades. IR lasers have been fabricated using ternary and quaternary semiconductor alloys containing the group III elements aluminum (Al), gallium (Ga) and indium (In) in combination with the group V elements phosphorus (P), arsenic (As) and antimony (Sb). The antimonides (compounds containing antimony) are of interest for mid-IR optical applications due to their relatively small band-gap. $InAs_{1-x}Sb_x$ is currently of particular interest to the Air Force because of the spectral range accessible by varying the antimony mole fraction and because the lattice parameter is near the lattice parameter of GaSb for low antinomy mole fraction alloys. High quality thin film epitaxy requires

near perfect lattice matching and as a result, high quality $InAs_{1-x}Sb_x$ structures can be grown on commercially available substrates.

Although the first $InAs_{1-x}Sb_x$ semiconductor p-n junction laser was fabricated by the Soviets in 1966 (Basov, 1966), this alloy system was virtually ignored for two decades. Since 1985, however, $InAs_{1-x}Sb_x$ alloys have received increased attention. Recently, at the Massachusetts Institute of Technology / Lincoln Laboratory (MIT/LL) an ongoing effort to produce antimonide based semiconductor lasers has shown great promise (Choi, 1993; Le, 1994; Eglash, 1994; Turner, 1995). This effort has been supported and funded by the Air Force Phillips Laboratory (PL/LIDA) for potential use in IR countermeasures systems.

The principle concern currently affecting progress in the MIT/LL mid-IR laser effort is a thorough understanding of how growth parameters affect the relative magnitudes of radiative and non-radiative recombination rates. The key parameters affecting non-radiative contributions are thought to be growth temperature (which affects the laser structure interfaces), strain, and composition. The ability to experimentally measure recombination rates and distinguish recombination processes is a powerful tool and could very likely help improve these lasers. Theoretical and experimental investigations of similar semiconductor materials for IR lasers indicate that Auger recombination, a non-radiative process, is the dominant deleterious mechanism limiting high power and efficiency (Casey, 1984). Defect related recombination, commonly known as Shockley-Read-Hall (SRH) recombination, may be the dominant effect at lower carrier injection levels and could be an important factor to consider regarding the MIT/LL laser structure. In either case, Auger or SRH, non-radiative transitions reduce laser performance. The ability to measure and understand these processes could aid significantly in the development of mid-IR semiconductor lasers.

In addition to controlling growth parameters to reduce non-radiative recombination rates, it may be possible to employ band-gap engineering techniques to

15

modify the band structure in such a way that Auger recombination is dramatically reduced (Adams, 1986; Yablonovitch and Kane, 1986). The ability to measure and quantify recombination phenomena is a critical element in determining whether a particular structure has succeeded in reducing the non-radiative recombination rates. With a better understanding of recombination phenomena coupled with the ability to modify the band structure, more efficient lasers may be designed and fabricated.

1.2. *Problem Statement*

The objective of a laser design is to efficiently produce coherent electromagnetic energy of a particular wavelength in a convenient and robust package. Toward this end, semiconductor lasers have been and will continue to be very attractive. In the case of mid-IR semiconductor lasers, non-radiative mechanisms siphon a significant portion of the excess carriers away from the coherent radiation producing process and ultimately heat the crystal by generating phonons.

Excess carriers in a semiconductor recombine through a large number of mechanisms that can be categorized into three types, SRH, radiative, and Auger. The carrier recombination rate processes, assuming intrinsic material ($n \approx p$) are related to the carrier density through the differential equation

$$-\frac{dn}{dt} = A_{SRH}n + B_{rad}n^2 + C_{Auger}n^3 . \tag{1-1}$$

Here n is the volumetric carrier density (carriers/cm^3) and A_{SRH}, B_{rad} and C_{Auger} represent the SRH, radiative, and Auger recombination coefficients respectively. Note the differing dependence on carrier density between these processes.

Auger recombination is thought to be a highly temperature dependent phenomena and has been accused of being the primary culprit for the unwanted strong temperature dependence of the laser threshold current (Agrawal, 1986). Theory and experiment both

point to Auger recombination as the Achilles heel for narrow band-gap semiconductor lasers.

Auger recombination rates are difficult to calculate theoretically and even more difficult to determine experimentally. Calculated Auger recombination coefficients, C_{Auger}, have been reported with variations over 8 orders of magnitude for nearly identical materials systems by separate authors in the literature. The only reasonable way to resolve the magnitude of the Auger term is by comparing theoretical Auger recombination coefficients with experimentally measured values.

1.3. Research Objectives

The goal of virtually all research on low band gap materials for mid-IR lasers is to improve the quality and efficiency of the lasers so they may be operated at elevated temperatures and become more practical to use. The specific goal of this research is to experimentally determine the radiative and non-radiative recombination coefficients in narrow band-gap semiconductor laser structures, particularly $InAs_{1-x}Sb_x$. With this capability, it may be possible to determine growth conditions and laser structure design that will reduce the Auger and other non-radiative recombination rates.

A significant difficulty researcher's face in trying to improve mid-IR laser performance is knowing where to focus their effort. If Auger is shown to be the dominant non-radiative recombination mechanism, then a new laser structure should be designed which may suppress Auger processes. On the other hand, if defect related recombination dominates, then the crystal growth technique should be improved to reduce the number of crystal or interfacial defects, if possible. By reducing the dominant non-radiative rates, the ratio of electron-hole pairs that recombine radiatively to the total electron-hole pairs recombining, will increase. The result is a more efficient semiconductor laser.

17

Non-radiative contributions cannot be measured directly. As a result, an indirect technique that is capable of measuring sub-picosecond phenomena in mid-IR materials must be developed. Time resolved luminescence, with a wavelength at approximately 4 μm from these narrow band-gap materials, would provide a suitable method. With this tool, coupled with an understanding and model of the quantum well laser structure, an accurate characterization of the recombination phenomena can emerge and our ability to design, grow, and fabricate mid-IR lasers will be greatly enhanced.

The research performed at AFIT provides, for the first time, measured Auger recombination rates and SRH recombination rates in antimonide based, mid-IR strained quantum well laser structures. The samples were selected because threshold current data as a function of temperature was available for each sample, and the samples were identical save the quantum well thickness (t_{qw}). An additional feature regarding these samples is that the laser threshold characteristic temperature (T_0) differed by approximately 25%.

The experimental results indicate that Auger is not nearly as dominant a mechanism as was originally thought. SRH may be the significant non-radiative mechanism for these structures.

1.4. Approach

Measuring temporal characteristics of long wavelength radiation (> 2 μm) is difficult due to the limited bandwidth of detectors in this range. Other techniques must be employed to access this wavelength region to obtain the experimental data. The experimental technique used in this dissertation was photoluminescence "upconversion." Upconversion is a $\chi^{(2)}$ phenomenon that involves frequency summation of two photons in a non-linear crystal. This general technique is described in detail by Shah (Shah, 1988). The determination of Auger recombination from time resolved luminescence data requires an understanding of the quantum well effects and the ability to fit experimental

data to a model for the recombination processes. The details of the quantum well model will be given in Chapter 3 and the details of the analysis will be described in Chapter 7.

Photoluminescence upconversion will be described in detail in Chapter 5, but is briefly described here. A beam-splitter is used on an ultrafast laser source to send one pulse to excite excess carriers in the material being studied, while the second pulse travels through an adjustable optical delay stage. The luminescence is combined with the delayed pulse in a non-linear crystal through a process known as sum frequency generation (SFG) or simply frequency upconversion (Yariv, 1984). The criteria for SFG phase matching is conservation of energy and conservation of momentum given by

$$
\begin{aligned}
h\nu_{SFG} &= h\nu_{pump} + h\nu_{PL} \\
\vec{k}_{SFG} &= \vec{k}_{pump} + \vec{k}_{PL}
\end{aligned}
\tag{1-2}
$$

where $h\nu_{SFG}$, $h\nu_{pump}$, and $h\nu_{PL}$ are the photon energies and k_{SFG}, k_{pump}, and k_{PL} are the wave vectors in the crystal of the upconverted, luminescence, and pump laser respectively . The resulting signal, $h\nu_{SFG}$, has a shorter wavelength and can be designed such that photon counting is possible. A spectrometer is used to spectrally resolve the luminescence as well as block out spurious signals. Signal-to-noise can be optimized by using a cooled photo-multiplier tube.

Because the upconversion process takes place only when luminescence photons and laser photons are present, the temporal resolution of the measurement is limited only by the temporal extent of the laser pulse. In addition, by controlling the optical path length of the "delayed" pulse, time resolved images from the luminescence are possible. The carrier density can be controlled by modifying either the focus of the excitation laser beam on the sample, or by modifying the pulse energy impinging the material sample. With this feature, the luminescence decay rate as a function of carrier density can be measured.

At the time of this writing, only three papers in the literature report experimental determination of Auger coefficients for materials that emit beyond 2 μm (Youngdale, 1993; Lindle, 1995 and McCahon, 1995), and none of them studied $InAs_{1-x}Sb_x$. Further, only two publications report performing upconversion at wavelengths longer than 2 μm (Heyen, 1989 and Jang, 1997). A thorough review of the literature is found in Chapter 2 and Appendix A.

1.5. *Organization of the Dissertation*

The dissertation is divided into eight chapters. Chapter 2 provides a brief literature review of the field, a more complete review is included in Appendix A. Chapter 3 and 4 provide an introduction to the fundamental concepts and theory for quantum wells and recombination phenomena in semiconductors respectively. An introduction to nonlinear optics and details of the upconversion experiment are provided in Chapter 5, while Chapter 6 provides a detailed description of experimental procedures and results obtained during this effort. Chapter 7 presents the analysis techniques used to extract meaningful recombination coefficients from the experimental data presented in Chapter 6. Finally, Chapter 8 concludes the dissertation with observations regarding the impact of this research in addition to recommendations for future work. An alphabetical bibliography follows Chapter 8.

2. Review of Field

This chapter provides a brief literature review of prior research efforts related to this dissertation. An expanded literature review is included in Appendix A, which provides a written description of most of the related papers. Tables at the end of each section provide a list of relevant papers, but only the most significant related prior research is described here. This chapter is subdivided into four main sections corresponding to the relevant topical areas, with each of the first four sections ending with comments regarding the current state of the field. Section 2.1 provides background information on mid-infrared (between 2 μm and 5 μm) semiconductor lasers, section 2.2 provides a brief synopsis of materials research on the alloy $InAs_{1-x}Sb_x$, section 2.3 gives a synopsis or experimental studies of Auger recombination, and section 2.4 gives a synopsis of research using the upconversion technique. Finally, Section 2.5 provides a summary of the key elements from the literature relating to this dissertation.

2.1. Mid-Infrared Semiconductor Lasers

A very good review of previous studies on the $InAs_{1-x}Sb_x$ ternary system has been provided by Marciniak (1994); therefore, only the most recent and relevant references are provided in this section. The method chosen to review the current status in the development of III-V mid-IR semiconductor lasers is chronological. With this in mind, the following section summarizes the progress and contributions made in the development of mid-IR semiconductor lasers with particular emphasis on the $InAs_{1-x}Sb_x$ material system.

The motivation for the proposed material can largely be explained in Figure 2-1. It can be seen from the figure that in order to exploit the transmission window of the atmosphere near 4 μm using semiconductor lasers, the III-V quaternary material $Ga_yIn_{1-y}As_{1-x}Sb_x$ is of particular interest.
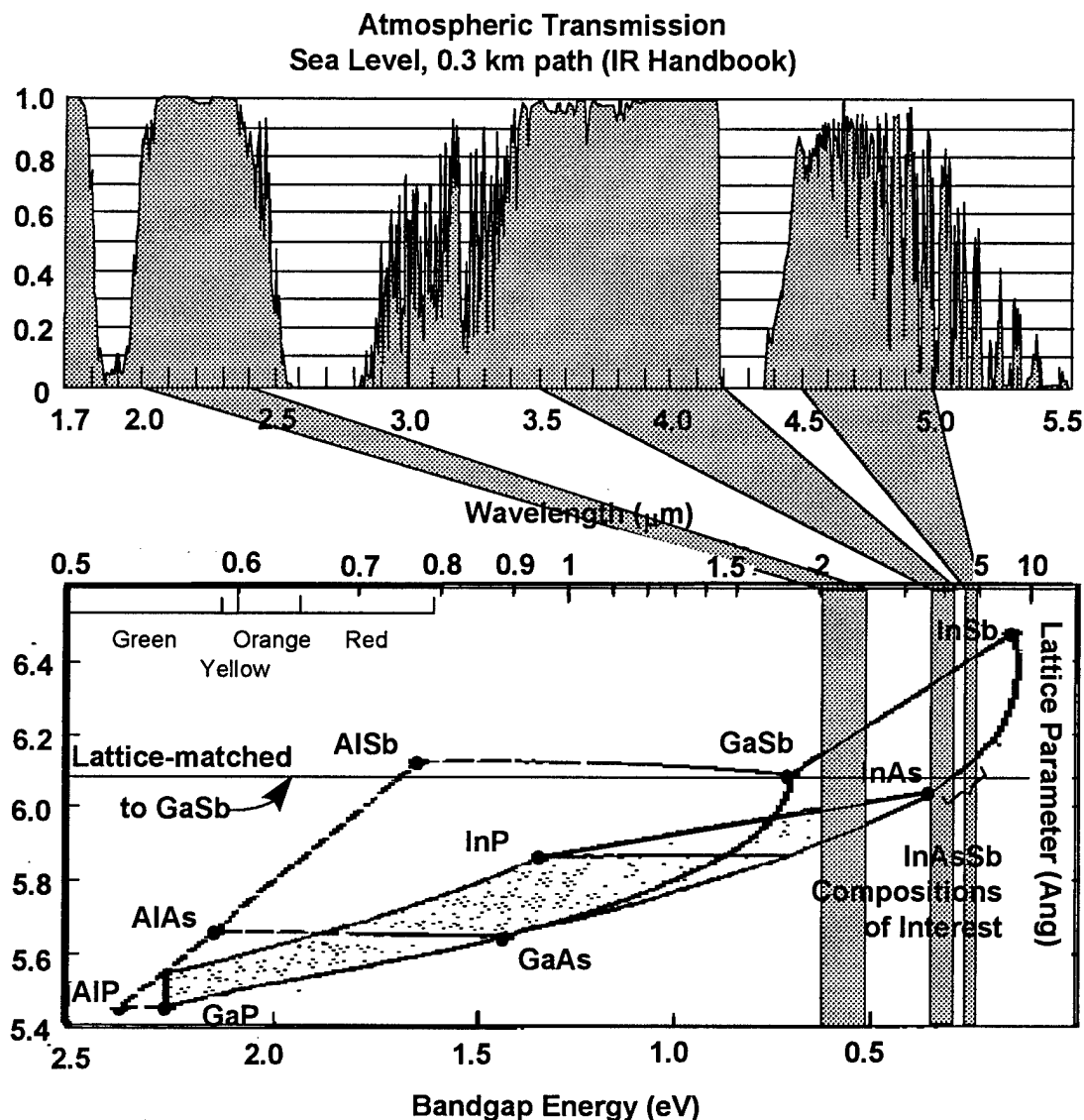
Figure 2-1: Atmospheric Transmission Window and related band-gap vs. lattice parameter for III-V semiconductor compounds and their alloys after Marciniak (1995).

Two other significant factors must be considered for material selection associated with crystal growth of optoelectronic devices. First, the ability to accurately control the composition of a semiconductor alloy is paramount. This factor frequently motivates crystal growers to prefer ternary alloys (composed of three elements) over quaternary alloys (composed of four elements) and thus, eliminate one degree of freedom. The second issue is associated with the availability of substrates with a lattice constant very

near the lattice constant of the proposed alloy. High quality monolithic structures can be grown on a crystalline substrate material which have a lattice constant that matches or nearly matches the lattice constant of the alloy. The availability of high quality GaSb wafers makes the quaternary alloy $Ga_yIn_{1-y}As_{1-x}Sb_x$ and the ternary alloy $InAs_{1-x}Sb_x$ lattice matched to GaSb particularly attractive.

In order to develop mid-IR diode lasers, the band gap of the active region material must be in the range 0.25-0.62 eV, corresponding to wavelengths of 5 - 2 μm. The semiconductor quaternary material system, which consists of $Ga_yIn_{1-y}As_{1-x}Sb_x$ alloys, provides this wavelength coverage. The energy gap of the quaternary composition *lattice matched* to a GaSb substrate, ranges from 0.71 eV ($\lambda \approx 1.7$ μm) for GaSb to 0.3 eV ($\lambda \approx$ 4.0 μm) for $InAs_{0.91}Sb_{0.09}$.

2.1.1. Semiconductor Laser Review

There are many parameters that can be used as a metric to characterize electrically pumped semiconductor lasers. Three important parameters most frequently used, especially with regard to long wavelength semiconductor lasers, are the threshold current density (J_{th}), the characteristic temperature (T_0), and the internal quantum efficiency (η).

Threshold current (J_{th}) is simply the electric current required for lasing to begin. The nuances associated with the issue of *when lasing begins* is outside the scope of this effort. The threshold current of the device (J_{th}) is governed largely by the optical characteristics of the laser. These include the reflectivity of the facets, the internal optical losses, and the wave-guide characteristics. The recombination mechanisms play a significant role in determining threshold since lasing cannot begin until a state of population inversion has been reached. This effectively means the "pump" working to generate the population inversion must increase as non-radiative recombination processes increase that act to return the system to thermal equilibrium.

23

The empirical temperature dependence of J_{th} is well known (Pankove, 1971:231) and is given by the equation

$$J_{th}(T) = J_{th}\left(T_{ref}\right)\exp\left(\frac{T - T_{ref}}{T_0}\right),$$ (2-1)

where $J_{th}(T)$ is the laser threshold current at temperature "T." Note that the characteristic temperature T_0 is purely an empirical quantity. A commonly used expression for the internal quantum efficiency (η), involves the radiative (τ_{rad}) and non-radiative (τ_{nr}) lifetimes (Casey, 1984) given by

$$\eta = \frac{1}{1 + \dfrac{\tau_{rad}}{\tau_{nr}}}.$$ (2-2)

The lifetimes can be related to the recombination coefficients in a straightforward manner given by

$$\tau_{rad} = \left(B_{rad} \cdot n_{th}\right)^{-1}$$
$$\tau_{nr} = \left(\tau_{SRH}^{-1} + \tau_{Auger}^{-1}\right)^{-1} = \left(A_{SRH} + C_{Auger} \cdot n_{th}^{2}\right)^{-1},$$ (2-3)

where n_{th} is the volumetric carrier density at threshold. From these equations it is easy to see how the magnitude of a laser's non-radiative coefficients will affect the efficiency of the device. It can also be seen that the magnitude of the Auger term, τ_{Auger}, is nonlinear with carrier density. Thus SRH and Auger recombination processes are both important for lasing!

2.1.2. Relevant Prior Research

Recent mid-IR semiconductor laser results from the MIT/LL group are encouraging particularly with regard to Auger recombination in strained quantum wells.

24

Turner *et al.* (Turner, 1995) fabricated mid-IR laser structures using ten $InAs_{0.86}Sb_{0.14}/In_{0.85}Al_{0.15}As_{0.86}Sb_{0.14}$ strained quantum wells as the active region with $AlAs_{0.08}Sb_{0.92}$ cladding layers. They obtained a threshold current density as low as 70 A/cm^2 at 70K and were able to operate cw up to 123K. The characteristic temperature of their laser was $T_0 = 30K$, which is significantly higher than the value obtained for the best $InAs_{0.91}Sb_{0.09}$ double heterostructure lasers ($T_0 \approx 20K$) (Choi, 1994). One of the key reasons for the success at MIT/LL has been the significant effort put into understanding the non-equilibrium growth conditions during MBE and accounting for these conditions at heterojunctions and key interfaces (Turner, 1994).

The latest paper by the MIT/LL group varied the thickness (10, 15, and 20 nm wells) in compressively strained quantum wells grown on InAs substrates, which are described thoroughly in Chapter 6 since these same laser structures are used as the samples studied in this dissertation. The threshold current density at 80 K was as low as 30 A/cm^2. The lasers operated at a wavelength near 3.5 μm and in the case of the 15 nm well, maintained continuous wave operation up to 175 K. The temperature dependence of the threshold current between 100 and 200 K exhibited T_0 values as small as 30 - 40 K, a significant improvement over previous T_0 values near 20 K. Auger recombination was again thought to be the limiting mechanism to higher temperature operation and lower threshold currents.

A synopsis of mid-IR semiconductor laser work is provided in Table 2-1. Note the optically pumped lasers are listed with an equivalent current to indicate the equivalent current injection required to reach threshold.

2.1.3. Current State of Mid-IR Laser Development

The difficulties with current mid-IR diode lasers are their inability to operate at high temperatures, as well as their low power levels. These are both related to the small empirical characteristic temperature parameter T_0 that is frequently attributed to CHSH

Auger recombination. The parameter space for MBE growth of laser structures is very large. Experimental determination of Auger recombination coupled with the theoretical backbone needed to make sense of the data promises to reduce the parametric space for crystal growers as well as provide understanding of the Auger process.

Table 2-1. Synopsis of Mid-IR semiconductor laser progress.

λ μm	Active Region	Growth	Pump el/op	T_0 K	J_{th} A/cm^2	T_{max}(K) cw/pulse	Ref	Year
3.5	InAs$_{91}$Sb$_{09}$	CZR	el		8000	77	Basov	1966
3.8	InAs$_{91}$Sb$_{09}$	MBE	op	15.9	14000	/135	van der Ziel	1985
3.1	InAs	LPE/DH	op	20	70000	/100	van der Ziel	1985
3.9	InAs$_{87}$Sb$_{13}$	LPE/DH	op	27.0	30000	/125	van der Ziel	1985
2.1	GaInAsSb	LPE/DH	el	80.0	7000	190/290	Caneau(b)	1986
2.2	GaInAsSb	LPE/DH	el	55.0	3500	220/290	Caneau	1986
3.9	InAs$_{91}$Sb$_{09}$	MBE	op	17.0	4000	/135	Chiu	1986
2.2	GaInAsSb	MBE/DH	el	26.0	4200	300/300	Caneau(c)	1987
2.0	GaInAsSb	LPE/DH	el		5400	77/300	Akimova	1988
2.4	GaInAsSb	LPE/DH	el		7600	77/300	Akimova	1988
2.2	GaInAsSb	LPE/DH	el	92.5	7000	/300	Joullie	1988
3.2	InAs$_{95}$Sb$_{05}$	LPE/DH	el	30.0	4500	/110	Mani	1988
2.2	GaInAsSb	LPE/DH	el	45.0	2600	/300	Zyskind	1989
3.2	InAs$_{95}$Sb$_{05}$	LPE/DH	el	38.0	1500	/110	Mani	1990
2.3	GaInAsSb	MBE/DH	el	50.0	1700	300	Eglash	1990
2.2	GaInAsSb	MBE/DH	el	25.0	940	300	Choi(b)	1991
2.3	GaInAsSb	MBE/DH	el	50.0	1500	300	Choi	1991
2.1	GaInAsSb	MBE/QW	el	113	260	300	Choi	1992
3.9	InAs$_{87}$Sb$_{13}$	LPE/DH	el		200	4.2	Aydaraliev	1993
2.0	GaInAsSb	MBE/QW	op		330	300	Choi	1993
2.2	GaInAsSb	LPE/DH	el	65	3000	300	Morosini	1993
3.0	GaInAsSb	MBE/DH	op	26.0		/210	Le	1994
4.0	InAsSb	MBE/DH	op	17.5		/150	Le	1994
4.0	InAs$_{91}$Sb$_{09}$	MBE/DH	el	17.0	33	80/155	Eglash	1994
2.0	GaInAsSb	MBE/QW	el		143	300	Turner	1994
3.9	InAs$_{91}$Sb$_{09}$	MBE/DH	el	20.0	36	105/175	Choi	1994
3.9	InAs$_{91}$Sb$_{09}$	MBE/QW	el	30.0	70	123/165	Turner	1995
3.5	InAs$_{91}$Sb$_{09}$	MBE/QW	el	35.0	30	175/225	Choi	1996

2.2. InAsSb Material Characterization

Very little effort has been devoted to understanding $InAs_{1-x}Sb_x$ relative to other materials over the past several decades. With the advent of non-equilibrium epitaxial growth techniques and a renewed interest in mid-IR semiconductor lasers, the material properties of $InAs_{1-x}Sb_x$ are being more thoroughly studied (Marciniak, 1995).

A necessary starting point for understanding and being able to use a particular semiconductor is knowledge of the parameters that characterize it. Some of these are the band gap (E_g), the split-off band energy (Δ), and the effective mass of the heavy valence band (m_{hh}), light valence band (m_{lh}), split-off valence band (m_{sh}), and the conduction band (m_c). A knowledge of these parameters for binary compounds (III-V), ternary alloys ($III_{1-x}III_x$-V and III-$V_{1-x}V_x$), or quaternary alloys ($III_{1-x}III_x$-$V_{1-y}V_y$) is at the heart of semiconductor material characterization. Understanding how these parameters change as the mole fraction of the species changes is a significant challenge in ternary and quaternary alloys.

2.2.1. Relevant Prior Research on InAs₁₋ₓSbₓ

In 1993, Mao and Krier used LPE grown material (Mao, 1993) while Elies (Elies, 1993) used MBE grown material to study the temperature dependence of the band-gap in $InAs_{1-x}Sb_x$ lattice matched to GaSb via photoluminescence. From the temperature dependence they determined the band-gap versus temperature relation and fit it to the Varshni equation, which describes semiconductor band-gap versus temperature relationship, given by

$$E_g(T) = E_g(0) - \frac{\alpha T^2}{\beta + T}, \qquad (2\text{-}4)$$

where $E_g(0)$ is the band-gap at zero temperature, and α and β are fitting parameters. They found that for $InAs_{0.91}Sb_{0.09}$, $E_g(0) = 0.3216$ eV, $\alpha = 2.6 \times 10^{-4}$ eV/K, and $\beta = 113$ K.

Marciniak studied MBE $InAs_{1-x}Sb_x$ via photoluminescence by varying

temperature, excitation power, and the antimony fraction, "x" between $0 \leq$ "x" ≤ 0.20.

The energy band gap as a function of temperature for $InAs_{0.91}Sb_{0.09}$ from Marciniak

(1995) is provided in Figure 2-2.
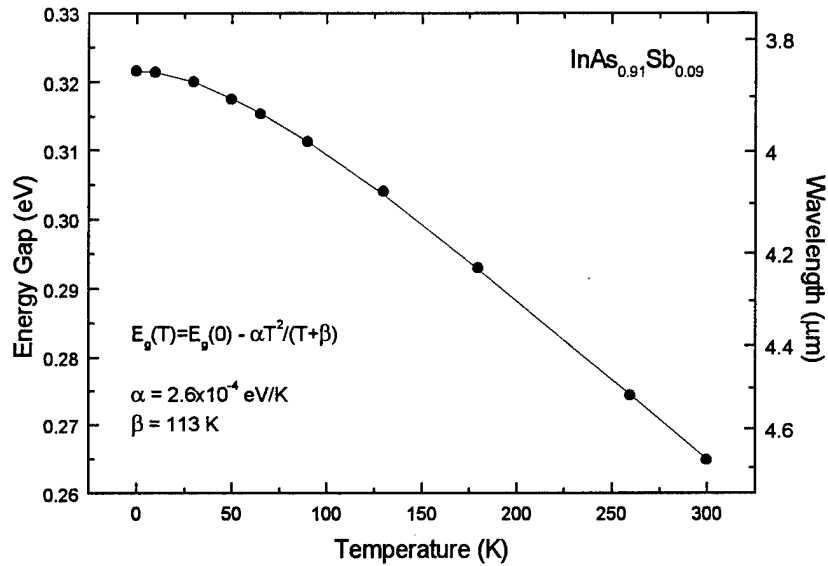
Figure 2-2: Band-Gap versus temperature for $InAs_{1-x}Sb_x$ alloy (x = 0.09). The circles represent experimentally determined values for the band-gap while the dotted line is a fit to the Varshni equation (Marciniak, 1995).

2.2.2. Current State of InAsSb Research

$InAs_{1-x}Sb_x$ is an important III-V alloy for mid-IR semiconductor lasers, about

which comparatively little is known. Mike Marciniak's dissertation research contributed

significantly to the characterization of epitaxial grown material. The lack of knowledge

available for this material system is illustrated by the limited published research which, in

turn, contributes to our inability to understand and improve InAsSb lasers for the mid-IR.

2.3. Auger Recombination

Auger recombination coefficients (C_{Auger}) in semiconductors were first estimated

in 1958 by Beattie and Landsberg (Beattie, 1958). Although difficult, several research

28

groups have attempted to experimentally measure Auger recombination rates. One difficulty associated with experimentally determining C_{Auger} is that the phenomenon is very fast, typically on the order of picoseconds. Another difficulty is related to the fact that Auger recombination cannot be *directly* measured. This is due to the fact that the Auger recombination process is fundamentally a loss of excess carriers, with the balance of the energy generating phonons that heat the crystal. If Auger were the only such process, we would have a chance at directly measuring it. However, because it competes with other non-radiative processes, Shockley-Read-Hall (SRH) recombination, which also contributes to carrier loss with the balance of energy producing phonons, there is no way to separate these two processes directly. If there were a mechanism to measure very small heat changes on an ultrafast time scale, one could more directly separate Auger from SRH recombination. Because that technology does not exist, and because we cannot connect electrical leads to a semiconductor and measure an Auger recombination current, indirect means are the only option. A synopsis of past experimental efforts will be given at the end of this section.

Although time resolved photoluminescence (TRPL) has great appeal because it is one of the most direct measures, it has not been used extensively. There are several reasons for this, among them, the fact that ultrafast spectroscopy is difficult and has become possible only in the last decade. The techniques available for high speed measurements are: 1) use of a very fast photodetector, which is limited to visible or near IR spectral ranges; 2) use of a streak camera, which again has a limited spectral range and is very expensive but enables temporal resolution down to approximately 10 picoseconds (Kohl, 1990); 3) use of a timed population correlation technique, which exploits the material luminescence response at a frequency difference $\varpi = \varpi_1 - \varpi_2$ from two excitation frequencies and is capable of time resolution from 250 ps (Bergman, 1991) down to 100 fs (Christanell, 1989); and 4) use of a frequency upconversion (Shah, 1988) with a temporal resolution typically near 100 fs.

2.3.1. Relevant Prior Research

B. Sermage *et al.* (1983; 1984; 1985) measured the luminescence decay rate of InGaAsP radiative emission at 1.3 μm and estimated the Auger recombination rate. Their experiment consisted of a mode locked Nd:YAG pump, a temperature controlled sample holder, and a very fast photodiode (response time 150 ps). They calculated the radiative recombination rate using Kane's **k•p** method (Kane, 1966:75-100) incorporating parabolic and later, non-parabolic band models. The carrier density range studied was from 4×10^{16} cm^{-3} to 2×10^{19} cm^{-3}. They presented analytic calculations for the number of carriers generated in the region of interest, as well as a means of extracting the non-radiative recombination rate from the time dependent luminescence (TRPL). The relationship of Auger recombination to the temperature parameter of a semiconductor laser (T_0) was emphasized.

In 1986, B. Sermage *et al.* compared Auger recombination in bulk $Ga_{1-x}In_xAs$ to the experimentally measured Auger rate in $Ga_{1-x}In_xAs$ / $Al_{1-x}In_xAs$ double heterostructures and multiple quantum wells. No appreciable difference in the Auger recombination coefficient could be detected between the double heterostructure and the quantum well structures. The determination of carrier density and the determination of carrier lifetime were discussed in detail. The 2-dimensional carrier sheet density (n_{2D}) and the 3D volumetric density (n_{3D}) are related by the quantum well (QW) thickness (t_{QW}) by

$$n_{3D} = \frac{n_{2D}}{t_{QW}}. \tag{2-5}$$

Auger recombination rates were experimentally determined by Hausser *et al.* (1990) in bulk and quantum wells composed of $In_xGa_{1-x}As$ using the frequency upconversion technique (Hausser, 1990). Because their research used upconversion, this paper is reviewed in the following section (2.4).

E.R. Youngdale *et al.* (1994) investigated InAs - $Ga_{1-x}In_xSb$ and InAs - GaSb superlattices by measuring the temporal photoconductive response at liquid nitrogen temperatures (77 K) and room temperature (300 K). They calculated the Auger recombination coefficient as a fitting parameter, along with the Shockley-Read-Hall lifetime (τ_{SRH}) and found that for low excitation levels, the carrier lifetime τ_{SRH} was 0.13 ns in InAs - GaSb and 6 ns in InAs - $Ga_{1-x}In_xSb$. They attributed the short τ_{SRH} in the InAs - GaSb to defect centers in InAs-based heterostructures, about which little is known. At high excitation levels they fit the Auger coefficient to meet their data. Radiative recombination was not mentioned or considered, a potentially serious shortcomings of this technique and their results. In their defense, theoretical investigations of the InAs - $Ga_{1-x}In_xSb$ superlattice (Grein, 1993) indicate that for high carrier concentrations at 77 K, radiative recombination is approximately one order of magnitude lower than the Auger recombination rate.

2.3.2. Current State of Auger Recombination Research

The best analysis of time resolved luminescence related to Auger recombination has been done by Sermage *et al.* (1983; 1984; 1985; 1986). Their reports included 1) detailed analysis of the determination of carrier concentration resulting from laser excitation, 2) consideration of the dependence of carrier ambipolar diffusion on carrier concentration, and 3) deviations of the radiative recombination rate when the quasi-Fermi level enters the bands (e.g. $R_{rad} \neq Bn^2$ but rather $R_{rad} = Bn^{\gamma+1}$).

The group from Germany, led by Hausser and Fuchs, used the upconversion technique for time resolved luminescence (Hausser, 1990) (Fuchs, 1991) and seem to have obtained reasonable Auger recombination results. They claim to have considered the appropriate issues. However, their papers lacked the clarity demonstrated by Sermage *et al.* regarding key elements related to their analysis. They claim to have done a calculation for the radiative recombination rate as a function of carrier concentration,

much like Sermage *et al.*, and cite references that outline their calculation (Zielinski, 1989; 1987), but leave the reader unsure of the details.

Table 2-2: Synopsis of experimental efforts for Auger and Shockley-Reed-Hall recombination coefficients.

Material	Structure	Method	Temp (K)	C_{Auger} $x10^{-29}$ (cm^6/s)	τ_{SRH} (ns)	Year	REF
Si	Bulk	TRPL	80	0.02		1972	Nilsson
InAs	Bulk	Decay	300			1974	Dalal
Ge	Bulk	TR-FCA	300	0.011		1975	Auston
GaAs	Bulk	TRPL	77	0.01		1976	Benz
GaSb	Bulk	TRPL	77	10000		1976	Benz
GaSb	Bulk	spin	77	2.5		1981	Titkov
InGaAsP	Bulk	TRPL	300	2.3		1983	Sermage
InGaAs	Bulk	P-Probe	300	25.0		1984	Prise
InGaAsP	Bulk	TRPL		2.6		1985	Sermage
InGaAsP/InP	MQW	f - Resp	300	3.3		1986	Olshansky
InGaAs	Bulk	TRPL		7.0		1986	Sermage
InGaAs-AlInAs	MQW	TRPL		6.0		1986	Sermage
GaSb	Bulk	TRPL	250	30		1989	Snow
InGaAs	Bulk	TRPL	300	32.0		1990	Hausser
InGaAs/InP	MQW	TRPL	300	0.9		1990	Hausser
GaSb/AlSb	MQW	TRPL		48.0		1991	Fuchs
InAs	Bulk	P-Probe	77	1000		1992	Vodopyan
InGaAsP/InP	MQW	f - Resp	300	4		1993	Dapkus
InGaAsP/InP	MQW	Eg+Δ	300	5		1993	Mozer
InAs/GaInSb	SL	TRPC	300	80000	6	1993	Youngdale
InAs/GaInSb	SL	TRPC	77	130	6	1994	Youngdale
InAs/GaSb	SL	TRPC	300		0.13	1994	Youngdale
InAs(Sb)	MQW	TRPC	77/300	2100	14	1995	Lindle
GaInSb/InAs	LS	P-Probe	300	700	4.1	1995	McCahon

2.4. Upconversion Experiments

This section contains a short review of key upconversion experiments related to the current effort. Upconversion is described in detail in Chapter 5. Briefly, upconversion is the result of mixing luminescence from a material, generated by a pulsed laser, with a portion of the pulsed laser (pump) in a non-linear crystal designed to sum the frequencies, resulting in a shorter wavelength signal. By varying the delay time between

the luminescence and the laser pulse at the crystal, temporal profiles of the luminescence are obtained. Other techniques used for ultrafast spectroscopy include the use of a very fast photodiode, pump-probe techniques, and time-correlation techniques. Some of these techniques are briefly presented in the Appendix A literature review along with the upconversion technique for completeness and comparison.

In 1988, Jagdeep Shah wrote a frequently cited paper for the IEEE Journal of Quantum Electronics on ultrafast luminescence spectroscopy (1988). This paper could justifiably be titled "everything you need to know about luminescence upconversion."

At the time of this writing, a total of approximately 40 papers exist that report data using the upconversion technique. Of these, four are particularly related to this dissertation, the first because upconversion was accomplished with long wavelength luminescence (4 µm) and the other three because upconversion was used to study Auger recombination. These four papers are reviewed below.

2.4.1. Relevant Prior Research

The longest wavelength upconversion to date was done at Brown University by Heyen, Hagerott & Nurmikko (1989) with some assistance from Partin of the General Motors Research Lab. They successfully used $AgGaS_2$ to upconvert luminescence from PbTe quantum wells to measure radiative recombination rates. The time resolved luminescent (TRPL) signals they measured were taken from the peak of the steady state infrared spectrum corresponding to $h\nu \sim 255\text{-}310$ meV ($\lambda = 4.0$ to 4.9). The laser used in their experiment was a mode-locked cw Nd:YAG ($\lambda = 1.06$ µm) with a pulse width of $\sim$ 100 ps and an average power of 100 mW.

The first paper to use upconversion as a technique to measure Auger recombination coefficients was by Snow et al. (1989), in which they studied GaSb. They used a synchronously pumped R6G dye laser with a pulse width of 3 ps to upconvert the 1.5 µm luminescence, and found that the temporal behavior is strongly influenced by the

relatively small energy difference between the Γ-valley and the L-valley in the conduction band. Using the time dependence of spectrally integrated luminescence, they fit radiative and Auger recombination coefficients (SRH was not considered) and report $C_{Auger} \leq 10^{-29}$ cm^{6}s^{-1} at 4 K and $C_{Auger} = 3 \times 10^{-28}$ cm^{6}s^{-1} at 275 K in GaSb.

Upconversion was used by Hausser $et\ al.$ (1990) to determine Auger recombination rates in In$_x$Ga$_{1-x}$As and In$_x$Ga$_{1-x}$As/InP quantum wells. Their upconversion experiment was done with a mode-locked, Q-switched Nd:YAG laser operating at 1.06 μm with a pulse width of about 150 ps. The excitation laser spot on the sample was estimated to be 30 μm. Each data point in their TRPL trace represents the integrated intensity of a complete luminescence spectrum at a given delay time. The Auger coefficient was determined as a fitting parameter along with the Shockley-Read-Hall coefficient. The radiative recombination was theoretically calculated using **k•p** based on a model they developed previously (Zielinski, 1987 and 1989). Although they display a luminescence spectrum from their sample obtained using upconversion at 0.5 nsec, the luminescence $decay$ curves are obtained from a spectrally $integrated$ luminescence signal. The carrier density for a given excitation was determined by fitting the spectral shape of their measured luminescence at 500 psec to a model of the laser structure that predicted the luminescence spectral line shape. They believe the accuracy of their carrier density to be within 5% of the actual carrier density.

The same group from Germany published a second work (Fuchs, 1991) using upconversion to study Auger recombination rates in GaSb/AlSb multiple quantum well structures (MQW). Their experimental configuration was the same as the 1990 paper. Stimulated emission was avoided, as in similar research efforts, by focusing the excitation spot down to a diameter of about 20 μm. The thickness of the GaSb/AlSb quantum well was L$_z$ $\geq$ 4.0 nm. The strain associated with this system based on lattice mismatch between GaSb and AlSb is 0.65%. Their results indicate a strong influence of the small energetic separation (90 meV) between the Γ-valley and the L-valleys. As a

result, the carriers excited into the Γ minimum are scattered on a time scale estimated to be about 1 psec, into the four L-valleys. This pins the quasi-Fermi level near the band edge of the L minima. These qualitative arguments explained both the comparatively narrow spectra and the lack of higher sub-band transitions seen during this investigation. The room temperature Auger recombination coefficient estimate using a least-squares fit was $C = 4 \times 10^{-28} cm^6 s^{-1}$. The Auger coefficient C_{Auger} exhibited a monotonic increase with temperature up to 400K in contrast with theory for this system. They monitored the luminescence spectra 500 ps after excitation because they argued the momentum relaxation of the carriers is completed within an accuracy of 5 % by this time.

2.4.2. Current State of Research Using Upconversion

The upconversion technique is a powerful technique for studying temporal behavior of luminescing materials. As a result, upconversion has been used to study a variety of ultrafast phenomena in semiconductor materials as can be seen in Table 2-3. It is a difficult technique to use, requiring a significant capital investment (principally an ultrafast laser) and extreme care since the upconverted signals are typically small, particularly with relatively long wavelength luminescence ($\lambda_{pl} > 2 \mu m$). The details of the upconversion process efficiencies are given in Chapter 5. One can readily see the dearth of reported upconversion results with luminescence beyond 2 μm. To date, only two studies have been carried out as seen in Table 2-3, at these wavelengths. In the case of InAsSb alloys, there are no reports of upconversion experiments, or for that matter temporal luminescence experiments.

Table 2-3: Synopsis of upconversion experiments performed to date that relate to studying semiconductors.

Application	Crystal	λ_{signal}	λ_{laser}	$\tau_{resolve}$	Peak	REF	Year
Demonstrate Principal	LiNbO$_3$	0.1.7	0.694	10 ns		Midwinter	1966
Laser Pulse Profile	ADP	0.515	0.600	20 ps	50 W	Mahr	1975
Laser Pulse Profile	LiIO$_3$	0.85	0.620	1 ps		Duguay	1982
Carrier Relaxation	LiIO$_3$	1.53	0.610	10 ps	200 W	Shah	1984
Luminescence from QW	NNP/1	1-1.6	0.620	100 fs		Hulin	1986
Carrier Relaxation GaAs	LiIO$_3$	0.870	0.617	350 fs	5.0 kW	Shah	1986
PL from GaAs	LiIO$_3$	0.800	0.610	400 fs	3.3 kW	Shah	1987
Inter-valley Scattering	LiIO$_3$	0.87	0.608	500 fs	3.3 kW	Shah	1987
Bloch Transport	LiIO$_3$	0.74	0.610	400 fs	81 W	Deveaud	1987
Laser Pulse Profile	ADP	0.515	0.600	20 ps	50 W	Mahr	1975
Carrier Relaxation	LiIO$_3$	1.53	0.610	10 ps	200 W	Shah	1984
Luminescence from QW	NNP/1	1-1.6	0.620	100 fs		Hulin	1986
Carrier Relaxation GaAs	LiIO$_3$	0.870	0.617	350 fs	5.0 kW	Shah	1986
PL from GaAs	LiIO$_3$	0.800	0.610	400 fs	3.3 kW	Shah	1987
Inter-valley Scattering	LiIO$_3$	0.87	0.608	500 fs	3.3 kW	Shah	1987
Bloch Transport	LiIO$_3$	0.74	0.610	400 fs	81 W	Deveaud	1987
Exciton Transfer QW	LiIO$_3$	0.732	0.610	400 fs	6.1 kW	Deveaud	1987
Radiative Rec PbTe	AgGaS$_2$	4.0-4.8	1.064	100 ps	20 W	Heyen	1989
Auger GaSb	LiIO$_3$	1.55	0.607	3 ps		Snow	1989
Carrier Relaxation inQW	BBO	0.870	0.636	60 fs		Wise	1989
Exciton Life InGaAs QW	LiIO$_3$	1.0	1.064	180 ps		Cebulla	1989
Tunneling and Transport				700 fs		Oberli	1989
Phonon-assisted tunneling	LiIO$_3$	0.800	0.725	750 fs		Oberli	1989
QW-Capture		0.639		800 fs	10 kW	Deveaud	1990
Relaxation GaAs & InP	BBO	0.920	0.630	80 fs		Zhou	1990
Spin-Polarization in QW	LiIO$_3$	0.790	0.670	1 ps		Freeman	1990
Polarization magnetic QW	LiIO$_3$	0.790	0.670	150 fs	10 kW	Freeman	1990
Auger in InGaAs		1.2-1.7	1.064	150 ps		Hausser	1990
Auger GaSb/AlSb QW		1.7	1.064	100 ps		Fuchs	1991
Relaxation in GaAs	LiIO$_3$	0.7-0.9	0.642	100 fs		Elsaesser	1991
Relaxation- doped GaAs	BBO	0.920	0.620	100 fs		Zhou	1991
Relaxation-doped GaAs	Urea	0.7-0.9	0.620	90 fs	9.3 kW	Gale	1992
Relaxation in GaAs & InP	LiIO$_3$	0.7-0.9	0.642	100 fs		Elsaesser	1992
Strained InGaAs/InP	BBO	0.7-1.8	0.713	150 fs	3.7 kW	Kersting	1992
Transport-capture InGaAs	BBO	0.7-1.8	0.630	300 fs	3.7 kW	Kersting	1992
Transport-capture InGaAs	BBO	0.7-1.8	0.630	300 fs	3.7 kW	Kersting	1992
Relaxation in GaAs & InP	LiIO$_3$	0.920	0.642	120 fs		Shah	1993
Transport in GaAs MSM	BBO	0.855	0.710	100 fs	3.7 kW	Kersting	1993
Dynamics in InGaAs/InP	BBO	0.7-1.8	0.630	300 fs		Kersting	1994
Low Temp CVD InGaAs	LiIO$_3$	0.8-1.7	0.770	100 fs	18.7 kW	Krotkus	1994
PPPV polymers	BBO	0.7-0.8	0.795	150 fs	70 W	Mollay	1994
Carrier Dynamics in QW		0.7-0.8	0.603	120 fs		Deveaud	1994
Relaxation in GaInSb SL	KTA	2.3	0.840	140 fs		Jang	1997

2.5. *Summary*

Mid-IR semiconductor lasers are important for a variety of applications and as a result, continue to be an area of active research as is apparent from the literature (Section 2.1). One of the most promising material systems, $InAs_{1-x}Sb_x$, has been studied over the past three decades (Section 0), but because crystal growth techniques have matured significantly over this time, only the most recent studies contribute significantly to laser development. Auger recombination is, almost without exception, cited as the most probable contributor to poor laser performance, both in terms of a its strong temperature dependence, low T_o value, and low total power. There are, however, relatively few reports of experimental measurements of the Auger recombination coefficient (Section 2.3), particularly semi-direct measurements like time resolved luminescence (recall direct measurements are currently not possible). Luminescence upconversion, although difficult, is a technique for measuring temporal behavior of luminescent materials (Section 2.4).

Several elements are particularly noteworthy from this review: 1) Auger recombination is thought to be the limiting factor for mid-IR lasers, 2) there is no method to directly measure Auger recombination mechanisms yet, 3) time-resolved luminescence is arguably the *most* direct means of characterizing the temporal behavior in solids, particularly for Auger recombination processes, 4) there are a total of three reports of upconversion used to study Auger recombination, and 5) there are only two reports of upconversion with luminescence beyond 2 μm, and neither of them treats InAsSb structures.

37

3. Quantum Wells in Semiconductors

Each of the samples studied in this experimental effort were strained quantum wells, as a result, the basics for calculating quantum well density of states, envelope functions and understanding strain effects are presented in Section 3.1, 3.2, and 3.3 respectively.

3.1. Density of States

An important parameter used to characterize semiconductor material is the density of states, represented by g(E). The bulk, or free particle, density of states in a semiconductor including the spin states for the 3D case (given in number of states per volume) and the 2D case (in number of states per area) are (McKelvey, 1966:134,151)

$$g_{3D}\left(E, m^*\right) = 4\pi \left(\frac{2m^*}{h^2}\right)^{3/2} \sqrt{E}$$

$$g_{2D}\left(E, m^*\right) = \frac{4\pi m^*}{h^2}$$

$$(3-1)$$

where m^* is the effective mass associated with the band of interest. Note the 2D density of states is independent of energy. Because a quantum well confines the electrons and holes in one dimension, convention usually calls this the "z" direction, we know from basic quantum mechanics (Anderson, 1971) that the energy levels will be quantized in that dimension. In terms of a density of states, a one-dimensional quantum well looks like discrete states separated in energy according to the calculated energy levels (see Section 3.2 below for calculation of the energy levels). We expect the remaining two unrestricted dimensions will likely result in the 2D density of states showing up in the expression for the density of states in a quantum well. Figure 3-1 provides a qualitative picture of the 1-dimensinal quantum well, 2D and 3D density of states, and a quantum well (QW) described below.
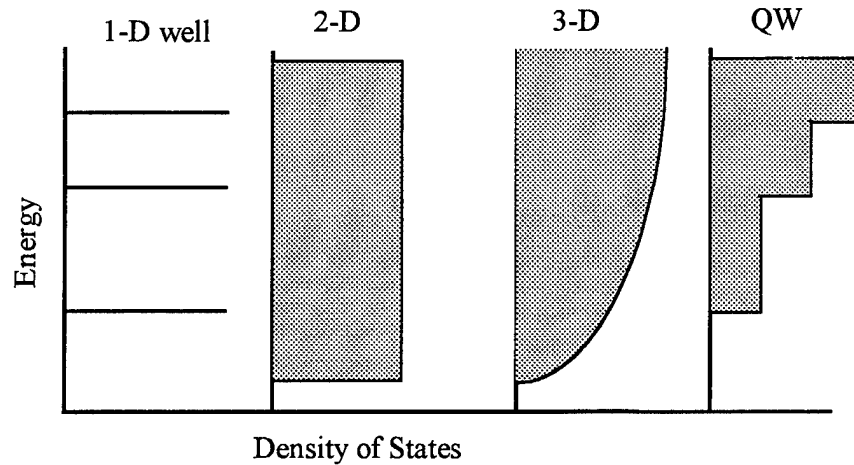
Figure 3-1: Qualitative picture of the density of states for a 1-dimensional particle confined to a well (1-D well), 2-dimension free particle (2-D), 3-dimension free particle (3-D), and a 3-dimensional particle confined in a one dimensional quantum well (QW).

The density of states is fundamentally about counting all accessible quantum states of the system at a particular energy. We recall from basic quantum mechanics that the particle (in this case electron or hole) has associated with it momentum in each direction, k_x, k_y, and k_z. The "x" and "y" directions and associated momentum k_x and k_y are not restricted and result in a "free particle" 2-dimensional constant density of states as depicted in Figure 3-1. The quantum well places restrictions on k_z such that in can only take on discrete values. For each accessible value of k_z, we have a new series of quantum states associated with k_x and k_y. Thus, the density of states is additive, that is the quantum well density of states looks like a staircase, with each additional quantized state adding another 2-D step to the density of states (see Figure 3-1).

3.2. Square Well Envelope Functions

Because a semiconductor quantum well affects the density of states, energy levels available to the system, and the location and nature of particles in the well, we must calculate the energy eigenvalues and wave functions of the well. This section outlines the fundamentals required to solve the one dimensional quantum mechanical problem

posed by semiconductor quantum wells. Beginning with the Schrodinger equation in one dimension we write

$$H\psi_n(z) = \left[-\frac{\hbar^2}{2m}\nabla^2 + V(z) \right]\psi_n(z) = E_n\psi_n(z) \qquad (3\text{-}2)$$

where $\psi_n(z)$ is the envelope function in band n, E_n are the discrete energy states accessible by the system, $V(z)$ is the potential energy and the remaining symbols take on their usual meaning.

It is important to note here that $\psi_n(z)$ is the envelope function and not the wave function of the electron (or holes). The full wave function is a product of the envelope function and the Wannier function (Yu and Cardona, 1996). Two important assumptions are made at this point to solve for the energy eigenvalues and the envelope function. The first is that parabolic bands reasonably characterize the bands inside and outside of the quantum well. The second assumption is that the effective masses (m^*) reasonably characterize the shape of the bands, and in so doing specifies the density of states in the structure as well as the inertial behavior of the particles.

1-D Quantum Well
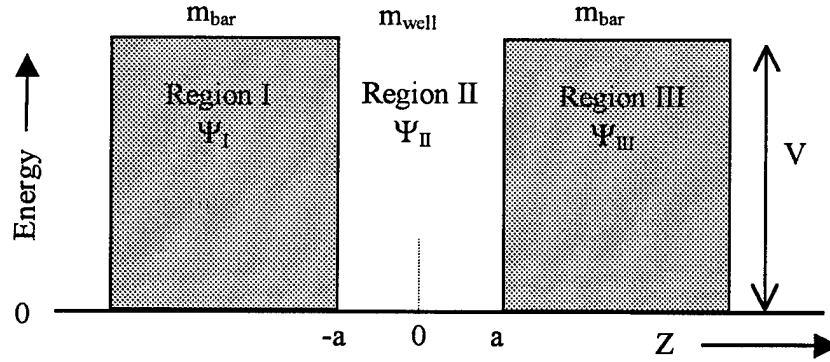
Figure 3-2: Qualitative picture of a one dimensional quantum well (QW).

A schematic diagram of a one-dimensional quantum well is given in Figure 3-2. The labeling and general approach to solving the 1-dimensional particle in a well is taken from Anderson (1971). The potential energy of the quantum well simply takes on a constant value inside the well region, and a larger constant value outside the well region in what is referred to as the barrier. The boundary conditions are 1) the wave function be continuous across the well/barrier region, and 2) the particle flux is continuous across the well/barrier interface. In general the effective masses of the well and barrier are not the same, thus, the two boundary conditions satisfied at the well/barrier interface are given by (Yu and Cardona, 1996:496)

$$\Psi_{well} = \Psi_{barrier}$$

$$\frac{1}{m^*_{well}}\left(\frac{\partial \Psi_{well}}{\partial z}\right) = \frac{1}{m^*_{barrier}}\left(\frac{\partial \Psi_{barrier}}{\partial z}\right)$$

(3-3)

where Ψ_{well} and $\Psi_{barrier}$ are the envelope functions in the well and barrier region respectively. Assuming the particle is confined, i.e. the particle energy "E" is less than

the potential energy of the barrier "V," can write an expression for the momentum in the well and barrier regions as

$$k_2 = \frac{\sqrt{2m_{well}^* E}}{\hbar}$$

$$K_1 = \frac{\sqrt{2m_{bar}^* (V - E)}}{\hbar}$$

(3-4)

and guess the form of the wave function solution. Solutions to the Schrodinger equation (3-2) in the three regions are

$$\Psi_I(z) = A \exp(K_1 z)$$
$$\Psi_{II}(z) = C \exp(ik_2 z) + D \exp(-ik_2 z).$$
$$\Psi_{III}(z) = F \exp(-K_1 z)$$

(3-5)

Now applying the boundary conditions at x = a and x = -a we find that

$$\frac{C}{D} = \frac{K_1/m_{bar}^* + ik_2/m_{well}^*}{-K_1/m_{bar}^* + ik_2/m_{well}^*} \exp(2ik_2 a)$$

$$\frac{C}{D} = \frac{-K_1/m_{bar}^* + ik_2/m_{well}^*}{K_1/m_{bar}^* + ik_2/m_{well}^*} \exp(-2ik_2 a)$$

(3-6)

The product of these two equations is 1, such that $(C/D)^2 = 1$, or $C = \pm D$. As expected we find a symmetric case (C = D) and asymmetric case (C = -D). Now with some straightforward manipulation and by defining

$$\alpha = k_2 a$$

$$\beta = a\sqrt{\frac{2m_{well}^* V}{\hbar^2}},$$

(3-7)

we can solve for the eigenenergies. Now we can write our symmetric and asymmetric solutions as

$$\alpha \tan(\alpha) = \left(\frac{m_{well}^*}{m_{bar}^*}\right) \cdot K_1 a = \left(\frac{m_{well}^*}{m_{bar}^*}\right) \cdot \sqrt{\frac{m_{bar}^*}{m_{well}^*}\left(\beta^2 - \alpha^2\right)}$$
$$-\alpha \cot(\alpha) = \left(\frac{m_{well}^*}{m_{bar}^*}\right) \cdot K_1 a = \left(\frac{m_{well}^*}{m_{bar}^*}\right) \cdot \sqrt{\frac{m_{bar}^*}{m_{well}^*}\left(\beta^2 - \alpha^2\right)} \quad (3\text{-}8)$$

If we return to our introductory quantum mechanics text, we find the only modification associated with using different effective masses in the well and barrier region shows up in Equation 3-7 and 3-8. The solution can then be found in the usual way, i.e. graphically, or with a numerical root finding routine. Appendix B presents additional detail of the mathematical manipulation from a Mathcad file.

We now have the eigenenergies and their associated eigenfunctions, which are our envelope functions. As we expected, the envelope functions in the well are symmetric (cosine functions) and antisymmetric (sine functions) solutions while the solutions in the barrier region are decaying exponential functions.

Figure 3-3 provides a graphical illustration of the energy levels and envelope functions calculated for a 10 nm InAsSb/InAlAsSb strained quantum well structure, identical to one of the samples studied in this dissertation. Because the structure is pseudomorphic, the quantum well is strained while the barrier is unstrained, the result being that the energy bands in the quantum well are shifted, while the barrier states effectively are unchanged from their bulk state. The shift in the heavy hole valence band (hh) and light hole valence band (lh) are reflected in the model and can be seen in Figure 3-3. The envelope functions associated with the first heavy hole state, and the first and second conduction band states are shown.
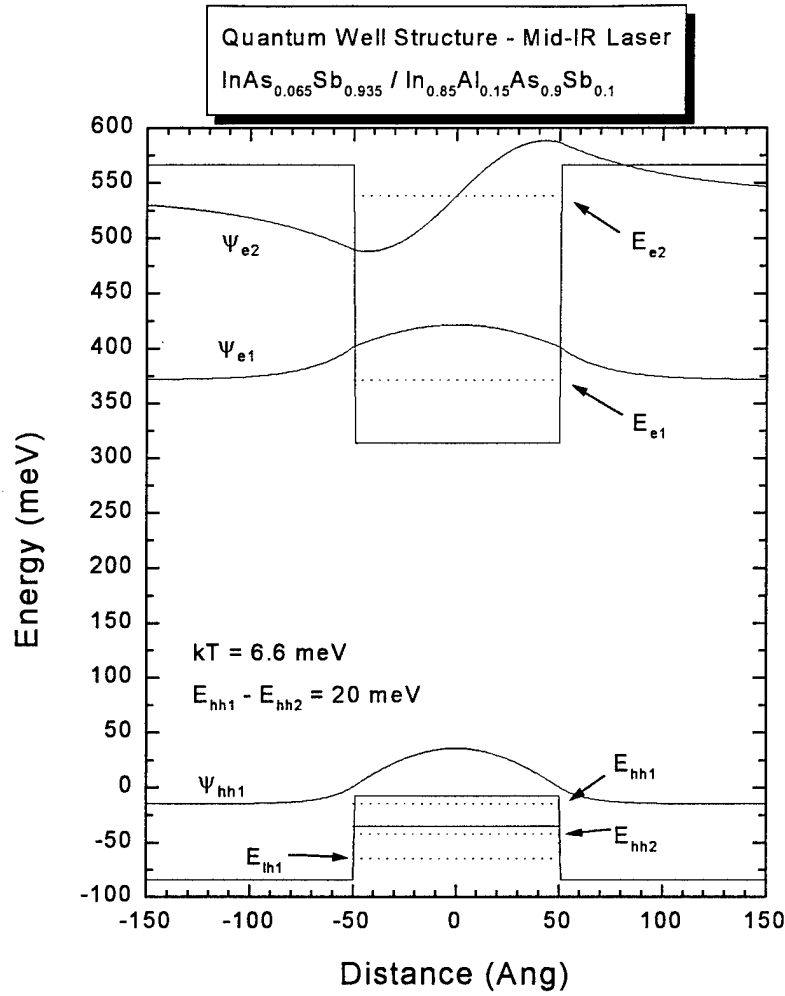
Figure 3-3: Energy band diagram of a single quantum well and the associated energy eigenvalues and envelope functions. Note that compressive strain splits the valence band by shifting the heavy hole band down and light hole band up in energy. Fermi energy levels were calculated for a carrier density of 10^{13} cm^{-2}.

3.3. Strain Effects

Because the samples studied in this research effort were strained quantum wells, the shift in energy associated with the energy bands, particularly the light hole and heavy hole bands, must be considered.

The valence band energies relative to the conduction band for the heavy-hole (hh), light-hole (lh), and split-off band (so) can be calculated using the $\mathbf{k} \bullet \mathbf{p}$ technique. The band energies can be determined as a function of strain if the elastic stiffness parameters C_{11} and C_{12} and the valence band deformation potentials A and B are known. Values for these and other important material parameters for important binary III-V materials are provided in Table 3-1. The modifications to the heavy-hole, light-hole and split-off bands are (Manasreh, 1993)

$$\delta E^{hh} = \left[-2A\left(\frac{C_{11}-C_{12}}{C_{11}}\right) + B\left(\frac{C_{11}+2C_{12}}{C_{11}}\right) \right]\varepsilon$$

$$\delta E^{lh} = \left[-2A\frac{C_{11}-C_{12}}{C_{11}} - B\left(\frac{C_{11}+2C_{12}}{C_{11}}\right) \right]\varepsilon \ . \qquad (3\text{-}9)$$

$$\delta E^{so} = -2A\left(\frac{C_{11}-C_{12}}{C_{11}}\right)\varepsilon.$$

The strain in the plane of the epitaxial layer ($\varepsilon_\parallel$) is calculated by comparing the equilibrium or bulk lattice constant of the layer material (a_L) with the lattice constant of the substrate (a_s). The in-plane strain is given by

$$\varepsilon_{II} = \frac{a_s}{a_L} - 1. \qquad (3\text{-}10)$$

Because the perpendicular direction is under no external stress, the strain in the perpendicular direction ($\varepsilon_\perp$) is related to the strain in the parallel direction ($\varepsilon_\parallel$) via Poisson's ratio (σ) and is given by

$$\varepsilon_\perp = \frac{-\varepsilon_{II}}{\sigma} \qquad (3\text{-}11)$$

where $\sigma \equiv C_{11}/2C_{12}$ and C_{11} and C_{12} are the elastic stiffness constants of the layer.

Table 3-1: Material parameters of III-V semiconductors.

Material	$E_g(0)$ (eV)	Δ (eV)	γ_1	γ_2	γ_3	C_{11}	C_{12}	C_{44}	A (eV)	B (eV)
GaAs	1.519	0.343	7.65	2.41	3.28	11.81	5.32	5.92	-8.23	-1.7
AlAs	2.974	0.28	4.04	0.78	1.57	11.81	5.32	5.92	-8.23	-1.7
InAs	0.418	0.38	19.7	8.4	9.28	8.329	4.526	3.96	-5.8	-1.8
InSb	0.235	0.803	35	15.7	16.8	6.918	3.788	3.02	-7.7	-2.0
GaSb	0.8133	0.758	11.7	4.1	5.19	8.834	4.023	4.32	-7.2	-1.8

The qualitative nature of the shift is depicted in Figure 3-4. One can see that in the case of negative strain, compression ($\varepsilon < 0$), the light-hole exhibits a downward shift in energy relative to the heavy-hole. Conversely, if the lattice is under positive strain, tension ($\varepsilon > 0$), the light-hole moves upward relative to the heavy-hole. This feature has had significant implications on semiconductor lasers as will be discussed in Chapter 4.

$$\varepsilon < 0 \qquad \varepsilon = 0 \qquad \varepsilon > 0$$
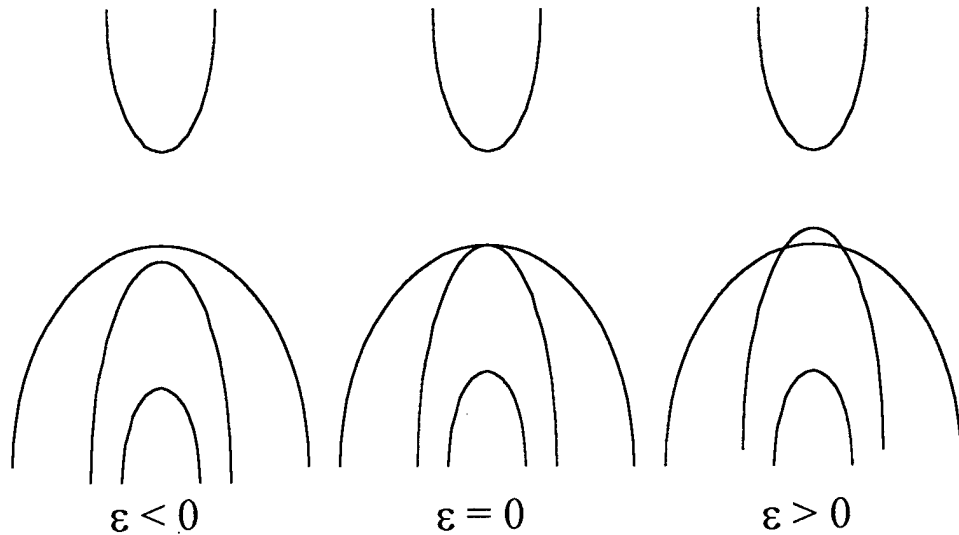
Figure 3-4: Qualitative picture of semiconductor band structure under strain. Strain is designated by ε (Agrawal and Dutta, 1993).

4. Recombination Phenomena in Semiconductors

This chapter provides the theoretical background for understanding recombination of excess electrons and holes in semiconductor materials. The recombination rate equation is usually expressed as (Agrawal and Dutta, 1993)

$$-\frac{dn}{dt} = A_{SRH} \cdot n + B_{rad} \cdot n^2 + C_{Auger} \cdot n^3, \qquad (4\text{-}1)$$

where Shockley-Read-Hall (SRH) recombination is characterized by the coefficient A_{SRH}, band-to-band radiative recombination is characterized by the coefficient B_{rad}, and Auger recombination is characterized by the coefficient C_{Auger}. Toward that end, the chapter is subdivided into five parts. Sections 4.1, 4.2 and 4.3 give a qualitative and quantitative description of the three types of recombination phenomena, SRH, radiative and Auger, respectively. Finally, section 4.4 discusses the effect of a strained quantum well on these recombination mechanisms.

4.1. Shockley-Read-Hall (SRH) Recombination

SRH recombination is associated with energy levels within the semiconductor band-gap that act as intermediary stages for recombination. The transition of carriers into or out of a state can take place radiatively, with the emission of a photon, or non-radiatively. In the case of nonradiative recombination, ignoring Auger for the time being, transitions can occur by emitting a cascade of phonons (Pankove, 1971). This processes increases as the number of available states in the energy gap increase. A qualitative picture of SRH recombination is given in Figure 4-1.

Conduction band
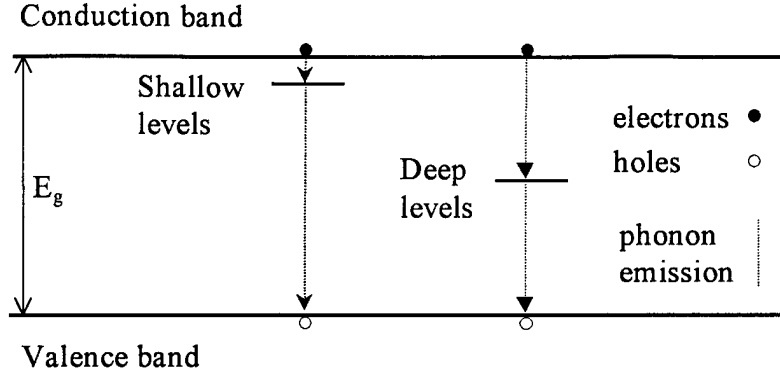
Figure 4-1: Schematic diagram of Shockley-Read-Hall recombination via shallow and deep levels in a semiconductor through phonon emission.

The rate of recombination is dominated by the number and character of states in the energy gap, and not by the concentration of excess carriers. As a result, SRH recombination is typically characterized in the semiconductor laser community by a single coefficient, A_{SRH} with units of s^{-1}, and the rate or recombination due to these processes in number of carriers per second $(dn/dt)_{SRH}$ is simply $A_{SRH}n$. A common and convenient term used is the SRH lifetime which is simply given by $\tau_{SRH} = A_{SRH}^{-1}$. If we write the SRH recombination in terms of a differential equation we have

$$-\frac{dn}{dt} = A_{SRH} \cdot n ,$$

(4-2)

which is easily solved giving

$$n(t) = n(0)\exp\left(\frac{-t}{\tau_{SRH}}\right).$$

(4-3)

Thus, if the dominant recombination mechanism is SRH, the carrier density time dependence can be characterized by an exponential decay.

There are a multitude of defects possible in semiconductor lasers, including heterojunction interface defects, vacancies, interstitials, and crystal growth defects. As a

48

result there may be several SRH recombination mechanisms contributing to the recombination of carriers at the same time, each with potentially a different lifetime associated with it. In this case, the decay is the result of a sum of exponentials, which can be treated with a single SRH lifetime and fit to a simple exponential. This makes the situation more complicated, however the defect types can be independently separated by their behavior with temperature. One feature to keep in mind regarding SRH recombination is that many of these defects have activation energies associated with them. As a result, their effectiveness may be a strong function of temperature. Because the exact nature and behavior of SRH recombination is complex and outside the scope of this effort, no further discussion is given. The important issue to keep in mind with regard to SRH is that at a constant temperature, the SRH contribution(s) can be characterized with an exponential decay lifetime, τ_{SRH}.

4.2. *Band-to-Band Radiative Recombination*

In the general case we can write the spontaneous emission rate $R_{sp}(hv)$ given in photons per unit time, per unit volume, per unit frequency range in some spectral range $d(hv)$ as

$$R_{sp}(hv)d(hv) = \sum_i \sum_f W_{if} G(hv) P_i P_f d(hv) \qquad (4\text{-}4)$$

where W_{if} is the transition rate between an initial state "i" and a final state "f," $G(hv)$ is a joint density of states and P_i and P_f are occupation probabilities. Specifically, P_i is the probability that the initial state is occupied and P_f is the probability the final state is unoccupied. In the case of a semiconductor, $G(hv)$ is a joint density of states between the conduction and valence bands and the occupation probabilities, P_i and P_f, are Fermi-Dirac distribution functions for an electron in the conduction band and a hole in the valence band respectively.

The transition rate, W_{if}, or rate of spontaneous emission from some excited state to a lower state is given in MKS units by (Ridley, 1993),

$$W_{if} = \frac{4\pi q^2 \eta}{3\varepsilon_0 m_0^2 h^2 c^3} h\nu \sum_{j=1,2,3} \langle \psi_f | P_j | \psi_i \rangle^2 \qquad (4\text{-}5)$$

where q is the charge of an electron, η is the refractive index, ε_0 is the permittivity of free space, m_0 is the mass of an electron, h is Plank's constant, c is the velocity of light in vacuum, hν is the energy of the emitted photon, ψ_i is the initial state wave function and ψ_f is the final state wave function, and P_j is the momentum operator summed over three orthogonal directions (x, y, z). In order to calculate radiative rates in a semiconductor, we can quantify the effect of the momentum operator on the initial and final wave functions via the "matrix element" approximation (Ridley, 1990) which defines

$$M_{cv} = \frac{2}{m_o} \sum_{j=1,2,3} \left| \langle \psi_f | P_j | \psi_i \rangle \right|^2 , \qquad (4\text{-}6)$$

where M_{cv} is the momentum matrix element for transitions between the conduction and valence band of the semiconductor with units of energy. It turns out that the value for most III-V semiconductors is near ~20 eV (Yu & Cardona, 1996, p.66). Our transition rate can now be written as

$$W_{if} = \frac{2\pi q^2 \eta M_{cv}}{3\varepsilon_o m_o h^2 c^3} h\nu , \qquad (4\text{-}7)$$

where W_{if} has the units of s^{-1}. This is the same expression given by Ridley (1990). The value of W_{if} for InAs, where M_{cv} is taken as 22.2 eV (Loehr, 1997), $\eta = 3.9$ and hν = 0.41 eV is 5.2×10^8 sec^{-1}. This quantity can now be related to the number of photons being emitted per unit volume per second.

We may write the density of states in a semiconductor including the spin states for the 3D case and the 2D case (McKelvey, 1966) as

$$G(h\nu) = g_{3D}\left(h\nu, m^*\right) = 4\pi\left(\frac{2m^*}{h^2}\right)^{2/3}\sqrt{h\nu - E_g},$$

$$G(h\nu) = g_{2D}\left(h\nu, m^*\right) = \frac{4\pi m^*}{h^2} \qquad (4\text{-}8)$$

where m* is the effective mass associated with the joint density of states (discussed below). The probability of occupation is given by

$$P_i = f(E_i, E_{fc}, T) = \frac{1}{\exp\left(\dfrac{E_i - E_{fc}}{kT}\right) + 1}$$

$$P_f = 1 - f(E_f, E_{fv}, T) = 1 - \frac{1}{\exp\left(\dfrac{E_f - E_{fv}}{kT}\right) + 1}, \qquad (4\text{-}9)$$

where E$_i$ is initial energy in the conduction band, E$_{fc}$ is the Fermi energy in the conduction band, E$_f$ is the final energy state in the valence band and E$_{fv}$ is the Fermi energy in the valence band.

We are now in a position to impose conservation of momentum. Because the momentum of a photon is much less than the crystal momentum of a phonon, we may write

$$\hbar k_{h\nu} \ll \hbar k_{phonon}. \qquad (4\text{-}10)$$

Thus, when a radiative recombination event takes place in a semiconductor with this constraint, the transition is direct, meaning the initial crystal momentum must equal the final crystal momentum. This constraint applies to a transition from the conduction band (subscript "c") to the heavy hole valence band (subscript "hh"), and invoking the parabolic band approximation we can write

51

$$E_i - E_f = h\nu = E_g + \frac{(\hbar k)^2}{2m_c} + \frac{(\hbar k)^2}{2m_{hh}}$$

$$(h\nu - E_g) = \frac{(\hbar k)^2}{2}\left(\frac{1}{m_c} + \frac{1}{m_{hh}}\right) = \frac{(\hbar k)^2}{2\mu} \tag{4-11}$$

where μ is a joint density of states mass between the conduction band and the heavy hole valence band given by the standard reduced mass relation

$$\frac{1}{\mu} = \frac{1}{m_c} + \frac{1}{m_{hh}}. \tag{4-12}$$

The energy associated with a particular transition energy $h\nu$ in each band is a weighted function of the effective masses relative to our joint density of states mass. So that now our initial energy state (E_i) and final energy state (E_f) for a particular $h\nu$ are given by

$$E_i = \frac{\mu}{m_c}(h\nu - E_g)$$

$$E_f = \frac{-\mu}{m_{hh}}(h\nu - E_g) \tag{4-13}$$

Thus, there is a direct relationship between $h\nu$ and an initial state (E_i) and final state (E_f).

One observation worth making at this point is our expectation of the radiative recombination rates dependence on strain. The discussion of strain in Chapter 3 indicated that in addition to quantization effects resulting from quantum confinement in the well, strain causes the valence bands, heavy-hole and light-hole, to move relative to one another. Strain also slightly modifies the shape of the band and in so doing modifies the density of states in the valence band. We note from Equations 4-11 and 4-13 that the effective mass term that shows up in these equations is the joint density of states given in Equation 4-12. Because the electron effective mass is approximately 10 times smaller than the heavy-hole mass in InAs, the radiative rate is not likely to be affected by strain.

We are now in a position to write an expression for the spontaneous emission rate for 3D and 2D semiconductor transitions from the conduction band to the heavy hole valence band, by inserting these relationships into Equation 4-4 giving

$$\left[R_{sp}(h\nu)\right]_{3D}^{hh} = \frac{2\pi q^2 \eta M_{cv}}{3\varepsilon_o m_o h^2 c^3} h\nu \left[4\pi \left(\frac{2\mu}{h^2}\right)^{2/3} \sqrt{h\nu - E_g}\right] f\left(E_i, E_{fc}, T\right)\left[1 - f\left(E_f, E_{fv}, T\right)\right]$$

$$\left[R_{sp}(h\nu)\right]_{2D}^{hh} = \frac{2\pi q^2 \eta M_{cv}}{3\varepsilon_o m_o h^2 c^3} h\nu \left[\frac{4\pi\mu}{h^2}\right] f\left(E_i, E_{fc}, T\right)\left[1 - f\left(E_f, E_{fv}, T\right)\right]$$

.(4-14)

To include transitions to the light hole valence band, we must sum the transitions from the conduction band to the light hole valence band. The analysis for the light hole contribution is identical that of the heavy hole, the exception being the substitution of effective mass ($m_{hh} \Rightarrow m_{lh}$). Thus we may write

$$R_{sp}(h\nu)_{3D}^{total} = \left[R_{sp}(h\nu)\right]_{3D}^{hh} + \left[R_{sp}(h\nu)\right]_{3D}^{lh}$$
$$R_{sp}(h\nu)_{2D}^{total} = \left[R_{sp}(h\nu)\right]_{2D}^{hh} + \left[R_{sp}(h\nu)\right]_{2D}^{lh}$$

(4-15)

The carrier dependence of spontaneous emission is accounted for through the occupation probabilities given by the Fermi energy level in the conduction (E_{fc}) and valence (E_{fv}) bands. The relationship between carrier density, n, and Fermi energy level in the conduction band, defining $E = 0$ at the valence band edge, is given as

$$n = \int_{E_g}^{\infty} G(E) f\left(E, E_{fc}, T\right) dE$$

$$n_{3D} = 4\pi \left(\frac{2m_c}{h^2}\right)^{3/2} \int_{E_g}^{\infty} \frac{\sqrt{E - E_g}}{\exp\left(\dfrac{E - E_{fc}}{kT}\right) - 1} dE$$

(4-16)

$$n_{2D} = \left(\frac{4\pi m_c}{h^2}\right) \int_{E_g}^{\infty} \frac{1}{\exp\left(\dfrac{E - E_{fc}}{kT}\right) - 1} dE$$

In the 3D case no closed form solution exists to relate n_{3D} and E_{fc}. In the 2D case, an analytic solution exists making it very attractive and convenient to use a 2D model so long as the 2D approximation is valid. For a 2D-electron gas in semiconductors the relationship is given by

$$E_{fc}^{2D} = kT \cdot \ln\left[\exp\left(\frac{n_{2D}h^2}{4\pi m_c} \cdot \frac{1}{kT} \right) - 1 \right]. \tag{4-17}$$

To calculate the "radiative lifetime," we simply integrate our expression for the spontaneous emission and divide by the carrier density. This gives us the total number of photons emitted per second per unit volume, divided by the number of carriers per unit volume. The result is then an integrated average recombination rate in $\sec^{-1}$. The radiative lifetime is simply the inverse of this quantity. The expression for an average radiative lifetime is then given by

$$\tau_{rad} = \frac{n}{\int_{E_g}^{\infty} R_{sp}^{total}(h\nu)d(h\nu)}. \tag{4-18}$$

A very important note at this point is that, although the term radiative lifetime is found in the literature and is often used out of convenience or because it is simple to understand, this is not a valid way to understand radiative recombination, qualitatively or quantitatively. Characterizing radiative recombination as a lifetime implies exponential decay behavior, however, one can clearly see from Equation 4-18 that τ_{rad} is a function of n, not independent of it. Therefore radiative recombination does *not* decay exponentially for *any* value of n.

Calculations of radiative recombination rates ($R_{rad}(n)$), which can be thought of as inverse radiative lifetime when care is taken, have been made using the material parameters for $InAs_{1-x}Sb_x$ with an antimony mole fraction of 6.5% at 77 K. Parabolic bands are assumed, and the material parameters were taken from previous work

(Marciniak, 1995) or, in the case of effective masses, are linear fits to the binary alloys. The spontaneous emission plot for three carrier densities and the integrated radiative lifetimes are plotted in Figure 4-1 and Figure 4-2 respectively.
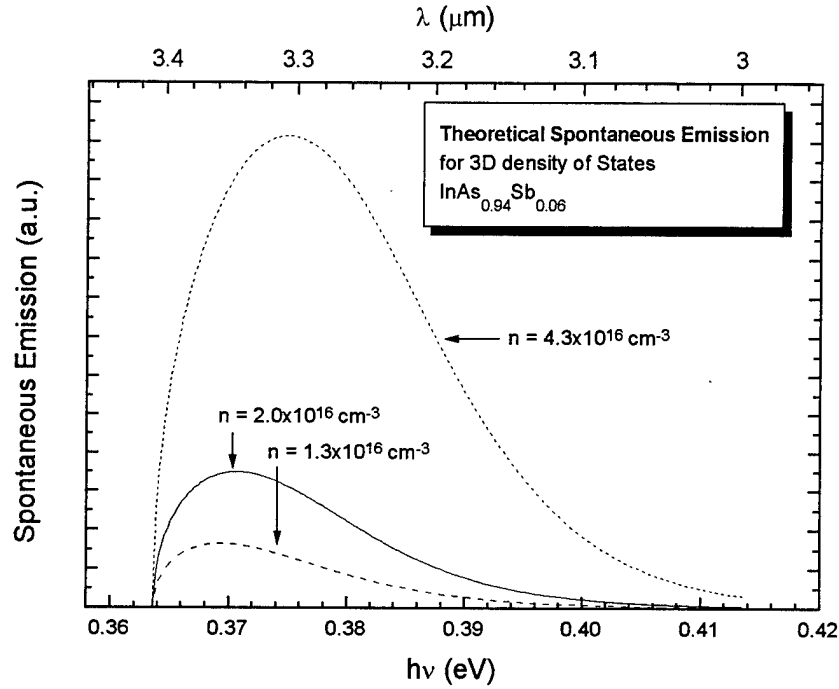
Figure 4-2: Theoretical calculation of the spontaneous emission from a 3D density of states for $InAs_{0.94}Sb_{0.06}$ with T = 77K
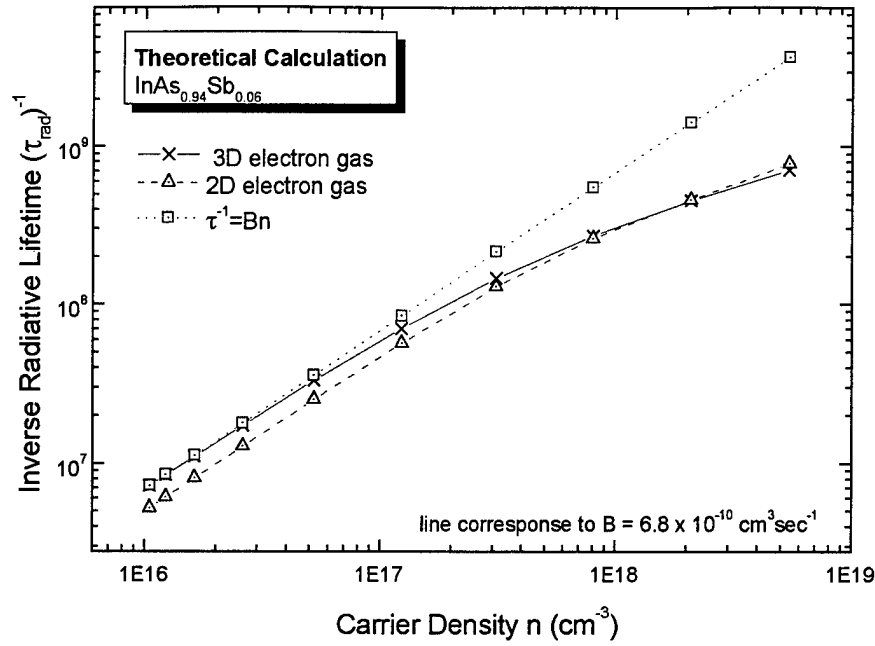
Figure 4-3: Inverse Radiative lifetimes (spontaneous emission rate) calculated for a 3D and 2D electron gas. Also plotted is the relation $\tau^{-1} = Bn$.

Since our objective is to study carrier recombination mechanisms modeled by the carrier recombination rate given in Equation 4-1, deviations from this fairly simple, yet widely accepted, approach must be considered. It is clear from Figure 4-2 that characterizing the radiative recombination rate with $dn/dt = Bn^2$ becomes a poor approximation at high carrier densities (it is very often convenient to speak of the "radiative lifetime" τ_{rad} which is defined as $\tau_{rad} = (Bn)^{-1}$). Returning to the equation for spontaneous emission, Equation 4-14, we can see the cause of this effect.

$$R_{sp} = \frac{2\pi q^2 \eta M_{cv}^2}{3m_o h^2 c^3 \varepsilon_o} h\nu \cdot g(E,\mu) f_{fc}\left(\frac{\mu}{m_c^*}(h\nu - Eg), E_{fc}\right)\left[1 - f_{vc}\left(\frac{\mu}{m_{hh}^*}(h\nu - Eg), E_{fv}\right)\right] \quad (4\text{-}19)$$

The carrier dependence for spontaneous emission manifests itself through the distribution function. Since we are dealing with electrons, the distribution function is

56

Fermi-Dirac and the probability of occupation is between 0 and 1. At the lowest carrier density, the rate of radiative recombination is governed principally by occupation, that is, in order for an electron to combine with a hole, a hole must exist in the valence band, and at low carrier densities this probability is small. The result is the typical bimolecular recombination ($R_{sp} \propto B_{rad}n^2$) where the radiative rate for a single electron in the conduction band (the inverse radiative lifetime τ_{rad}^{-1}) increases proportionately to n (Sermage, 1985). At large carrier density, the Fermi energies enter the bands and all conduction band states are filled with electron and all valence band states are filled with holes within ~kT of the respective Fermi levels. As a result, the limiting criterion for radiative recombination is related to the radiative transition strength between the initial and final states, and not occupation probability which dominates the low carrier density regime. As a result, at high carrier densities when the Fermi energies enter both conduction and valence bands, the radiative transition rate begins to saturate.

Previous efforts have attempted to consider this effect by expanding the radiative coefficient (B_{rad}) in a Taylor series expansion in carrier density n (Olshansky, 1984) and by modifying the exponent associated with the radiative term (Sermage, 1985). The first two terms in a Taylor series expansion of the radiative coefficient in n results in (Olshansky, 1984)

$$B(n) = B_o - B_1 n .\qquad (4\text{-}20)$$

The interesting thing regarding this approach is that "B_1" has the same order dependence on carrier density n as the Auger coefficient, with an opposite sign. In effect, B_1 is mathematically a negative Auger coefficient. The utility of such an approximation used in efforts attempting to determine Auger coefficients is questionable because the phenomena being measured is also being used to characterize radiative rate saturation.

Another technique for approximating this rate limiting phenomena is to write (Sermage, 1985)

$$\frac{1}{\tau_{rad}} = B(n)n = Bn^{\gamma} \tag{4-21}$$

where $1 > \gamma > 0$. Thus at low carrier densities $\gamma \approx 1$ while at very high carrier densities $\gamma \approx 0$.

4.2.1. Radiative Coefficients (B_{rad}) from Theory

The value of the radiative recombination coefficient can, to first order, be calculated from theory. Taking the result from Equation 4-7 we calculate the transition rate from conduction to valence band as

$$W_{if} = \frac{2\pi q^2 n_{h\nu} M_{cv}}{3\varepsilon_o m_o h^2 c^3} h\nu \tag{4-22}$$

where $h\nu = E_g$ and the notation is defined above. Assuming a non-degenerate distribution, Ridley (1990) has shown that the radiative coefficient is given by

$$B_{rad} = \frac{W_{if} N_{cv}}{N_c N_v}, \tag{4-23}$$

where N_{cv}, N_c and N_v are the density of states in the Boltzmann approximation for the joint density, conduction band, and valence band respectively given by

$$N_x = 2\left(\frac{2\pi m_x^* kT}{h^2}\right)^{3/2}. \tag{4-24}$$

Using the material parameters for the samples under study, we can calculate an initial approximation for the value of the radiative recombination coefficient at 77 K to be $B_{rad} \approx 2.5 \times 10^{-10}$ cm^3/sec. Note the theoretical temperature dependence of the radiative recombination coefficient, B_{rad}, coming from the above relations is $T^{-3/2}$.

An additional calculated data point in bulk $InAs_{0.91}Sb_{0.09}$ from a more detailed model by Flatte' (Flatte', 1995), assuming the radiative lifetime at lasing threshold is dominated by spontaneous emission at 77 K, finds $B_{rad} \approx 2.7 \times 10^{-10}$ cm^3/sec.

Our theoretical calculations provide a starting point estimate for the radiative coefficient B_{rad}. Experimentally, the calculated radiative coefficient was used as an initial value and then, if necessary, used as a free parameter to best fit the data. Because the order dependence differs for each of the recombination phenomena, we expect the radiative coefficient to most influence the intermediary carrier densities. The results obtained for B_{rad} are discussed in Chapter 7.

4.3. Auger Recombination

Auger recombination is a process in which an electron and a hole recombine, giving up their energy and momentum to another electron or hole in the system in the form of kinetic energy. If the energy is transferred to an electron, which is then pushed up higher into the conduction band, then the Auger process is referred to as CHCC. The nomenclature simply refers to the bands of the particles involved. The initial state always involves an electron in the conduction band (C) and almost always involves a hole in the heavy-hole valence band (H), giving us the first two letters. In the case where an electron receives the energy and is moved higher into the conduction band, we have another conduction band electron (C), going to a final state in the conduction band (C). Other bands that get involved with the Auger process are the light-hole band (L) and the split-off band (S). The process most often thought to dominate in long wavelength materials (low band-gap) is the CHSH process depicted in Figure 4-4.
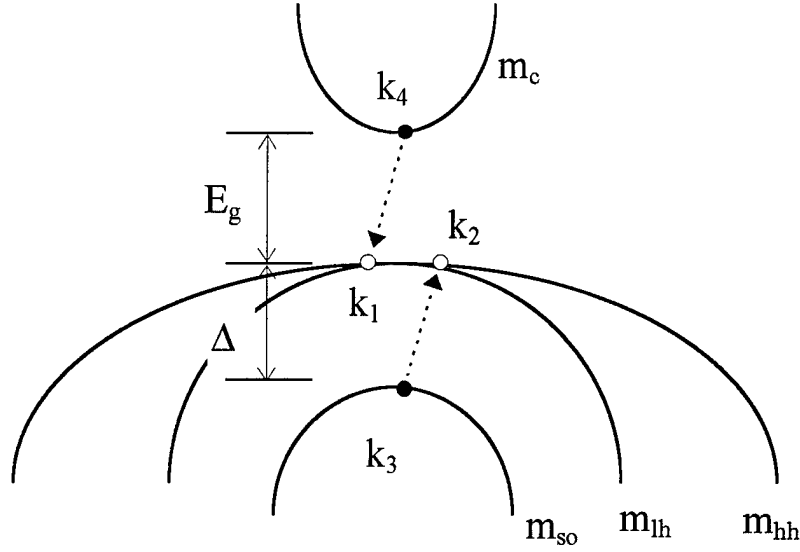
Figure 4-4: "CHSH" Auger Recombination Process.

To calculate the rate of Auger recombination, we must use Fermi's Golden Rule (Bransden, 1983) given as

$$W_{if} = \frac{4\pi^2}{h} \left| \langle f | V | i \rangle \right|^2 \delta\left(E_i - E_f\right).$$ (4-25)

The symbols are interpreted in the usual way: W_{if} is the transition rate, $\langle f |$ is the final state, $| i \rangle$ is the initial state, V is the coupling between the two states, and δ is the Dirac delta function.

For the case of Auger recombination, the coupling matrix element $|\langle i | V | f \rangle|^2 = |M|^2$ is the matrix element of the electron-electron interaction. The dominant Auger process for mid-IR semiconductor lasers is thought to be the "CHSH" process illustrated in Figure 4-3. In this, the initial state consists of 2 heavy holes in states k_1 and k_2. One of the holes recombines with an electron in the conduction band at state k_4 and the balance of energy and momentum is transferred to the other hole that is scattered to a state k_3 in

the split-off band. The rate of the Auger process can be written in the general form (Loehr, 1993)

$$R_{Auger} = 2\frac{4\pi^2}{h}\left(\frac{4\pi q^2}{\varepsilon}\right)\frac{1}{(2\pi)^9}\iiint |M|^2 \Theta\delta\left(E_3(k_3) + E_4(k_4) - E_1(k_1) - E_2(k_2)\right)dk_1 dk_2 dk_3$$

(4-26)

where ε is the dielectric constant, q is the electronic charge, $E_j(k_i)$ is the energy of the state k_i in band j. For the CHSH process I have adopted Loehr's notation with the band numbers given as: 1 $\equiv$ Heavy hole band, 2 $\equiv$ Heavy hole band, 3 $\equiv$ Split-off band, and 4 $\equiv$ Conduction band. Θ is the product of initial state occupation and final state vacancy that can be calculated using Fermi statistics and the full non-parabolic band structure. In a simplified form Θ is given by

$$\Theta = \left(\frac{1}{1+\exp\left(\frac{E_1(k_1)-E_{fv}}{kT}\right)}\right)\left(\frac{1}{1+\exp\left(\frac{E_2(k_2)-E_{fv}}{kT}\right)}\right)\left(\frac{1}{1+\exp\left(\frac{E_3(k_3)-E_{fv}}{kT}\right)}\right)\left(\frac{1}{1+\exp\left(\frac{E_4(k_4)-E_{fc}}{kT}\right)}\right)$$

(4-27)

where E_{fv} = Fermi energy level in the valence bands and E_{fc} = Fermi energy level in the conduction band.

For non-degenerate carrier concentrations (i.e. the low carrier density regime when use of Maxwell-Boltzmann (MB) statistics is valid), the integration of Θ over all states gives a recombination rate proportional to the cube of the carrier density $R_{Auger} \propto n^3$. Note the exponent is three and not four because the carriers near the band edge dominate the occupation probability. In the case of the CHSH process illustrated in Figure 4-3, the state labeled k_3 is assumed to be initially occupied by an electron for all reasonable values of n, lowering the dependence of R_{Auger} on n from 4 to 3. For the degenerate case, where MB statistics are no longer valid, this is no longer strictly valid. We expect a saturation phenomena begins to effect the Auger rate, similar to the

saturation of the radiative recombination discussed above. This phenomena has never been directly observed or addressed in the literature. Saturation phenomena will not be considered in this effort as the carrier densities were not high enough to warrant this additional consideration.

The matrix element $|M|^2$ for the transition, summing over all spin states and including direct and exchange terms, is given by

$$|M|^2 = \left| \frac{\langle 3, k_3 | 1, k_1 \rangle \langle 4, k_4 | 2, k_2 \rangle}{|k_1 - k_3|^2} - \frac{\langle 3, k_3 | 2, k_2 \rangle \langle 4, k_4 | 1, k_1 \rangle}{|k_2 - k_3|^2} \right|^2$$
$$+ \left| \frac{\langle 3, k_3 | 1, k_1 \rangle \langle 4, k_4 | 2, k_2 \rangle}{|k_1 - k_3|^2} \right|^2 + \left| \frac{\langle 3, k_3 | 2, k_2 \rangle \langle 4, k_4 | 1, k_1 \rangle}{|k_2 - k_3|^2} \right|^2, \qquad (4\text{-}28)$$

where $\langle i, k_i | j, k_j \rangle$ represents the overlap integral between the wave functions of band i at wave vector k_i and band j at wave vector k_j.

With a significant amount of mathematical manipulation and substitution, this nine dimensional integral can be reduced to a five dimensional integration over the Brillouin zone (Loehr, 1991:129). It is clear that an accurate model of the bands is required in order to calculate the wave functions and overlap integrals needed in the calculation of radiative and Auger recombination rates. Further detail for theoretically calculating Auger coefficients is outside the scope of this research effort.

4.4. Modification Introduced by a Strained Quantum Well

Recall from Section 3.3, strain in a semiconductor shifts the energy bands relative to one another, and in the case of the valence band, splits the light-hole from the heavy-hole band. Adams (1986) suggested that by growing a quantum well in such a way that the bulk lattice constant of the well material is slightly larger than the bulk lattice constant of the barrier material, the quantum well would be under bi-axial compression. This would result in the third direction being elongated and under tensile strain ($\varepsilon > 0$), as

was reviewed in section 3.3 via Poisson's ratio. The strain pushes the heavy-hole and the light hole apart relative to one another, in such a way that in the quantized direction, the higher energy band has a lighter effective mass (lh).

Using this as a tool, researchers can use "band-structure engineering" to lower the laser threshold and make higher efficiency semiconductor lasers. Adams argued that with bi-axial compressive strain, a population inversion can be achieved at lower injection current densities due to the reduced density of states at the valence band edge. Also, Auger recombination will be greatly reduced by the reduced density of states for holes, as well as the ability to shift the bands away from possible Auger resonance. Burt and Taylor (1985) and later Adams (1986) expressed the CHSH Auger rate in the form

$$R_{CHSH} \propto p^2 n \cdot \exp\left(\frac{-E_a}{kT}\right) \qquad (4\text{-}29)$$

where the activation energy E_a is given by

$$E_a = \left(\frac{m_s}{2m_{hh} + m_c - m_s}\right) \cdot \left(E_g - \Delta\right). \qquad (4\text{-}30)$$

Here, E_g is the band gap, Δ is the energy difference between valence band edge and the split off valence band, m_s is the spin orbit split-off band effective mass, m_{hh} is the heavy hole effective mass and m_c is the conduction band effective mass. Although this analytic expression is valid only for the non-degenerate regime, i.e. before the Fermi energy level enters the bands, the theoretical trend relating Auger recombination to the material parameters is qualitatively useful for illustrating Auger resonance. One can see from Equation 4-30, that if $E_g \approx \Delta$, the activation energy associated with Auger processes is a minimum and we are likely to have a large Auger recombination rate. Adams concluded that with effective band-structure engineering, the CHSH Auger recombination rate could be reduced by orders of magnitude (Adams, 1986).

4.4.1. *What to Consider and What to Ignore*

Strained quantum wells introduce a multitude of modifications to the un-strained bulk semiconductor model. Besides shifting energy bands relative to one another, the shape of the energy bands are modified in complicated ways, such that even the effective mass approximation can be called into question. This leaves the experimentalist with the task of deciding which effects are significant enough to consider, and which are safe to ignore.

Energy bands moving relative to one another in the quantum well will modify the relationship between Fermi energy and carrier density. Because this is an important aspect in understanding the analysis discussed in Chapter 7, it has been included in this effort where applicable. Although modifications to the shape of the bands are important for a number of interesting semiconductor problems, they require significant theoretical effort, and were considered a less important phenomenon impacting our ability to understand and model carrier recombination. As a result, only the quantization energies and the energy shifts due to strain are considered in this dissertation.

5. The Upconversion Technique

This chapter provides both the theoretical and experimental details related to sum-frequency-generation (SFG) used to perform photoluminescence upconversion. Briefly, upconversion is the performed by splitting a pulsed laser into two optical paths, one of which travels through a variable optical path delay stage. One of the paths, referred to here as the "luminescence" path, is used to excite a sample to produce luminescence, while the other path, referred to here as the "pump" path is used to mix with the luminescence in a nonlinear crystal. The purpose of mixing is to obtain SFG photons which has two benefits, 1) the SFG photons are of higher energy than either the luminescence or the pulsed laser enabling photon counting, and 2) the SFG signal only takes place when both luminescence and pump photons are present. This allows us to
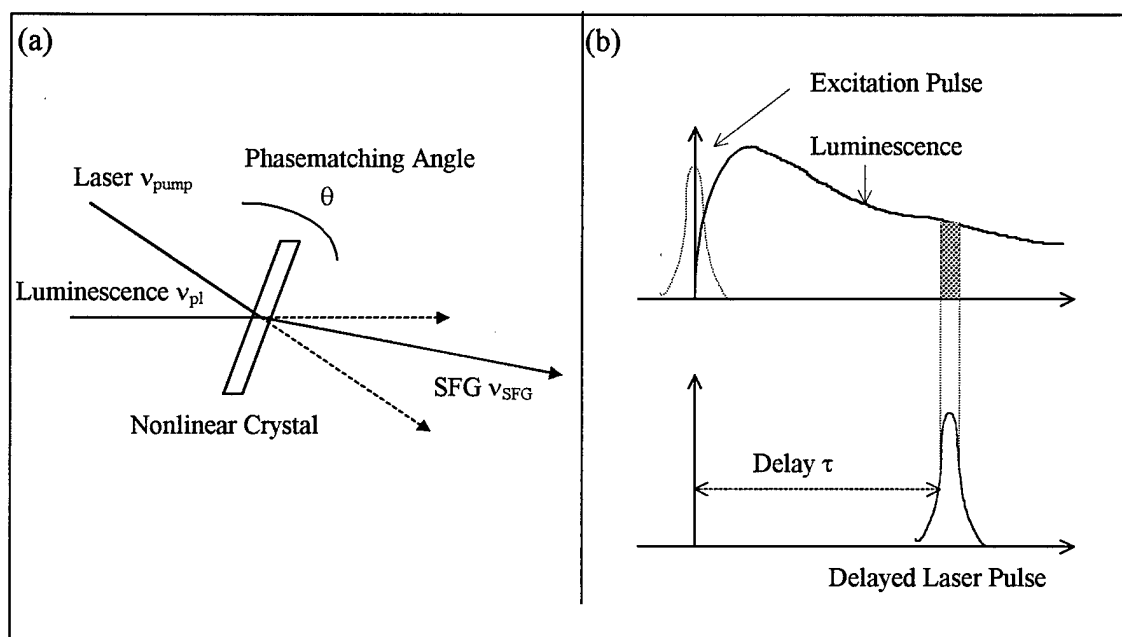
Figure 5-1: Schematic diagram for luminescence upconversion after Shah (1988). Sum-frequency radiation is generated in a nonlinear crystal (a), only during the time that a delayed laser pulse is present (b).

change the optical path difference between to luminescence and the pump and thereby obtain the temporal behavior of the luminescence. An illustrative figure of upconversion is presented in Figure 5-1.

The first section in this chapter, 5.1, provides a background in nonlinear optics needed to understand SFG, particularly as it pertains to the photoluminescence upconversion experiment. Section 5.2 and 5.5 describe the upconversion experimental configuration and some of the experimental difficulties and lessons learned in this effort respectively. A noteworthy subsection 5.3 presents the efficiency calculation for upconversion used to predict the upconversion signal strength. The chapter concludes with a discussion of energy bandwidth issues in Section 5.4.

Recall from the introduction in Chapter 1, our desire is to measure phenomena in mid-IR material on a very short time scale (sub-picosecond) to quantify the contributions of Auger and SRH recombination. Because there are no direct techniques to measure and identify non-radiative phenomena, an indirect technique is our only choice. Among indirect techniques that are possible for studying mid-IR structures (refer to Table 2-2) we have 1) time resolved photoconductivity (TRPC), 2) time resolved photoluminescence (TRPL), 3) pump-probe techniques, and 4) frequency response techniques.

Of these, the frequency response techniques are the least direct and require the most assumptions regarding behavior in the semiconductor. Pump-probe requires the probe photon energy be equal to the energy being studied in the sample; so in the case of mid-IR material, a mid-IR probe is required. The only group to have studied recombination rates using mid-IR pump-probe is the University of Iowa group lead by Professor Thomas F. Boggess. TRPC can be used to obtain time resolved information. However, this experiment has shortcomings in that electrical probes are used to measure the time dependence of the sample conductance, and as a result, depend on assumptions associated with the behavior of the electrical connections, carrier transport from the active region to the electrical connections, the geometry of the experiment, and a

knowledge of the samples optical parameters. An additional difficulty has been the assumptions required to analyze TRPC data.

TRPL along with pump-probe, are the most direct measures available to characterize carrier recombination dynamics. Time resolved data can be obtained from a short pulsed laser in conjunction with a fast detector. Unfortunately, the time constant for currently available mid-IR detectors is near 1 ns, meaning the shortest time a mid-IR detector is capable of resolving is approximately 1 ns. As a result, ultrafast phenomena in mid-IR materials must be obtained through other more elaborate techniques, such as a nonlinear frequency mixing upconversion technique.

5.1. Non-Linear Optics

Upconversion is the mixing of two electromagnetic waves in a non-linear crystal to create a third electromagnetic wave. Because the interaction requires an intense electromagnetic field, upconversion is most easily performed with a laser pump. In this dissertation we mix the long wavelength luminescence signal (also called photoluminescence because our excitation mechanism is photons, $\nu_{pl} = c/\lambda_{pl}$) with the laser (referred to here as the pump, $\nu_{pump} = c/\lambda_{pump}$) which results in an upconverted signal from sum frequency generation ($\nu_{SFG} = c/\lambda_{SFG}$). For sum frequency generation (SFG), also called upconversion, to take place, the conditions

$$\nu_{SFG} = \nu_{pl} + \nu_{pump}$$
$$\vec{K}_{SFG} = \vec{K}_{pl} + \vec{K}_{pump}$$

$$(5\text{-}1)$$

must be satisfied where ν is the frequency of the electromagnetic radiation and K is the wave vector given by

$$K = n\frac{2\pi}{\lambda}.$$

$$(5\text{-}2)$$

The relations in Equation (5-1) embody conservation of energy and conservation of momentum respectively. The relationship between the vacuum wavelengths of the two input beams (taken here as the photoluminescence electromagnetic field specified by λ_{pl} and the pump laser specified by λ_{pump}) and the upconverted beam (λ_{SFG}) is given by

$$\frac{1}{\lambda_{SFG}} = \frac{1}{\lambda_{pl}} + \frac{1}{\lambda_{pump}}.$$

(5-3)

SFG takes place as a result of $\chi^{(2)}$ which is the first non-linear term in the polarization of a nonlinear medium (Fowles, 1975:153). The polarization (P) of a medium can be expanded in a Taylor series expansion

$$P_i = \varepsilon_o\left(\chi_{ij}^{(1)}E_j + \chi_{ijk}^{(2)}E_jE_k + \chi_{ijkl}^{(3)}E_jE_kE_l + \cdots\right)$$

(5-4)

where P_i is the ith component of the instantaneous polarization and E_i is the ith component of the instantaneous field. Summations over repeated indices are assumed. The same equation can be written in a more convenient form (adopting the notation from Yariv and Yeh (Yariv, 1984:504)).

$$P_i = \varepsilon_o\left(\chi_{ij}^{(1)}E_j + 2d_{ijk}E_jE_k + 4\chi_{ijkl}^{(3)}E_jE_kE_l + \cdots\right)$$

(5-5)

By writing it this way we can represent the second-order non-linearity $P_i = 2\varepsilon_0 d_{ijk}E_jE_k$ in matrix form and discuss the specific phenomena responsible for upconversion. The matrix form is given by

$$\begin{pmatrix} P_x \\ P_y \\ P_z \end{pmatrix} = 2\varepsilon_o \begin{pmatrix} d_{11} & d_{12} & d_{13} & d_{14} & d_{15} & d_{16} \\ d_{21} & d_{22} & d_{23} & d_{24} & d_{25} & d_{26} \\ d_{31} & d_{32} & d_{33} & d_{34} & d_{35} & d_{36} \end{pmatrix} \begin{pmatrix} E_x^2 \\ E_x^2 \\ E_x^2 \\ 2E_xE_y \\ 2E_xE_y \\ 2E_xE_y \end{pmatrix}$$

(5-6)

68

For example, because LiIO$_3$ has a hexagonal crystal structure and C$_6$ point group, the "d" matrix is given by

$$\begin{pmatrix} 0 & 0 & 0 & d_{14} & d_{15} & 0 \\ 0 & 0 & 0 & d_{15} & -d_{14} & 0 \\ d_{31} & d_{32} & d_{33} & 0 & 0 & 0 \end{pmatrix}. \qquad (5\text{-}7)$$

In a similar manner, because LiNbO$_3$ has a trigonal crystal structure and has C$_{3v}$ symmetry, the "d" matrix is given by

$$\begin{pmatrix} 0 & 0 & 0 & 0 & d_{15} & -d_{22} \\ -d_{22} & d_{22} & 0 & d_{15} & 0 & 0 \\ d_{31} & d_{32} & d_{33} & 0 & 0 & 0 \end{pmatrix}. \qquad (5\text{-}8)$$

The primary crystal used for upconversion in this effort was KTiOAsO$_4$ (KTA) which has a C$_{2v}$ point group symmetry and so the "d" matrix is given by

$$\begin{pmatrix} 0 & 0 & 0 & 0 & d_{15} & 0 \\ 0 & 0 & 0 & d_{24} & 0 & 0 \\ d_{31} & d_{32} & d_{33} & 0 & 0 & 0 \end{pmatrix} \qquad (5\text{-}9)$$

The phase matching condition is also critical for upconversion. This requires that the nonlinear polarization wave induced at the sum frequency travel through the crystal at the same phase velocity as the generated electromagnetic wave of the same frequency. This requires knowledge of the index of refraction for the ordinary and extraordinary wave vectors for the wavelengths of interest given by the Sellmeier equations. Since KTA is a bi-axial crystal, there are three Sellmeier equations for each of the principal axes (Fenimore, 1995) given by

$$n_x(\lambda) = \sqrt{1.90713 + \frac{1.23522}{1 - \left(\frac{0.19692}{\lambda}\right)^2} - 0.01025\lambda^2}$$

$$n_y(\lambda) = \sqrt{2.15912 + \frac{1.00099}{1 - \left(\frac{0.21844}{\lambda}\right)^2} - 0.01096\lambda^2} \quad . \qquad (5\text{-}10)$$

$$n_z(\lambda) = \sqrt{2.14786 + \frac{1.29559}{1 - \left(\frac{0.22719}{\lambda}\right)^2} - 0.01436\lambda^2}$$

It is convenient to speak of ordinary and extraordinary waves in the crystal, which are defined by the orientation of the crystal relative to the polarization of the optic fields. The KTA crystal used in this research was cut in the X-Z plane at an angle of $\theta_x = 43°$ according to the vendor, θ_x being the angle between the crystal axis and the normal to the crystal surface. This means that the "ordinary" ray has a polarization in the Y direction and the extraordinary ray is in the X-Z plane. The refractive index then for the ordinary (o) and extraordinary (e) rays are

$$n_o(\lambda) = n_y(\lambda)$$

$$n_e(\lambda) = \frac{n_x(\lambda)n_z(\lambda)}{\sqrt{n_z(\lambda)^2 \cos(\theta)^2 + n_x(\lambda)^2 \sin(\theta)^2}}, \qquad (5\text{-}11)$$

where θ is the angle between the Z axis and the "e" ray inside the crystal. Using wave vector notation we can write the phase matching condition for collinear geometry simply as $K_{SFG} = K_{PL} + K_{pump}$. This situation is made somewhat more complicated when non-collinear phase matching is attempted as in Figure 5-2.
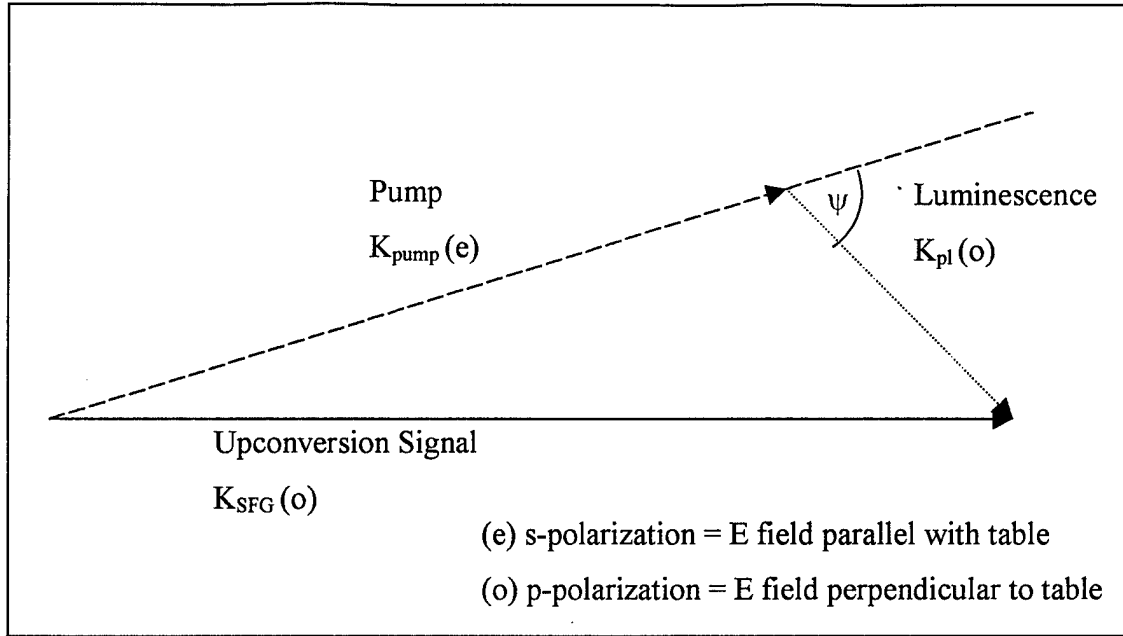
Figure 5-2: Non-collinear phase matching geometry used in experiment.

For the non-collinear case, the direction of the wave vectors must sum so that

$$\vec{K}_{SFG} = \vec{K}_{PL} + \vec{K}_{pump}$$
$$K^2_{SFG} = K^2_{PL} + K^2_{pump} - 2K_{PL}K_{pump} \cos(\psi)$$

(5-12)

where we have used the law of cosines and ψ is the angle between the two interacting

waves inside the crystal (note the expression involves only the magnitudes of the wave

vectors). Since the wave vectors are linearly proportional to the index of refraction, and

our "e" ray varies with angle θ, we can phase match various wavelengths by simply

rotating the KTA crystal to a predetermined tilt, and obtain a sum frequency signal.

Returning to matrix equations 5-6 and 5-9 we see that our ordinary ray P_{SFG} field is

generated by the interaction of E_y and E_x components of the input beams via d_{24}. The

magnitude of this coupling term will determine the effectiveness of our nonlinear crystal.

The efficiency of the process is provided below in section 5.3.

5.2. Experimental Configuration

Figure 5-3 is a schematic diagram of the photoluminescence upconversion experiment developed at AFIT for this dissertation.

5.2.1. Optical Path

The pulse coming from the Ti:Sapphire (described below in 5.2.3) travels through two lenses that expand and collimate the beam. This is done to insure the beam diameter changes a negligible amount as the delay stage is moved. The next optical element the beam encounters is a half-wave plate ($\lambda/2$) that is used to rotate the polarization of the beam. The beam is horizontally polarized coming out of the Ti:Sapphire cavity (s-polarization with respect to the optics table) but must be rotated to controllably split the beam into two legs with a polarizing beam splitter, which immediately follows the $\lambda/2$ wave plate. The two beams coming out of the polarizing beam splitter become the pump beam (s-polarization) and the luminescence beam (p-polarization).
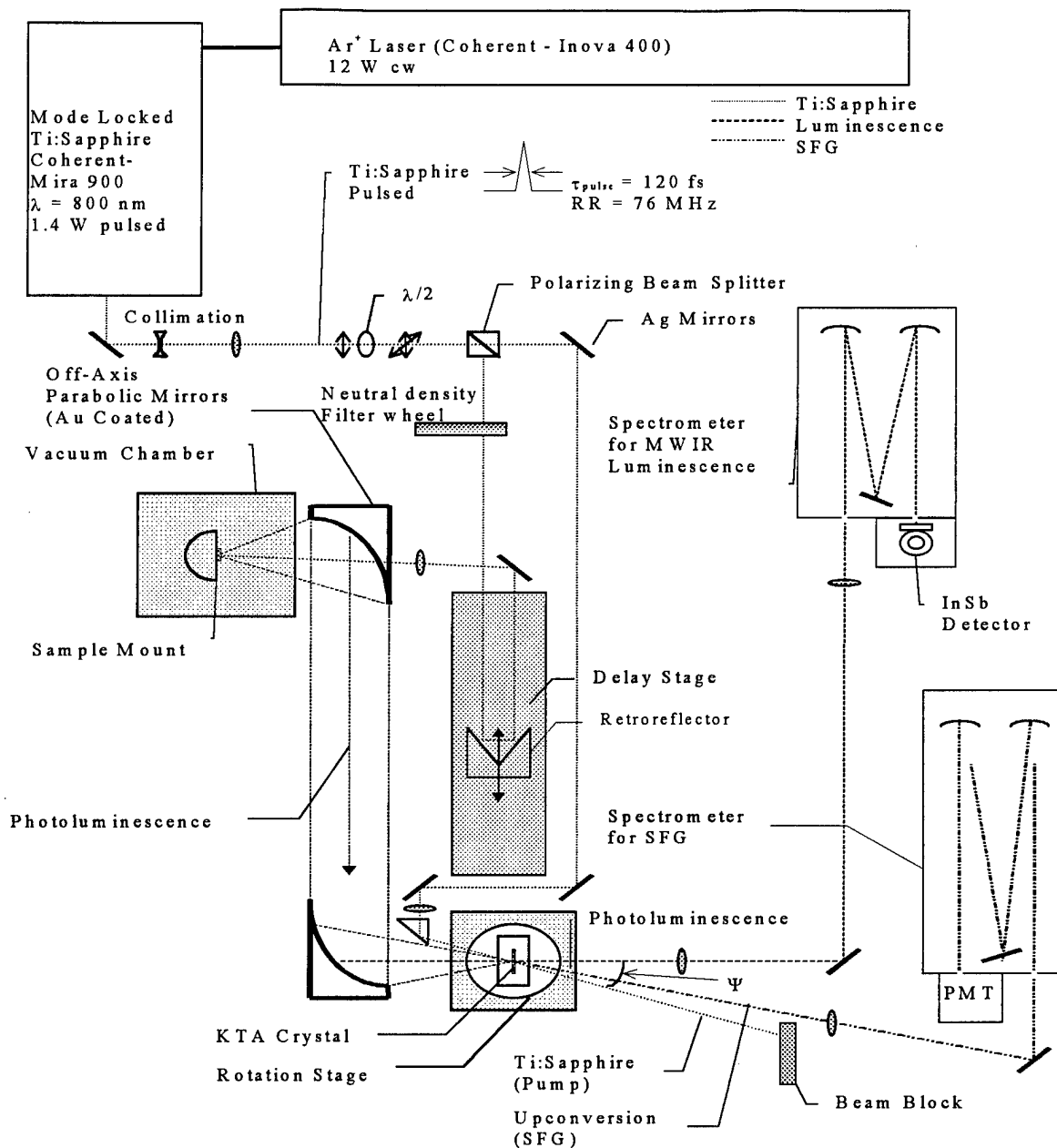
Figure 5-3: Experimental configuration of upconversion experiment constructed at AFIT

5.2.1.1.Pump Beam Path

The pump beam, with polarization in the plane of the table, propagates through a

fixed distance before it is focused onto the nonlinear crystal with a 100 mm focal length

lens. The Ti:Sapphire spot size on the KTA crystal was measured to be 50 μm in diameter (the techniques of this measurement are discussed below in section 5.5.3). The angle of separation between the luminescence path and the pump path was set at $\psi = 16°$ for non-collinear type-II SFG. The non-collinearity enabled spatial separation of the SFG signal from the pump. Silver mirrors were used throughout to insure the temporal extent of the pulse was not modified as it propagated, a feature characteristic of dielectric mirrors. The reflection just prior to the nonlinear crystal was made with a prism in order to insert the beam spatially close to the luminescence path.

5.2.1.2.Luminescence Beam Path

The luminescence beam, the vertical polarized beam leaving the beam splitter, passes through a neutral density filter wheel to control of the power to the sample, before it is sent through a computer controlled delay stage and focused to a spot on the semiconductor sample. The neutral density filter allowed the setup to remain unchanged while varying the luminescence excitation power. The delay stage is only capable of translating a total of 30 cm, which corresponds to a maximum delay of 2 ns (30 cm/c = 1 ns) if only one pass in and out of the Au coated corner-cube retroreflector is used. In order to take data out to 3 ns, two passes in and out of the retroreflector were used. The shortcoming with this configuration is that the Au coated corner-cube is only about 88% efficient, which is a significant improvement over the first glass corner-cube that was only 65% efficient. With limited Ti:Sapphire power, two passes was all the system would successfully support.

The luminescence excitation beam was then focused by a lens before striking the sample mounted in the sample chamber described in section 5.2.2. The spot on the sample was measured to be 70 μm in diameter. The details of this measurement are described in section 5.5.3. Luminescence was collected with a 2 in Au coated off-axis parabolic (OAP) mirror with a focal length $f_{OAP} = 150$ mm, and a 90° turning angle. The

mid-IR luminescence propagated to a second identical OAP that focused the luminescence onto the nonlinear crystal, thus the system was a 1:1 image of the luminescence excitation spot. The Au coated OAP mirrors were acquired from Janos Optics, of New Hampshire. Au coating was used for its uniformly high reflection characteristics across the mid-IR.

5.2.1.3. Nonlinear Crystal

The nonlinear crystal chosen for SFG of the pump ($\lambda_{pump} \approx 800$ nm) and the luminescence ($\lambda_{PL} \approx 3.5$ μm) was a 1 mm thick, KTA crystal, with an X-Z cut at 43°. This means the Y-axis is perpendicular to the surface normal, and the X-axis and Z-axis both have components of the surface normal. A 43° cut means the angle between the surface normal and the Z-axis is 43°. The crystal was mounted in a commercially available crystal holder from Inrad Inc. that was held in a 3 in Al adapting mount made by the AFIT machine shop. The 3 in adapter was placed in a 3 in optics mount with tilt control. This mount was placed on two linear translation stages mounted perpendicular to one another, which was itself mounted on a rotation stage.

5.2.1.4. Signal Detection

Beyond the nonlinear crystal were two optical collection paths, one to collect the mid-IR luminescence and the other to collect the SFG upconversion signal. The luminescence collection path used CaF_2 optics to re-image the spot at the nonlinear crystal onto the slits of a ½ meter McPherson spectrometer. This configuration enabled the simultaneous measurement of the luminescence signal and the upconversion signal. Simultaneity was not a requirement. However the need to switch back and forth between the two signals was critical. The McPherson spectrometer used a 300 grooves/mm grating, ideal for mid-IR wavelengths, and was equipped with a liquid nitrogen (LN_2)

cooled InSb detector. Time integrated luminescence spectral scans were acquired using a computer controlled EG&G lock-in amplifier.

The SFG upconversion signal was collected with BK7, 2 in optics which re-imaged the spot on the nonlinear crystal onto the entrance slits of a ¾ meter Spex spectrometer. The Spex used a 1200 grooves/mm grating and a GaAs photomultiplier tube (PMT) detector. The PMT was biased at its maximum allowable bias voltage (1200 volts) during operation to insure the sensitivity was near peak performance. The PMT was cooled to –40 °C to reduce the dark current by placing it in a LN_2 cooled housing made by Products for Research. The signal from the PMT was sent through a high bandwidth three stage amplifier before going to a Stanford Research SR400 Photon Counter to count photon events. The voltage used to discriminate actual photon counts varied somewhat. However a useful guide in setting the discriminator voltage was a measure of the dark counts, which at –40 °C was near 40 counts per second (cps).

Other important elements to the configuration included the beam block, high pass filters, low pass filters, and kinematic mounts. The kinematic mount was used to insert a mirror into the luminescence excitation path and thereby, divert it into a power meter. This arrangement insured the alignment was not disturbed during the necessary process of measuring the power to the sample. Because the kinematic mount was placed before the focusing lens and the LiF window, the offset associated with the losses due to these additional optical components was measured and used to ensure that accurate power measurements were made at the sample. The beam block, high pass filter and low pass filter will be discussed in the noise section (5.5.4).

5.2.2. Sample Chamber

In order to prevent condensation on the cold sample surface, the sample is held under vacuum, typically maintaining a pressure of 10^{-6} torr. This was accomplished with an Alcatel turbo pump backed-up by an Alcatel mechanical pump. The sample was

placed on a liquid helium transfer system (also called the Helitran) cold-finger, capable of cooling samples to approximately 4 K. Each sample was attached to the cold-finger copper mount of the Helitran system with Crycon grease. Crycon is an industry name for a particular cryogenic thermal grease that is loaded with copper to insure sufficient thermal conductivity and temperature uniformity. Xylene was used to clean grease off the front surface as needed. The flow of helium was controlled with simple gas flow valves, and the temperature was stabilized with a wire-wrap type resistive heater on the cold-finger. The temperature was measured by a calibrated temperature sensitive silicon diode.

The vacuum chamber was surrounded by 4 in flanges equipped with two quartz windows, and a LiF window. The luminescence excitation laser came through and the mid-IR luminescence excited through the LiF window. The primary concern associated with the LiF window is it's strong susceptibility to water damage. This was a continuous concern because there was no backup for the LiF window, and the need to cool the sample meant condensation was constantly forming on the cryogenic transfer lines above the LiF window.

5.2.3. Laser Characteristics

The Ti:Sapphire beam temporal, spectral, and spatial characteristics, strongly influenced the performance of the upconversion experiment.

5.2.3.1. How it Works

An argon-ion (Ar^+) laser was used to pump a Coherent Mira 900, mode-locked Ti:Sapphire laser which was tuned with a birefringent filter to lase near the peak of the Ti:Sapphire gain at 800 nm. By physically limiting the spatial volume of the cavity, we force the laser into a mode-locked state. This happens because the limited spatial volume introduces significant losses for cw modes oscillating in the cavity, but allows high field

pulses to oscillate loss-free because they are unaffected by the spatial volume limit. This happens because the Ti:Sapphire index of refraction exhibits a field dependence, known as the Kerr effect, which results in the Ti:Sapphire crystal behaving like a lens for mode-locked pulses.

5.2.3.2. Temporal Characteristics

The laser operated at a repetition rate (RR) of 76 MHz, which translated to 13.2 ns between pulses. These were the specifications from the Ti:Sapphire manufacturer, which were verified with a fast photodiode and oscilloscope. The mode-locked Ti:Sapphire pulse exhibited an autocorrelation width of 200 fs shown in Figure 5-4. The autocorrelation full-width at half-max (FWHM) is written as $\Delta\tau_{ac}$ and is experimentally measured. This is done with a nonlinear crystal used to mix the pump with itself in a non-collinear geometry. The upconversion experimental configuration could easily be adapted for this measurement by insuring the position of the excitation spot on the sample scattered a significant portion of the Ti:Sapphire light. This would then be collected by the OAP mirrors and delivered to the nonlinear crystal the same as the luminescence. The scattered laser pulse could then be translated temporally by changing the delay stage until it temporally overlapped with the pump pulse. KTA is not capable of phase matching k_{pump} with k_{pump} (i.e. second harmonic generation – SHG), so $LiIO_3$ was used as the nonlinear crystal in an ooe type-I phase matching. This required the insertion of an additional half-wave plate ($\lambda/2$) to rotate the pump polarization from E_{pump} being parallel to the table (s) to E_{pump} being perpendicular to the table (p).
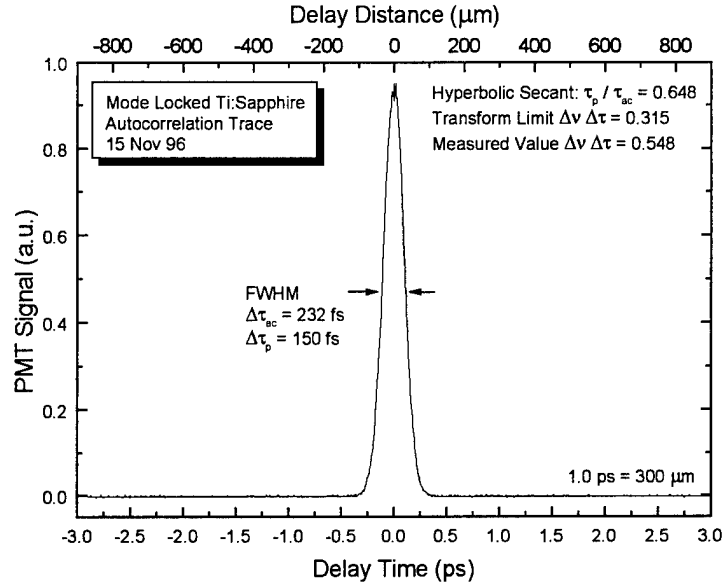
Figure 5-4: Autocorrelation of Ti:Sapphire taken with AFIT's upconversion experimental setup.

By monitoring the SHG signal as the delay stage is moved, we can measure the autocorrelation trace of the pulse. To find the temporal pulse width ($\Delta\tau_p$), a line shape must be assumed; in the mode-locked Ti:Sapphire case, a hyperbolic secant line shape is typically assumed by the laser manufacturer $\{I(t) = \text{sech}^2(1.76 \cdot t / \Delta\tau_{ac})\}$. With this assumption, the relationship between $\Delta\tau_{ac}$ and $\Delta\tau_p$ is given as $\Delta\tau_p/\Delta\tau_{ac} = 0.648$ and our measured pulse width is $0.648 \times (200 \text{ fs}) = 130$ fs.

5.2.3.3. Spectral Characteristics

The Ti:Sapphire was tuned to a center wavelength of 800 nm. A spectral scan of the mode-locked Ti:Sapphire is shown in Figure 5-5. The energy bandwidth of the Ti:Sapphire was measured to be $\Delta h\nu = 14.2$ meV. An additional measure of pulsed lasers is the product $\Delta\nu\Delta\tau$ that can be compared to the transform limit. Again, assuming a hyperbolic secant line shape, the transform limit is $\Delta\nu\Delta\tau_p = 0.315$. Using the data from Figures 5-4 and 5-5 to obtain $\Delta\tau_p$ and $\Delta\nu$ respectively, our measured value for this

quantity was $\Delta v \Delta \tau_p = 0.548$. This value is quite reasonable and indicates the mode-locked performance of the laser is good.
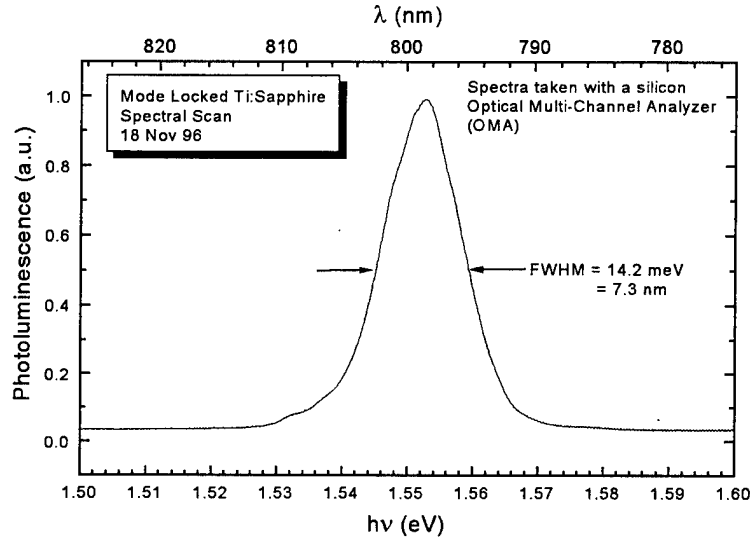
Figure 5-5: Spectra of the Ti:Sapphire while mode-locked

5.2.3.4. Spatial Characteristics

As will be discussed in Chapter 7, the measured value of the spot sized is critical in determining carrier density as well as calculating the SFG efficiency (see section 5.3). To do this accurately, a razor blade technique and a pin-hole technique were employed to measure spot size and used to compare against one another. These techniques are described in section 5.5.3. An additional comparison that proved to be quit useful was simply calculating the expected stop size through a lens assuming a Gaussian beam profile. This is simply done using the relation (Verdeyen, 1989)

$$2 \cdot \omega_o = \frac{4}{\pi} \frac{\lambda f}{D},$$

(5-13)

80

where ω_o is the spot size at the focus (defined as the radius at which the intensity has decreased to $1/e_2$), λ is the wavelength of the laser, f is the focal length of the lens, and D is the diameter of the beam before entering the lens. Each of these approaches (razor blade, pin-hole, and Equation 5-13) rely on the assumption that the beam profile is Gaussian. To insure this assumption was reasonable, a Coherent Mode-Master was used to determine its nearness to a Gaussian profile. The Mode-Master measures M^2, which is a parameter frequently used to describe the spatial profile of a beam relative to a Gaussian (for a perfect Gaussian $M^2 = 1.0$). The Ti:Sapphire was consistently measured to have a value of $M^2 = 1.1$.

5.3. SFG Efficiency Calculation

The calculation of conversion efficiency in MKS units given by (Dmitriev, 1991:42) as

$$\eta = \frac{2\pi^2 d_{eff}^2 L_{eff}^2 \left(P_{pump} \Big/ A_{pump} \right)}{c \varepsilon_o \lambda_{PL} \lambda_{SFG} n_o^{PL} n_e^{pump} n_o^{SFG}} \tag{5-14}$$

where d_{eff} is the effective nonlinear coefficient, L_{eff} is the effective interaction length, P_{pump} is the peak power of the pump laser, A_{pump} is the area of the pump laser in the non-linear crystal, λ_x is the wavelength of x, and n^y is the refractive index of the non-linear crystal for y photons. We can see that the efficiency of this process is related fundamentally to the "nonlinear" coefficient "d_{eff}" and the interaction length "L_{eff}." Both quantities are discussed below for the particular case of interest.

For the current experiment using KTA, the "o" rays were K_{PL} and K_{SFG} and the "e" ray was K_{pump}. Given the wavelengths for this experiment, this type of interaction is referred to as "oeo" which is a type II interaction (Dmitriev, 1991). The effective nonlinear coefficient is then given by

$$d_{\textit{eff}} = d_{oeo} = d_{32}\sin(\theta), \qquad (5\text{-}15)$$

where θ is the angle between the Z axis and the propagating K_{SFG} vector. The value of d_{32} for KTA is 4.2×10^{-12} m/V. There is a strong angle dependence through the phase matching angle θ, over the range of wavelengths of interest in this research (2 - 4 μm), the phase matching angle in KTA varied from $55°$ - $40°$.

A similar analysis can be performed for other candidate nonlinear crystals. For this effort, $LiIO_3$, $LiNbO_3$ and KTA were the three crystals of principal interest. Because the conversion efficiency is proportional to $d_{\textit{eff}}^2$, the magnitude associated with each crystal is critically important and is provided in Table 5-1 (Dmitriev, 1991:71-107).

Table 5-1: Comparison of non-linear crystals for use in Mid-IR PL upconversion.

Crystal	Type	D_{eff} =	~ θ_{pm} (°)	d_{critical} Value
$LiIO_3$	ooe	$d_{15}\sin(\theta)$	22-19	d_{15}= -5.5x10^{-12} m/V
$LiNbO_3$	ooe	$d_{15}\sin(\theta)$ - $d_{22}\cos(\theta)\sin(3\varphi)$	50-40	d_{15}= -5.4x10^{-12} m/V d_{22}= +2.7x10^{-12} m/V
KTA	oeo	$d_{32}\sin(\theta)$	55-40	d_{32}= 4.2x10^{-12} m/V

The effective interaction length (L_{eff}) is related to geometric considerations as well as group velocity considerations (Edelstein, 1990:96-99). The effective length is given by

$$L_{\textit{eff}} = \left(\frac{1}{L_s^2} + \frac{1}{L_t^2}\right)^{-\frac{1}{2}} \cdot \textit{erf}\left[\frac{\sqrt{\pi}}{2} \cdot L_c \cdot \left(\frac{1}{L_s^2} + \frac{1}{L_t^2}\right)^{\frac{1}{2}}\right] \qquad (5\text{-}16)$$

where L_s is the spatial effective length, L_t is the temporal effective length and L_c is the thickness of the nonlinear crystal. In the case of non-collinear SFG, if we assume the beams are Gaussian, than the spatial effective length is related to the angle between the

interacting beams, referred to here as the angle of non-collinearity (ψ). L_s is given by (Edelstein, 1990)

$$L_s = \frac{\sqrt{\pi}}{2}\left[\psi^2\beta^2 + \frac{(\rho-\psi)^2}{w_{pump}^2} - \frac{\left(\psi\beta^2 + \frac{(\rho-\psi)^2}{w_{pump}^2}\right)^2}{2\beta^2}\right]^{-\frac{1}{2}}$$

(5-17)

where w_{pump} is the spot size of the pump at the crystal, ρ is the walk-off angle of the extraordinary ray in the crystal and β is a convenient parameter and β and ρ are defined by

$$\beta = \sqrt{\frac{1}{w_{pump}^2} + \frac{1}{w_{PL}^2}}$$

$$\rho = a\tan\left[\frac{n_o(\lambda_{PL})^2}{n_e(\lambda_{pump})^2}\tan(\theta_{pm})\right] - \theta_{pm}$$

(5-18)

where w_{PL} is the spot size of the imaged luminescence at the non-linear crystal, and θ_{pm} is the phase matched angle of the SFG beam. Note that all angles are angles internal to the crystal.

In the most general case, group velocity mismatch between the interacting pulses contributes to decreased overlap length. This degradation mechanism is primarily a concern for optical parametric oscillators (OPO's) in which case the temporal overlap of signal and idler is critically important. In the case of PL upconversion, the fact that the pulse energy propagates at a slightly different velocity through the crystal is of negligible concern since the "pulse width" of the PL signal is significantly larger than the pump pulse width. In the interest of completeness, however, the temporal effective length (L_t) is given by (Edelstein, 1990)

$$L_t = \frac{\sqrt{\pi}}{2}\left[v_{p\text{-}SFG}^2 \gamma^2 + \frac{v_{p\text{-}PL}^2}{\tau_{pump}^2} - \frac{\left(v_{p\text{-}SFG}\gamma^2 + \frac{v_{p\text{-}PL}^2}{\tau_{pump}^2} \right)^2}{2\gamma^2} \right]^{-\frac{1}{2}} \tag{5-19}$$

where τ_{pump} is the pulse width of the pump, $v_{p\text{-}SFG}$ is the group velocity mismatch between the pump and the SFG beams, $v_{p\text{-}PL}$ is the group velocity mismatch between the pump and the luminescence beams, and γ is a convenient parameter. The group velocity mismatch ($v_{p\text{-}SFG}$ and $v_{p\text{-}PL}$) and γ are defined by

$$v_{p\text{-}SFG} = \left[\frac{n_e(k_p,\theta_{pm})}{c} + \frac{k_p}{c}\frac{\partial}{\partial k}n_e(k_p,\theta_{pm}) \right] - \left[\frac{n_o(k_{SFB})}{c} + \frac{k_{SFG}}{c}\frac{\partial}{\partial k}n_o(k_{SFB}) \right]$$
$$v_{p\text{-}PL} = \left[\frac{n_e(k_p,\theta_{pm})}{c} + \frac{k_p}{c}\frac{\partial}{\partial k}n_e(k_p,\theta_{pm}) \right] - \left[\frac{n_o(k_{PL})}{c} + \frac{k_{PL}}{c}\frac{\partial}{\partial k}n_o(k_{PL}) \right] \tag{5-20}$$

$$\gamma = \sqrt{\frac{1}{\tau_{pump}^2} + \frac{1}{\tau_{PL}^2}} \quad . \tag{5-21}$$

where τ_{PL} is the pulse width of the luminescence signal ($\approx$ 1 ns), k_p, k_{PL} and k_{SFG} are wave vectors for the pump, luminescence, and SFG respectively, $n_o(k)$ is the ordinary index and $n_e(k, \theta)$ is the extraordinary index, and θ_{pm} is the phase matched angle of the SFG beam.

5.3.1.1. Predicted Counts Per Second (cps)

An instructive exercise is to calculate theoretically the number of photons one expects to count per second in an upconversion experiment. Let us assume KTA is used to mix $\lambda_{PL} = 3.5$ μm with $\lambda_{pump} = 800$ nm with a non-collinear angle in the crystal of $\psi = 16°$, waist sizes $w_{PL} = 35$ μm and $w_{pump} = 25$ μm and a Ti:Sapphire pump operating at RR = 76 MHz with a pulse width of 130 fs and average power of $P_{pump} = 400$ mW. The equations for effective length give a value of $L_{eff} = 106$ μm. The resulting efficiency is

calculated using Equation 5-14 and found to be $\eta = 0.1029\%$. This number should be interpreted as the likelihood a mid-IR photon is mixed, or summed, with a pump photon, to produce a SFG photon.

To estimate the cps, we must know the number of mid-IR photons available per pulse for mixing in the KTA. To estimate this number we use a typical peak signal from the InSb detector, $S_{InSb} = 10 \; \mu V$. The value of the resistor and quantum efficiency at λ_{PL} in the InSb detector according to the manufacturer (Cincinati Electronics) was $R_{InSb} = 23.18 \; k\Omega$ and $QE = 82\%$ respectively. Using our known geometry, index of refraction for optical components, and an estimated grating efficiency for the McPherson spectrometer, we estimate the efficiency of delivering light from the spot at the nonlinear crystal to the detector to be $\eta_{optic} = 36\%$. The average number of mid-IR photons at the nonlinear crystal that are available for mixing with the pump, per pulse is given by

$$\# \; photons = \frac{S_{InSb}}{R_{InSb} \cdot QE \cdot RR \cdot \eta_{optic}} \cdot \left(\frac{1}{e^-} \right). \qquad (5\text{-}22)$$

Plugging in the numbers gives 120 mid-IR photons per pulse. Because the Ti:Sapphire oscillates at 76 MHz, the total number of mid-IR photons available for mixing at the nonlinear crystal per second is $120(76 \times 10^6) = 9.1 \times 10^9$. Now we must account for the fact that these photons do not all arrive at the same time. We do this by estimating a pulse width of the luminescence signal. For this experiment, a reasonable pulse width was $\tau_{PL} = 1$ ns. Now the number of photons that are in the crystal interaction region at the same time the pump pulse is present is reduced by a factor $\tau_{pump}/\tau_{PL} = 1.3 \times 10^{-4}$. We are now in a position to estimate the expected counts per second (cps) from this upconversion experiment. The calculation is simply

$$cps = \frac{S_{InSb}}{e^- \cdot R_{InSb} \cdot QE \cdot \eta_{optic}} \cdot \left(\frac{\tau_{pump}}{\tau_{PL}} \right) \eta_{SFG}, \qquad (5\text{-}23)$$

which gives us a value of approximately 1225 cps.

5.4. Phase-Matching Bandwidths

In addition to the efficiency calculation for the SFG process, the energy bandwidth of the process is very important. This is related to the conservation of momentum constraint on the SFG process. Simply put, the efficiency calculated above assumes $\Delta K = 0$ where ΔK is defined by

$$\Delta K = \left| \vec{K}_{PL} + \vec{K}_{pump} - \vec{K}_{SFG} \right| \tag{5-24}$$

where we recognize K_{PL} as the wave vector of the photoluminescence photons, K_{pump} as the wave vector of the pump laser, and K_{SFG} as the wave vector of the sum-frequency photons. ΔK can be written (Dmitriev, 1991:32) as the sum of components that contribute to the wave vector mismatch given here as

$$\Delta K \approx \left(\frac{\partial (\Delta K)}{\partial T} \right) \Delta T + \left(\frac{\partial (\Delta K)}{\partial \theta_{pm}} \right) \Delta \theta_{pm} + \left(\frac{\partial (\Delta K)}{\partial h\nu} \right) \Delta h\nu \tag{5-25}$$

where "T" is the crystal temperature, θ_{pm} is the SFG phasematching angle, and $\Delta h\nu$ is the spectral bandwidth of the interacting photons. In the case of KTA, the first term in Equation (5-25) is negligible. The second term is related to the geometry of the optics and the type of interaction. For the experimental setup used in this effort, and assuming KTA "oeo" interaction we can calculate the angle at which the efficiency drops to half the maximum value (Dmitriev, 1991:33) as

$$\Delta \theta = \frac{0.886 \lambda_{pump} \left[1 + \left(n_{opump} \middle/ n_{epump} \right)^2 \tan^2(\theta_{pm}) \right]}{L_{eff} \tan(\theta_{pm}) \left[1 - \left(n_{opump} \middle/ n_{epump} \right)^2 \right] n^e_{pump}(\theta_{pm})} \tag{5-26}$$

where n_{opump} is the ordinary index at the pump wavelength, n_{epump} is the extraordinary index at the pump wavelength, and $n^e_{pump}(\theta_{pm})$ is the index of the phase-matched extraordinary photons. For the case of KTA with the wavelengths used in this effort, $\Delta\theta \approx 3.6$ degrees corresponds to an f# ≈ 8. The implication of such a large f# is that any light outside this cone of light is not sufficiently phase matched and will not result in an SFG signal. This sets limits on upconversion efficiency and experimental considerations.

The last term in determining ΔK is related to the bandwidth of the mixing photons. For this calculation we need to assume which of the two added frequencies has the largest bandwidth. In our case, the photoluminescence has a bandwidth of $h\nu_{pl} \approx 16$ meV to 22 meV depending on the temperature, while the bandwidth of the Ti:Sapphire measured at $h\nu_{pump} \approx 14$ meV. Because the bandwidths are of the same order, both are presented here for completeness and in recognition that the limiting bandwidth will dominate. If we assume the lower frequency wave (λ_{PL}) has a wide bandwidth, the corresponding $\Delta h\nu$ that results in a decrease in efficiency of conversion by 50% is given for "oeo" interaction by Dmitriev (1991:36) as

$$\Delta h\nu = \frac{h \cdot 0.886}{L_{eff}\left[n_{PL} - n_{SFG} - \lambda_{PL}\left(\frac{\partial n_{PL}}{\partial \lambda_{PL}}\right) + \lambda_{SFG}\left(\frac{\partial n_{SFG}}{\partial \lambda_{SFG}}\right)\right]}, \qquad (5\text{-}27)$$

where n_{PL} is the ordinary index at the luminescence wavelength, n_{SFG} is the ordinary index of KTA at the sum-frequency, and partial derivatives come from the Sellmeier equations for KTA. For luminescence wavelengths between 2 and 4 μm, the energy range over which the efficiency decreases to 50%, corresponds to $\Delta h\nu \approx 100$ meV. Thus the decrease due to wavelength detuning should be very small based on these calculations.

If we assume the higher frequency wave (λ_{pump}) has a wider bandwidth than the luminescence, than the corresponding $\Delta h\nu$ that results in a decrease in efficiency of conversion by 50% is given for "oeo" interaction is (Dmitriev, 1991:37)

$$\Delta h\nu = \frac{h \cdot 0.886}{L_{eff}\left[n_{pump}(\theta_{pm}) - n_{SFG} - \lambda_{pump}\left(\dfrac{\partial n_{pump}(\theta_{pm})}{\partial \lambda_{pump}}\right) + \lambda_{SFG}\left(\dfrac{\partial n_{SFG}}{\partial \lambda_{SFG}}\right)\right]}, \quad (5\text{-}28)$$

where $n_{pump}(\theta_{pm})$ is the extraordinary index at the pump wavelength, n_{SFG} is the ordinary index of KTA at the sum-frequency wavelength, and partial derivatives come from the Sellmeier equations for KTA. Again, for luminescence wavelengths between 2 and 4 μm, the energy range over which the efficiency decreases to 50%, corresponds to $\Delta h\nu \approx$ 1000 meV. Thus, the bandwidth for efficient upconversion is limited to approximately $\Delta h\nu \approx 100$ meV. We recognize that for the case where the luminescence spectra is near 100 meV, time resolved spectra can only be accurately measured if the system is calibrated in such a way to permit the simultaneous rotation of the crystal with the scanning spectrometer.

5.4.1. Measured States and Bandwidth

The material being studied in this effort is dominated by band to band radiative recombination (Marciniak, 1995). Thus, the luminescence peak is due to recombination from and initial energy state (E_i) at or near the lowest energy point in the conduction band to a final energy state (E_f) at or near the highest point in the valence band.

The spectral width of the signals and our measurement system challenge the assumption that we are only sampling the peak of the photoluminescence spectra. The configuration used for these series of experiments resulted in the signal energy-bandwidth, set by the slit-width of the spectrometer (FWHM $\approx$ 9 meV at 640 nm), within the photoluminescence energy bandwidth (FWHM $\approx$ 16 meV), the Ti:Sapphire

bandwidth (FWHM $\approx$ 15 meV) and the SFG energy-bandwidth ($\Delta h\nu \approx 100$ meV) calculated above. As a result, our upconversion signal effectively probes only the band-edge luminescence.

5.5. *Experimental Difficulties & Lessons Learned*

In view of the fact that this is the first experimental report of upconversion for wavelengths longer than 3 μm with sub-picosecond resolution, some of the experimental challenges and potential obstacles are presented here. In addition to the sensitivities described above, a number of difficulties were encountered while attempting luminescence upconversion that are worthy of additional discussion. These include discussions on laser behavior and sensitivity (5.5.1), shopping for nonlinear crystals (5.5.2), the necessity for precision optics and measurements (5.5.3), and noise (5.5.4).

5.5.1. *Laser Sensitivity*

Although the Ar^+ laser and the Ti:Sapphire, both from Coherent, used in this effort were arguably some of the best commercially available, their operation was not without difficulties. During the course of this dissertation, it was discovered that the beam quality of the Ti:Sapphire is dominated by the beam quality of the Ar^+ laser. This is no surprise to anyone, however what was surprisingly difficult was maintaining the beam quality from the Ar^+. The Ar^+ operating at approximately 12 watts produced ionized radicals just outside the Brewster window. These radicals would react with the sheath that was designed to cover the Brewster window resulting in free particles that can best described as "black junk," which rained down onto the Brewster window. The solution from the laser manufacturer was to periodically etch the window to remove the particles. Unfortunately, Coherent was not able to sell the etching solution, sodium-sulfate, as it is a harsh chemical. Further, ordering the solution was ruled out of the question due to government regulations on acquiring such a chemical. Fortunately, a local businessman in the glass etching business donated just enough sodium-sulfate

89

crystals to put into solution and etch the window. The entire tube was replaced approximately six months afterward. The mode-locked Ti:Sapphire would produce approximately 1.2 watts when it was running efficiently, which was primarily driven by the cavity alignment.

5.5.2. Nonlinear Crystals

Phase matching conditions and effective non-linear coefficients are relatively straightforward to calculate and find in the literature, respectively. The Handbook of Nonlinear Optical Crystals (Dmitriev, 1991) was a valuable resource for such theoretical investigations when considering various nonlinear crystal options for both SFG and SHG. A promising candidate for SFG of mid-IR with near-IR wavelengths was $LiNbO_3$ as can be seen in Table 5-1. $LiNbO_3$ has been used as a Q-switching material for many years and as a result, is fairly well developed and manufactured by several vendors, including international vendors. A small firm that represents a Chinese crystal growth house had by far the best price as well as references within the Air Force, on $LiNbO_3$, so two 1 mm thick samples were ordered. To date, no frequency mixing has been seen as a result of these crystals. This included a careful attempt to double a flash lamp pumped Ho:YAG laser ($\lambda_{Ho:YAG} \approx 2.1 \mu m$).

Although KTA is a newer material in the sense that it has not been available for long, at the guidance of the University of Iowa ultrafast spectroscopy group led by Professor Thomas F. Boggess, a KTA crystal was purchased and has successfully mixed frequencies. This is not to imply the task is trivial; in fact, the details of crystal orientation and crystal cut verification are quite difficult and tedious, and can be accomplished only via close comparison with theoretical models.

5.5.3. Precision Optics – Precision Measurements

The initial design of this experiment called for refractive optics to re-image the luminescence spot onto the non-linear crystal. Two inch diameter CaF_2 lenses were identified and purchased for the purpose of collecting the most luminescence possible and phase matching with the pump laser. The experiment was constructed and attempted numerous times in an effort to find a SFG signal. Autocorrelation was successfully performed to identify the zero-delay distance, a difficult task in its own right discussed below. The telling symptom of the problem was subtle yet apparent; when scattered light was collected by the lenses and viewed with a near-IR viewer in an attempt to collimate the light, the collimation was poor and contained circular rings. Several researchers with years of experience (who will remain nameless) were brought in and shown the setup and the poor collimation effect, yet no one identified it on sight. The problem was of course spherical aberrations. It is not clear when or how this insight came about, but once it did the future direction was clear, off-axis parabolic (OAP) mirrors.

The task of finding the zero-delay point was cited by Shah (1988) as being the single most difficult element about the experiment. This is certainly the case once the experiment is working. One need only realize that c x 130 fs = 40 μm. This means that in addition to insuring that a 35 μm spot overlaps inside the crystal with a 25 μm spot, the temporal delay stage accuracy must be inside 40 μm before any autocorrelation signal is given off. To make matters somewhat more challenging, the autocorrelation signal competes with the SHG signal from the pump mixing with itself. This is due to the fact that the phase matched angle for collinear phase-matching is very near the phase matching angle for the non-collinear geometry when ψ is small. Also, scattering centers on the surface of the crystal act to divert light in the direction of perfect phase matching with the pump. The true autocorrelation signal must be distinctly identified by separating it from these other SHG photons.

As mentioned above, the measurement of the luminescence excitation spot size on the sample ω_{PL} and the nonlinear pump spot size on the crystal ω_{pump} were both critical measurements. For this reason, redundancy of measurement techniques and great care in employing the techniques was insured. The two measurement techniques used were the razor blade and pin-hole. The razor blade measurement is simply performed by translating a razor blade or knife edge across the beam with a micrometer while monitoring the power on the down side of the blade. The resulting data is power versus distance which can be compared to the theory if the beam profile is known.

The pin-hole technique is fundamentally identical to the razor blade in that the power through a pin-hole is compared with theory of an assumed beam profile. Spot sizes were determined by measuring the power through a 50 μm pinhole. Both techniques consistently resulted in beam sizes within about 5% of one another. Both techniques assume a Gaussian profile which was measured using a Coherent "Mode Master" and found to be approximately $M^2=1.1$.

5.5.4. Fighting Noise

A particularly troublesome aspect of this experiment with samples that are relatively inefficient photon emitters, was low signal-to-noise. The number of luminescence photons collected by the collection optics and delivered to the non-linear crystal, effectively sets the signal available for SFG. The efficiency of the process discussed in section 5.3, determines the number of photons available for counting with the PMT. The noise on the other hand is a combination of multiple noise sources: 1) PMT dark current, 2) electrical "cross-talk" noise associated with the counting electronics and spurious electrical signals that can register a count, 3) room light entering the spectrometer from either the open slits or gaps in the spectrometer, 4) photon noise associated with the randomness of counting a modest number of photon events (associated with Poisson statistics), 5) Ti:Sapphire noise associated with fluctuations in

the pump beam causing fluctuations in the luminescence intensity and non-linear mixing process, and finally 6) Ti:Sapphire noise associated with pump photons, either from stimulated or spontaneous emission, that reach the PMT and are counted as photon events.

Dark current noise was minimized by cooling the PMT to -40 °C which effectively brought the dark current down to less than 100 counts-per-second (cps). Shielding the cabling minimized electrical cross talk and running the experiment without external light sources minimized room light. This meant that in addition to keeping the room lights off, all other light sources, (e.g. light emitting diodes, Ar ion laser scatter, other indicator lights on equipment) were covered. Care was taken to stabilize fluctuations in the Ti:Sapphire by using a vibration isolation table. Noise associated with the random nature of photon arrival is a fundamental limit.

The final contribution to noise, and as it turned out the most significant, was from photons from the Ti:Sapphire reaching the PMT. From the start, a beam block was used to spatially block the pump beam from the SFG upconversion collection optic path. This dramatically reduced noise associated with pump beam photons reaching the PMT. Even with the spatial separating beam block in place, a large number of pump photons still reach the PMT. This is clearly illustrated in Figure 5-6, which shows three spectral scans over the wavelength range of interest taken with the ¾ meter spectrometer using the PMT as the detector with identical settings and scanning rates. The bottom trace labeled "Background (No Ti:Sapphire)" was taken with the Ti:Sapphire blocked at the laser output aperture while the slits were wide open to measure noise contributions from dark current, electrical cross-talk, room light, and photon statistics. Note the sum of these contributions is very near 100 cps. A second scan was taken with the Ti:Sapphire un-blocked, but without luminescence. The result was the top trace with a peak up to 100000 cps at 690 nm. It was apparent immediately that the laser signal ($\lambda \approx 800$ nm +/- 6 nm) must be attenuated before entering the spectrometer.

To accomplish this, two short-pass filters (< 700 nm and < 750 nm) were placed at the entrance slit to the ¾ meter spectrometer. Because the short-pass filters were in place in front of the entrance slits, and because the spectral scan exhibited structure in the signal, the signal must be a result of spontaneous emission of photons from the highly excited Ti:Sapphire crystal within the scanned energy range. To reduce this dominate noise contribution, a long-pass filter (λ > 700 nm) was placed just outside the Ti:Sapphire laser. The result is shown by the middle trace in Figure 5-6.
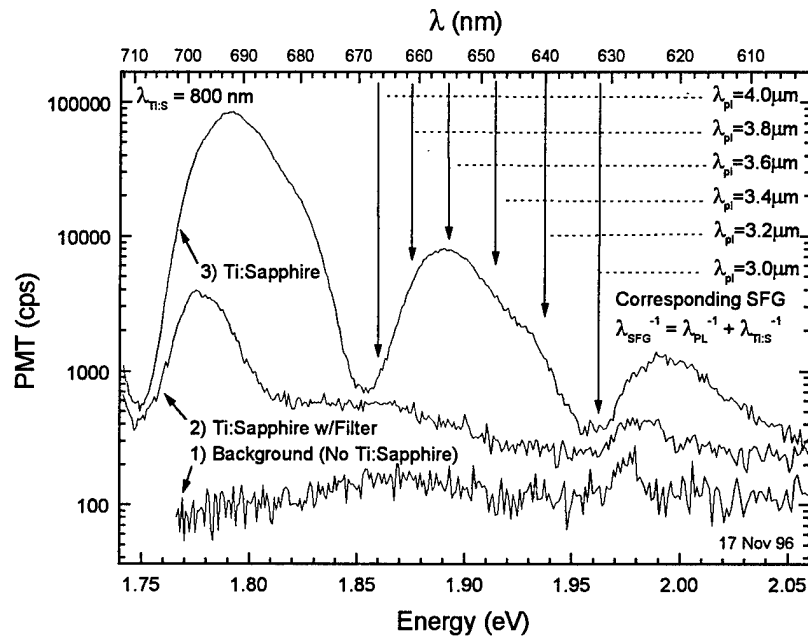
Figure 5-6: Spectral scan of the spectrometer used to filter the SFG photons with the slits wide open (3mm) 1) with the Ti:Sapphire completely blocked (bottom curve), 2) with a long-pass filter at 700 nm placed before the polarizing beam splitter used to attenuate noise (middle curve), and 3) without the long-pass filter.

6. Experimental Results

This chapter provides details of the samples studied, the upconversion experiment, and results obtained from the experiment. Section 6.1 provides details of the sample structure and section 6.2 provides information relevant to the experimental procedure, and finally, section 6.3 provides time resolved luminescence results obtained via luminescence upconversion on the MIT/LL samples at a variety of temperatures. The Chapter ends with concluding remarks on the samples and data obtained.

6.1. Sample Information and Structure

The three samples studied in this effort were chosen from among several laser structures grown at MIT/LL. They were chosen because the structures were nearly identical, except in quantum well and barrier thickness. This conveniently provided a single parameter variation to study and characterize its influence. A complete description and characterization of the lasers used in this study is given elsewhere (Choi, 1996) and briefly described here. Growth details are also published elsewhere (Turner, 1995). The QW laser structures were grown on (100) n-InAs substrates by molecular beam epitaxy using a cracked As_2 source. After an n^+ InAs buffer region was grown, the structures consisted of an n-$AlAs_{0.16}Sb_{0.84}$ cladding, and $In_{0.85}Al_{0.15}As_{0.9}Sb_{0.1}$ tensile strained barrier alternating with a compressively strained $InAs_{0.935}Sb_{0.065}$ well with either 8 or 10 wells, followed by p-$AlAs_{0.16}Sb_{0.84}$ cladding and a p^+ GaSb cap layer. The cladding regions were nominally 2.0 μm thick. The structure of the laser samples is given in Table 6-1, and a scaled energy-band diagram of the structure is given in Figure 6-1.

Table 6-1: Detailed structure of three InAsSb/InAlAsSb/AlAsSb QW lasers grown on InAs Substrates (Choi, 1996).

Wafer	Well Thickness (t_{qw}) (nm)	Number of wells	Barrier Thickness (t_{bar}) (nm)	Number of barriers	Cladding thickness (μm)
A	15	10	30	11	2.0
B	10	10	20	11	2.5
C	20	8	40	9	2.0

MIT/LL Mid-Infrared Laser Structure ($\lambda = 3.4$ µm)

Energy

Cladding Layer: $AlAs_{0.16}Sb_{0.84}$

Quantum Well $InAs_{0.935}Sb_{0.065}$

Barrier Layer $In_{0.85}Al_{0.15}As_{0.9}Sb_{0.1}$

Conduction Band Offset $E_c = 220$ meV

Ti:Sapphire $\lambda = 800$ nm $h\nu = 1.55$ eV

1.65 eV

0.65 eV

0.36 eV

10 Wells Total

Valence Band Offset $E_v = 70$ meV

Cladding Thickness = 2.0 µm

	Well Width	Barrier Width
"A"	15 nm	30 nm
"B"	10 nm	20 nm
"C"	20 nm	40 nm

Refractive Index

$n = 3.17$

$n_{eff} = 3.87$ (effective index of well/barrier region)

Figure 6-1: Energy and refractive index diagram of laser structure with band offsets drawn to scale. Also drawn to scale is the photon energy $h\nu$ of the Ti:Sapphire pump used to generate excess carriers in the well/barrier region.

The samples were also particularly interesting because the temperature dependence parameter (T_0) of the samples differed over the range tested at MIT/LL. The threshold current density as a function of temperature for the three lasers is provided in Figure 6-2. Details of the laser characterization are presented in the paper from which the figure was taken (Choi, 1996).

The samples were studied using time-integrated photoluminescence (PL) at temperatures as low as 4K. Virtually all of the upconversion results were performed at higher sample temperatures in the interest of observing Auger phenomena. The peak of the luminescence from all three shifted by approximately -0.18 meV/K.
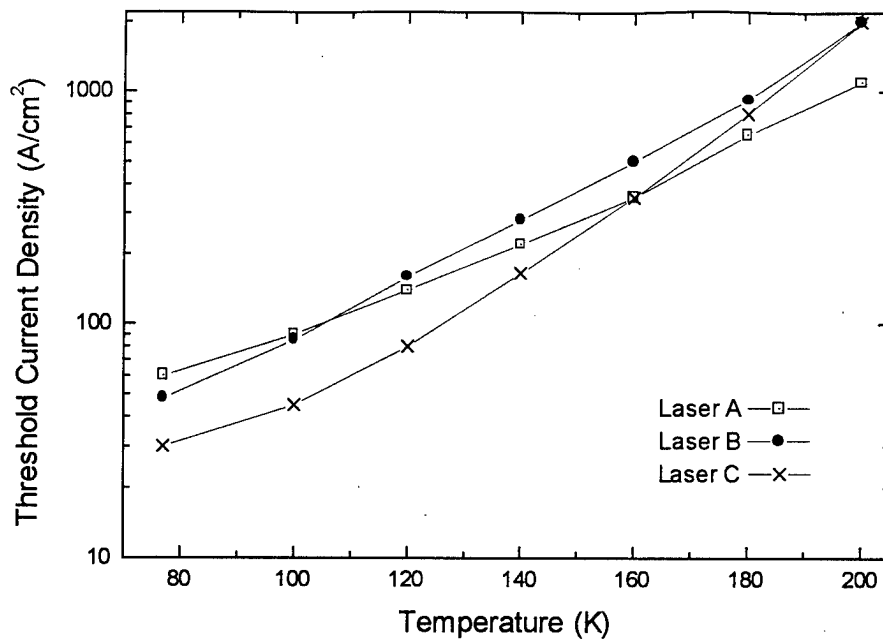
Figure 6-2: Pulsed threshold current density versus temperature of the three InAsSb/InAlAsSb quantum well diode lasers studied, taken from (Choi, 1996).

Figure 6-3 and Figure 6-4 gives the time integrated luminescence emission spectra for the samples at 77 K and 150 K respectively. A noteworthy feature of the PL taken at 77 K is the variation of the high-energy slope between the three samples. The high energy side slopes correspond to the effective carrier temperatures (T_e) (Marciniak, 1995:7-35). The best fit values for T_e for the three samples at a lattice temperature of 77 K were 157 K, 92 K and 383 K for samples A, B, and C respectively.

The PL taken at 150 K was a much lower signal overall, which reduces the signal to noise proportionately as can be seen in Figure 6-4. One feature worth noting on the 150 K PL data is the high-energy shoulder showing up on the "B" laser sample. This is thought to be the result of carriers populating the higher energy quantized states in the quantum well. This hypothesis is consistent with that of Dr. George Turner at MIT/LL, who grew the samples as well as performed characterization on these samples, including PL.
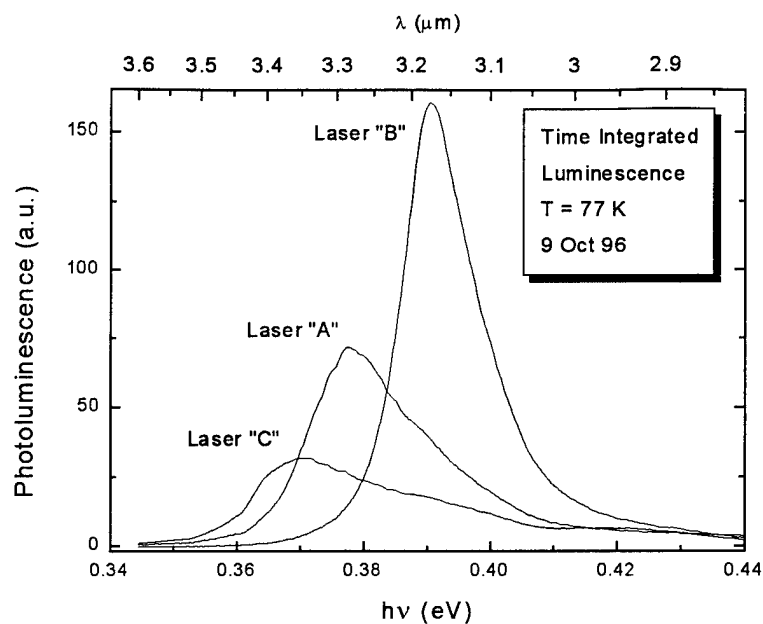
Figure 6-3: Time integrated luminescence spectra from laser samples A, B, and C taken at 77 K.
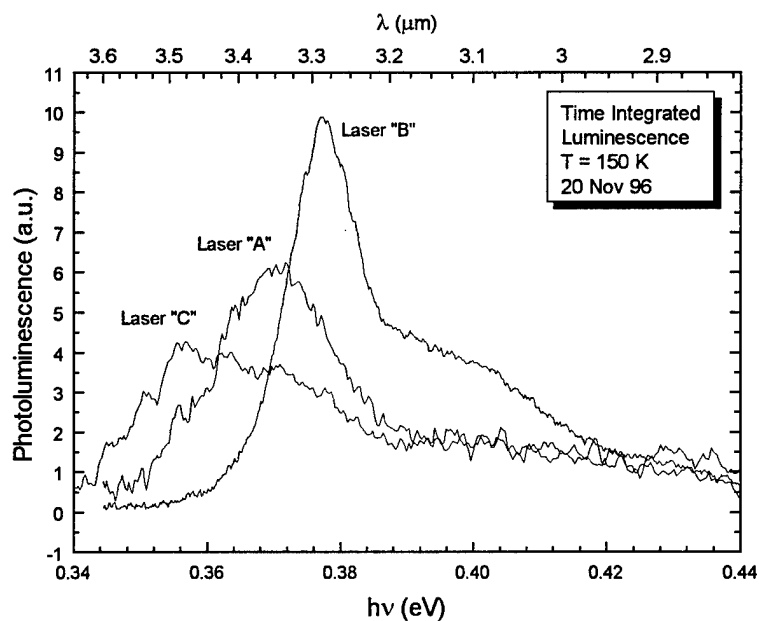
Figure 6-4: Time integrated luminescence spectra from laser samples A, B, and C taken at 150 K

6.2. Procedural Details

The data required for the analysis was not known a priori. As a result, the procedure to collect the required data evolved with time, experience, and requirements of the analysis. In the interest of brevity, only the procedure used for collecting the data presented in this dissertation, which is the most recent and best measured data, is presented here.

Procedural details included measuring or aligning activities on a periodic or as-needed basis, for those things that would likely not change with time, and measurements made before each data set was acquired. Each type is described below.

6.2.1. Periodic Procedure

1. *Align System*: A pin-hole was used in place of the nonlinear crystal to align the pump beam with the luminescence beam. It was highly desirable for the two interacting beams to overlap at the axis of rotation for the rotation stage. This allowed the nonlinear crystal to be rotated without changing the alignment of the rest of the system. By placing a pin-hole in the 3 in mount, the rotation axis could be found by viewing the pump beam through the pin-hole as the stage was rotated. Once the axis of rotation was identified, the luminescence could be focused thought the pin-hole. The magnitude of the PL was monitored via the McPherson spectrometer and the InSb detector.

2. *Measuring Angles*: A HeNe laser was used as an alignment aid by propagating the HeNe beam down the luminescence optical path in the reverse direction. Reflections off the surface of the nonlinear crystal allowed an absolute crystal rotation angle to be defined. The rotation stage could then be used to rotate to a particular angle Φ, which would send the HeNe down a path at 2Φ. This allowed experimental angles to be compared with angles calculated from the nonlinear model.

3. *Measure Spot Size*: The techniques used to measure the spot size were discussed in Chapter 5. Briefly they are the razor blade technique and the pin-hole technique. Both techniques are based on monitoring the laser power as an object of known size and shape is introduced is such a way that the object obscures the laser beam path. By assuming a beam profile, we can theoretically calculate the affect of the obscuring object, compare it with the experimental results, and thus determine the spatial extent of the spot.

4. *Find Zero-Delay*: This technique was also discussed in Chapter 5. Briefly, a nonlinear crystal capable of phase-matching for SHG in the Ti:Sapphire, in our case LiIO$_3$, is placed on the rotation stage in the place of the KTA crystal. The sample vacuum chamber, which is placed on an X-Y-Z translation stage, is translated perpendicular to the incoming luminescence excitation beam, until a strong scattering spot on the sample is found. The scattered Ti:Sapphire light was collected and delivered to the nonlinear crystal, same as the mid-IR luminescence. The translation stage was moved until SHG resulting from the non-collinear phase matching of the pump and the scattered Ti:Sapphire off the sample, was seen. As was discussed in Chapter 5, this procedure is rather difficult. A critical element used to uniquely identify the SHG resulting from the two beam mixing, versus SHG from the pump by itself, was to block the luminescence path entirely with a card and then unblock it manually while observing the signal either with the PMT or with a human eye.

5. *Improving Upconversion Signal*: Once an upconversion signal was identified, fine adjustments were made with the position of the nonlinear crystal, the angle of crystal rotation, and the upconversion collecting optics.

6.2.2. Each Data Set Procedure

1. *Measure Power at Sample*: Before collecting upconversion data, it was critical to know the power used to generate luminescence in the sample. As was described in

Chapter 5, a silver mirror was mounted on a kinematic mount which could be inserted in the luminescence path just prior to the focusing lens used to excite the sample. A calibrated silicon power meter was used with a 1000:1 attenuation filter on it. Because the beam experienced reflective losses at the focusing lens as well as at the LiF window, and because the attenuation filter was not exactly 1000:1, the offset between the permanent power meter used for each data set, and the actual power at the sample was measured and found to differ by a factor of 1.11.

2. *Measure PL signal and wavelength λ_{PL}:* The peak of the PL emission was identified with the McPherson spectrometer and InSb detector. This was done by using a chopper wheel with a lock-in amplifier described in Chapter 5.

3. *Set Upconversion Wavelength:* The Spex spectrometer grating was rotated to the appropriate upconversion wavelength (λ_{SFG}). The slits were left wide open for both the input and exit slits of the spectrometer.

4. *Scan Inputs:* The computer interface (constructed during this effort) controlled the delay stage as well as the photon counter electronics, allowing the user to select important parameters such as the photon counter integration time, (i.e. how long the PMT will count photons per data point), and the delay time step size. Scans were typically made with a 30 second PMT integration time, and were taken from –250 ps to 3.050 ns with 50 ps steps.

5. *Calibrating for L(n) versus n:* The requirement for empirically relating the upconversion signal "L(n)" with the carrier density "n" is discussed in the analysis section, Chapter 7. These required upconversion measurements made with the delay stage set a 50 ps, while the power was varied and measured. This is discussed in more detail in Chapter 7.

6.3. Upconversion Results

The experiment and analysis technique used in the current study differs from previous attempts to characterized carrier recombination dynamics, in that the TRPL here is for a fixed photon energy with finite band-width. Other similar efforts used a time resolved, *integrated* luminescence signal (Snow, 1989a; 1989b; Hausser, 1990; Fuchs, 1991) to characterized carrier recombination dynamics.

A series of consecutive time resolved photoluminescence traces were performed on each sample. Because the luminescence from laser sample "B" was more intense, it was used extensively to improve experimental technique and data collection. As a result, the best upconversion data is on sample "B" which includes data from77 K, 120K, 150 K and 180K. There is far less quality data for laser samples "A" and "C." All the best data from this effort is provided this section.

6.3.1. Laser Sample "A"

The upconversion signal for the "A" laser was not nearly as strong as the "B" laser, however, SFG was possible and traces with acceptable signal to noise were obtained. The temporal traces from upconversion on the "A" laser are shown in Figure 6-6 and 6-7, while a calibration of the upconversion signal (L(n)) versus the excitation power is shown in Figure 6-5. Note the calibration was take on the same date under the same conditions as the highest signal trace in Figure 6-6. The relevance of this calibration will be discussed in Chapter 7.
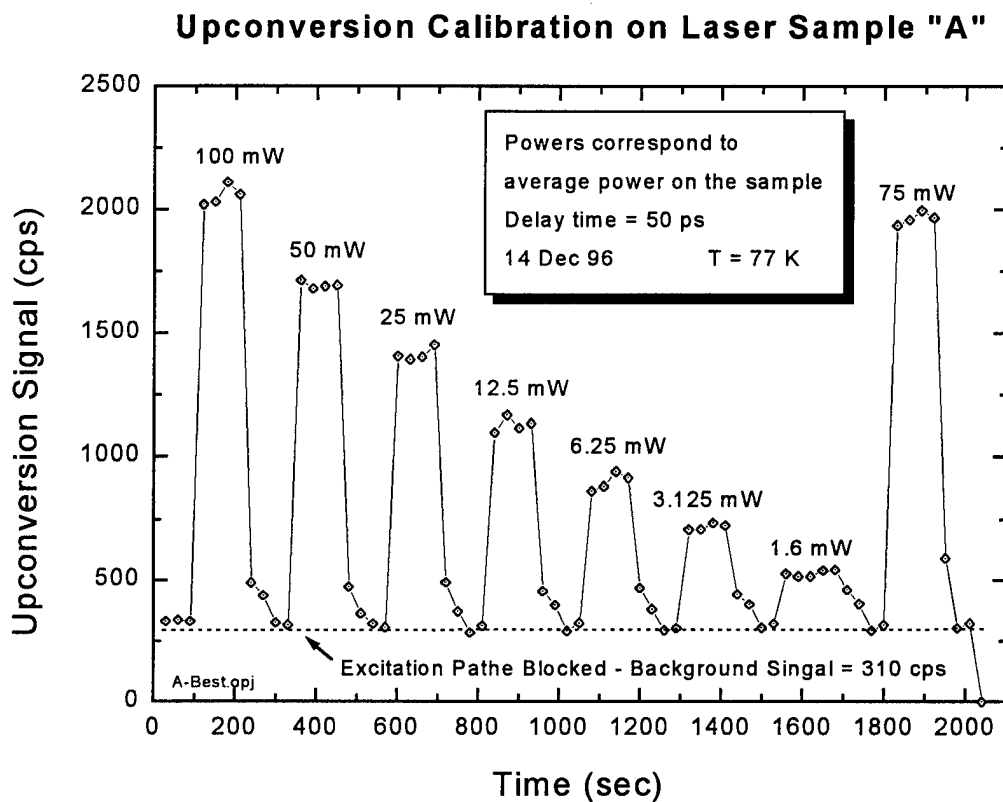
Figure 6-5: Calibration relationship between luminescence intensity (*L(n)*) and excitation power for Laser Sample "A" at 77K.
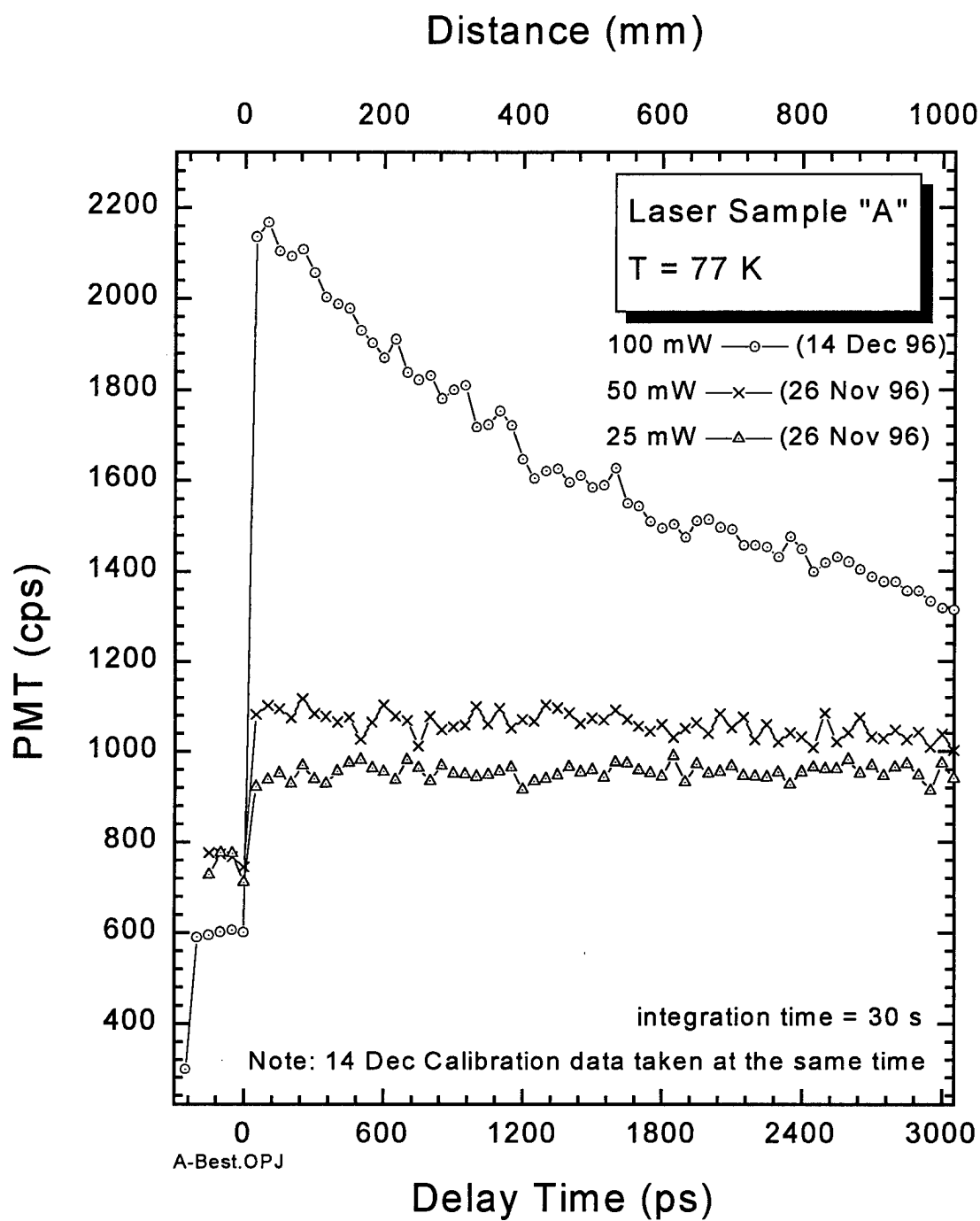
Figure 6-6: Luminescence upconversion on Laser Sample "A" at 77 K.
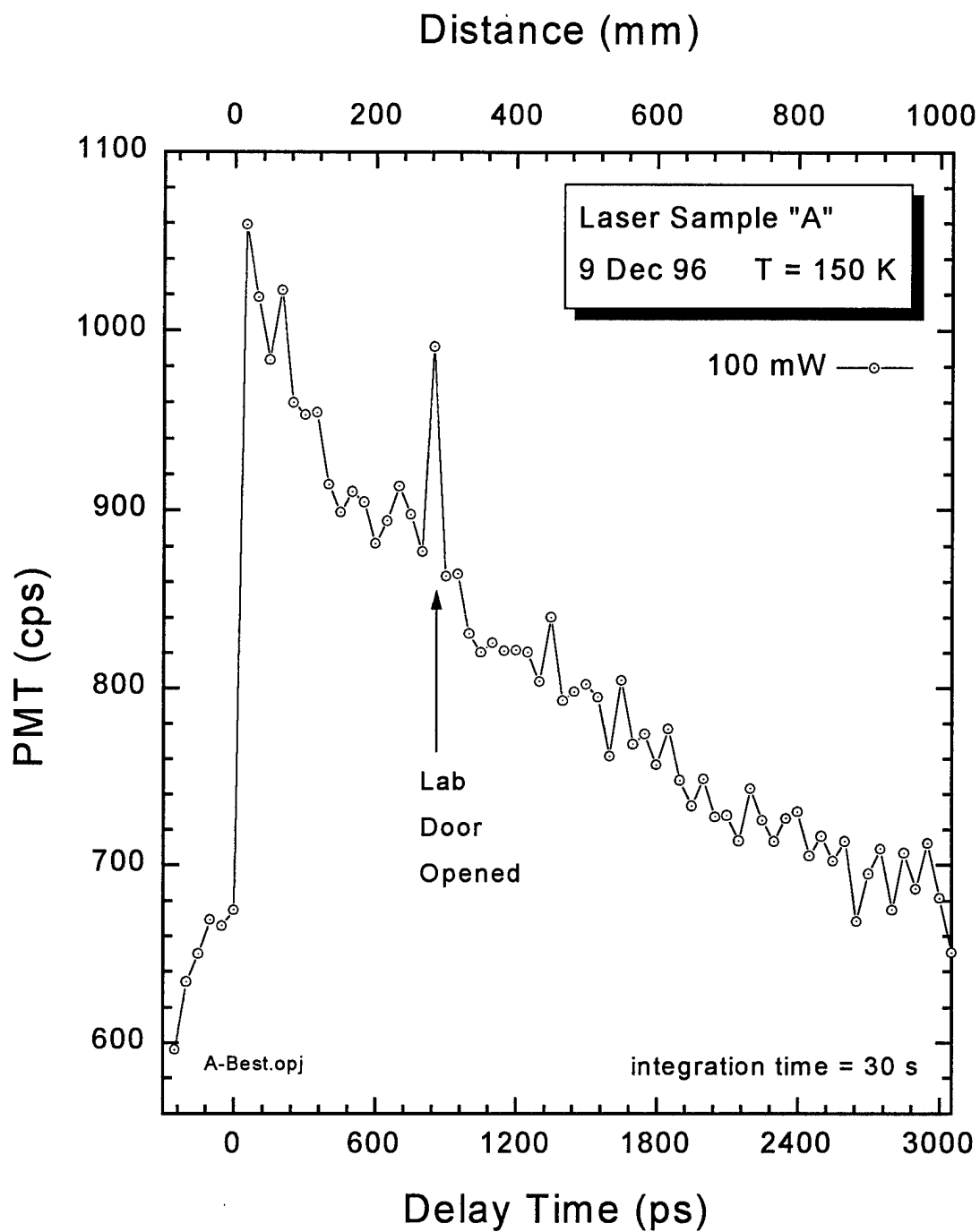
Figure 6-7: Luminescence upconversion on Laser Sample "A" at 50K.

6.3.2. Laser Sample "B"

Laser sample "B" was the brightest and the best overall data was obtained from it. Figure 6-8 through 6-12 are the luminescence upconversion traces obtained on laser sample "B", at 77 K, 77 K, 120 K, 150 K and 180 K respectively. The traces were made after identifying the peak of the time-integrated photoluminescence (Figure 6-3 and 6-4) and tuning the spectrometer to the appropriate energy sum while translating the delay stage. Note, the same calibration information obtained for sample "A" above is available from Figures 6-8 to 6-12 by taking the luminescence intensity signal, from each trace, at the initial highest point (at 50 ps) for each of the initial excitation energies. Figure 6-8 and 6-9 are traces of the same conditions taken at different times. Both traces are included to demonstrate the consistency in this type of measurement. Figure 6-9 includes excitation levels as high as 200 mW. This level of excitation was not possible without rotating the half-wave plate and sending increased energy into the luminescence excitation path and decreasing the energy into the pump path. When this is done, the efficiency of the upconversion process changes, and it is no longer reasonable to plot new data, with one upconversion efficiency, along side old data, taken with a different upconversion efficiency, unless this efficiency is accounted for by re-scaling. To do this, upconversion traces were made at 200 mW, 100 mW, and 50 mW in order compare the 100 mW and 50 mW traces with data taken at the previous half-wave plate settings. This allowed for a re-scaled 200 mW trace to be included.
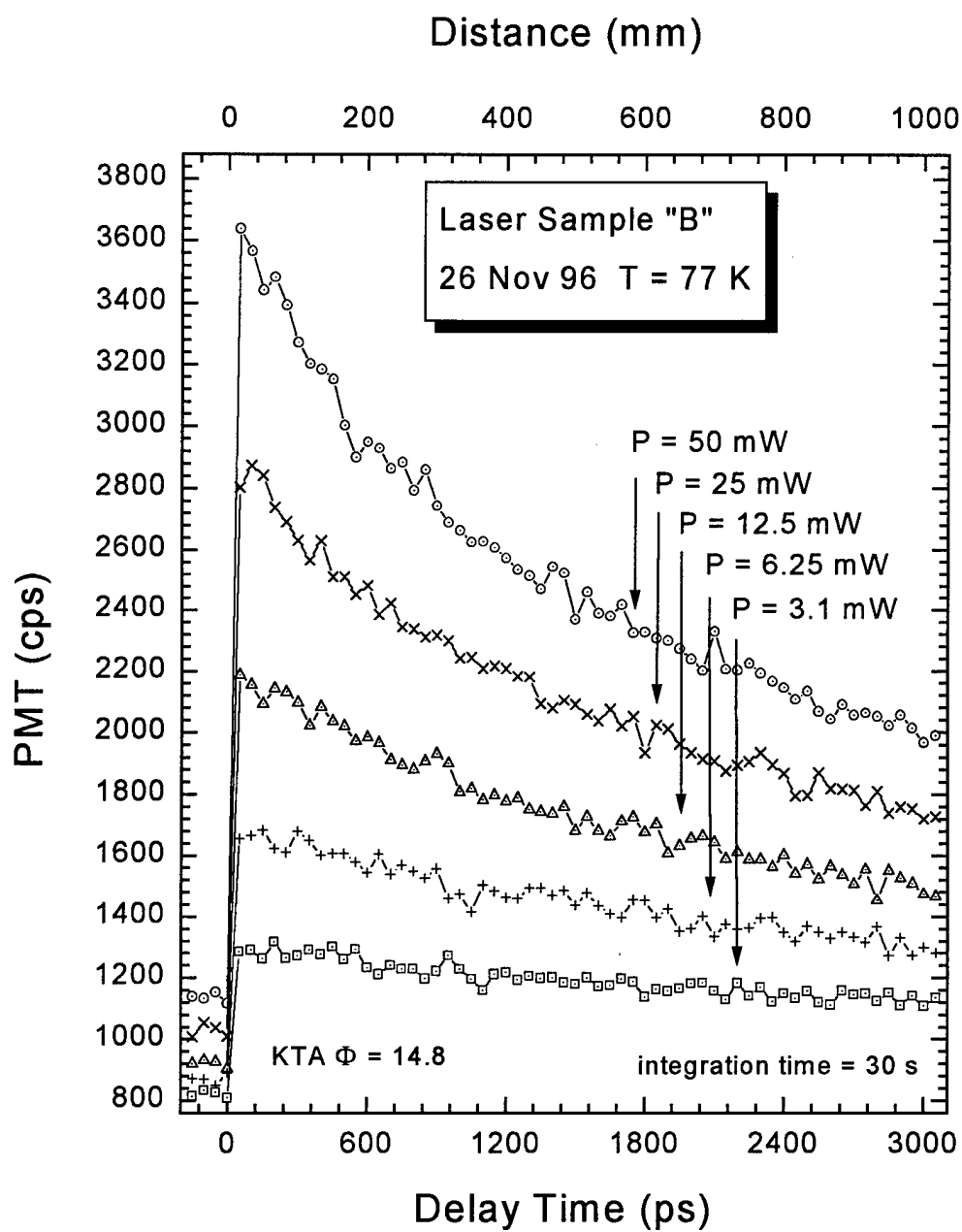
Figure 6-8: Luminescence upconversion on Laser Sample "B" 77K.
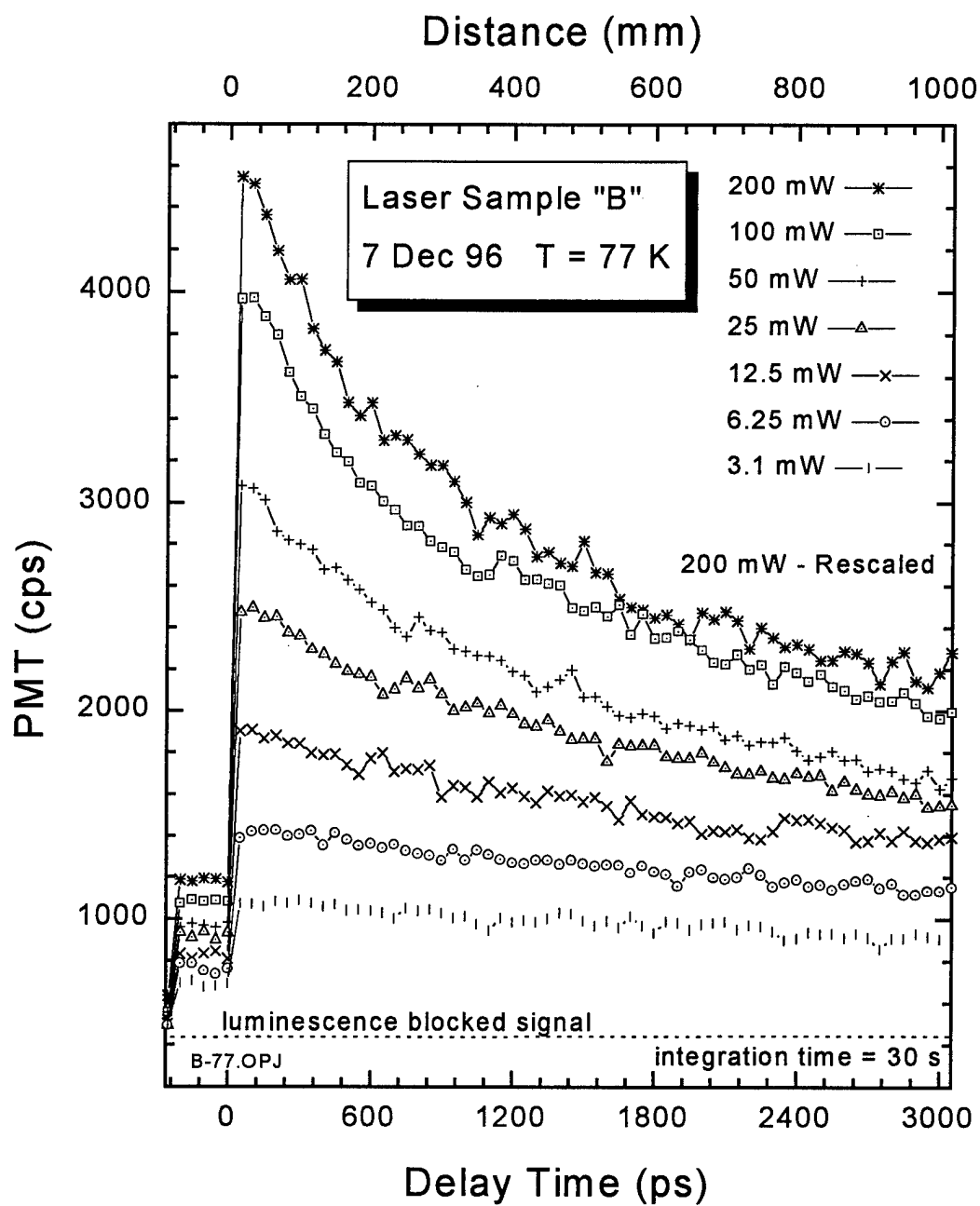
Figure 6-9: Luminescence upconversion on Laser Sample "B" at 77K. Note the highest excitation energy is re-scaled (see text for description).
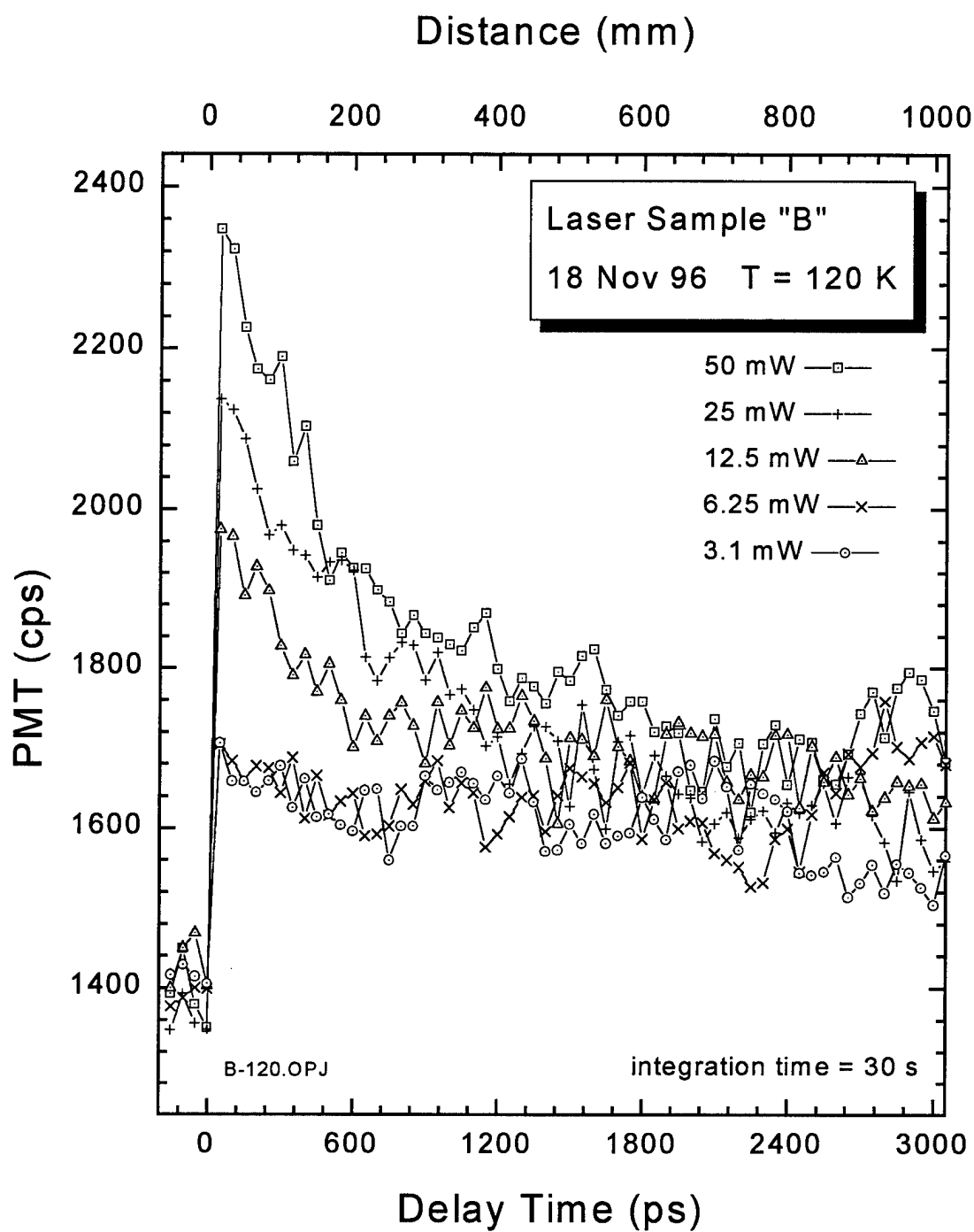
Figure 6-10: Luminescence upconversion on Laser Sample "B" at 120 K.
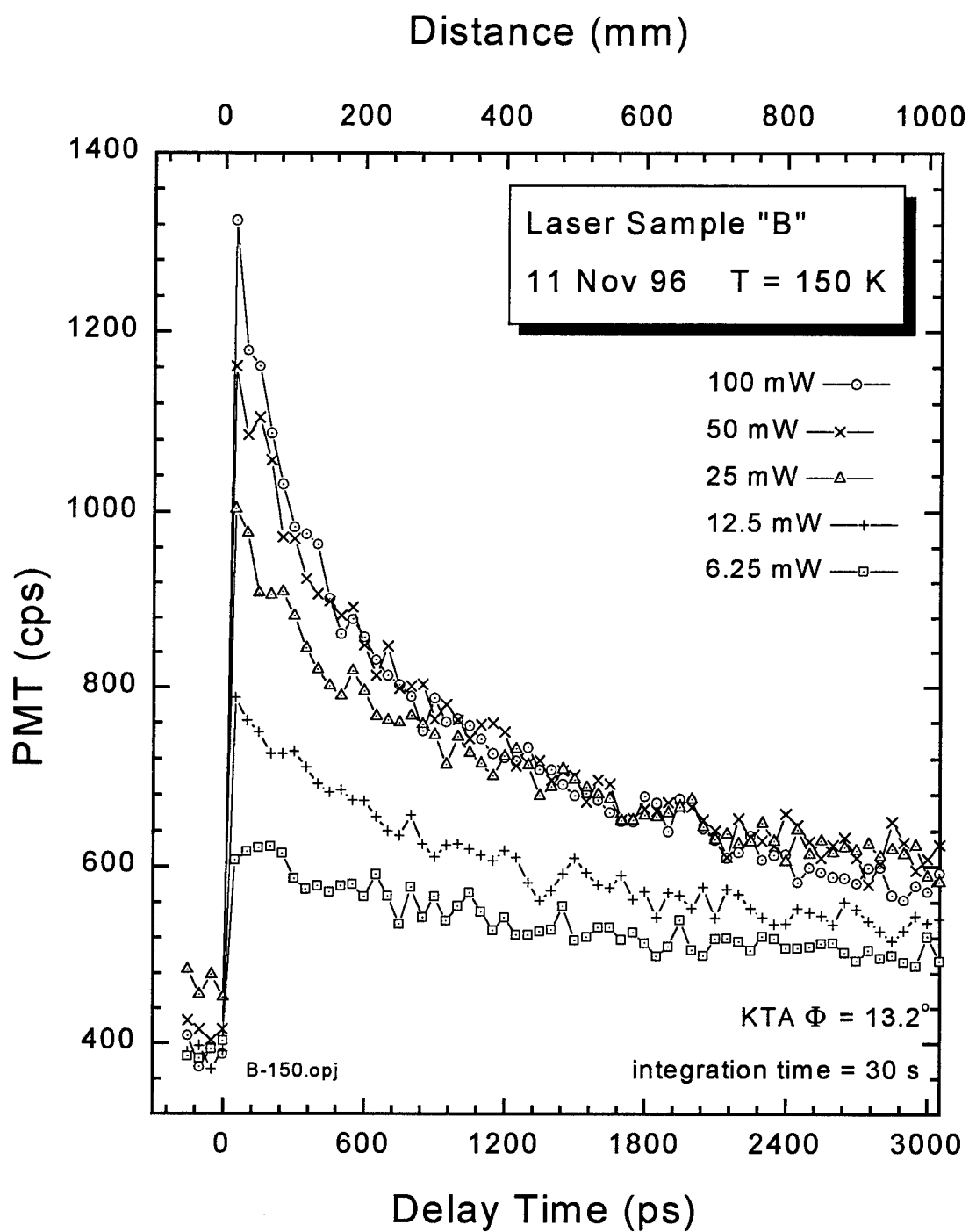
Figure 6-11: Luminescence upconversion on Laser Sample "B" at 150 K.
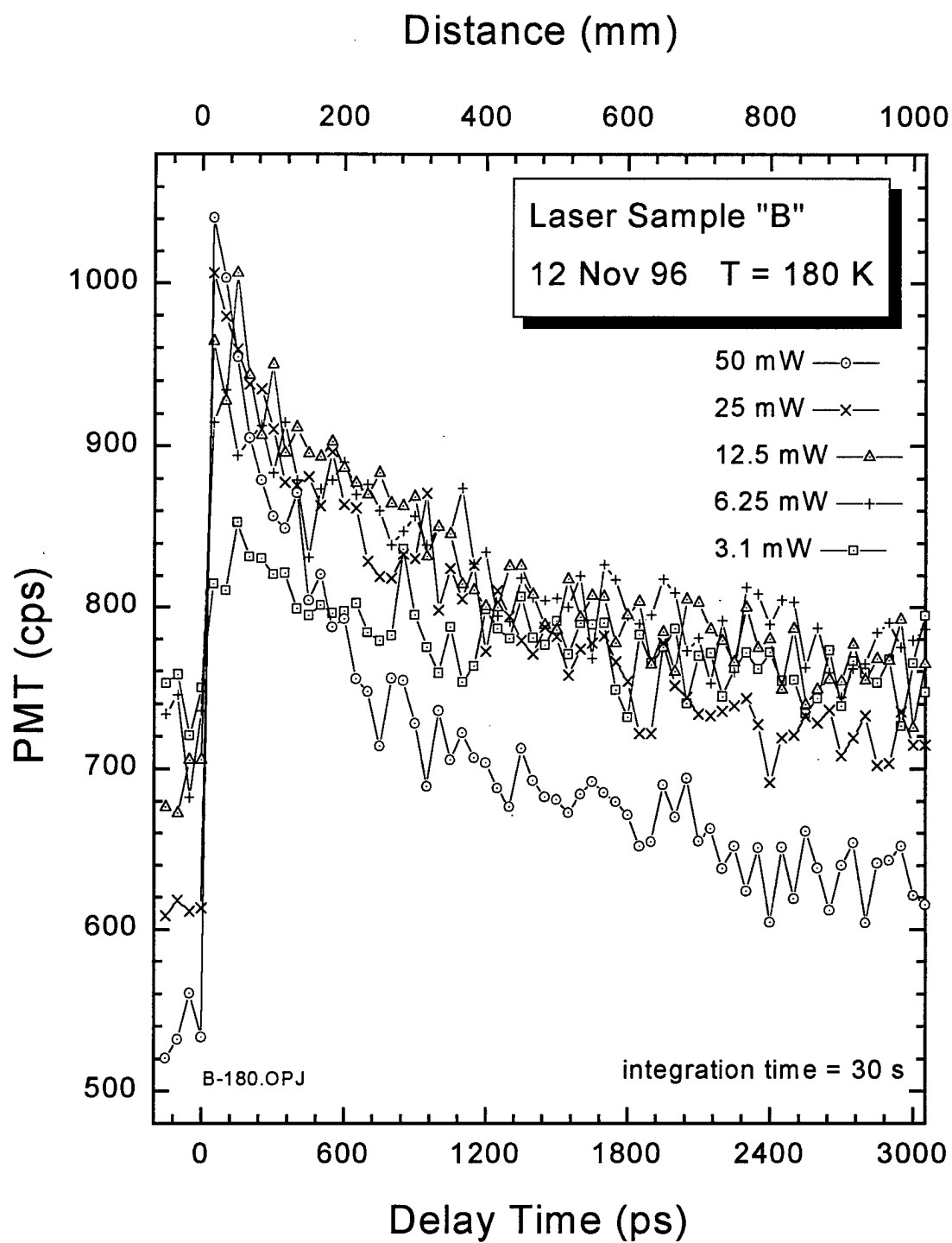
Figure 6-12: Luminescence upconversion on Laser Sample "B" at 180K.

6.3.3. Laser Sample "C"

Laser "C" was the least bright in terms of time integrated and time resolved luminescence. As a result, very little data was taken with laser sample "C." Traces from laser sample "C" are provide in Figure 6-13 and 6-14. Note that no calibration data exists for this sample.
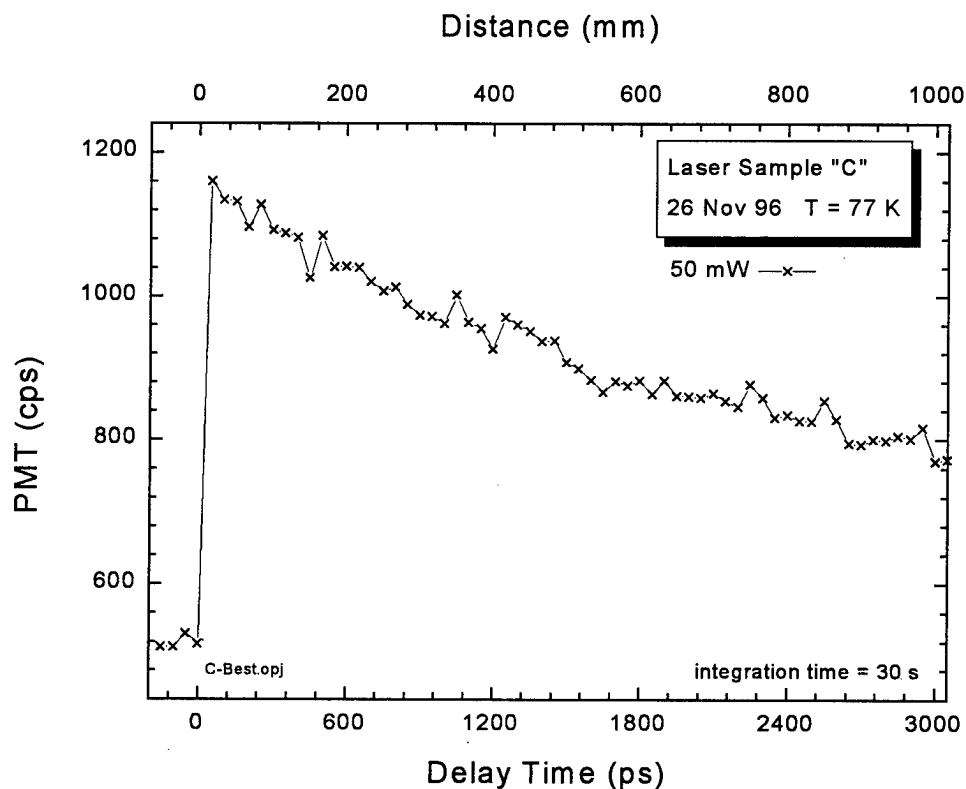
Figure 6-13: Luminescence upconversion on Laser Sample "C" at 77 K. No calibration data exists for this sample.
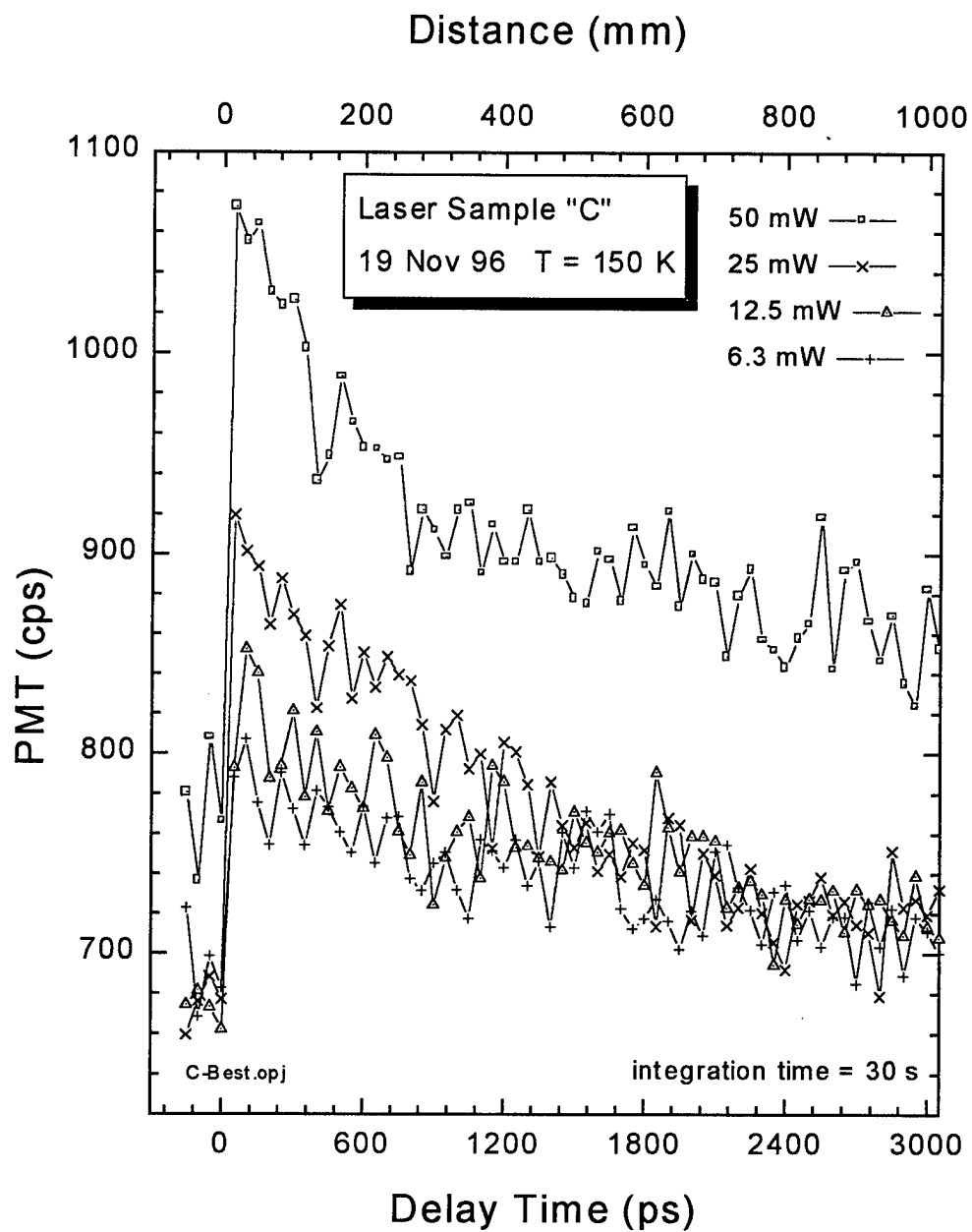
Figure 6-14: Luminescence upconversion on Laser Sample "C" at 150K.

6.4. Conclusion

The samples studied in this effort provided an isolated variable (quantum well/barrier thickness) while their threshold behavior versus temperature (T_0) differed substantially. Although the available samples did not allow for a wide parameter space study, their differing laser threshold characteristics hinted that their variations may significantly affect Auger recombination rates. These samples provide a valid but limited basis to study recombination dynamics versus well/barrier thickness.

The quality of the time resolved upconversion data obtained from these samples was critically dependent on the magnitude of the luminescence. As a result, most of the data, and the best data, is on the brightest sample, laser sample "B." The ability to characterize the Auger recombination rate for the other two laser samples "A" and "C" will depend on how well the available data matches up with what is required to perform the analysis.

Recall the expected upconversion signal calculation from Chapter 5 that resulted in ≈ 1200 (cps), which is surprisingly close to the magnitude of the signal actually measured.

7.Analysis

The objective of this research is to experimentally determine the recombination coefficients, and in particular the Auger coefficient. To do this we must compare our measured $n_m(t)$ with the calculated $n_c(t)$ where the subscript "m" indicates measured and "c" indicates calculated. Unfortunately, as was discussed in Chapter 4, there is no direct means to measure the carrier density $n_m(t)$. To obtain $n_c(t)$ we need only solve the differential equation

$$-\frac{dn}{dt} = A_{SRH}n + B_{rad}n^2 + C_{Auger}n^3,\qquad(7\text{-}1)$$

which is the standard recombination rate equation assuming intrinsic material (i.e. $n \approx p$). This differential equation can be solved for $n(t)$ at all times $t > t_o$ if the recombination coefficients A_{SRH}, B_{rad} and C_{Auger}, are known and if the initial condition at time $t = t_o$ is known. The initial condition in this case is the value of the carrier concentration at t_o, referred to here as $n(t_o)$, where t_o is our delay stage "zero" point.

In the upconversion experiment we have access only to the luminescence signal as a function of time, $L_m(t)$, which was the experimentally *measured* data presented in Chapter 6. In order to compare this experimental data, $L_m(t)$, with the calculated carrier densities $n_c(t)$ obtained from equation 7-1, we must devise a means to relate the luminescence signal "L" to the carrier density "n." For the current effort, an empirical means was devised to define the relationship between luminescence and carrier density referred to here as $L(n)$. The empirical method is discussed below in section 7.3. Once $L(n)$ is determined, the recombination coefficients used in equation 7-1 can be used as fitting parameters. The fit can be compared with the measured data $L_m(t)$ by using our $L(n)$ relationship to plot $L(n_c(t))$ with the data $L_m(t)$. With this, we can directly compare the fit of our recombination coefficients with the experimental data.

Unfortunately, TRPL experiments in the literature that report quantitative information about carrier dynamics, specifically the reporting of Auger recombination coefficients, are either applicable to significantly different experimental conditions (Sermage, 1986), or incomplete in communicating the $L(n)$ relationship assumed between the measured luminescence and the carrier density (Hausser, 1990). In some cases, experimental details and techniques are never mentioned (Snow, 1988). As a result of these differences, no clear analysis technique exists to analyze the TRPL for a fixed photon energy with finite band width, prior to this effort.

This chapter will address the issues associated with determining the initial carrier density $n(t_o)$ in section 7.1. Section 7.2 will present a method for solving the differential equation (7-1), and section 7.3 will present the method used to determine $L(n)$ for this effort with a detailed discussion of carrier relaxation. Section 7.4 presents the fits $L_c(t)$ with the data $L_m(t)$. Finally section 7.5 discusses potential sources of error.

7.1. Solving the dn/dt Rate Equation for n(t)

Our first step is to solve the differential equation given in Equation 7-1 to obtain $n(t)$ for a given initial carrier density $n(t_o)$. Recall, $n(t_o)$ is known from our calculation in Equation 7-2, 7-4 and 7-5. With the initial volumetric carrier density known, $n(t_o) = n_o$, we can solve the differential Equation 7-1 by writing

$$\int_{t_o}^{t} dt = \int_{n_o}^{n} \frac{-dn}{A_{SRH}n + B_{rad}n^2 + C_{Auger}n^3}. \qquad (7-2)$$

Because the right side of this equation has an analytic solution, we can write time as a function of volumetric carrier density $t(n)$. Making the substitution $A_{SRH} = A$, $B_{rad} = B$, and $C_{Auger} = C$, so the solution will fit on the page we can write the solution to this definite integral as $t - t_o = t(n) - t(n_o)$ where we have defined the function

116

$$t(n) = \frac{-1}{2A} \ln \left[\frac{n^2}{A + Bn + Cn^2} \right] + \frac{B}{2A} \frac{2}{\sqrt{4AC - B^2}} \arctan \left[\frac{2Cn + B}{\sqrt{4AC - B^2}} \right]. \quad (7\text{-}3)$$

By numerically inverting this equation, we can compute $n(t)$ for given values of A, B, C, and n_o. Since our initial volumetric carrier density $n(t_o)$ is known, we can calculate and plot the carrier density for subsequent times $t > t_o$.

7.2. Determination of Initial Carrier Density n(t_o)

From Equation 7-1 we can see that the recombination mechanisms can be identified by their power dependence on carrier density. As a result, knowledge of the *initial* carrier density at zero delay (i.e. $t = t_o$), referred to here as $n(t_o)$, is critical for determining the recombination coefficients. Accuracy in carrier density is limited primarily by our knowledge of the material's optical characteristics and excitation beam size. In this current study, the carrier density was determined by experimentally measuring the energy per laser pulse (determined by dividing the average power by the repetition rate of the laser, or $E_p = P_{avg}/RR$), the wavelength of the laser (λ_{laser}), the radius of the laser spot at the sample (w_o defined as the $1/e^2$ point for intensity), and the absorption coefficient (α) of the sample at λ_{laser}. Assuming a Gaussian profile for the luminescence excitation laser pulse, the *initial* peak 2-dimensional carrier density in each quantum well is given by (Sermage, 1986)

$$n_{2D-max}(t_o) = \left(\frac{E_p}{h\nu_{laser}} \right) \left(\frac{2}{N_{qw}\pi w_o^2} \right) L_{int} L_{pulse} \left[1 - \exp\left(-\alpha \cdot N_{qw}\left(t_{qw} + t_{bar} \right) \right) \right], \quad (7\text{-}4)$$

where $h\nu_{laser}$ is the photon energy of the laser used to create the carriers, N_{qw} is the number of quantum wells, t_{qw} and t_{bar} are the thickness' of the quantum well and barrier respectively, α is the absorption coefficient (related to the extinction coefficient "k" by α

117

$= 4\pi k/\lambda$), L_{int} quantifies the power losses associated with the focusing lens and reflections off the front surface and internal to the sample, and L_{pulse} quantifies the carrier losses which occur during the pulse. Note the factor of 2 is a result of the fact that we are interested in the peak carrier density in a Gaussian distribution. Also note that we assume the absorption coefficient α is applicable to both the well and barrier material. This is a reasonable assumption since α is experimentally measured on a heterostructure sample. The expressions for L_{int} and L_{pulse} are

$$L_{int} = T_{fl}\left[1-\left(\frac{n_s-1}{n_s+1}\right)^2\right]\left[1+\left(\frac{n_s-1}{n_s+1}\right)^2 \cdot \exp\left(-\alpha N_{qw}\left(t_{qw}+t_{bar}\right)\right)\right]$$

$$L_{pulse} = \left(\frac{\tau_{PL}}{t_p}\right)\left(1-\exp\left(-t_p\middle/\tau_{PL}\right)\right)$$

(7-5)

where T_{fl} is the combined transmission of the focusing lens and vacuum chamber window, n_s is the index of refraction for the semiconductor, τ_{PL} is the approximate sample carrier lifetime, and t_p is the pulse width of the laser. As was stated in Chapter 5, the laser used in this effort was a mode-locked Ti:Sapphire with $\lambda_{laser} \approx 800$ nm and $t_p \approx$ 130 fs. Typical lifetimes for carriers ranged from 500 ps to 10 ns, thus, even for the shortest lifetime (500 ps) the percent of carriers lost during the pulse (1 -L_{pulse}) was approximately 0.013% and was neglected in this analysis.

Area carrier densities, or sheet densities were obtained using the $n_{2d}(t_o)$ calculation given in equation (7-2). A common practice for converting 2D area densities to 3D volumetric carrier densities is to simply divide by the quantum well thickness (Sermage, 1986), so the volumetric, or 3-dimensional carrier density is given by

$$n_{3d}\left(t_o\right) = \frac{n_{2d}\left(t_o\right)}{t_{qw}}.$$

(7-6)

This approach was compared with a more complex approach which considers the envelope function in the quantum well, but was found to give the same results within less than 10%. As a result, considering the other uncertainties in this experiment, the more simple and widely used relation given in Equation 7-4 was used in this effort to calculate volumetric carrier density.

The photons emitted from the sample represent some average carrier density, n_{eff}, that mixes in the nonlinear crystal with the pump laser. This sampling factor is related to the overlap of the imaged luminescence spot size and the nonlinear pump spot size. It is calculated by comparing the luminescence spot size ($w_{PL} \approx 35$ μm) and shape that is re-imaged onto the nonlinear crystal, with the "pump" laser spot size ($w_p \approx 25$ μm) and shape. We can imagine that if the pump spot were infinitely small, the luminescence that would mix with the pump would come from the center of the luminescent spot where the peak density is found given by Equation 7-2. Because the pump spot size has a spatial extent, it mixes with a finite region of the luminescence. To obtain the effective carrier density that is being sampled via upconversion, we integrate over the two Gaussian spots which gives

$$\frac{n_{eff}}{n_{max}} = \int_0^\infty \left[\exp\left(\frac{-r^2}{2w_{PL}^2}\right) \right] \left[\frac{1}{\pi w_p^2} \exp\left(\frac{-r^2}{2w_p^2}\right) \right] \pi r dr = \frac{1}{1 + \dfrac{w_p^2}{w_{PL}^2}} . \quad (7\text{-}7)$$

If we use our spot size values we find $n_{eff} \approx 0.67 \, n_{max}$.

The final, usable, result for the *initial* effective carrier density is given by

$$n_{eff}(t_o) = \left(\frac{1}{1 + \dfrac{w_p^2}{w_{PL}^2}} \right) \left(\frac{E_p}{h\nu_{laser}} \right) \left(\frac{2}{t_{qw} N_{qw} \pi w_o^2} \right) L_{int} \left[1 - \exp\left(-\alpha \cdot N_{qw} \left(t_{qw} + t_{bar} \right) \right) \right], (7\text{-}8)$$

The most critical material parameters in the carrier concentration calculation are the absorption coefficient of the well/barrier region (α) and the index of refraction (n_s). Both of these quantities have been experimentally determined by ellipsometry measurements at MIT/LL for a laser structure without the top cladding layer. In all other respects however they were identical to the samples used in this study and the MIT/LL values will be assumed to be valid here. The results of the MIT/LL measurements are provided in Table 7-1.

Table 7-1: Optical properties of InAsSb quantum well samples from ellipsometer measurements.

λ (nm)	N_s	k	α (cm^{-1})
830	3.26	1.29	1.95×10^5
633	3.12	1.75	3.47×10^5
405	1.62	2.19	6.80×10^5

7.3. Relating Luminescence Intensity (L) to Carrier Density (n)

As was discussed at the beginning of this chapter, an important aspect of the analysis is determining the relationship between that which is observed, time resolved photoluminescence (TRPL) via upconversion, and that which is inferred, carrier density. Because upconversion experiments measure luminescence intensity as a function of time, L(t), and not carrier density, n(t), as a function of time, it is necessary to determine the relationship between L and n.

The most natural and logical method for relating the TRPL signal strength to carrier density is empirical. This means that data is taken in such a way that we correlate the luminescence signal "L" directly with a known carrier density "n." Because carrier concentration evolves with time, we chose to correlate the luminescence with the *initial* carrier density, $n(t_o)$, as that is the only time we "*know*" the value of the carrier density. The TRPL signal is a directly measurable quantity; the carrier density and distribution on the other hand must be carefully calculated as a function of other measurable quantities

described above in section 7.2. This empirical approach was chosen as the most direct method of relating upconversion signal to carrier concentration. Figure 7-1 illustrates the empirical scheme used to define the relationship between luminescence L and carrier density n. The luminescence signal is take from the PMT to obtain L, which corresponds to the carrier density value, n, obtained from Equation 7-8 for a given excitation power.
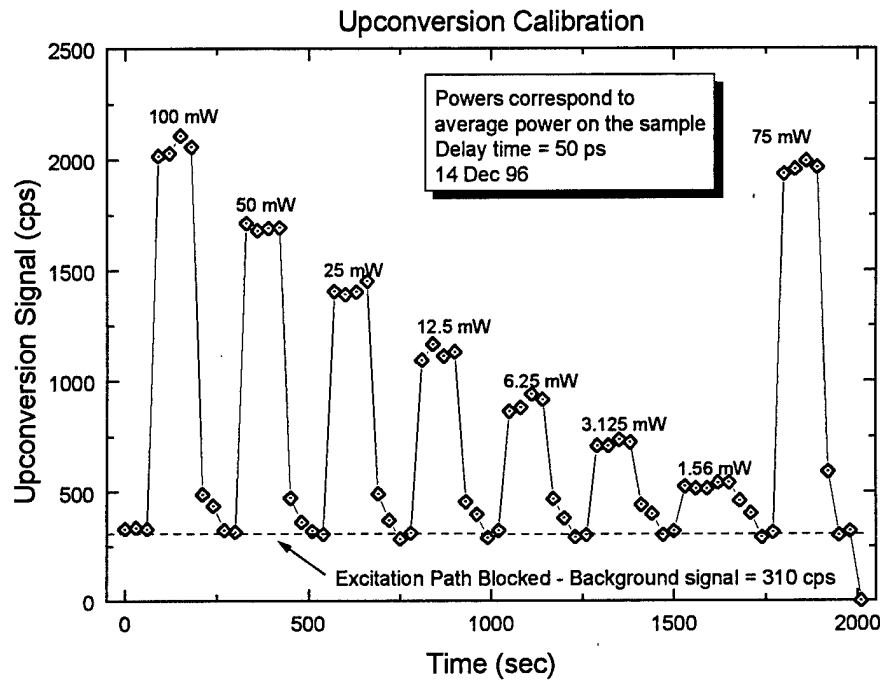
Figure 7-1: Upconversion calibration plot used to correlate the upconversion signal with carrier density. Sample "A" was at 77 K and a neutral density filter was used to attenuate the power to the sample while all other parameters were held constant.

With empirical data collected, we can easily define a fitting function expression to relate L to n. The fitting function expression chosen to relate L and n was

$$L(n) = u_0 n + u_1 n^{u_2},\qquad(7\text{-}9)$$

where u_0, u_1, and u_2 are fitting parameters. This function was used because it was easy to implement and fit the data well. The fitting parameters in Equation (7-9) were found for

<div align="center">121</div>

each data set by using the upconversion signal strength obtained at a delay stage setting of *50 ps*. The rationale for choosing 50 ps is discussed below. Figure 7-2 illustrates the empirical data used to define the relationship between L and n as well as the fitting function for laser samples "A" and "B" at 77 K and 150 K respectively.
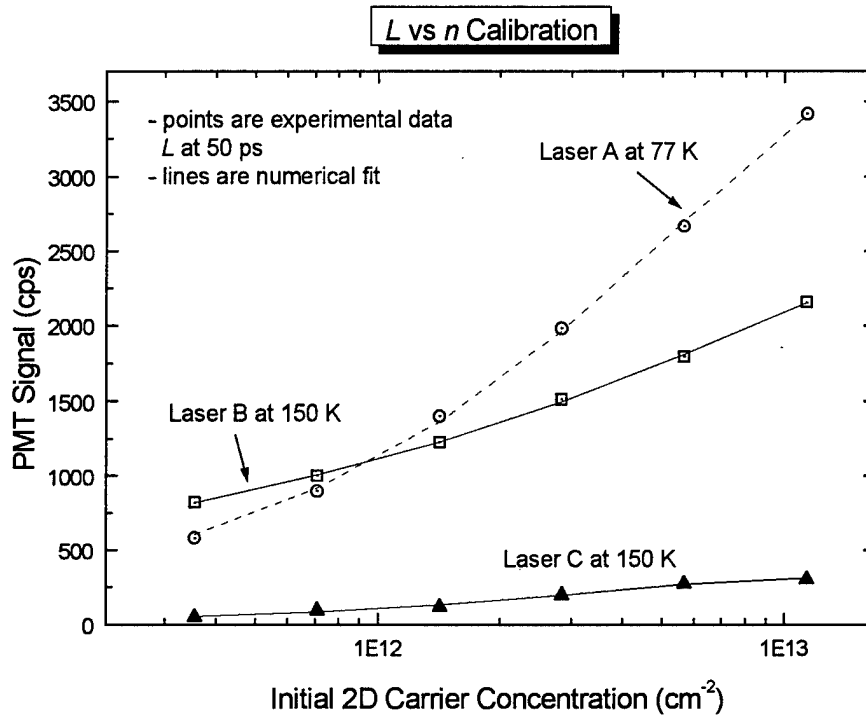
Figure 7-2: Sample of the empirical data used to define a relationship between the upconverted signal and carrier density. The lines are numerical fits to Equation (7-9).

7.3.1. Carrier Cooling and the 50 ps Assumption

In addition to upconversion performed to study recombination dynamics, laser sample "B" was used to optimize the experimental configuration. In doing so, sample "B" was cooled to 5 K and luminescence upconversion was performed with the spectrometer wavelength set for the SFG signal. Figure 7-3 provides the resulting temporal trace from this experiment.
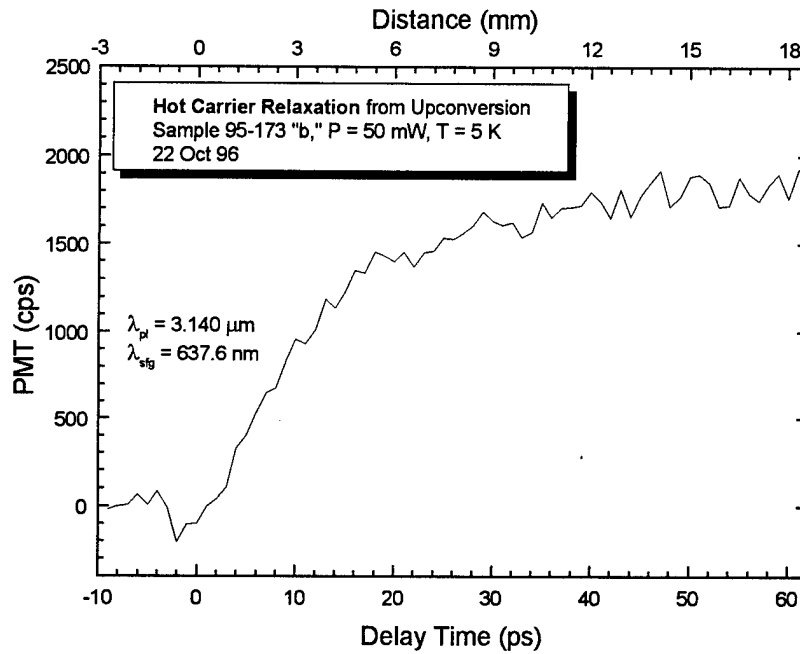
Figure 7-3: Luminescence upconversion from laser sample "B" at 5 K.

Note the upconversion signal requires approximately 50 ps to reach a maximum. This is very similar to findings by other researchers studying momentum relaxation of hot carriers (Shah, 1996). On very short time scales (< 10 ps) carrier-carrier scattering dominates the cooling of hot carriers which results in a thermal distribution of the carriers characterized by a temperature (T_c) which is greater than the lattice temperature (T_L). As time progresses, optical phonons and acoustic phonons continue to cool the carriers toward equilibrium with the lattice temperature $(T_c => T_L)$.

The issue of carrier temperature is significant in ultrafast experiments of this type because the carrier distribution is highly dependent on the temperature characterizing the lattice. Using optical phonon energy data we can estimate the carrier cooling times. By averaging over the carrier distribution, we obtain a carrier cooling rate from optical phonons (Shah, 1996:163) given as

$$\left\langle \frac{dE}{dt} \right\rangle = \frac{h\nu_{LO}}{\tau_{LO}} \exp\left(-h\nu_{LO} \Big/ kT\right), \tag{7-10}$$

where $\langle dE/dt \rangle$ is the average energy loss rate to the lattice per electron-hole pair by optical phonon scattering mechanisms, $h\nu_{LO}$ is the energy of the longitudinal optical (LO) phonon, and τ_{LO} is defined as

$$\left(\tau_{LO}^{3D}\right)^{-1} = \frac{q^2 \pi \sqrt{2mh\nu_{LO}}}{h^2}\left(\frac{1}{\varepsilon_\infty} - \frac{1}{\varepsilon_s}\right), \tag{7-11}$$

$$\tau_{LO}^{2D} = \left(2 \Big/ \pi\right)\tau_{LO}^{3D}, \tag{7-12}$$

for the 3D and 2D cases. Here m is the carrier mass, ε_∞ and ε_s are the optical and static dielectric permittivities equal to $12.25\varepsilon_o$ and $15.15\varepsilon_o$ for InAs respectively. The LO and transverse optical (TO) phonons are related by the Lyddane-Sachs-Teller relationship given by

$$\left(\frac{\nu_{LO}}{\nu_{TO}}\right)^2 = \frac{\varepsilon_s}{\varepsilon_\infty}, \tag{7-13}$$

Using time integrated photoluminescence, Marciniak determined energy values of optical phonons for $InAs_{1-x}Sb_x$ (low "x" values) by observing the optical phonon replica energy 27 - 29 meV below the luminescence peak (Marciniak, 1995:7-22). The energy of acoustic phonons is estimated to be only a few meV (Marciniak, 1995:7-42).

Using these values we calculate an estimate phonon scattering lifetime for the quantum well material to be $\tau_{LO}(3D) = 225$ fs and $\tau_{LO}(2D) = 143$ fs. Using this simple approach, the average energy-loss rate to the lattice per electron-hole by optical scattering mechanisms for carriers characterized by a temperature $T_c = 150$ K, is approximately 5 meV/ps, a very fast cooling mechanism!

Other researchers studying the cooling of hot carriers in antimonide semiconductors have found that cooling by optical phonon emission is essentially complete 15 ps after injection with a lattice temperature of 8 K which corresponds to a phonon scattering lifetime of $\tau_{LO} \approx 1.2$ ps (Jang, 1997).

The distribution of carriers in the bands as a function of time also impacts the luminescence intensity. Other researchers have shown (Shah, 1996 and Jang, 1997) that hot carriers can be characterized by a thermal distribution on very short time scales (1 - 2 ps) primarily due to optical phonon emission. The carriers continue to interact with the lattice via optical and acoustic phonons, reducing the excess energy in the carriers, and cooling them toward the lattice temperature.

We may conclude that at modest time delays after the initial excitation (tens of ps) the carriers are characterized by a thermal distribution near the lattice temperature. Experimental observation of the upconversion signal indicates the L(t) signal reaches a peak very near 50 ps for samples in the temperature range of interest (77 - 200 K). As a result, the empirical calibration of relating upconversion signal to carrier density was performed at a time delay of 50 ps.

It is important to note that the temperature that characterizes the carriers may be somewhat higher than the lattice temperature due to the slow down of optical phonon emission and mechanisms that heat the carriers. The magnitude of the temperature that the carriers quickly arrive at is not critical to the analysis. What is critical to the analysis is that the temperature that describes the carrier distribution remain reasonably constant after 50 ps. Ideally we desire the carrier temperature to remain constant over the 3 ns that make up the TRPL traces. This is due to the fact that the $L(n)$ relationship assumes a constant carrier temperature. Other researchers have observed this very fast cool-down of carriers, attributed to optical phonon scattering, followed by a dramatic slow-down of the cooling and the carrier temperature remaining approximately constant for nanosecond time scales (Jang, 1997 & Snow, 1989).

7.3.2. Comparison with Theory

By examining the *L(n)* relationship from a purely theoretical standpoint, we may improve our understanding of this experimental technique and the empirical relationship measured between *L* and *n*. Assuming carrier occupation is governed by Fermi-Dirac statistics, we can view the carrier dynamics in terms of the conduction and valence band "Fermi" functions, f_c and f_v, which evolve in time. Returning to Equations 4-7 and 4-9, we see that the magnitude of spontaneous emission (photoluminescence) is directly proportional to the product of occupation probabilities in the conduction (P_c) and valence (P_v) bands. Thus we may write

$$I_{lum} \propto P_c P_v = \left[\exp\left(\frac{E_i - E_{fc}}{kT_{cc}} \right) + 1 \right]^{-1} \left[\exp\left(\frac{E_f - E_{fv}}{kT_{vc}} \right) + 1 \right]^{-1} . \qquad (7\text{-}14)$$

Since E_i and E_f are fixed by tuning the spectrometer to a particular hv, the only variables affecting the occupation probability are the quasi-Fermi levels in both bands (E_{fc} & E_{fv}) and the carrier temperatures. Note that the carrier temperatures are not necessarily the same; T_{cc} is the carrier temperature in the conduction band while T_{vc} is the temperature of carriers in the valence band.

The PMT mounted on a stationary spectrometer, which effectively acts as a narrow spectral filter, measures the signal at the sum frequency photon energy (hv_{SFG}). This energy is directly related to a particular energy in the mid-IR, hv_{PL}, where $hv_{PL} = hv_{SFG} - hv_{pump}$. The mid-IR energy ($hv_{PL}$) in turn is directly related to energies in the quantum well, E_i and E_f, by Equation 4-13. The luminescence intensity from these two states is proportional to the occupation probability by Equation 4-16. The occupation of the discrete energy states, E_i and E_f, is a function of the Fermi energy level in the conduction and valence bands, E_{fc} and E_{fv} respectively, as given by the Fermi-Dirac distribution function, Equation 4-9. If we know the density of states for the system, we can relate E_{fc} and E_{fv} to the carrier densities, *n* and *p*. Putting this all together we have a

theoretical relationship between the carrier density and the measured upconversion signal *L(n)*. Stepping through these relationships again we have

$$L_{hv_{SFG}} \propto L_{hv_{PL}}$$

$$L_{hv_{PL}} \propto P_c\left(E_i, E_{fc}\right)P_v\left(E_f, E_{fv}\right)$$

$$P_c\left(E_i, E_{fc}\right)P_v\left(E_f, E_{fv}\right) \propto P_c(n)P_v(p \approx n) \qquad (7\text{-}15)$$

$$P_c(n)P_v(n) \propto L(n)$$

It is helpful to keep in mind the image that upconversion is a sampling of the occupation of discrete energies in the conduction band (E_i) and the valence band (E_f), at a particular moment in time.
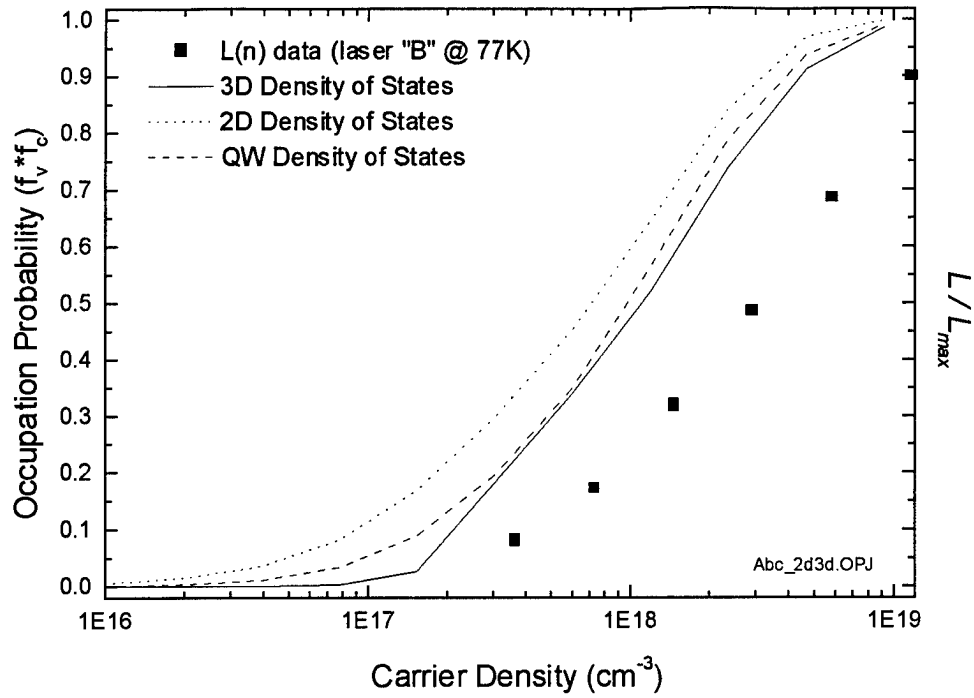
Figure 7-4: Theoretical behavior of luminescence intensity "L" versus carrier density "n" assuming a carrier temperature of 100 K, plotted with scaled empirical data from laser sample "B" at 77 K to illustrate the consistent trend.

The theoretical behavior for the variation of $L(n)$ based on the relationships described above and found in Chapter 4, and using a quantum well model described in Chapter 3, is plotted in Figure 7-4. Also plotted in the figure is the expected occupation probability for a 2-dimensional and 3-dimensional density of states discussed in Chapters 3 and 4 along with the empirical relations obtained by the methods described in section 7.3. The empirical data was scaled by a constant factor to plot the $L(n(t_o))$ along side the theoretical occupation probability. The empirical $L(n)$ data seems to be shifted to higher carrier densities by a factor of 3. This may point to a possible error that will be discussed at the end of this chapter. The point of the figure is to illustrate that the measured behavior is consistent with the expected theoretical behavior.

128

7.4. Plotting $L_m(t)$ versus $L_c(t)$

From section 7.2 we saw that given an initial carrier density $n(t_o)$, and the recombination coefficients A_{SRH}, B_{rad}, and C_{Auger}, we can find $n(t)$ for all $t > t_o$. With $n(t)$ available, we are now in a position to use Equation 7-9 and plot our expected luminescence from the calculated $n(t)$. Our calculated luminescence, referred to here as $L_c(t) = L(n_c(t))$, is our expected luminescence signal as a function of time for the recombination coefficients. This can then be directly compared with the actual luminescence versus time measured in the upconversion experiment, referred to here as the measured luminescence, $L_m(t)$.

Although data was taken on several samples at various temperatures as presented in Chapter 6, the best data was for laser samples "A" and "B" at 77 K and laser sample "B" at 150 K. Because the rest of the data taken was of poorer quality, principally due to the very low luminescence strength of the samples and the background noise, only the data from these three TRPL series is analyzed here to extract recombination coefficients.

7.4.1. SRH Coefficient (A_{SRH}) from an Independent Technique

Recall from the discussion in section 4.1, SRH recombination is characterized by exponential decay. For the samples at lower temperatures (77 K) shown in Figures 6-6 to 6-12, the signal just prior to zero delay is above the background signal (luminescence blocked condition) indicating the presence of excess carriers 13.2 ns after the excitation pulse and beyond. This is readily seen even in the low initial excitation levels in Figures 6-6, 6-8, and 6-11. The assumption here is that Shockley-Read-Hall recombination dominates in the low carrier regime between $\approx$ 3 ns to 13.2 ns. The Shockley-Read-Hall (A_{SRH}) coefficient was calculated by fitting an exponential decay using the upconversion signal magnitude at 3 ns ($L_m(t = 3\ ns)$) as the starting point and the residue signal at 13.2 ns ($L_m(t = 13.2\ ns)$ just before the following pulse excites additional carriers in the

sample) as the ending point. Considering the contribution from all previous pulses, the equation for calculating the SRH lifetime was given by

$$\frac{I_{13ns}}{I_{3ns}} = \sum_{j=0}^{\infty} \exp\left(\frac{-10ns - j \cdot 13.2ns}{\tau_{SRH}}\right) = \exp\left(\frac{-10ns}{\tau_{SRH}}\right)\left[1 - \exp\left(\frac{-13.2ns}{\tau_{SRH}}\right)\right]^{-1} .(7\text{-}20)$$

Note, the relation $\Sigma x^n = (1\text{-}x)^{-1}$ for $x < 1$ was used. With this we can write a straightforward expression that requires a numerical root finder. Because both radiative and Auger recombination processes take place during the duration, and likely dominated in the early times for high initial carrier densities, the contribution from prior pulses was used only for the low initial excitation energies. For large initial carrier density cases, the SRH lifetime was simply given by

$$\tau_{SRH} = \frac{10ns}{\ln\left(I_{3ns}\middle/I_{13ns}\right)} .$$

(7-21)

To insure accuracy of this measure, several small to medium excitation levels were used and compared on each sample. Variations between the samples at 77 K were modest, and are attributed to variations in growth quality. This technique was possible for the low temperature samples because the SRH coefficient was found to be reasonably small for the laser samples under these conditions.

For laser samples at higher temperatures, no appreciable signal remained after 13 ns from excitation. As a result, it was impossible to use the technique described above to determine the Shockley-Read-Hall coefficient. Consequently, A_{SRH} was used as a fitting parameter in these situations to obtain an estimate for the A_{SRH} coefficient at these elevated temperatures.

7.4.2. Best Fit for 77 K Data

The calculated and measured luminescence, $L_c(t)$ and $L_m(t)$, are plotted for laser sample "B" at 77 K in Figure 7-5. The fit of the recombination coefficient values used to calculate $n_c(t)$ can be compared directly. The best-fit recombination coefficients used to fit the measured data are displayed in the figure. A_{SRH} was obtained independently by fitting the upconversion signal at 3 ns, to the upconversion signal at 13.2 ns, assuming exponential decay. This technique was described in detail above. The value was found to be $A_{SRH} \approx 1.0 \times 10^8$ sec^{-1} ± 10% for sample "B" at 77 K ($\tau_{SRH} = 1/A_{SRH} \approx 10$ ns) under varying initial excitation conditions.

Although the theoretical radiative coefficient (B_{rad}) from section 4.2 was initially used where $B_{rad} \approx 2.5 \times 10^{-10}$ cm^{3}sec^{-1}, a superior fit to the data is obtained in Figure 7-5 if the radiative coefficient value is taken as $B_{rad} \approx 2.0 \times 10^{-10}$ cm^{3}sec^{-1}. It is not surprising that the "theoretical" value differs from the measured value because the theoretical value is limited by our knowledge of material parameters, particularly the effective masses. The situation is even less known because the strained quantum well system modifies the effective mass further.

TRPL with Fit for Laser "B" at 77 K

$$-dn/dt = A_{SRH}n + B_{rad}n^2 + C_{Auger}n^3$$

$A_{SRH}^{-1} = 10 \text{ ns}$

$B_{rad} = 2.0 \times 10^{-10} \text{ cm}^3\text{s}^{-1}$

$C_{Auger} = 1.0 \times 10^{-30} \text{ cm}^6\text{s}^{-1}$

100 mW □
50 mW ×
25 mW ○
12.5 mW +
6.25 mW ◇
3.125 mW ✳

B150fit.OPJ

11 Nov 96 Data

Figure 7-5: Time resolved photoluminescence data (marked points) and calculated fits (dashed lines) for laser sample "B" at 77 K for various excitation conditions.

The Auger coefficient found to fit best to the 77 K TRPL data was a negligible value! The implication is that Auger is not a contributing factor for the low temperature data.

There seems to be a deviation on the top trace at approximately 1 ns delay time, which seems to have shifted the PMT signal up a constant amount. The cause of this is unknown at this point but it is likely to be directly attributable to a temporal change in the room light. Unfortunately, nothing out of the ordinary was noted in the lab notebook for this particular day.

The series of traces shown in Figure 7-5 were arguable the best data taken for that sample at that particular temperature. However, it is not the only data taken on that sample. The traces were repeatable, and because the significance of the result is substantial, an additional TRPL series of traces on the same sample at the same

temperature are given in Figure 7-6. This data was taken approximately two weeks prior to the data given in Figure 7-5. Using the analysis technique discussed in this chapter, the recombination coefficients are identical within experimental uncertainty.

TRPL with Fit for Laser "B" at 77 K

$$-dn/dt = A_{SRH}n + B_{rad}n^2 + C_{Auger}n^3$$

$$A_{SRH}^{-1} = 10 \text{ ns}$$

$$B_{rad} = 1.8 \times 10^{-10} \text{ cm}^3\text{s}^{-1}$$

$$C_{Auger} = 1.0 \times 10^{-30} \text{ cm}^6\text{s}^{-1}$$

50 mW □
25 mW ×
12.5 mW o
6.25 mW +
3.125 mW ◇

APL.OPJ

Delay Time (ns)

26 Nov 96 Data
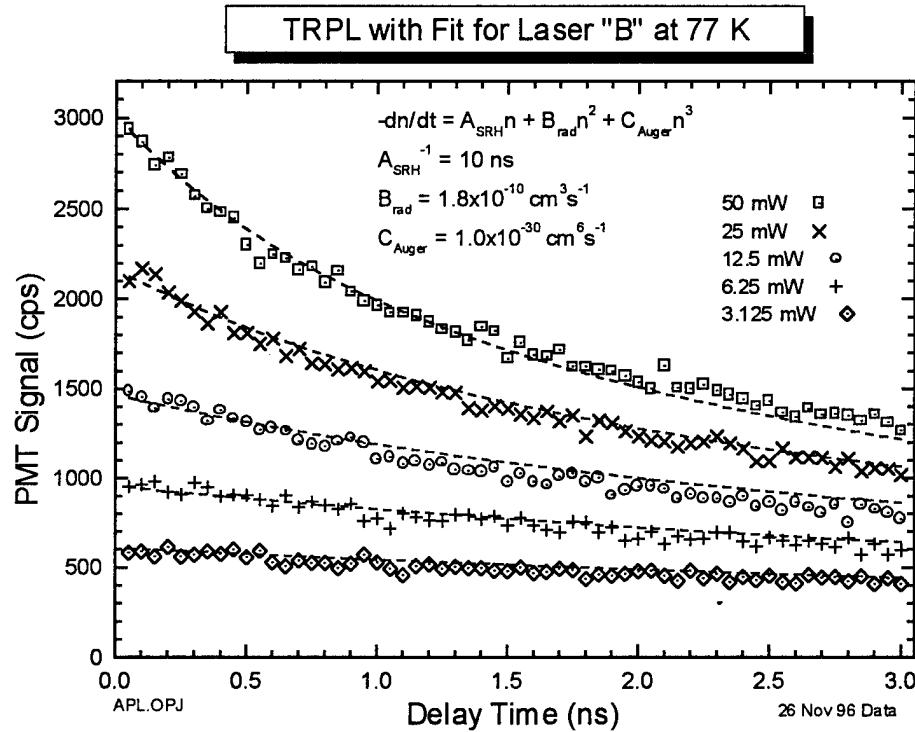
Figure 7-6: Time resolved photoluminescence data (marked points) and calculated fits (dashed lines) for laser sample "B" at 77 K for various excitation conditions. Data take under identical conditions to Figure 7-5 data on separate days.

Similar results were obtained for laser "A" at 77 K plotted in Figure 7-7. Only the highest carrier density data was taken on this particular TRPL series, along with the *L(n)* calibration plotted in Figure 7-1. The SRH coefficient was calculated using the technique described in section 7.5 without considering the prior pulse contributions because the initial carrier density was high. The resulting SRH coefficient was found to be 12.5 ns. Again, the radiative coefficient was found to fit extremely well with $B_{rad} \approx$

2.0×10^{-10} cm^{3}sec^{-1}. As in the case of laser "B," the Auger coefficient was found to be negligible for laser sample "A" at 77 K.
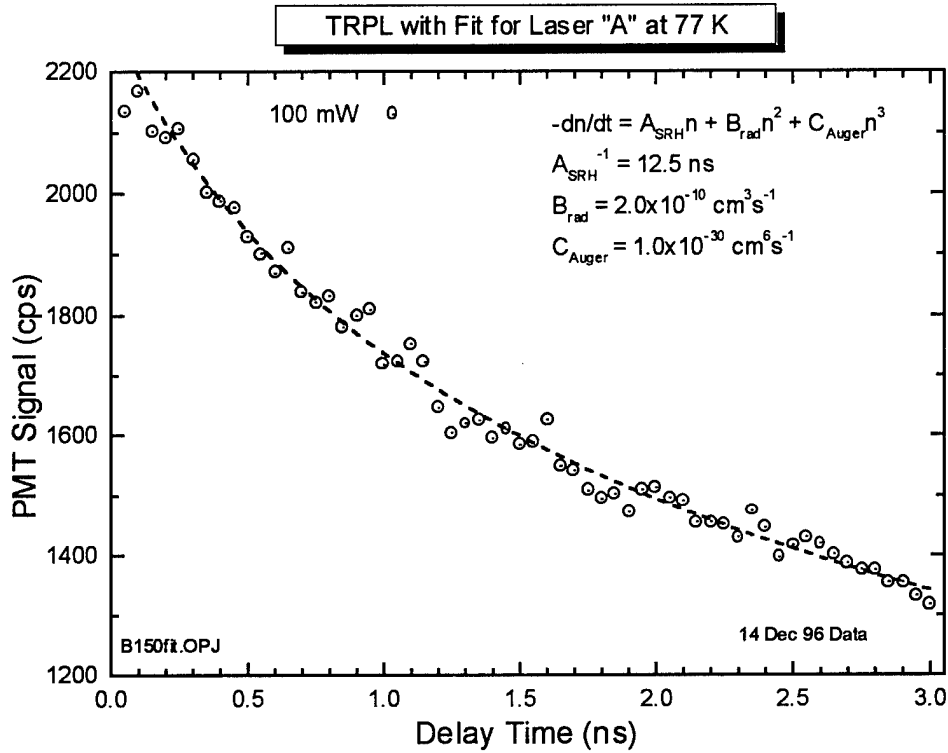
Figure 7-7: Time resolved photoluminescence data (marked points) and calculated fit (dashed line) for laser sample "A" at 77 K 100 mW excitation condition.

7.4.3. Best Fit for 150 K Data

The calculated and measured luminescence, $L_c(t)$ and $L_m(t)$, are plotted for laser sample "B" at 150 K in Figure 7-8 along with the best fit values for the A_{SRH} and C_{Auger} recombination coefficients. No identifiable signal was found just prior to the zero delay point (i.e. at 13 ns after luminescence excitation). As a result, the ability to "independently" fit the SRH recombination coefficient was impossible. For these series of TRPL traces, B_{rad} was taken as known from the 77 K data scaled by the theoretical

$(kT)^{-3/2}$, coming from Equation 4-22, giving a value of $B_{rad} \approx 0.78 \times 10^{-10}$ cm^{3}sec^{-1}. The recombination coefficients, A_{SRH} and C_{Auger} were used as fitting parameters.

Because the parameter space for fitting two unknown recombination coefficients can be difficult, a systematic and iterative error reduction approach was used. The first observation that can be made directly from Equation 7-1 is the dominance of the Auger term at high volumetric carrier densities. As a result, the fitting of the Auger coefficient was accomplished by minimizing the squared error considering only the highest excitation trace.

Figure 7-9 plots the squared error between the calculated luminescence $L_c(t)$ and the measured $L_m(t)$ given by

$$ERROR = \sum_{i=data} \left[L_c(t_i) - L_m(t_i) \right]^2 . \qquad (7\text{-}16)$$

The fitting error for the highest excitation TRPL trace, referred to as the "top TRPL," is plotted in Figure 7-9. The best fit value for the Auger coefficient is $C_{Auger} \approx 7.0 \times 10^{-28}$ cm^{6}s^{-1}.

Using this as our Auger recombination coefficient, our next step is to find the best fit for the SRH recombination coefficient. A_{SRH} was determined in effectively the same way, however because the low carrier density regime is strongly affected by SRH recombination, the fitting error was minimized over the sum of all TRPL excitation traces. Figure 7-10 is a plot of the squared error for various values of A_{SRH}, with our previously obtained values for C_{Auger} and B_{rad}. Table 7-1 provides a synopsis of the measured recombination coefficients.

TRPL with Fit for Laser "B" at 150 K

$$-dn/dt = A_{SRH}n + B_{rad}n^2 + C_{Auger}n^3$$

$$A_{SRH}^{-1} = 1.7 \text{ ns}$$

$$B_{rad} = 0.78 \times 10^{-10} \text{ cm}^3\text{s}^{-1}$$

$$C_{Auger} = 7.0 \times 10^{-28} \text{ cm}^6\text{s}^{-1}$$

50 mW □
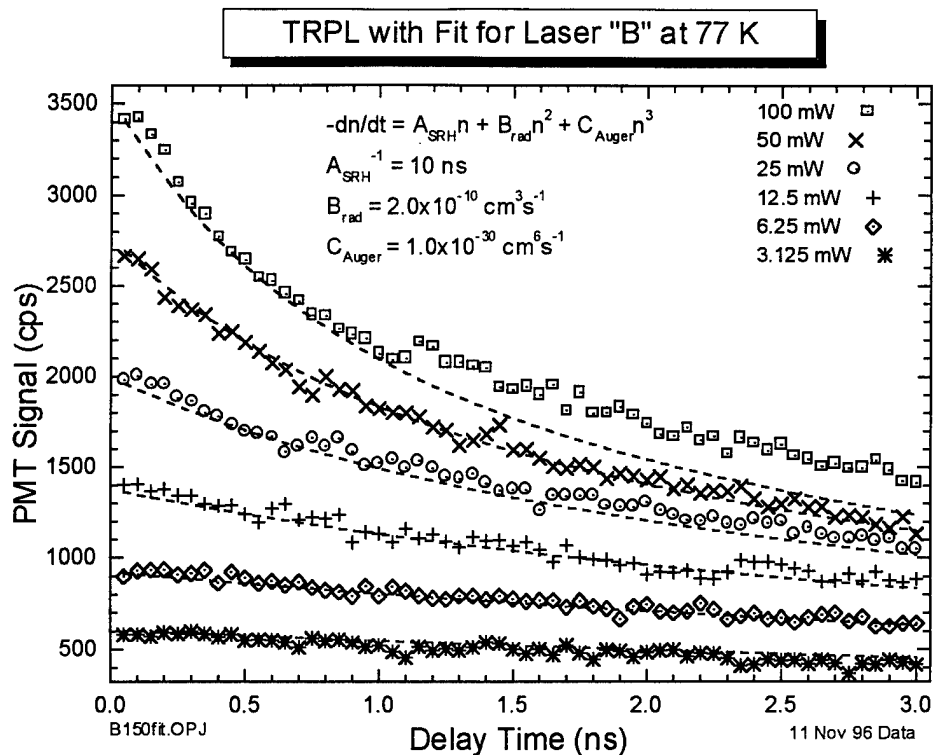25 mW ✕
12.5 mW ⊙
6.25 mW +
3.125 mW ◇

11 Nov 96 Data
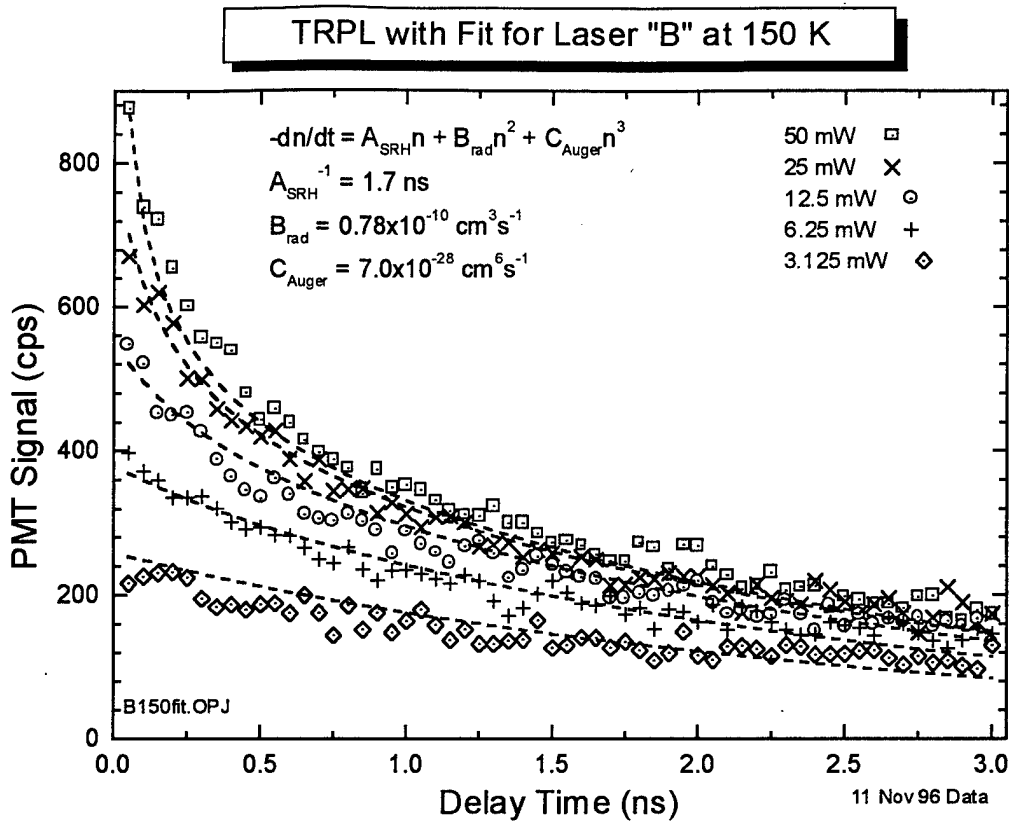
Figure 7-8: Time resolved photoluminescence data (marked points) and calculated fits (dashed lines) for laser sample "B" at 150 K for various excitation conditions.

Table 7-1: Summary of laser sample characteristics and the measured recombination coefficients.

Laser Sample	QW/Barrier Thickness (nm/nm)	Number of Wells (t_{qw})	τ_{SRH} (ns)	B_{rad} (cm^3/s)	C_{Auger} (cm^6/s)
A (77 K)	15/30	10	12.5	2.0×10^{-10}	$< 1 \times 10^{-29}$
B (77 K)	10/20	10	10.0	2.0×10^{-10}	$< 1 \times 10^{-29}$
B (150 K)	20/40	8	1.7	0.78×10^{-10}	7.0×10^{-28}
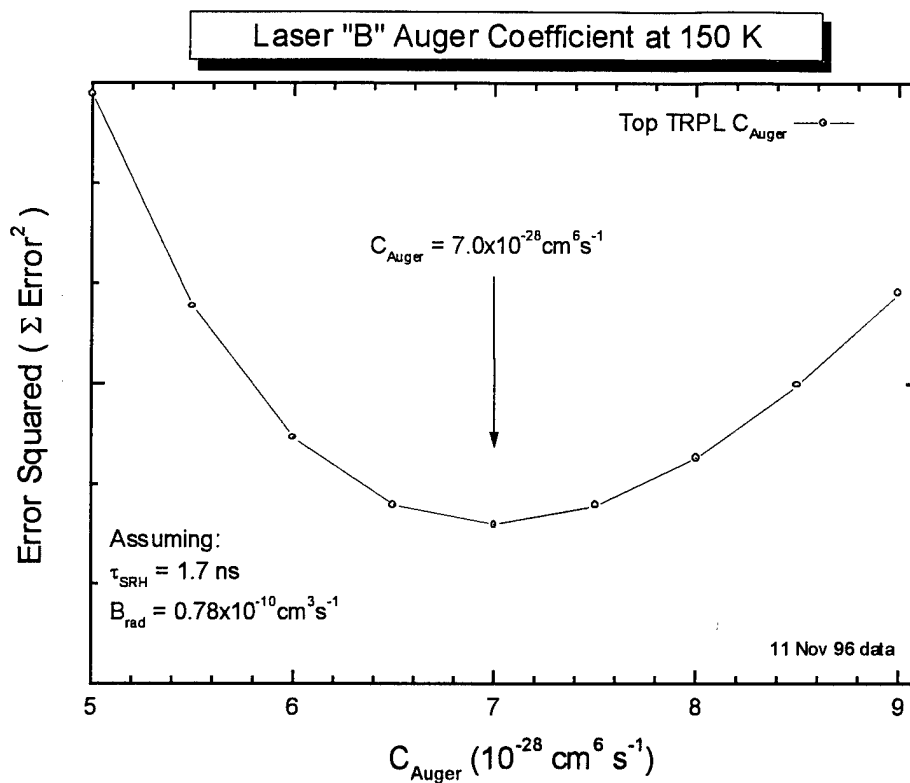
Figure 7-9: Squared error between the measured data ($L_m(t)$) and calculated fit ($L_c(t)$) for various values of C_{Auger} on laser sample "B" at 150 K.

7.5. Factors Considered in Analysis

Measuring ultrafast phenomena is challenging and requires assumptions to evaluate and analyze data. This section discusses some of these assumptions and critical experimental measures to quantify or test the reasonableness of the error that may be associated them.

7.5.1. Error Analysis

The sensitivity to measurement errors and fitting errors is fundamental to assigning either quantitative or qualitative degrees of confidence to experimental results. Measurement error dominates the error bars for the determination of recombination coefficients.
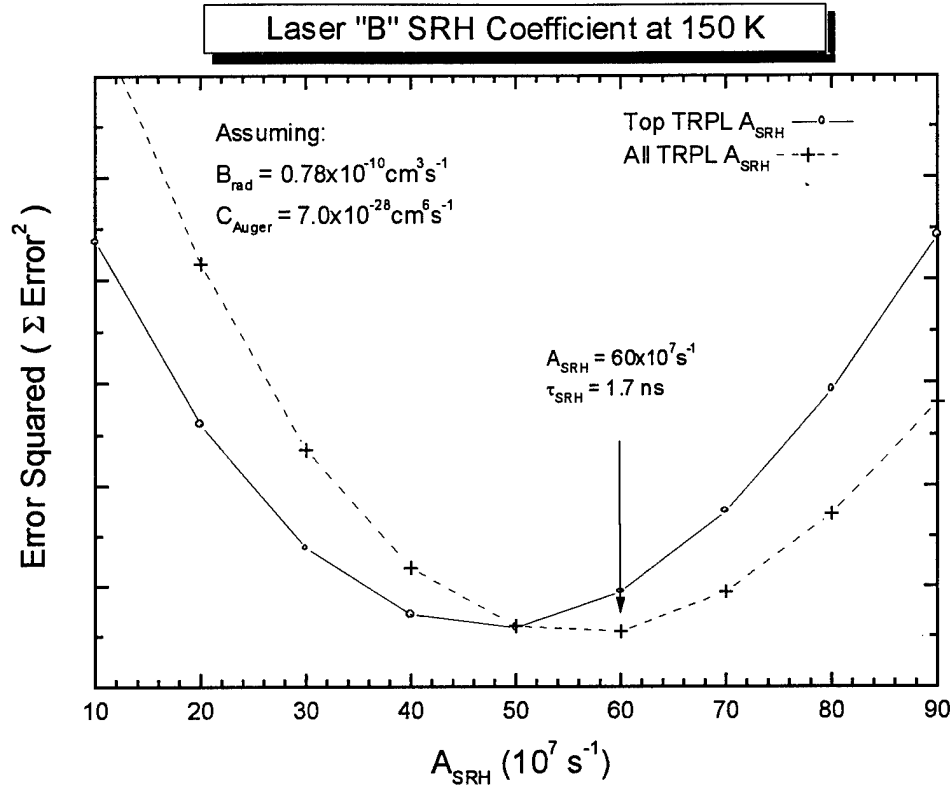
Figure 7-10: Squared error between the measured data $(L_m(t))$ and calculated fit $(L_c(t))$ for various values of A_{SRH} on laser sample "B" at 150 K.

The error associated with the experimental determination of an Auger coefficient is dominated by the strong dependence on initial carrier density. To illustrate, an error of 10% in excitation spot radius (w_o) results in a carrier density error of approximately 20% ($n_{2d} \propto w_o^2$), and because Auger recombination has a cubic dependence on power of carrier density from Equation (7-1) ($dn/dt|_{Auger} \propto n^3$) the result is 100% error or a factor of 2 in the resulting Auger coefficient. Section 5.5.3 presented the experimental details associated with measuring the spot size as well as accuracy estimates for the values found. The measurement error associated with determining the excitation spot size (ω_o) is $\pm 10\%$. As a direct result of this strong dependence, the accuracy of the value for Auger coefficients in this effort is estimated to be within a factor of ± 2 of the true value.

Because the spot size measurement is a global offset error, the relative error between samples is estimated to be $\pm 20\%$. This is based on a fitting sensitivity of the recombination coefficients.

In addition to the strong dependence on excitation spot size measurements, an additional factor to consider is the assumption that the carriers are evenly distributed among the 8 or 10 quantum wells. This assumption was made for simplicity and convention. After consulting with other researchers facing the same task (Boggess and Jang), and discussing the complexities of the problem, it was clear that a simplifying assumption was required. The uniform distribution assumption was used because the carriers enter the region in very excited states and are well above the quantum wells and barriers. The assumption then is that their high initial injection temperature allows the carriers to penetrate into the sample farther than Beer's law would predict.

The physics associated with each recombination process exhibits a unique power dependence as expressed in Equation 7-1. For this reason, fitting the recombination coefficients is reasonably straightforward and introduces surprisingly little error. For the highest carrier excitation levels ($n_{3d} \approx 10^{19}$ cm^{-3}) the Auger coefficient dominated the fitting in the region from 0 time delay to 500 ps. Modifications to the radiative coefficient and Shockley-Read-Hall (SRH) had little effect for the highest excitation fit, particularly in the time near zero delay. Likewise, the radiative coefficient dominated the "intermediary" carrier density ranges while the Auger and SRH had less of an effect in fitting the TRPL traces in the 500 ps to 3 ns range. Finally, the ability to independently measure A_{SRH} by comparing the residue signal remaining at 13 ns with the signal at 3 ns for a series of power levels reduces the fitting error significantly by removing A_{SRH} as a fitting parameter and taking it as a known. The Auger and radiative contribution to carrier recombination was small in this time domain, particularly in the very low carrier density cases. Because the dominant recombination phenomena differed in distinct temporal regions, the fitting accuracy is estimated to within 25%. This is based on

varying each recombination coefficient independently and observing the quality of the fit as measured by the squared error term.

7.5.2. Carrier Diffusion Effects

The diffusion of carriers results in an increasing area of the 2D spot with time. If we assume a Gaussian spot, then the beam radius w is given as a function of time by

$$w(t) = \sqrt{w_o^2 + 2D_h t} \qquad (7\text{-}17)$$

where, for ambipolar diffusion, D_h, is the diffusion coefficient for holes (McKelvey, 1966) given by

$$D_h = \frac{\mu_h kT}{q}. \qquad (7\text{-}18)$$

Using material parameters for InAs, with mobility and hole effective mass values of $\mu_{InAs} = 460$ cm^2/volt sec and $m_h = 0.40$ m$_e$ (Sze, 1981), and if our initial beam waist is 25 μm we can calculate the effect ambipolar diffusion has on carrier density. Because Sze's data is for 300 K, we must approximate the mobility for 150 K using the expression given by McKelvey for the temperature dependence of mobility given as

$$\mu(T) = \mu(300K) T^{-\frac{3}{2}}. \qquad (7\text{-}19)$$

Even if we assume D_h is 5 times larger than the low-density coefficient to account for plasma expansion, we find that after 1.5 ns, $w \approx 26$ μm. Thus, the carrier density would only be approximately 8 % lower due to expansion in the most extreme case. The error in carrier density associated with measuring the excitation spot size is approximately 20% - 25%. As a result, diffusion of carriers will be ignored in the current study.

7.5.3. Distribution of Carriers in the Wells

Assuming Beer's law describes the absorption behavior of the luminescence excitation as it propagates through the sample, the intensity of the beam decreases exponentially. The beam energy is, of course, generating hot carriers in the structure proportional to the energy absorbed in the region. This would intuitively cause an uneven distribution of carriers between the first well near the top, and the last well at the bottom. In addition to the non-uniform carrier distribution normal to the sample, both the well region and the barrier region absorb the luminescence excitation energy, and because samples A, B, and C had well/barrier varying thickness characteristics, the non-uniform distribution of carriers may have caused additional variations between samples.

This issue was discussed at length with other researchers, particularly Professor Thomas F. Boggess and Professor Michael Flatte both of the University of Iowa, who have wrestled with an identical or near identical situation. The assumption / approximation that was used for their effort and the current effort, was that because the carriers are generated with significant excess energy above the band-gap, they initially have excess kinetic energy available to move and redistribute themselves in the wells. This redistribution and cooling of carriers results in a fairly uniform distribution of carriers in the wells. As a result, the assumption used in the calculation of carrier density is that the carriers are evenly distributed across the multi-well structure. The Iowa team has seen some anecdotal evidence that indicates the approximation is not completely unreasonable. However, without a thorough study of carrier transport, it is an approximation.

7.5.4. Error Associated with a Factor of 3

Recall Figure 7-5, the trend in the empirical data matched our expectation from theory, however the initial carrier density was shifted by a factor of approximately 3. This raises a question regarding the dependence of the reported recombination

141

coefficients on the carrier density. In particular, what would the best fit for Auger recombination be if the carrier density was in fact a factor of 3 lower than the values used in this analysis. To determine the effect of lowering the initial carrier density by 3, the analysis was repeated for the lower initial carrier density. The best-fit analysis found that for the low temperature traces (77 K), the Auger recombination coefficient was still negligible ($C_{Auger} < 0.5 \times 10^{-28}$ cm^{6}s^{-1}). To get a fit that was reasonable, the value for B_{rad} was found to be $B_{rad} \approx 6.0 \times 10^{-10}$ cm^{3}s^{-1}. Because the SRH coefficient does not depend on initial carrier density, and could be obtained independently for the low temperature traces, the value did not change from $A_{SRH}^{-1} \approx 10$ ns.

Now if the revised B_{rad} is used for the higher temperature analysis by scaling as we did before by $(kT)^{-3/2}$, then our best fit coefficients for the "B" laser at 150 K were found to be $A_{SRH}^{-1} \approx 2.0$ ns, $B_{rad} \approx 3.0 \times 10^{-10}$ cm^{3}s^{-1}, $C_{Auger} < 5.0 \times 10^{-27}$ cm^{6}s^{-1}. Thus, if the initial carrier density were wrong by a factor of 3, the best-fit Auger coefficient would be in error by an order of magnitude.

To some degree, this bounds the absolute error associated with this technique and the analysis for C_{Auger}. It is not likely that the initial carrier density is off by this large an amount, however, because Auger recombination coefficients vary by multiple orders of magnitude in the literature, this approach provides absolute error bars for the reported Auger coefficients given here.

It is worth pointing out again that Figure 7-4 motivated this analysis because the apparent discrepancy between the expected occupation probability (i.e. the expected L(n) relationship) and the measure L(n) relationship. This discrepancy could also be explained entirely by our ignorance of the material parameters, particularly the heavy-hole mass (m_{hh}) in the quantum well. Because the heavy-hole mass dominates the occupation statistics at the valence band edge, a modest change in the value of m_{hh} results in a significant shift in the occupation probability curve relative to the initial carrier density.

8. Conclusion

In this final chapter, the impact of this study on our understanding of the MIT/LL mid-IR lasers is discussed. Section 8.1 identifies the uniqueness of this work and highlights the contribution. Recombination coefficients are compared with prior research efforts in section 8.2. Section 8.3 presents the relative importance of Auger recombination in these structures from the laser operation perspective in terms of current. Section 8.4 provides recommendations for follow-on efforts.

8.1. Contribution and Uniqueness of Effort

The most significant contribution of this effort is the experimental determination of the non-radiative recombination coefficients in the mid-IR material. Previous theoretical and experimental research has speculated that Auger recombination was the limiting non-radiative mechanism. The conclusion of this effort is that at low temperatures (77 K), the Auger coefficient is very small, while at higher temperatures (150 K), the Auger coefficient becomes appreciable, however it is still significantly smaller by more than an order of magnitude than other researchers have thought. The exact value of the recombination coefficients reported here is not as important as the order of magnitude since Auger recombination coefficients reported for similar materials varied over several orders of magnitude. Further comparison with other researcher's results is presented in Section 8.2.

Three experimental aspects of this effort make it unique: 1) the wavelength upconverted (3 μm < λ_{PL} < 4 μm) with a sub-picosecond laser, 2) the application of upconversion for determination of recombination dynamics in mid-IR semiconductor lasers and 3) the method developed to interpret the data. Although approximately 30 publications using upconversion spectroscopy exist at the time of this research, only one publication (by Nurmikko's group at Brown University) performed upconversion with a

wavelength as long as that reported here (Heyen, 1989), and in that effort, a Nd:YAG laser ($\lambda = 1.064$ µm) with a pulse width on the order of 100 ps was mixed with luminescence wavelengths from 4 - 5 µm. Nurmikko had a significant advantage because SFG was possible with silver thiogallate ($AgGaS_2$) which has a non-linear coefficient approximately 2 to 4 times larger than $LiIO_3$, $LiNbO_3$ or KTA (Dmitriev, 1991). $AgGaS_2$ was not an option for this effort because it absorbs wavelengths shorter than ≈ 700 nm (recall that $\lambda_{SFG} \approx 650$ nm).

Two publications from a German research team reported upconversion as a method to study carrier recombination dynamics including Auger recombination (Hausser, 1989 and Fuch, 1989). They used a Nd:YAG laser with a pulse width of 150 ps to mix with the 1.5 µm luminescence. Unfortunately, the details of their analysis are not provided in their published article making it difficult to understand exactly how they derived recombination coefficients. Their upconversion experiment exploited a ¼ meter spectrometer and a linear silicon array at the exit slit, allowing for the measurement of an integrated luminescence signal. They fit recombination coefficients to the time dependence of the integrated luminescence and said nothing regarding the relationship between $L(t)$ and $n(t)$. The current research then not only experimentally determines Auger coefficients at longer wavelengths than previously reported, but also provides a clear and sensible approach to the analysis for interpreting time resolved luminescence data.

8.2.   *Comparison with Other Reported Results*

Most of the literature related to mid-IR antimonide based lasers, both theoretical and experimental, indicate two things: 1) the dominant deleterious mechanism limiting the performance, both in terms of threshold current density and maximum operating temperature, is Auger recombination and 2) superior performance is possible through band-gap engineering.

144

Two previously reported results are available for comparison, both report significantly larger Auger coefficients than those found in this effort. Naval Research Laboratory (NRL) reported on a similar material system using time-resolved photoconductivity (TRPC) Auger coefficients values two orders of magnitude larger ($\approx$ 4.0×10^{-26} cm^6sec^{-1}) at 77 K (Lindle, 1995). The shortcomings of the time-resolved photoconductivity (TRPC) are stated here due to their significance. The TRPC results suffer from similar experimental difficulties as were described in the current effort such as determination of initial carrier density. In addition to the standard experimental difficulties, two important differences are worth noting regarding the NRL effort: 1) they assumed no radiative transitions ($B_{rad} = 0$) and 2) all samples were grown by molecular beam epitaxy (MBE) onto [100] semi-insulating GaAs substrates. Because GaAs has a significantly different lattice constant than InAsSb, the crystal quality is likely very poor, and as a result, the usefulness of their results for laser designers concerned with quantum well laser structures with good crystalline quality is questionable.

Theoretical calculations of the Auger coefficient were made for bulk $InAs_{0.91}Sb_{0.09}$ (Flatte, 1996). Three critical concerns exist regarding these results; 1) the model is limited by our knowledge of the material parameters, which in the case of InAsSb is poor, 2) the structures of interest are strained quantum well lasers, not bulk material, and 3) experimental results are intrinsically tied more strongly to reality.

These theoretical results continue to support the paradigm that Auger recombination is the Achilles heel for mid-IR laser structures. The recombination coefficients determined in these two studies along with those obtained in this study are provided in Table 8-1 for comparison.

It is possible that the particular samples studied in this effort exhibited Auger suppression properties far superior to other material systems or structures. The samples studied by NRL were for a 15% antimony composition rather than the 6.5% antimony

quantum wells used in this effort. This may explain the significant difference between their results and the results presented here.

Table 8-1: Summary of results and comparison with other researcher findings. Note, Flatte' is from theoretical calculations (Flatte', 1995) and NRL-TRPC are experimental where B_{rad} has been assumed to be negligible (Lindle, 1995).

Source	Sample /Material	Temp (K)	Auger (C_{Auger}) 10^{28} cm^{6}s^{-1}	Radiative (B_{rad}) 10^{-10} cm^{3}s^{-1}	SRH lifetime A_{SRH}^{-1} ns
This effort	"A"	77	< 0.1	2.0	12
This effort	"B"	77	< 0.1	2.0	10
This effort	"B"	150	7.0	0.78	1.7
Model-Flatte	InAs$_{0.91}$Sb$_{0.09}$	77	23.3	2.7	
"	InAs$_{0.91}$Sb$_{0.09}$	150	29.0		
"	InAs$_{0.91}$Sb$_{0.09}$	300	24.5		
TRPC-NRL	InAs$_{0.85}$Sb$_{0.15}$	77	400	0	14
"	InAs$_{0.85}$Sb$_{0.15}$	300	90	0	16

8.3. *Impact on mid-IR Laser Research*

The results of this research indicate that the Auger recombination coefficients in the laser samples studied are smaller than originally thought. The impact of the value of the recombination coefficients is readily seen in Figure 8-1 which is a plot of current contributions from J_{SRH}, J_{rad}, J_{Auger} and J_{total} vs volumetric carrier density, $n(cm^{-3})$.

The trends correspond reasonably well to the laser performance and predicted Auger trends from the previously reported laser characterization (Choi, 1996). Based on the assumption that threshold is achieved at a carrier density of 5×10^{17} cm^{-3} and using the recombination values found in laser B at 150 K in this effort, the current required to reach threshold is 680 A/cm^2. The previously reported results measured laser threshold for laser B at 150 K to be $\approx$ 400 A/cm^2.

Contributions to Laser Current

Legend shown in figure:
- $A_{SRH} = 60^7 \, sec^{-1}$ ($\tau_{SRG} = 1.7$ ns)
- $B_{rad} = 0.78 \times 10^{-10} \, cm^3 \, sec^{-1}$
- $C_{Auger} = 7.0 \times 10^{-28} \, cm^6 \, sec^{-1}$
- $J_{SRG} + J_{rad} + J_{Auger}$

$J = e(dn/dt)$

$n_{th} = 5 \times 10^{17} \, cm^{-3}$
@ T = 150 K

Current contributions @ n_{th}
$J_{SRH} = 76\,\%$
$J_{Rad} = 5\,\%$
$J_{Auger} = 19\,\%$

Y-axis: Amp/cm^2
X-axis: Carrier Density (cm^{-3})

Current.OPJ
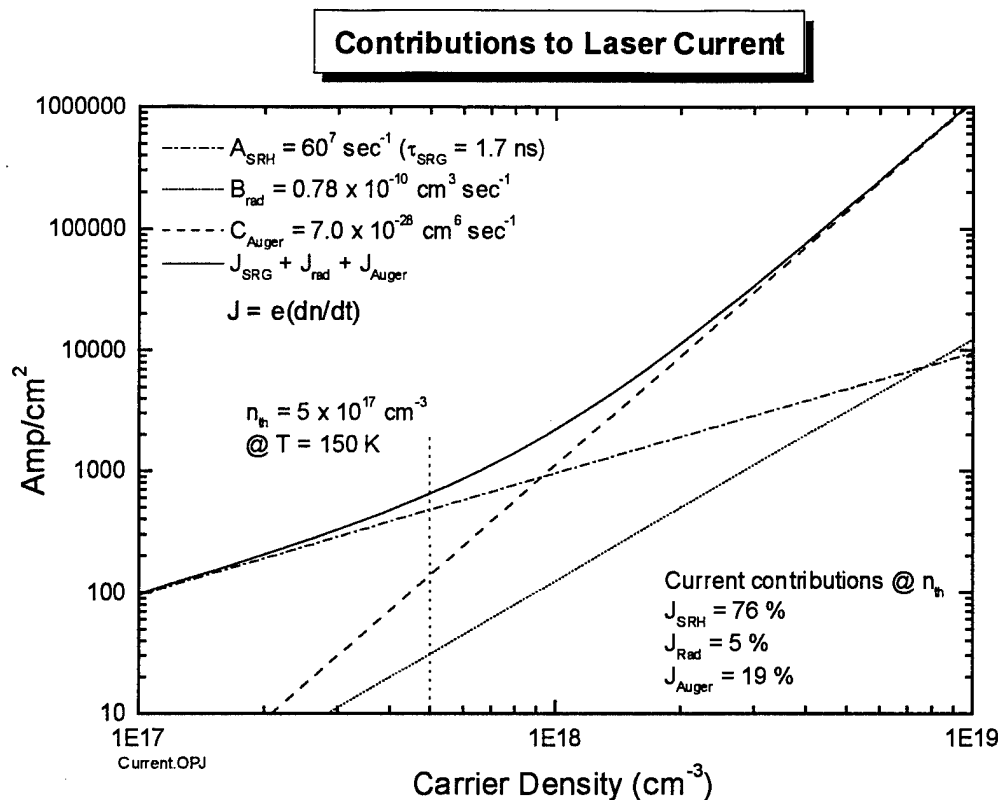
Figure 8-1: Current contributions from recombination mechanisms as a function of volumetric carrier density. The vertical line indicates the approximate value for threshold.

Semiconductor laser researchers need to know where to focus their efforts. If Auger recombination is shown to be the dominant mechanism, than the laser design needs to be improved to avoid resonance with Auger effects. If SRH is the limiting non-radiative mechanism, then the growth processes must be improved to reduce the number of non-radiative, defect related recombination sites. The finding of the current research and the most important result for laser designers is that the Auger coefficient may not be the dominating non-radiative mechanism. The results at 150 K indicate that the defect related SRH recombination effects are significant, and dominate the efficiency of the device. Further improvement in crystal quality and interfacial effects may yield the most dramatic improvement in these laser structures.

147

8.4. Recommendations for Future Work

The analysis technique for determination of recombination coefficients is critical for this experiment. The empirical approach to relate $L(t)$ to $n(t)$ was used here in this effort after several elegant theoretical approaches were attempted. Although the calibration technique used to define the relationship between $L(t)$ and $n(t)$ at 50 ps has proved to be a reasonable assumption that holds up under scrutiny (other researchers at the University of Iowa have similar findings), it is not as satisfying as calibrating the system to collect precise luminescence spectra as a function of time, $L(h\nu,t)$. In any case, a thorough study of the time evolution of the luminescence spectra, coupled with a detailed model of the structure and what we expect the luminescence to look like as a function of time, would provide valuable insight to carrier relaxation and carrier recombination phenomena.

Other possible follow-on research is the study of carrier transport in these mid-IR laser structures. Other researchers have grown novel devices to assist in the temporal carrier transport phenomena (Deveaud, 1987), but the luminescence wavelengths have all been short (less than 1 μm) relative to the capabilities of the current effort.

Because the SRH recombination was found to be significant, other techniques should be used that are superior for measuring and characterizing defect related SRH recombination. Deep level transient spectroscopy (DLTS) is a likely candidate for such an investigation.

A. Appendix – Expanded Literature Review

This appendix is intended to augment the literature review provided in Chapter 2 and has been included here in the interest of keeping the literature review brief and directly relevant. Chapter 2 contains only the papers that have significantly impacted this dissertation research, in addition to the tables that provide a helpful list of published research in the four main areas. This appendix provides a written description of prior work in the four areas reviewed in Chapter 2 and they are A.1 mid-infrared semiconductor lasers, A.2 materials research on the $InAs_{1-x}Sb_x$ alloy, A.3 theoretical and experimental background on Auger recombination research, A.4 photoluminescence upconversion technique. In the interest of completeness, the description of significant papers is also included here as well as the tables giving the publication list for each area.

A.1. Mid-Infrared Semiconductor Lasers

High quality monolithic structures can be grown on a crystalline substrate material, which have a lattice constant that matches or nearly matches the lattice constant of the alloy. The availability of high quality GaSb wafers makes the quaternary alloy $Ga_yIn_{1-y}As_{1-x}Sb_x$ and the ternary alloy $InAs_{1-x}Sb_x$ lattice matched to GaSb particularly attractive. The lattice matched condition for the quaternary removes the independence of either "y" or "x" and can thus be expressed as a dependent function. When the quaternary is expressed as $Ga_yIn_{1-y}As_{1-x}Sb_x$ we can write "y" in terms of "x" in Equation (3-1) (Adachi, 1987).

$$y = \frac{0.3835 - 0.3835x}{0.421 + 0.216x} \qquad (A-1)$$

A.1.1. Early Work - Before 1990

The first $InAs_{1-x}Sb_x$ laser was made by the Soviets in 1966 by Basov (Basov, 1966). The Czochralski method was used for crystal growth, and the composition of antimony varied in the boule, allowing Basov to investigate a variety of compositions. The peak wavelength of the laser emission discussed in their paper was at approximately 3.5 μm with an injection current density threshold of J_{th} = 8000 A/cm² at T = 77 K.

In 1985 and 1986, researchers from AT&T Bell Labs (van der Ziel, 1985a, 1985b, and 1986) investigated laser structures that were optically pumped. The active region was made of $InAs_{0.91}Sb_{0.09}$. The peak wavelength of coherent light was approximately 3.9 μm. They fabricated lasers using different types of cladding layers. Their first effort (van der Ziel, 1985a) used InAs as the cladding layer and the crystal was grown by liquid phase epitaxy (LPE). The values for the threshold current and the temperature parameter were J_{th} = 30,000 A/cm² and T_0 = 27K. The second effort (van der Ziel, 1985b) used GaSb as the cladding layer and the crystal was grown by molecular beam epitaxy (MBE). The values for the threshold current and the temperature parameter were J_{th} = 14,000 A/cm² and T_0 = 16K. Their third effort (van der Ziel, 1986) used $Al_{0.5}Ga_{0.5}Sb$ as the cladding layer and the crystal was grown by MBE. The values for the threshold current and the temperature parameter were J_{th} = 4000 A/cm² and T_0 = 17K.

A.1.2. Recent Work - Since 1990

Significant progress has been made recently for lasers operating at 4 μm by researchers at the (MIT/LL). In 1991 under Air Force funding, Eglash and Choi grew MBE $InAs_{0.91}Sb_{0.09}/AlAs_{0.08}Sb_{0.92}$, fabricated, and demonstrated optically pumped lasers, first at 3.71 μm, then at 3.99 μm (Eglash, 1994; Marciniak, 1995). The lasers operated at temperatures as high as 155K with a temperature parameter T_0 = 17K.

In 1994, the same group from MIT/LL succeeded in producing optically pumped (Le, 1994) and electrically pumped (Eglash, 1994) $InAs_{0.91}Sb_{0.09}$ lasers. Optically

pumped lasers use a shorter wavelength laser to obtain a population inversion while a direct electrical current drives electrically pumped lasers. The MIT/LL group made use of a novel approach for optical pumping using a diode array (Le, 1993). The laser emitted at 4 μm, operated at temperatures as high as 150K, and exhibited exponential threshold behavior $\exp(T/T_0)$ with characteristic temperature $T_0 = 17.5$K. Auger recombination was cited as the critical temperature dependent parameter limiting the operation at higher temperatures.

The electrically pumped version of their mid-IR laser (Eglash, 1994) consisted of a double heterostructure of $AlAs_{0.08}Sb_{0.92}$ and $InAs_{0.91}Sb_{0.09}$ for electrical confinement. The lasers emitted at 4 μm, exhibited a threshold current of only $J_{th} = 33$ A/cm^2 and possessed a characteristic temperature of $T_0 = 17$K. The lasers exhibited continuous wave operation at temperatures up to 80K and pulsed operation up to 155K. The prospect of using compressively strained quantum wells was discussed as a possible method to reduce the effects of Auger recombination as had been done in previous efforts on InGaAsSb at 2.1 μm (Choi, 1992).

In terms of the figures of merit, the goal is to reach continuous wave (cw) operation at room temperature with as much power as possible, a goal already realized for semiconductor lasers emitting at 2.2 μm (Choi, 1991). Toward that end, Choi *et.al.* used an amplifier to increase the optical power. The addition of a tapered oscillator gain region to enhance the optical power and was successfully used with 2 μm lasers is a reasonable approach for the 4 μm laser (Choi, 1993).

More recent mid-IR semiconductor laser results from the MIT/LL group are encouraging, particularly with regard to Auger recombination in strained quantum wells. Turner *et.al.* (Turner, 1995) fabricated mid-IR laser structures using ten $InAs_{0.86}Sb_{0.14}/In_{0.85}Al_{0.15}As_{0.86}Sb_{0.14}$ strained quantum wells as the active region with $AlAs_{0.08}Sb_{0.92}$ cladding layers. They obtained a threshold current density as low as 70 A/cm^2 at 70K and were able to operate cw up to 123K. The characteristic temperature of

their laser was $T_0 = 30K$, which is significantly higher than the value obtained for the best InAs$_{0.91}$Sb$_{0.09}$ double heterostructure lasers ($T_0 \approx 20K$) (Choi, 1994). One of the key reasons for the success at MIT/LL has been the significant effort put into understanding the non-equilibrium growth conditions during MBE and accounting for these conditions at heterojunctions and key interfaces (Turner, 1994).

The latest paper by the MIT/LL group varied the thickness (10, 15, and 20 nm wells) in compressively strained quantum wells grown on InAs substrates, which are described thoroughly in Chapter 4 since these same laser structures are used as the samples studied in this dissertation. The threshold current density at 80 K was as low as 30 A/cm^2. The lasers operated at a wavelength near 3.5 μm and in the case of the 15 nm well, maintained continuous wave operation up to 175 K. The temperature dependence of the threshold current between 100 and 200 K exhibited T_0 values as small as 30 - 40 K, a significant improvement over previous T_0 values near 20 K. Auger recombination was again thought to be the limiting mechanism to higher temperature operation and lower threshold currents.

A different approach to designing mid-IR and longer wavelength lasers has been recently proposed by Capasso and Faist of AT&T Bell Labs (Capasso, 1995). They produced a "quantum-cascade" mid-IR laser that emits at 4.3 μm. Although their approach is applicable out to longer wavelengths (e.g. 10 μm), to date this approach only works in pulse mode with peak powers of 30 mW at a temperature of 100K.

A synopsis of mid-IR semiconductor laser work is provided in Table 1. Note the optically pumped lasers are listed with an equivalent current to indicate the equivalent current injection required to reach threshold.

A.1.3. Current State of Mid-IR Laser Development

The difficulties with current mid-IR diode lasers are their inability to operate at high temperatures, as well as their low power levels. These are both related to the small

empirical characteristic temperature parameter T_0 which is frequently attributed to CHSH Auger recombination. The parameter space for MBE growth of laser structures is very large. Experimental determination of Auger recombination coupled with the theoretical backbone needed to make sense of the data promises to reduce the parametric space for crystal growers as well as provide understanding of the Auger process.

Table 1. Synopsis of Mid-IR semiconductor laser progress.

λ μm	Active Region	Growth	Pump el/op	T_0 K	J_{th} A/cm²	T_{max}(K) cw/pulse	Ref	Year
3.5	InAs$_{91}$Sb$_{09}$	CZR	el		8000	77	Basov	1966
3.8	InAs$_{91}$Sb$_{09}$	MBE	op	15.9	14000	/135	van der Ziel	1985
3.1	InAs	LPE/DH	op	20	70000	/100	van der Ziel	1985
3.9	InAs$_{87}$Sb$_{13}$	LPE/DH	op	27.0	30000	/125	van der Ziel	1985
2.1	GaInAsSb	LPE/DH	el	80.0	7000	190/290	Caneau(b)	1986
2.2	GaInAsSb	LPE/DH	el	55.0	3500	220/290	Caneau	1986
3.9	InAs$_{91}$Sb$_{09}$	MBE	op	17.0	4000	/135	Chiu	1986
2.2	GaInAsSb	MBE/DH	el	26.0	4200	300/300	Caneau(c)	1987
2.0	GaInAsSb	LPE/DH	el		5400	77/300	Akimova	1988
2.4	GaInAsSb	LPE/DH	el		7600	77/300	Akimova	1988
2.2	GaInAsSb	LPE/DH	el	92.5	7000	/300	Joullie	1988
3.2	InAs$_{95}$Sb$_{05}$	LPE/DH	el	30.0	4500	/110	Mani	1988
2.2	GaInAsSb	LPE/DH	el	45.0	2600	/300	Zyskind	1989
3.2	InAs$_{95}$Sb$_{05}$	LPE/DH	el	38.0	1500	/110	Mani	1990
2.3	GaInAsSb	MBE/DH	el	50.0	1700	300	Eglash	1990
2.2	GaInAsSb	MBE/DH	el	25.0	940	300	Choi(b)	1991
2.3	GaInAsSb	MBE/DH	el	50.0	1500	300	Choi	1991
2.1	GaInAsSb	MBE/QW	el	113	260	300	Choi	1992
3.9	InAs$_{87}$Sb$_{13}$	LPE/DH	el		200	4.2	Aydaraliev	1993
2.0	GaInAsSb	MBE/QW	op		330	300	Choi	1993
2.2	GaInAsSb	LPE/DH	el	65	3000	300	Morosini	1993
3.0	GaInAsSb	MBE/DH	op	26.0		/210	Le	1994
4.0	InAsSb	MBE/DH	op	17.5		/150	Le	1994
4.0	InAs$_{91}$Sb$_{09}$	MBE/DH	el	17.0	33	80/155	Eglash	1994
2.0	GaInAsSb	MBE/QW	el		143	300	Turner	1994
3.9	InAs$_{91}$Sb$_{09}$	MBE/DH	el	20.0	36	105/175	Choi	1994
3.9	InAs$_{91}$Sb$_{09}$	MBE/QW	el	30.0	70	123/165	Turner	1995
3.5	InAs$_{91}$Sb$_{09}$	MBE/QW	el	35.0	30	175/225	Choi	1996

A.2. InAsSb Material Characterization

A.2.1. Early Work on InAs$_{1-x}$Sb$_x$

From 1964 till 1976, the only material characterization for InAs$_{1-x}$Sb$_x$ involved polycrystalline films. Properties including band-gap, split-off band energy, effective masses, and refractive indices were measured as a function of antimony mole fraction "x." Electron mobility, Hall coefficients, electroreflectance, phonon scattering, and far-

IR reflectivity studies were also used to understand and characterize $InAs_{1-x}Sb_x$. The details of these studies have been presented by Marciniak (Marciniak, 1995).

One paper from this period worth mentioning reports values for the split-off energy band Δ. Vishnubhatla et.al. used electroreflectance to study material parameters in mixed III-V alloys (Vishnubhatla, 1969). Among the alloys investigated was $InAs_{1-x}Sb_x$. They found a split-off energy Δ that varied quadratically. The exact form is given by the following equation:

$$\Delta = a - cx^2 \qquad\qquad (A-2)$$

where "a" is the split-off energy of the binary, in this case "a" = Δ_{InSb} = 0.85eV (Madelung, 1991), "c" is a constant determined experimentally or calculated theoretically (in eV), and "x" is taken as the *arsenic* mole fraction ($InAs_xSb_{1-x}$). In the case of $InAs_{1-x}Sb_x$ the value given for "c" from their electroreflectance *experiment* was "c" = 0.23 eV, while the value they predicted from *theory* was "c" = 0.32 eV. Vishnubhatla noted that of the alloys they investigated they found good agreement between the predicted values and the measured values, within the limits of their experimental error, with the *exception* of $InAs_{1-x}Sb_x$. Note the split-off energy in InAs was 0.42eV (Madelung, 1991), thus in order to fit the end points a value of "c" = 0.43 eV would be required.

Van Vechten (Van Vechten, 1970) studied the variation of band gap and split-off band energy for a number of alloys. Results generated in theory and compared with experiment for the $InAs_{1-x}Sb_x$ system were given in a later paper by Van Vechten et.al. (Van Vechten, 1972) who found the split-off band energy as a function of antimony composition to be given by

$$\Delta = x\Delta_{InSb} + (1-x)\Delta_{InAs} - x(1-x)1.18(eV). \qquad\qquad (A-3)$$

From 1976 to 1985, several researchers studied single crystalline properties of $InAs_{1-x}Sb_x$ grown via liquid phase epitaxy (LPE). Several of these efforts included the spectral response of an $InAs_{1-x}Sb_x$ photodetector, photoluminescence, Hall measurements and an optically pumped laser. The low photoluminescence intensity from $InAs_{1-x}Sb_x$ was attributed to Auger recombination (Esina, 1978).

Starting in 1985, epitaxial techniques were used to grow $InAs_{1-x}Sb_x$ films. Chiang and Bedair (Chiang, 1985) studied films grown via metal organic chemical vapor deposition (MOCVD) with an antimony mole fraction between 0.4 < "x" < 0.7 for detector applications between 8-12 μm. That same year, Tsang *et.al.* studied epi-layers of $In_{1-x}Ga_xAs_{1-y}Sb_y$ lattice matched to GaSb grown via molecular beam epitaxy (MBE) (Tsang, 1985). A photodetector made of LPE $InAs_{0.85}Sb_{0.15}$/InAs was fabricated by researchers at AT&T Bell Labs (Mohammed, 1986).

Electrical characterization of $InAs_{1-x}Sb_x$ was studied by Srivastava *et.al.* in 1986 (Srivastava, 1986). They experimentally determined the band off-set parameters for the heterojunction $InAs_{0.95}Sb_{0.05}$ on GaSb. That year Chiu *et.al.* studied heterojunctions and superlattices composed of GaSb and $InAs_{0.92}Sb_{0.08}$ lattice matched to GaSb grown via molecular beam epitaxy (Chiu, 1986).

In 1987 Yen *et.al.* studied $InAs_{1-x}Sb_x$ across the entire antimony mole fraction range (0 < "x" <1) via FTIR absorption (Yen, 1987). The expression they found for room temperature band gap in electron volts (eV) as a function of antimony mole fraction is given in the following equation.

$$E_g = 0.35 - 0.771x + 0.596x^2 \qquad (A-4)$$

Bethea and Yen continued studying the alloy $InAs_{1-x}Sb_x$ with high antimony mole fractions (large "x" values) for photoconductor detector applications (Bethea, 1987 and 1988). Electrical properties from Hall measurements for $InAs_{1-x}Sb_x$ with high antimony

mole fractions were presented by Yen (Yen, 1988). Also in 1988 Yen $et.al.$ studied the photoluminescence from $InAs_{1-x}Sb_x$ with low antimony mole fractions. Samples were grown on InAs (Yen, 1988) and GaAs (Yen(b), 1988).

Sandia National Laboratory has also shown interest in the $InAs_{1-x}Sb_x$ alloy. Kurtz $et.al.$ used photoluminescence and IR absorption to study a strained layer superlattice (SLS) of $InAs_{0.18}Sb_{0.87}/InSb$ (Kurtz, 1988). They concluded that a type-II structure exists at the heterointerface, meaning that in the narrower band-gap material, confinement takes place in either the conduction or valence band, but not both. This explained the photoluminescence peak observed at an energy smaller than the band-gap corresponding to the alloy $InAs_{0.18}Sb_{0.87}$. Dawson, also of Sandia, presented FTIR measurements from $InAs_{1-x}Sb_x$ /$In_yGa_{1-y}Sb$ SLS grown by MBE (Dawson, 1989).

Stringfellow $et.al.$ of the University of Utah studied Raman scattering in $InAs_{1-x}Sb_x$ alloys grown via MOCVD (Stringfellow, 1988). In 1989 they observed ordering in $InAs_{1-x}Sb_x$ for MOCVD samples with an antimony mole fraction $0.22 \le x \le 0.88$ (Stringfellow, 1989a). Stringfellow has also presented a thermodynamic model to understand miscibility gap and phase separation in III-V metastable alloy semiconductors (Stringfellow, 1989b).

A.2.2. Recent Work on $InAs_{1-x}Sb_x$

The propensity for $InAs_{1-x}Sb_x$ to phase separate during epitaxial growth was reported by Ferguson $et.al.$ (Ferguson, 1991) and Stradling (Stradling, 1991). They dramatically demonstrated this phenomena in a photo of a superlattice composed of $InAs_{0.33}Sb_{0.67}$ / $InAs_{0.69}Sb_{0.31}$. The superlattice was novel because it was grown under constant atomic flux conditions in an MBE, with nominal growth conditions predicting an alloy composition of $InAs_{0.5}Sb_{0.5}$. The natural phase separation/miscibility gap resulted in the superlattice.

Egan *et al.* studied scattering effects in $InAs_{1-x}Sb_x$ to include grain boundary scattering, dislocation scattering and alloy scattering. The motivation behind this effort was to exploit the very small effective mass of $InAs_{1-x}Sb_x$ alloy system (Egan, 1994).

In 1993, Mao and Krier used LPE grown material (Mao, 1993) while Elies (Elies, 1993) used MBE grown material to study the temperature dependence of the band-gap in $InAs_{1-x}Sb_x$ lattice matched to GaSb via photoluminescence. From the temperature dependence they determined the band-gap versus temperature relation and fit it to the Varshni equation, which describes semiconductor band-gap versus temperature relationship, given by

$$E_g(T) = E_g(0) - \frac{\alpha T^2}{\beta + T}, \tag{A-5}$$

where $E_g(0)$ is the band-gap at zero temperature, and α and β are fitting parameters. He found that for $InAs_{0.91}Sb_{0.09}$, $E_g(0) = 0.3216eV$, $\alpha = 2.6 \times 10^{-4} eV/K$, and $\beta = 113$ K.

Marciniak studied MBE $InAs_{1-x}Sb_x$ via photoluminescence by varying temperature, excitation power, and the antimony fraction, "x" between $0 \leq$ "x" ≤ 0.20 A sample of Marciniak's results on energy band gap as a function of temperature is provided in Figure A-1.
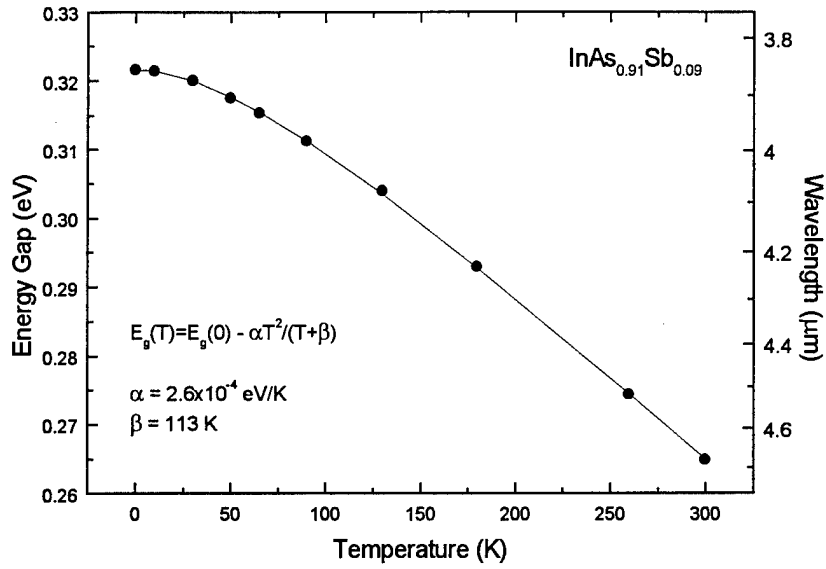
Figure A-1: Band-Gap versus temperature for InAs$_{1-x}$Sb$_x$ alloy (x = 0.09). The circles represent experimentally determined values for the band-gap while the dotted line is a fit to the Varshni equation (Marciniak, 1995).

A.2.3. Current State of InAsSb Research

InAs$_{1-x}$Sb$_x$ is an important III-V alloy for mid-IR semiconductor lasers, about which comparatively little is known. Mike Marciniak's dissertation research contributed significantly to the characterization of epitaxial grown material. The lack of knowledge available for this material system is illustrated by the limited published research for this alloy and contributes to our inability to develop InAsSb lasers for the mid-infrared.

A.3. Auger Recombination

Auger recombination rates (R$_{Auger}$) in semiconductors were first estimated in 1958 by Beattie and Landsberg (Beattie, 1958). Since that time, many researchers, particularly from a theoretical standpoint (Benz, 1976; Haug, 1984; 1988; Takeshima, 1978; 1984) have studied the effect of Auger recombination in bulk material. A number of theoretical investigations of Auger recombination in heterostructures and quantum wells is also available in the literature (Abram, 1988; Grein, 1992; 1993; Taylor, 1985; Tsou, 1992;

Young, 1993; Youngdale, 1994). The dominance of Auger recombination in mid-IR semiconductor lasers from theoretical investigations is also well known (Landsberg, 1986; Mozer, 1983; Oreilly, 1987; Sugimura, 1981; 1982). Although difficult, several research groups have attempted to experimentally measure Auger recombination rates. In addition to measuring very fast phenomena, one difficulty associated with experimentally determining Auger recombination coefficients is related to the fact that Auger recombination cannot be *directly* measured. A synopsis of past experimental efforts will be given at the end of this section.

A.3.1. Experiment

A modest number of researchers have experimentally determined Auger recombination rates. The limited activity in this area is primarily due to the inability to directly measure non-radiative phenomena. Among the methods used to measure Auger recombination are time-resolved free-carrier absorption (Auston, 1975), photoluminescence from the conduction band to the split-off band ($hv=Eg+\Delta$) (Benz, 1976; Mozer, 1983; Zielinski, 1989), intensity-dependent photoconductivity (Youngdale, 1994 a & b; Lindle, 1995), differential carrier lifetimes (Olshansky, 1984; 1987; Chen, 1991; Ongstad, 1995; 1996), doping (Titkov, 1981) and temperature (Kurtz, 1995) dependent photoluminescence, pump-probe (Prise, 1984) (Vodopyanov, 1992; McCahon, 1996), time-resolved-photoluminescence (TRPL) (Sermage, 1983; 1985; 1986) and TRPL using frequency upconversion (Snow, 1989a; b; Hausser, 1990; Fuchs, 1991).

Although time resolved luminescence has great appeal because it is the most direct measure among the options, it has not been used extensively. There are several reasons for this, among them, the ability to perform ultrafast spectroscopy is difficult and has only become possible in the last decade. The techniques available for high speed measurements are: 1) use of a very fast photodetector, which is limited to visible or near IR spectral ranges; 2) use of a streak camera, which again has a limited spectral range and

is very expensive but enables temporal resolution down to approximately 10 picoseconds (Kohl, 1990); 3) use of a timed population correlation technique, which exploits the material luminescence response at a frequency difference $\varpi = \varpi_1 - \varpi_2$ from two excitation frequencies and is capable of time resolution from 250 ps (Bergman, 1991) down to 100 fs (Christanell, 1989); and 4) use of a frequency up-conversion (Shah, 1988) with a temporal resolution typically near 100 fs.

The earliest experimental approach for determining Auger recombination coefficients was by Blinov et.al. (Blinov, 1968) who observed the photoconductive decay tail in silicon following photo-excitation by a Q-switched laser. The first report of optical determination of Auger recombination rates was made in 1972 by Nilsson and Svantesson (Nilsson, 1972). Using a fast photodetector, they measured the luminescence decay tail in silicon and fit the rates by assuming an Auger recombination process given by Equation (3-8).

$$\frac{-\partial n}{\partial t} = C \cdot n^3 \tag{A-6}$$

where "C" is the Auger recombination coefficient in $cm^6 sec^{-1}$. The cubic dependence is naturally assumed from the three-body character of Auger, whereby an electron recombines with a hole and the excess kinetic energy is transferred to another electron or hole.

Other techniques have been used to determine Auger recombination coefficients. Researchers at AT&T Bell Labs in 1975 used a free-carrier absorption technique to determine the Auger rate in germanium (Auston, 1975).

B. Sermage et.al. (Sermage, 1983; 1984; 1985) measured the luminescence decay rate of the 1.3 μm InGaAsP emission and estimated the Auger recombination rate. Their experiment consisted of a mode locked Nd:YAG pump, a temperature controlled sample holder, and a very fast photodiode (response time 150 ps). They calculated the radiative

recombination rate using Kane's $\mathbf{k \cdot p}$ method (Kane, 1966:75-100) incorporating parabolic and later, non-parabolic band models. The carrier density range studied was from 4×10^{16} cm^{-3} to 2×10^{19} cm^{-3}. They presented analytic calculations for the number of carriers generated in the region of interest, as well as a means of extracting the non-radiative recombination rate from the time dependent luminescence (τ_l). The relationship of Auger recombination to the temperature parameter of a semiconductor laser (T_0) was emphasized.

In 1986, B. Sermage et.al. compared Auger recombination in bulk $Ga_{1-x}In_xAs$ to the experimentally measured Auger rate in $Ga_{1-x}In_xAs$ / $Al_{1-x}In_xAs$ double heterostructures and multiple quantum wells. No appreciable difference in the Auger recombination coefficient could be detected between the double heterostructure and the quantum well structures. The determination of carrier density and the determination of carrier lifetime were discussed in their paper. The 2D carrier sheet density and the 3D volumetric density are related by the quantum well (QW) thickness (t_{qw}) such that $N_{3D} = N_{2D}/t_{qw}$.

C.H. Henry et.al.(Henry, 1983) studied the luminescence decay in $In_yGa_{1-y}As_{1-x}P_x$ / InP double heterostructures with varying doping densities. The objective of this effort was to understand the radiative and non-radiative recombination mechanism in order to make a more efficient semiconductor laser and reduce its temperature dependence (T_0). The temporal dependence of the luminescence was measured using a fast Ge avalanche photodiode and a mode locked Ar ion laser. The response time of this system was reported to be 90 ps. They found the Shockley-Read-Hall recombination time to be over 200 ns. The Auger lifetime (which is not a valid way to view Auger recombination because Auger exhibits a very strong dependence on carrier density) was estimated at 8 ns for p-type material and about 20 ns in n-type material.

In 1983, A. Mozer *et al.* inferred Auger recombination from the split-off band process CHSH by quantifying the photoluminescence from the $h\nu = E_g + \Delta$ transition in

$Ga_{1-y}In_yAs_{1-x}P_x$/InP and $Ga_{1-y}Al_ySb_xAs_{1-x}$/GaSb laser material. The photon energy of interest was approximately 1.29-1.31 eV.

E. Wintner and E.P. Ippen studied what they called the "non-linear carrier dynamics," which directly implied in their case Auger recombination, for $Ga_xIn_{1-x}As_yP_{1-y}$ using a pump-probe technique (Wintner, 1984). The pump and probe were both from a Nd:YAG at 1.06 μm. This meant that in order to evaluate the data, a computer model was used that accounted for temporal development of the carrier density and absorption, the spatial averaging of bleaching, and a convolution with the probe beam. The temporal extent of the laser was 85 ps. The Auger coefficient was extracted as a fitting parameter.

M.E. Prise *et al.* in 1984 measured Auger recombination rates in $In_xGa_{1-x}As$ using a pump-probe technique. They pumped the $In_{0.53}Ga_{0.47}As$ sample with a Nd:YAG optical parametric amplifier ($LiNbO_3$) at the band edge corresponding to $\lambda = 1.67$ μm. The recombination due to traps was ignored, and the radiative recombination rate was calculated using Kane's **k•p** method (Kane, 1966).

Auger recombination rates were experimentally determined by Hausser *et al.* in bulk and quantum wells composed of $In_xGa_{1-x}As$ using the frequency up-conversion technique (Hausser, 1990). The Auger coefficient was determined as a fitting parameter along with the Shockley-Read-Hall coefficient. The radiative recombination was again determined from a **k•p** calculation based on a model they developed previously (Zielinski, 1987 and 1989). Although they display a luminescence spectrum from their sample obtained using upconversion at 0.5 nsec, the luminescence *decay* curves are obtained from a spectrally *integrated* luminescence signal. The carrier density for a given excitation was determined by fitting the spectral shape of their measured luminescence at 500 psec to a model of the laser structure that predicted the luminescence spectral line shape. They believe the accuracy of their carrier density to be within 5% of the actual carrier density.

Time-resolved photoconductivity measurements have also been used to extract Auger recombination rates. I.H. Campbell et.al., in 1991 studied the far infrared photoresponse of a InAs/$Ga_{1-x}In_xSb$ superlattice using temporally resolved photoconductivity measurements. They measured two time constant responses, one at approximately 2 ns and a much slower recombination at approximately 2 µs. Both time constants were attributed to Shockley-Read-Hall mechanisms.

A research group at the Naval Research Laboratory lead by E.R. Youngdale and J.R. Meyer, collaborated with theoreticians from Chicago and Harvard to study Auger recombination in InAs - $Ga_{1-x}In_xSb$ superlattices (Youngdale, 1994). The experimental technique used was a time resolved photoconductive response technique (Youngdale, 1993). At low excitation levels, they measured a carrier lifetime less than 10 ns and attributed it to Shockley-Read-Hall recombination centers. The Shockley-Read-Hall seems to be dominant over the radiative recombination due to the large number of interface states. At high excitation levels, the carrier lifetime decreased and matched the theoretical Auger trend. The thrust of the paper was to directly compare $Hg_{1-x}Cd_xTe$ with InAs - $Ga_{1-x}In_xSb$ for long wavelength infrared detector applications.

E.R. Youngdale et. al. continued their investigation of InAs - $Ga_{1-x}In_xSb$ and InAs - GaSb superlattices by measuring the temporal photoconductive response at liquid nitrogen temperatures (77K) and room temperature (Youngdale, 1994). They calculated the Auger recombination coefficient as a fitting parameter, along with the Shockley-Read-Hall lifetime (τ_{SRH}) and found that for low excitation levels, the carrier lifetime τ_{SRH} was 0.13 nsec in InAs - GaSb and 6 ns in InAs - $Ga_{1-x}In_xSb$. The short τ_{SRH} in the InAs - GaSb is attributed to defect centers in InAs-based heterostructures, about which little is known. At high excitation levels they fit the Auger coefficient to meet their data. Radiative recombination was not mentioned or considered, an potentially serious shortcomming of this technique and their results. In their defense, theoretical investigations of the InAs - $Ga_{1-x}In_xSb$ superlattice (Grein, 1993) indicate that for high

carrier concentrations at 77K, radiative recombination is approximately one order of magnitude lower than the Auger recombination rate.

It is worth noting some of the work from the German group led by Hausser, Zielinski and Fuchs. In addition to being one of only two groups to use the "upconversion" technique to characterize Auger recombination in quantum wells (Hausser, 1990; Fuchs, 1991), a paper in the IEEE Journal of Quantum Electronics (Zielinski, 1989) is of particular interest. In this paper they measure CHSH Auger rates by monitoring the luminescence from the radiative recombination between the conduction and split-off band ($hv = E_g + \Delta$). This is possible because the CHSH Auger process results in hole states in the split-off band. By varying the carrier density while monitoring the E_g emission and the $E_g + \Delta$ emission, they were able to determine the recombination coefficients associated with Shockley-Read-Hall (A_{SRH}), radiative (B_{rad}) and Auger (C_{Auger}). Using their experimentally obtained values of the recombination rates with their model, they demonstrate the accuracy and utility of their model by calculating threshold current density as a function of temperature.

A.3.2. Current State of Auger Recombination Research

The best analysis of time resolved luminescence related to Auger recombination has been done by Sermage et al (Sermage, 1983; 1984; 1985; 1986). Their experiment and analysis included 1) detailed analysis of the determination of carrier concentration resulting laser excitation, 2) consideration of the dependence of carrier ambipolar diffusion on carrier concentration, and 3) deviation of the radiative rate when the quasi-Fermi level enters the bands (e.g. $R_{rad} \neq Bn^2$ but rather $R_{rad} = Bn^{\gamma+1}$).

The group from Germany, led by Hausser and Fuchs, used the upconversion technique for time resolved luminescence (Hausser, 1990) (Fuchs, 1991) and seem to have obtained reasonable Auger recombination results. They claim to have considered the appropriate issues, however, their papers lacked the clarity demonstrated by Sermage

et al. regarding key elements related to their analysis. They claim to have done a calculation for the radiative recombination rate as a function of carrier concentration, much like Sermage *et al.*, and they cite references that outline their calculation (Zielinski, 1989; 1987), but leave the reader unsure of the details.

Table 2: Synopsis of experimental efforts for Auger and Shockley-Reed-Hall recombination coefficients.

Material	Structure	Method	Temp (K)	C_{Auger} $\times 10^{-29}$ (cm^6/s)	τ_{SRH} (ns)	Year	REF
Si	Bulk	TRPL	80	0.02		1972	Nilsson
InAs	Bulk	Decay	300			1974	Dalal
Ge	Bulk	TR-FCA	300	0.011		1975	Auston
GaAs	Bulk	TRPL	77	0.01		1976	Benz
GaSb	Bulk	TRPL	77	10000		1976	Benz
GaSb	Bulk	spin	77	2.5		1981	Titkov
InGaAsP	Bulk	TRPL	300	2.3		1983	Sermage
InGaAs	Bulk	P-Probe	300	25.0		1984	Prise
InGaAsP	Bulk	TRPL		2.6		1985	Sermage
InGaAsP/InP	MQW	f - Resp	300	3.3		1986	Olshansky
InGaAs	Bulk	TRPL		7.0		1986	Sermage
InGaAs-AlInAs	MQW	TRPL		6.0		1986	Sermage
GaSb	Bulk	TRPL	250	30		1989	Snow
InGaAs	Bulk	TRPL	300	32.0		1990	Hausser
InGaAs/InP	MQW	TRPL	300	0.9		1990	Hausser
GaSb/AlSb	MQW	TRPL		48.0		1991	Fuchs
InAs	Bulk	P-Probe	77	1000		1992	Vodopyan
InGaAsP/InP	MQW	f - Resp	300	4		1993	Dapkus
InGaAsP/InP	MQW	Eg+Δ	300	5		1993	Mozer
InAs/GaInSb	SL	TRPC	300	80000	6	1993	Youngdale
InAs/GaInSb	SL	TRPC	77	130	6	1994	Youngdale
InAs/GaSb	SL	TRPC	300		0.13	1994	Youngdale
InAs(Sb)	MQW	TRPC	77/300	2100	14	1995	Lindle
GaInSb/InAs	LS	P-Probe	300	700	4.1	1995	McCahon

A.4. Ultrafast Spectroscopy and Upconversion Experiments

A.4.1. Early Work - Before 1990

The idea for the upconversion technique originally came from Midwinter and Warner in 1966 (Midwinter, 1967). They used $LiNbO_3$ to upconvert the emission spectrum of a mercury lamp with a ruby laser. The researchers credited with first using the "upconversion" technique as a "light gate" are Mahr and Hirsch of Cornell in 1975 (Mahr, 1975). They used an ADP crystal to measure sub-nanosecond optical pulses from

a mode-locked dye laser. The temporal resolution from their system was estimated to be 20 ps.

The upconversion technique was not applied to study the luminescence of solids until 1984 when Kash and Shah (Kash, 1984) measured carrier relaxation from the luminescence temporal decay of $In_{0.53}Ga_{0.47}As$. They used 10mm thick $LiIO_3$ crystal as the non-linear medium and calibrated the spectral response of the crystal/spectrometer system by using a tungsten lamp as an infrared source.

In 1986, Jagdeep Shah began working with Block and Gossard of AT&T Bell Labs studying ultrafast phenomena in GaAs using the upconversion technique (Shah, 1986). With a Rh 6G dye laser operating at 617 nm they obtained a pulse width of ~350 fs with an average power of 7 mW. They used a 2 mm thick $LiIO_3$ for mixing the frequencies.

In 1986, a French group led by Hulin (Hulin, 1986) demonstrated luminescence upconversion using a nonlinear organic crystal NPP [N-(4 nitrophenyl) - (L) - prolinol]. The transparency range extends from 0.5 to 2 µm and was used to upconvert luminescence from $In_xGa_{1-x}As$. The efficiency of NPP is high and so they were able to upconvert using a spot size of 1 mm^2 with a laser pulse duration of 100 fs. The thrust of the paper was the use of NPP as a nonlinear upconversion crystal.

In May of 1987, Shah, Damen, Deveaud and Block published an oft cited *Applied Physics Letter* (Shah, 1987) using the upconversion technique. In their experiment, they studied room temperature GaAs by collecting photoluminescence with Cassegrainian optics in order to keep the group velocity dispersion (GVD) to a minimum. The laser was a dye laser pumped by a frequency doubled Nd:YAG, modified to get ~80 mW of average power. $LiIO_3$ was again used with an upconversion luminescence bandwidth for a given θ of about 10-20 meV. The principle intent of this effort was to demonstrate upconversion with very short time scales.

In 1987, Deveaud, Shah, Damen, Lambert & Regreny used the ultrafast upconversion to study transport of electrons and holes in superlattice mini-bands (Deveaud, 1987). Using the same experimental set up, they observed time evolution of luminescence from a graded $Al_xGa_{1-x}As$ sample. They presented time resolved luminescence spectra at various delays for a 20nm/20nm stepwise, graded-gap superlattice sample of GaAs/AlGaAs. The average power used was 2 mW with a pulse width less than 300 fs. The emphasis of this paper is on understanding electron transport rather than the experimental details of ultrafast spectroscopy and upconversion.

Later in 1987, Deveaud, Damen, Shah and Tu used the upconversion technique to study the dynamics of excitons in $GaAs/Al_xGa_{1-x}As$ quantum wells (Deveaud, 1987). The same system was used (Rh6G laser, $LiIO_3$, 300 fs pulse width with ~400 fs temporal resolution). They showed that excitons travel from narrow regions in quantum wells to wider regions of the well in ~250 ps.

Shah *et al.*, using the same experimental set up, studied the inter-valley scattering rates in GaAs. In this effort he collaborated with an Italian theoretician to compare theory with experiment. They found that the spectra at 1, 2, and 10 ps can be well fitted by thermalized (Fermi-Dirac type) distribution functions with temperatures larger than the lattice temperature. One of the interesting findings was that the luminescence intensity near the band-gap shows significant increase for nearly 10 ps after the end of the excitation pulse.

In 1988, Jagdeep Shah wrote a frequently cited paper for the IEEE Journal of Quantum Electronics on ultrafast luminescence spectroscopy (Shah, 1988). This paper could justifiably be titled "everything you need to know about upconversion spectroscopy."

The longest wavelength upconversion to date was done at Brown University by Heyen, Hagerott & Nurmikko with some assistance from Partin of the General Motors Research Lab. They successfully used $AgGaS_2$ to upconvert luminescence from PbTe

quantum wells to determine the radiative recombination rate. The transient PL signals they measured were taken from the peak of the steady state infrared spectrum corresponding to hν ~255-310 meV (λ = 4.0 to 4.9). The laser used in their experiment was a mode-locked cw Nd:YAG (λ = 1.06 μm) with a pulse width of ~ 100 ps and an average power of 100 mW.

Researchers at Cornell University presented an upconversion experiment in 1989 by using a 1 mm thick barium meta-borate (BBO) crystal and Cassegrainian collection optics. Wise and Tang (Wise, 1989) studied relaxation of hot electrons in room temperature GaAs quantum wells with a 60 fs temporal resolution. Their emphasis was on temporal resolution with some discussion of the laser bandwidth and the upconverted bandwidth. For a 40 fs pulse, the transform-limited bandwidth is 30 meV. Their results were consistent with Shah *et al.* who studied carrier relaxation or "thermalization."

At the March 1989 Optical Society of America's Picosecond Electronics & Optoelectronics conference, Oberli with Shah *et al.* presented two papers using the upconversion technique. In the first they studied tunneling and perpendicular transport of carriers in GaAs/Al$_x$Ga$_{1-x}$As superlattices (Oberli, 1989a). In the second, they studied optical phonon assisted tunneling in double quantum well structures (Oberli, 1989b). The emphasis on both these papers was tunneling and transport, with virtually no discussion of the experimental details for the upconversion experiment.

Jagdeep Shah ended 1989 with a review paper in *Superlattices and Microstructures* titled "Ultrafast Studies of Carrier Relaxation in Semiconductors and their Microstructures" (Shah, 1989). No new experiments were reported, rather a review of hot carrier dynamics, theory and experiments was presented. It is worth noting here that in 1992 Jagdeep Shah edited a book for the Academic Press entitled "Hot Carriers in Semiconductor Nanostructures" (Shah, 1992).

A.4.2. Recent Work - Since 1990

Chronologically the next upconversion experiment was by Hausser *et al.* and was significant because their purpose was to determine Auger recombination rates in $In_xGa_{1-x}As$ and $In_xGa_{1-x}As/InP$ quantum wells. This paper will be discussed in greater detail in the Auger Recombination section. Their upconversion experiment was done with a mode-locked, Q-switched Nd:YAG laser operating at 1.06 μm with a pulse width of about 150 ps. The excitation laser spot on the sample was estimated to be 30 μm. Each data point in their TRPL trace represents the integrated intensity of a complete luminescence spectrum at a given delay time.

The 20th International Conference on "The Physics of Semiconductors" held in Thessaloniki, Greece in August of 1990 contained several papers that used the upconversion technique. Freeman *et al.* of IBM used the upconversion technique to study spin polarization in $GaAs/Al_xGa_{1-x}As$ quantum wells (Freeman, 1990). They found that the "polarization decay time" is much shorter in quantum wells than in bulk material. No experimental details of the upconversion technique were given.

At Thessaloniki, Benoit Deveaud presented a study on the luminescence from quantum wells (Deveaud, 1990). In it he studied the relaxation processes in two-dimensional quantum structures including radiative recombination, momentum relaxation, and carrier distributions. He also presented results of carrier tunneling between asymmetric quantum wells for on and off resonant structures. His experimental set up consisted of a double jet dye laser pumped with a frequency doubled YAG laser. The average power from this system is 500 mW. Luminescence was collected by two off axis parabolic mirrors.

Hot carrier relaxation was studied by Zhou *et al.* using a 1mm thick BBO crystal in the luminescence upconversion experiment, and was presented at Thessaloniki in 1990. Their ultrafast laser (temporal pulse = 50 fs with $\lambda \sim 630$ nm) and dispersion free luminescence collection system resulted in a time resolution better than 80 fs. They

concluded that in InP and GaAs with carrier densities between 2 x 10^{16} cm^{-3} and 2 x 10^{18} cm^{-3}, carrier-carrier scattering governs the initial relaxation leading to a Maxwellian-like broad carrier distribution during the first 100 fs.

The final paper related to the upconversion technique presented at Thessaloniki in 1990 was a review of ultrafast tunneling in quantum well structures by Jagdeep Shah *et al.* (Shah, 1990).

The third of three papers that used the upconversion technique to study Auger recombination rates, also by the group from Germany led by Hausser, was published in 1991 by Fuchs *et al.*(Fuchs, 1991). In this paper, GaSb/AlSb multiple quantum well structures (MQW) were studied using the upconversion technique with a simultaneously Q-switched and mode locked Nd:YAG laser with a pulse width of 100 psec. Stimulated emission is avoided, as in the similar research efforts, by focusing the excitation spot down to a diameter of about 20 μm. The thickness of the GaSb/AlSb quantum well was $L_z \geq 4.0$ nm. The strain associated with this system based on lattice mismatch between GaSb and AlSb is 0.65%. Their results indicate a strong influence of the small energetic separation (90 meV) between the Γ-valley and the L-valleys. As a result, the carriers excited into the Γ minimum are scattered on a time scale estimated to be about 1 psec, into the four L-valleys. This pins the quasi-Fermi level near the band edge of the L minima. These qualitative arguments explain both the comparatively narrow spectra and the lack of higher sub-band transitions seen during this investigation. The room temperature Auger recombination coefficient they estimated was $C = 4\times10^{-28}$cm^{6}s^{-1}. The Auger coefficient C_{Auger} exhibited a monotonic increase with temperature up to 400K in contrast with theory for this system. In their analysis of data, they used a least-squares fit and monitored the PL spectra 500 psec after excitation because they believed the momentum relaxation of the carriers is completed within an accuracy of 5 %.

At the International Symposium on Ultrafast Processes in Spectroscopy (Bayreuth, 1991) there were three papers that used the upconversion technique. Gale *et*

al. (Gale, 1992) studied minority carrier behavior in bulk doped semiconductors using a synchronously pumped dye laser operating at 620 nm, a pulse width of 65 fsec and an average power of 30 mW. The total system temporal response was estimated to be 90 fsec using the 100 μm thick urea crystal. The samples studied were n-doped GaAs and p-doped InP.

The second paper using upconversion at the International Symposium on Ultrafast Processes in Spectroscopy in 1991 was given by Zhou and Kurz (Zhou, 1991). They used a colliding pulse mode locked ring dye laser (CPM-laser) with a pulse width of 50 fsec, average power 25 mW and $\lambda \sim 610.0$ nm to study MOCVD grown GaAs and InP doped (both n and p doping) samples. As in the Gale paper (Gale, 1992) excitation levels are small relative to the doping level.

The final upconversion paper from the International Symposium on Ultrafast Processes in Spectroscopy in 1991 was given by Elsaesser, Shah, Rota and Lugli (Elsaesser, 1992). The information contained in their conference paper is virtually identical to their Physical Review Letter dated 1 April 1991 (Elsaesser, 1991) and the experimental results reported in a Physical Review B paper in February 1993 (Shah, 1993) The emphasis in the 1993 paper was the Monte Carlo simulations of carrier scattering and thermalization processes. In their study of thermalization in GaAs and InP, they used a dye laser emitting at 644.0 nm, a 0.5 mm thick $LiIO_3$ crystal, and obtained a 100 fsec temporal resolution

In 1992, Kersting *et al.* studied carrier transport and capture in $In_xGa_{1-x}As/InP$ heterostructures using the upconversion technique (Kersting, 1992a and 1992b). In their experiments, they used a CPM-laser with a pulse width of 80 fsec, average power 25 mW and $\lambda \sim 630.0$ nm. The non-linear crystal they used was a 1 mm thick β-barium borate (BBO) and the overall temporal resolution obtained was estimated to be shorter than 100 fsec. The spectral response of their setup was calibrated with a tungsten lamp.

Kersting *et al.* continued to study carrier dynamics using the upconversion technique in $In_xGa_{1-x}As/InP$ heterostructures in 1992 (Kersting, 1992) with a Kerr-lens mode-locked Ti:Sapphire laser ($\lambda = 710$ nm). The time resolution in these experiments is estimated to be 150 fsec. In this study, the transfer times of electrons and holes from barriers to wells in *strained* $In_xGa_{1-x}As/InP$ multiple quantum wells were reported. Few additional details of the experiment were provided.

In 1993, Kersting *et al.* used the upconversion technique to study carrier transport in GaAs metal-semiconductor-metal devices (MSM) Schottky diodes (Kersting, 1993). They found the time resolved luminescence signal depends strongly on bias voltage and carrier density.

In *Optical and Quantum Electronics* vol. 26, Kersting *et al.* provide an invited paper on carrier dynamics in $In_xGa_{1-x}As/InP$ heterostructures with an emphasis on applications to semiconductor lasers (Kersting, 1994). There did not appear to be any new data in this paper; rather it was a re-packaging of their previous data using the colliding pulse mode locked ring dye laser (CPM-laser $\lambda = 630$ nm) and the Kerr-lens mode-locked Ti-Sapphire laser ($\lambda = 710$ nm).

In that same issue of *Optical and Quantum Electronics*, Deveaud *et al.* present upconversion data illustrating the quantum mechanical versus semi-classical capture and transport properties in quantum well lasers (Deveaud, 1994). They used a hybrid dye laser to generate 600 fsec pulses centered around λ=603.4 nm. Using a compression prism system, they obtain a temporal resolution of 120 fsec. Using simple diffusion equations, they fit the observed data well. Real semiconductor laser structures were also discussed.

An obvious application of the upconversion technique is in the measurement of carrier lifetimes for low temperature grown GaAs and $In_xGa_{1-x}As$. Krotkus *et al.* used a mode-locked Ti:Sapphire with a central wavelength of $\lambda = 770$ nm, a 1 mm thick $LiIO_3$ crystal and off-axis parabolic mirrors to obtain a temporal resolution estimated to be 200

fsec (Krotkus, 1994). The hole and electron traps were measured, and found to have lifetimes on the order of 18 to 60 psec. The $In_xGa_{1-x}As$ samples used in their study were grown via MOCVD. The wavelength of the luminescence before upconversion was $\lambda_{IR} =$ 1.7 μm. All their measurements were performed at room temperature.

A review article worth noting was published in the International Journal of Modern Physics B in 1991 by Ockman, Wang and Alfano (Ockman, 1991). They discussed time resolved luminescence measurements using streak camera, optical Kerr gate and the "upconversion gate" in some detail.

A.4.3. Current State of Research Using Upconversion

The upconversion technique is a powerful technique for studying temporal behavior of luminescent materials. It is a difficult technique requiring a significant capital investment (principally an ultrafast laser) and extreme care as the upconverted signals are typically small, particularly for upconversion with relatively long wavelength luminescence ($\lambda_{pl} > 2$ μm). The details of the upconversion process efficinecies are given in Chapter 5. One can readily see the dearth of reported upconversion results with luminescence beyond 2 μm, only two (Heyen, 1989 and Jang, 1997) in Table 3 (note λ_{signal} is used in Table 3 rather than λ_{pl} for generality). Because the luminescence from low band gap materials like InAsSb is longer than 2 μm, there are no reports of upconversion, or for that matter temporal luminescence, on InAsSb.

Table 3: Synopsis of upconversion experiments performed to date that relate to studying semiconductors.

Application	Crystal	λ_{signal}	λ_{laser}	$\tau_{resolve}$	Peak	REF	Year
Demonstrate Principal	LiNbO$_3$	0.1.7	0.694	10 ns		Midwinter	1966
Laser Pulse Profile	ADP	0.515	0.600	20 ps	50 W	Mahr	1975
Laser Pulse Profile	LiIO$_3$	0.85	0.620	1 ps		Duguay	1982
Carrier Relaxation	LiIO$_3$	1.53	0.610	10 ps	200 W	Shah	1984
Luminescence from QW	NNP/1	1-1.6	0.620	100 fs		Hulin	1986
Carrier Relaxation GaAs	LiIO$_3$	0.870	0.617	350 fs	5.0 kW	Shah	1986
PL from GaAs	LiIO$_3$	0.800	0.610	400 fs	3.3 kW	Shah	1987
Inter-valley Scattering	LiIO$_3$	0.87	0.608	500 fs	3.3 kW	Shah	1987
Bloch Transport	LiIO$_3$	0.74	0.610	400 fs	81 W	Deveaud	1987
Laser Pulse Profile	ADP	0.515	0.600	20 ps	50 W	Mahr	1975
Carrier Relaxation	LiIO$_3$	1.53	0.610	10 ps	200 W	Shah	1984
Luminescence from QW	NNP/1	1-1.6	0.620	100 fs		Hulin	1986
Carrier Relaxation GaAs	LiIO$_3$	0.870	0.617	350 fs	5.0 kW	Shah	1986
PL from GaAs	LiIO$_3$	0.800	0.610	400 fs	3.3 kW	Shah	1987
Inter-valley Scattering	LiIO$_3$	0.87	0.608	500 fs	3.3 kW	Shah	1987
Bloch Transport	LiIO$_3$	0.74	0.610	400 fs	81 W	Deveaud	1987
Exciton Transfer QW	LiIO$_3$	0.732	0.610	400 fs	6.1 kW	Deveaud	1987
Radiative Rec PbTe	AgGaS$_2$	4.0-4.8	1.064	100 ps	20 W	Heyen	1989
Auger GaSb	LiIO$_3$	1.55	0.607	3 ps		Snow	1989
Carrier Relaxation inQW	BBO	0.870	0.636	60 fs		Wise	1989
Exciton Life InGaAs QW	LiIO$_3$	1.0	1.064	180 ps		Cebulla	1989
Tunneling and Transport				700 fs		Oberli	1989
Phonon-assisted tunneling	LiIO$_3$	0.800	0.725	750 fs		Oberli	1989
QW-Capture		0.639		800 fs	10 kW	Deveaud	1990
Relaxation GaAs & InP	BBO	0.920	0.630	80 fs		Zhou	1990
Spin-Polarization in QW	LiIO$_3$	0.790	0.670	1 ps		Freeman	1990
Polarization magnetic QW	LiIO$_3$	0.790	0.670	150 fs	10 kW	Freeman	1990
Auger in InGaAs		1.2-1.7	1.064	150 ps		Hausser	1990
Auger GaSb/AlSb QW		1.7	1.064	100 ps		Fuchs	1991
Relaxation in GaAs	LiIO$_3$	0.7-0.9	0.642	100 fs		Elsaesser	1991
Relaxation- doped GaAs	BBO	0.920	0.620	100 fs		Zhou	1991
Relaxation-doped GaAs	Urea	0.7-0.9	0.620	90 fs	9.3 kW	Gale	1992
Relaxation in GaAs & InP	LiIO$_3$	0.7-0.9	0.642	100 fs		Elsaesser	1992
Strained InGaAs/InP	BBO	0.7-1.8	0.713	150 fs	3.7 kW	Kersting	1992
Transport-capture InGaAs	BBO	0.7-1.8	0.630	300 fs	3.7 kW	Kersting	1992
Transport-capture InGaAs	BBO	0.7-1.8	0.630	300 fs	3.7 kW	Kersting	1992
Relaxation in GaAs & InP	LiIO$_3$	0.920	0.642	120 fs		Shah	1993
Transport in GaAs MSM	BBO	0.855	0.710	100 fs	3.7 kW	Kersting	1993
Dynamics in InGaAs/InP	BBO	0.7-1.8	0.630	300 fs		Kersting	1994
Low Temp CVD InGaAs	LiIO$_3$	0.8-1.7	0.770	100 fs	18.7 kW	Krotkus	1994
PPPV polymers	BBO	0.7-0.8	0.795	150 fs	70 W	Mollay	1994
Carrier Dynamics in QW		0.7-0.8	0.603	120 fs		Deveaud	1994
Relaxation in GaInSb SL	KTA	2.3	0.840	140 fs		Jang	1997

Quantum Well Calculation

**Bill Cooley
Appendix B**

Constants & Units

$k \equiv 1.380658 \cdot 10^{-23} \cdot J \cdot K^{-1}$ $eV \equiv 1.60217733 \cdot 10^{-19} \cdot J$ $nm \equiv 10^{-9} \cdot m$ $\mu m \equiv 10^{-6} \cdot m$ $ps := 10^{-12} \cdot s$ $Ang := 10^{-10} \cdot m$

$h \equiv 6.6260755 \cdot 10^{-34} \cdot J \cdot s$ $hbar := h \cdot (2 \cdot \pi)^{-1}$ $\varepsilon_0 \equiv 8.854187817 \cdot 10^{-12} \cdot F \cdot m^{-1}$ $ns := 10^{-9} \cdot s$ $meV := 10^{-3} \cdot eV$

$q_c \equiv 1.60217733 \cdot 10^{-19} \cdot C$ $m_e \equiv 9.1093897 \cdot 10^{-31} \cdot kg$ $c \equiv 2.99792458 \cdot 10^8 \cdot m \cdot s^{-1}$ $h \cdot c = 1.2398424 \text{ eV} \cdot \mu m$

Well Composition => $x_{well} := 0.065$

Well Width   => $L := 10 \cdot nm$ $a := L \cdot 2^{-1}$

Barrier Composition
"y" => Al mole fraction => $x_{bar} := 0.1$
"x" => Sb mole fraction => $y_{bar} := 0.15$

	InAs	**InSb**	**InAs$_{1-x}$Sb$_x$**
Lattice Constant:	$a_{InAs} := 6.0583 \cdot Ang$	$a_{InSb} := 6.47937 \cdot Ang$	
Dielectric Constant:	$\varepsilon_{InAs} := 12.25 \cdot \varepsilon_0$	$\varepsilon_{InSb} := 15.68 \cdot \varepsilon_0$	
Luttinger parameters:	$\gamma 1_{InAs} := 19.7$	$\gamma 1_{InSb} := 35$	
	$\gamma 2_{InAs} := 8.4$	$\gamma 2_{InSb} := 15.7$	
	$\gamma 3_{InAs} := 9.28$	$\gamma 3_{InSb} := 16.8$	
Stiffness parameters:	$c11_{InAs} := 8.329$	$c11_{InSb} := 6.918$	$c11(x) := c11_{InAs} \cdot (1 - x) + c11_{InSb} \cdot x$
	$c12_{InAs} := 4.526$	$c12_{InSb} := 3.788$	$c12(x) := c12_{InAs} \cdot (1 - x) + c12_{InSb} \cdot x$
	$c44_{InAs} := 3.96$	$c44_{InSb} := 3.02$	
Valence Band: Deformation potentials	$A_{InAs} := -5.8 \cdot eV$	$A_{InSb} := -7.7 \cdot eV$	$A(x) := A_{InAs} \cdot (1 - x) + A_{InSb} \cdot x$
	$B_{InAs} := -1.8 \cdot eV$	$B_{InSb} := -2.0 \cdot eV$	$B(x) := B_{InAs} \cdot (1 - x) + B_{InSb} \cdot x$

Effective Masses:
(m_c, m_{hh}, m_{lh}) $m_{InAs} := (0.0231 \quad 0.35 \quad 0.026)^T \cdot m_e$ $m_{InSb} := (0.0136 \quad 0.34 \quad 0.0158)^T \cdot m_e$

$m_{well}(x) := x \cdot m_{InSb} + (1 - x) \cdot m_{InAs}$

$me_{well} := m_{well}(x_{well})_0$ $mhh_{well} := m_{well}(x_{well})_1$ $mlh_{well} := m_{well}(x_{well})_2$

$m_{well} := [me_{well} \quad mhh_{well} \quad mlh_{well}]^T$

$m_{2dvds} := mhh_{well} + mlh_{well}$ $m_{3dvds} := (mhh_{well}^{1.5} + mlh_{well}^{1.5})^{\frac{2}{3}}$

Energy: $Eg0_{InSb} := 0.236 \cdot eV$ $Eg0_{InAs} := 0.418 \cdot eV$

$\Delta_{InSb} := 0.85 \cdot eV$ $\Delta_{InAs} := 0.38 \cdot eV$ $Eg0_{Mar} := 0.322 \cdot eV$

$\alpha_{InAs} := 0.38 \cdot meV \cdot K^{-1}$ $\alpha_{InSb} := 0.6 \cdot meV \cdot K^{-1}$ $\alpha_{Mar} := 0.26 \cdot meV \cdot K^{-1}$

$\beta_{InAs} := 215 \cdot K$ $\beta_{InSb} := 500 \cdot K$ $\beta_{Mar} := 113 \cdot K$

$Eg_{InAs}(T) := Eg0_{InAs} - \dfrac{\alpha_{InAs} \cdot T^2}{\beta_{InAs} + T}$ $Eg_{InSb}(T) := Eg0_{InSb} - \dfrac{\alpha_{InSb} \cdot T^2}{\beta_{InSb} + T}$

Set Temperature=> $T := 77 \cdot K$

Using Marciniak's Data => $Eg(T) := Eg0_{Mar} - \dfrac{\alpha_{Mar} \cdot T^2}{\beta_{Mar} + T}$ $E_g := Eg(T)$

$\Delta(x) := x \cdot \Delta_{InSb} + (1 - x) \cdot \Delta_{InAs} - x \cdot (1 - x) \cdot 1180 \cdot meV$ $E_g = 313.887 \text{ meV}$

Barrier Information In$_{1-y}$Al$_y$As$_{1-x}$Sb$_x$: $Eg_{AlSb} := 2.3 \cdot eV$ $Eg_{AlAs} := 3.13 \cdot eV$

$$bow_{bar}(x,y) := x \cdot (1 - x) \cdot 680 \cdot meV + y \cdot (1 - y) \cdot 670 \cdot meV$$

$$Eg_{bar}(x,y) := x \cdot y \cdot Eg_{AlSb} + x \cdot (1 - y) \cdot Eg0_{InSb} + (1 - x) \cdot y \cdot Eg_{AlAs} + (1 - x) \cdot (1 - y) \cdot Eg0_{InAs} - bow_{bar}(x,y)$$

$$Eg_{bar}(x_{bar}, y_{bar}) = 650.255 \cdot meV$$

Effective Masses:

$$m_{AlSb} := (0.259 \quad 0.336 \quad 0.123)^T \cdot m_e \qquad m_{AlAs} := (0.15 \quad 0.409 \quad 0.153)^T \cdot m_e$$

$$m_{bar}(x,y) := x \cdot y \cdot m_{AlSb} + x \cdot (1 - y) \cdot m_{InSb} + (1 - x) \cdot y \cdot m_{AlAs} + (1 - x) \cdot (1 - y) \cdot m_{InAs}$$

$$me_{bar} := m_{bar}(x_{bar}, y_{bar})_0 \qquad mhh_{bar} := m_{bar}(x_{bar}, y_{bar})_1 \qquad mlh_{bar} := m_{bar}(x_{bar}, y_{bar})_2$$

$$m_{bar} := \begin{bmatrix} me_{bar} & mhh_{bar} & mlh_{bar} \end{bmatrix}^T$$

Band Offset (measured relative to well valence band)

Conduction band (75%) => $EC1 := Eg(T) + 0.75 \cdot (Eg_{bar}(x_{bar}, y_{bar}) - Eg(T))$

Valence Band   (25%) => $EV1 := -0.25 \cdot (Eg_{bar}(x_{bar}, y_{bar}) - Eg(T))$

Accounting for Strain

Poison ratio => $\sigma(x) := \dfrac{c11(x)}{2 \cdot c12(x)}$

Strain => $\varepsilon_{11}(x) := \dfrac{a_{InAs}}{a_{InAs} \cdot (1 - x) + a_{InSb} \cdot x} - 1$ $\varepsilon_z(x) := \dfrac{-\varepsilon_{11}(x)}{\sigma(x)}$

$$\varepsilon_{11}(x_{well}) = -0.45 \cdot \% \qquad\qquad \varepsilon_z(x_{well}) = 0.489 \cdot \%$$

Energy Shifts due to Strain

$$E_{hh}(x) := \left[2 \cdot A(x) \cdot \left(\frac{c12(x) - c11(x)}{c11(x)} \right) + B(x) \cdot \left(\frac{c11(x) + 2 \cdot c12(x)}{c11(x)} \right) \right] \cdot \varepsilon_{11}(x) \qquad E_{hh}(x_{well}) = -7.297 \cdot meV$$

$$E_{lh}(x) := \left[2 \cdot A(x) \cdot \left(\frac{c12(x) - c11(x)}{c11(x)} \right) - B(x) \cdot \left(\frac{c11(x) + 2 \cdot c12(x)}{c11(x)} \right) \right] \cdot \varepsilon_{11}(x) \qquad E_{lh}(x_{well}) = -41.335 \cdot meV$$

$$E_{so}(x) := \left(2 \cdot A(x) \cdot \frac{c12(x) - c11(x)}{c11(x)} \right) \cdot \varepsilon_{11}(x) \qquad\qquad E_{so}(x_{well}) = -24.316 \cdot meV$$

Well Depth - Note, all Energies are measured relative to the unstrained valence band.

$$V_0 := EC1 - E_g \qquad\qquad V_1 := 0 \cdot meV + E_{hh}(x_{well}) - EV1 \qquad V_2 := 0 \cdot meV + E_{lh}(x_{well}) - EV1$$

Well Depth (e,hh,lh) => $V^T = \begin{bmatrix} 252.276 & 76.795 & 42.757 \end{bmatrix} \cdot meV$

The Square Well in One Dimension (modified Anderson, 1971)

Wave Functions

$$\Psi_I = A \cdot \exp(K_1 \cdot x)$$

$$\Psi_{II} = C \cdot \exp(i \cdot k_2 \cdot x) + D \cdot \exp(-i \cdot k_2 \cdot x)$$

$$\Psi_{III} = F \cdot \exp(-K_1 \cdot x)$$

Wave vectors

$$k_2 = \sqrt{\frac{2 \cdot m_{well} \cdot E}{hbar^2}} \qquad K_1 = \sqrt{\frac{2 \cdot m_{bar} \cdot (V - E)}{hbar^2}}$$

@ -a   **@ a**

$$\Psi_I = \Psi_{II} \qquad\qquad \Psi_{II} = \Psi_{III}$$

Boundary Conditions

$$\frac{1}{m_{bar}} \cdot \frac{d}{dx} \Psi_I = \frac{1}{m_{well}} \cdot \frac{d}{dx} \Psi_{II} \qquad \frac{1}{m_{well}} \cdot \frac{d}{dx} \Psi_{II} = \frac{1}{m_{bar}} \cdot \frac{d}{dx} \Psi_{III}$$

@ x = -L/2 or -a

$$A \cdot \exp(K_1 \cdot a) = C \cdot \exp(-i \cdot k_2 \cdot a) + D \cdot \exp(i \cdot k_2 \cdot a)$$

$$m_{bar}^{-1} \cdot A \cdot K_1 \cdot \exp(K_1 \cdot a) = m_{well}^{-1} \cdot C \cdot i \cdot k_2 \cdot \exp(-i \cdot k_2 \cdot a) - m_{well}^{-1} \cdot D \cdot i \cdot k_2 \cdot \exp(i \cdot k_2 \cdot a)$$

@ x = L/2 or a

$$F \cdot \exp(-K_1 \cdot a) = C \cdot \exp(i \cdot k_2 \cdot a) + D \cdot \exp(-i \cdot k_2 \cdot a)$$

$$-m_{bar}^{-1} \cdot F \cdot K_1 \cdot \exp(-K_1 \cdot a) = m_{well}^{-1} \cdot C \cdot i \cdot k_2 \cdot \exp(i \cdot k_2 \cdot a) - m_{well}^{-1} \cdot D \cdot i \cdot k_2 \cdot \exp(-i \cdot k_2 \cdot a)$$

Substituting for Aexp(K₁a):

$$K_1 \cdot m_{bar}^{-1} \cdot \left(C \cdot \exp(-i \cdot k_2 \cdot a) + D \cdot \exp(i \cdot k_2 \cdot a) \right) = m_{well}^{-1} \cdot \left(C \cdot i \cdot k_2 \cdot \exp(-i \cdot k_2 \cdot a) - D \cdot i \cdot k_2 \cdot \exp(i \cdot k_2 \cdot a) \right)$$

Substituting for Fexp(-K₁a):

$$-K_1 \cdot m_{bar}^{-1} \cdot \left(C \cdot \exp(i \cdot k_2 \cdot a) + D \cdot \exp(-i \cdot k_2 \cdot a) \right) = m_{well}^{-1} \cdot \left(C \cdot i \cdot k_2 \cdot \exp(i \cdot k_2 \cdot a) - D \cdot i \cdot k_2 \cdot \exp(-i \cdot k_2 \cdot a) \right)$$

Manipulating:

$$\frac{C}{D} = \frac{\left(K_1 \cdot m_{bar}^{-1} + i \cdot k_2 \cdot m_{well}^{-1} \right)}{\left(-K_1 \cdot m_{bar}^{-1} + i \cdot k_2 \cdot m_{well}^{-1} \right)} \cdot \exp(2 \cdot i \cdot k_2 \cdot a) \qquad \frac{C}{D} = \frac{\left(-K_1 \cdot m_{bar}^{-1} + i \cdot k_2 \cdot m_{well}^{-1} \right)}{\left(K_1 \cdot m_{bar}^{-1} + i \cdot k_2 \cdot m_{well}^{-1} \right)} \cdot \exp(-2 \cdot i \cdot k_2 \cdot a)$$

Multiplying:

$$\left(\frac{C}{D} \right)^2 = \left[\frac{\left(K_1 \cdot m_{bar}^{-1} + i \cdot k_2 \cdot m_{well}^{-1} \right)}{\left(-K_1 \cdot m_{bar}^{-1} + i \cdot k_2 \cdot m_{well}^{-1} \right)} \cdot \exp(2 \cdot i \cdot k_2 \cdot a) \right] \cdot \left[\frac{\left(-K_1 \cdot m_{bar}^{-1} + i \cdot k_2 \cdot m_{well}^{-1} \right)}{\left(K_1 \cdot m_{bar}^{-1} + i \cdot k_2 \cdot m_{well}^{-1} \right)} \cdot \exp(-2 \cdot i \cdot k_2 \cdot a) \right] = 1$$

Thus => $C = \sqrt{D^2}$ **or the two cases =>** $C = D$ $C = -D$

Case I (symetric) => $C = D$

$$\left[\left(K_1 \cdot m_{bar}^{-1} \right) \cdot \exp(2 \cdot i \cdot k_2 \cdot a) - -K_1 \cdot m_{bar}^{-1} \right] = \left[\left[i \cdot k_2 \cdot m_{well}^{-1} - \left(i \cdot k_2 \cdot m_{well}^{-1} \right) \cdot \exp(2 \cdot i \cdot k_2 \cdot a) \right] \right]$$

$$K_1 \cdot m_{bar}^{-1} \cdot \left(\exp(-i \cdot k_2 \cdot a) + \exp(i \cdot k_2 \cdot a) \right) = i \cdot k_2 \cdot m_{well}^{-1} \cdot \left(\exp(-i \cdot k_2 \cdot a) - \exp(i \cdot k_2 \cdot a) \right)$$

$$K_1 \cdot m_{bar}^{-1} = i \cdot k_2 \cdot m_{well}^{-1} \cdot \frac{\exp(-i \cdot k_2 \cdot a) - \exp(i \cdot k_2 \cdot a)}{\left(\exp(-i \cdot k_2 \cdot a) + \exp(i \cdot k_2 \cdot a) \right)} = k_2 \cdot m_{well}^{-1} \cdot \tan(k_2 \cdot a)$$

Recall => $\sin(\alpha) = \dfrac{\exp(i\alpha) - \exp(-i\alpha)}{2 \cdot i}$ $\cos(\alpha) = \dfrac{\exp(i\alpha) + \exp(-i\alpha)}{2}$

$$\tan(\alpha) = \frac{\exp(i\alpha) - \exp(-i\alpha)}{i \cdot (\exp(i\alpha) + \exp(-i\alpha))}$$

$$\cot(\alpha) = \frac{i \cdot (\exp(i\alpha) + \exp(-i\alpha))}{\exp(i\alpha) - \exp(-i\alpha)}$$

Lets Define convinient parameters=> $\alpha = a \cdot k_2 = a \cdot \sqrt{\dfrac{2 \cdot m_{well} \cdot E}{hbar^2}}$ $\beta := a \cdot \overrightarrow{\sqrt{\dfrac{2 \cdot m_{well} \cdot V}{hbar^2}}}$

$a \cdot K_1 = a \cdot \sqrt{\dfrac{2 \cdot m_{bar} \cdot (V - E)}{hbar^2}} = \sqrt{\dfrac{m_{bar}}{m_{well}} \cdot \left(\beta^2 - \alpha^2 \right)} = \sqrt{\dfrac{m_{bar}}{m_{well}}} \cdot \sqrt{\left(\beta^2 - \alpha^2 \right)}$ $\alpha \cdot \tan(\alpha) = \sqrt{\dfrac{m_{well}}{m_{bar}}} \cdot \sqrt{\left(\beta^2 - \alpha^2 \right)}$

Now we have the two cases, symetric and antisymetric =>

Putting in the numbers => $\beta^T = \begin{bmatrix} 1.929 & 4.196 & 0.843 \end{bmatrix}$ $-\alpha \cdot \cot(\alpha) = \left[\sqrt{\dfrac{m_{well}}{m_{bar}}} \cdot \sqrt{\left(\beta^2 - \alpha^2 \right)} \right]$
(m_c, m_{hh}, m_{lh})

Number of Bound Solutions => $sol := 1 + floor\left[\overrightarrow{\dfrac{\beta}{\left(\dfrac{\pi}{2}\right)}}\right]$ $sol = \begin{bmatrix} 2 \\ 3 \\ 1 \end{bmatrix}$

Defining convinient variables =>
$n := 0 .. \, sol_0 - 1$
$p := 0 .. \, sol_1 - 1 \qquad pq := 0 .. \left(sol_1 + sol_2 - 1 \right)$
$q := 0 .. \, sol_2 - 1$

Symmetric solution => $S(\alpha, i) := \left[\alpha \cdot \tan(\alpha) - \sqrt{\dfrac{m_{well_i}}{m_{bar_i}}} \cdot \sqrt{\left[\left(\beta_i \right)^2 - \alpha^2 \right]} \right]$

asymmetric solution => $aS(\alpha, i) := \alpha \cdot \cot(\alpha) + \sqrt{\dfrac{m_{well_i}}{m_{bar_i}}} \cdot \sqrt{\left[\left(\beta_i \right)^2 - \alpha^2 \right]}$

$f(\alpha, i, n) := \left| \, if(mod(n, 2) = 0, root(S(\alpha, i), \alpha), root(aS(\alpha, i), \alpha)) \, \right|$

Initial Guesses

$\alpha c_n := \pi \cdot (2.3)^{-1} + n \cdot \left(\pi \cdot 2^{-1} \right)$

$\alpha h_p := \pi \cdot (2.2)^{-1} + p \cdot \left(\pi \cdot 2^{-1} \right)$ **Now E(k) =>** $EK(k, m) := \dfrac{hbar^2 \cdot k^2}{2 \cdot m}$

$\alpha l_q := \pi \cdot (2.2)^{-1} + q \cdot \left(\pi \cdot 2^{-1} \right)$

Calculate α, k, E and EO (energy relative to origin) for each State:

$\alpha c_n := f\left(\alpha c_n, 0, n \right)$ $kc_n := \alpha c_n \cdot a^{-1}$

$\alpha h_p := f\left(\alpha h_p, 1, p \right)$ $kh_p := \alpha h_p \cdot a^{-1}$ $Kc_n := \sqrt{\dfrac{m_{bar_0}}{m_{well_0}}} \cdot \sqrt{\left[\left(\beta_0 \right)^2 - \left(\alpha c_n \right)^2 \right]} \cdot a^{-1}$

$\alpha l_q := f\left(\alpha l_q, 2, q \right)$ $kl_q := \alpha l_q \cdot a^{-1}$

$Kh_p := \sqrt{\dfrac{m_{bar_1}}{m_{well_1}}} \cdot \sqrt{\left[\left(\beta_1 \right)^2 - \left(\alpha h_p \right)^2 \right]} \cdot a^{-1}$ $Kl_q := \sqrt{\dfrac{m_{bar_2}}{m_{well_2}}} \cdot \sqrt{\left[\left(\beta_2 \right)^2 - \left(\alpha l_q \right)^2 \right]} \cdot a^{-1}$

The Quantized Energy relative to the "bottom" of the well (absolute value) are:

$Ec_n := EK\left(kc_n, m_{well_0} \right)$ $Ec^T = \begin{bmatrix} 57.934 & 224.513 \end{bmatrix} \cdot meV$

$Eh_p := EK\left(kh_p, m_{well_1} \right)$ $Eh^T = \begin{bmatrix} 6.949 & 27.235 & 58.179 \end{bmatrix} \cdot meV$

$El_q := EK\left(kl_q, m_{well_2} \right)$ $El^T = 22.888 \cdot meV$

Graphically the Solution is displayed below:

$$\alpha_p := 0.01, 0.02 .. \max(\beta)$$

$$\frac{\alpha_p \cdot \tan(\alpha_p)}{\left[-(\alpha_p \cdot \cot(\alpha_p))\right]}$$
$$\overline{\sqrt{\dfrac{m_{well_0}}{m_{bar_0}}} \cdot \sqrt{\left[(\beta_0)^2 - \alpha_p^2\right]}}$$
$$\overline{\sqrt{\dfrac{m_{well_1}}{m_{bar_1}}} \cdot \sqrt{\left[(\beta_1)^2 - \alpha_p^2\right]}}$$
$$\sqrt{\dfrac{m_{well_2}}{m_{bar_2}}} \cdot \sqrt{\left[(\beta_2)^2 - \alpha_p^2\right]}$$

$$\frac{\alpha_p}{\pi}$$
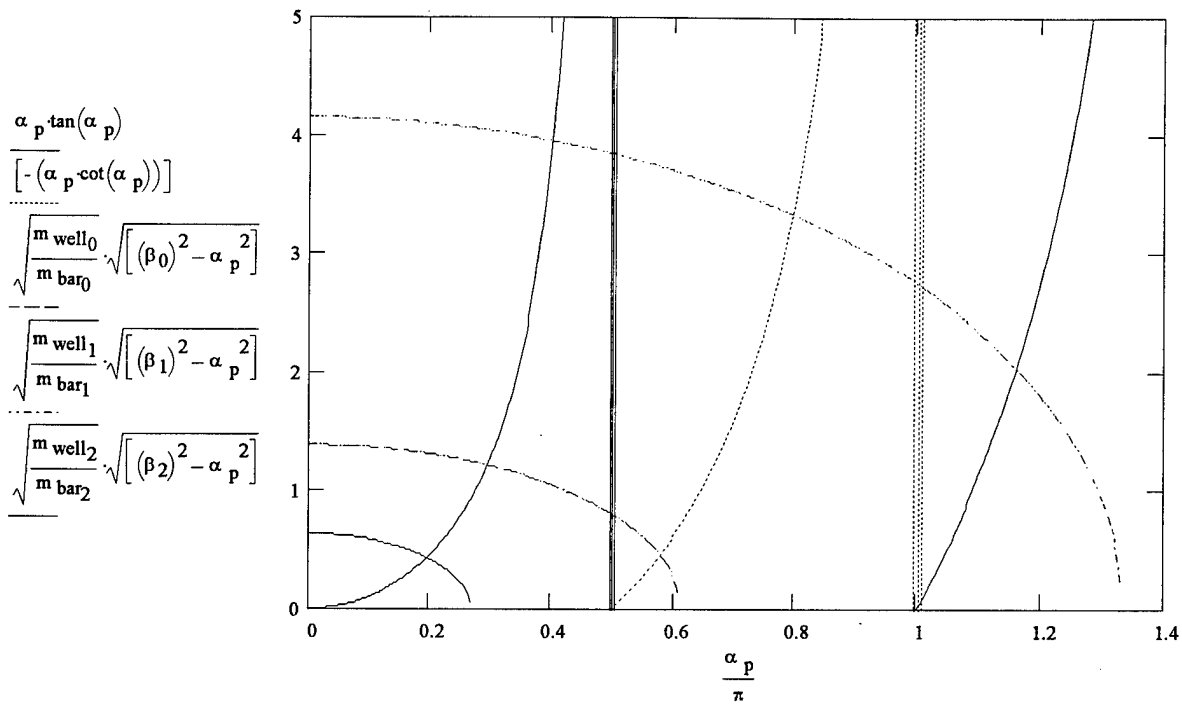
Calculating the Wave Functions:

$$\Psi_{II}{}^{sym} = N \cdot \exp(i \cdot k_2 \cdot x) + N \cdot \exp(-i \cdot k_2 \cdot x) = \frac{N}{2} \cdot \cos(k_2 \cdot x) \qquad \Psi_I{}^{sym} = \Psi_{III}{}^{sym} = N \cdot \exp(K_1 \cdot x)$$

$$\Psi_{II}{}^{asym} = N \cdot \exp(i \cdot k_2 \cdot x) - N \cdot \exp(-i \cdot k_2 \cdot x) = \frac{N}{2} \cdot \sin(k_2 \cdot x) \qquad \Psi_I{}^{sym} = -\Psi_{III}{}^{sym} = N \cdot \exp(K_1 \cdot x)$$

	Real (oscillitory)	**Imaginary (decay)**
Symmetric =>	$\Psi_{II}(x,k) := \left(\dfrac{\cos(k \cdot x)}{2}\right)$	$\Psi_I(x,k,K) := \dfrac{\Psi_{II}(a,k)}{\exp(-K \cdot a)} \cdot \exp(-K \cdot |x|)$
Asymmetric =>	$\Psi_{IIa}(x,k) := \left(\dfrac{\sin(k \cdot x)}{2}\right)$	$\Psi_{Ia}(x,k,K) := \dfrac{if(x \geq 0 \cdot nm, 1, -1) \cdot \Psi_{IIa}(a,k)}{\exp(-K \cdot a)} \cdot \exp(-K \cdot |x|)$

Un-Normalized Wave Functions =>

$$\Psi(x,k,K) := if\left(|x| \leq a, \Psi_{II}(x,k), \Psi_I(x,k,K)\right)$$

$$\Psi_a(x,k,K) := if\left(|x| \leq a, \Psi_{IIa}(x,k), \Psi_{Ia}(x,k,K)\right)$$

Quantized Energy States measured relative to the unstrained valence band.

$$EOc := E_g + Ec \qquad\qquad EOc^T = \left[\ 371.821 \quad 538.4\ \right] \cdot meV$$

$$EOh := E_{hh}(x_{well}) - Eh \qquad\qquad EOh^T = \left[-14.246 \quad -34.531 \quad -65.475\right] \cdot meV$$

$$EOl := E_{lh}(x_{well}) - El \qquad\qquad EOl^T = -64.223 \cdot meV$$

To Plot the QW, Quantized Energies, and Wavefunctions we define additional functions:

$$EC_{cav}(x1, x2, d) := if\left(|d| \leq a, E_g, EC1\right)$$
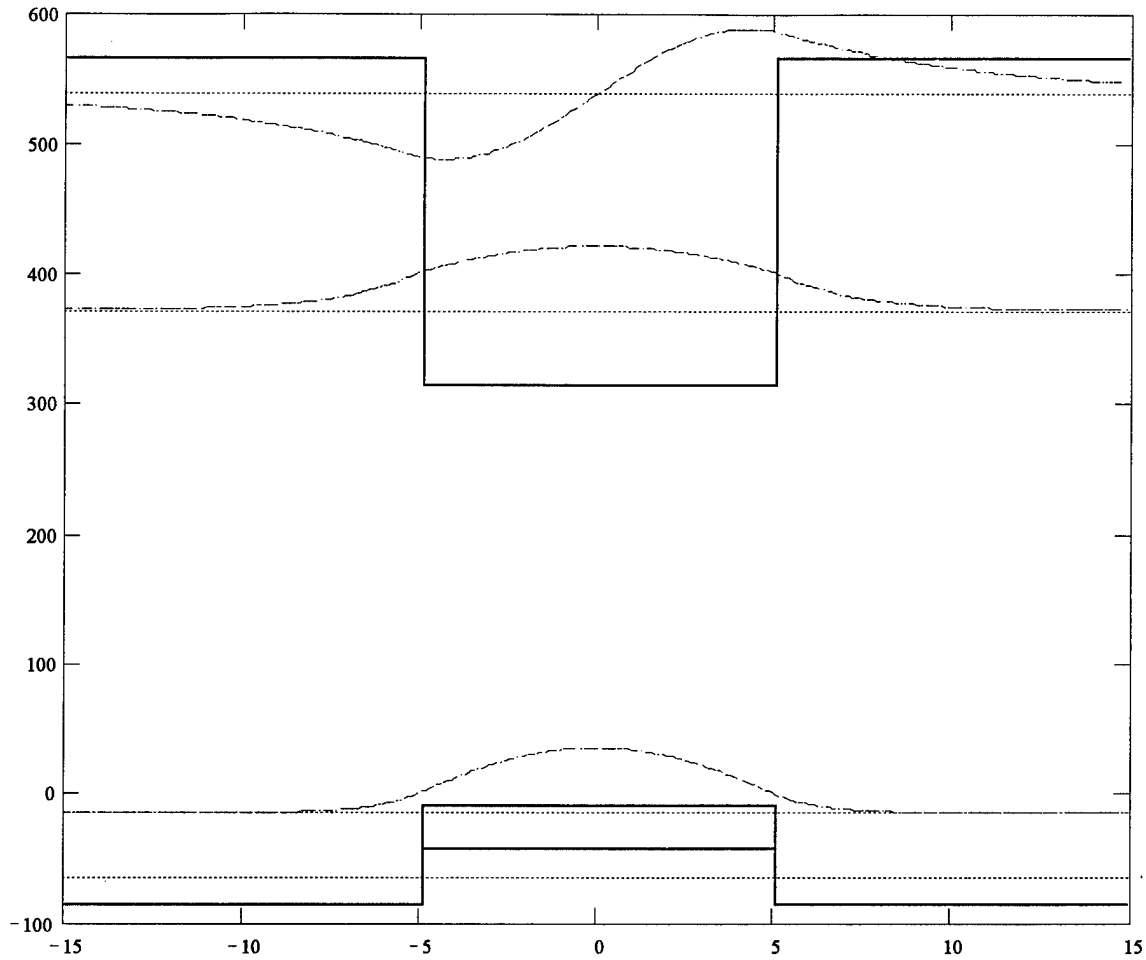
$$EC1 = 566.163 \cdot meV$$

$$EV_{cav}(x1, x2, d) := if\left(|d| \leq a, E_{hh}(x_{well}), EV1\right)$$

$$EVl_{cav}(x1, x2, d) := if\left(|d| \leq a, E_{lh}(x_{well}), EV1\right) \qquad\qquad E_{hh}(x_{well}) = -7.297 \cdot meV$$

$di := 0 .. 300$

$d_{di} := -15 \cdot nm + di \cdot 0.1 \cdot nm$

$QW_{di,0} := d_{di} \cdot Ang^{-1}$ $QW_{di,1} := \dfrac{EC_{cav}(x_{well}, x_{bar}, d_{di})}{meV}$ $QW_{di,2} := \dfrac{EV_{cav}(x_{well}, x_{bar}, d_{di})}{meV}$

$QW_{di,3} := \dfrac{EVl_{cav}(x_{well}, x_{bar}, d_{di})}{meV}$ $QW_{di,4} := \Psi(d_{di}, kc_0, Kc_0) \cdot 100 + \dfrac{EOc_0}{meV}$

$QW_{di,6} := \Psi(d_{di}, kh_0, Kh_0) \cdot 100 + \dfrac{EOh_0}{meV}$ $QW_{di,5} := \Psi_a(d_{di}, kc_1, Kc_1) \cdot 100 + \dfrac{EOc_1}{meV}$

$WRITEPRN("QW") := QW$

Valence Band Energy values => $EOv := stack\left(\dfrac{EOh}{eV}, \dfrac{EOl}{eV}\right) \cdot eV$

Calculated Transition Energies:

$E_{trans_{n,pq}} := EOc_n - EOv_{pq}$ $E_{trans} = \begin{bmatrix} 386.067 & 406.352 & 437.296 & 436.044 \\ 552.646 & 572.931 & 603.875 & 602.622 \end{bmatrix} \cdot meV$

$\lambda_{trans} := \dfrac{\overrightarrow{h \cdot c}}{E_{trans}}$ $\lambda_{trans} = \begin{bmatrix} 3.211 & 3.051 & 2.835 & 2.843 \\ 2.243 & 2.164 & 2.053 & 2.057 \end{bmatrix} \cdot \mu m$

Measured PL peak => $\lambda_b(77 \cdot K) = 3.175 \cdot \mu m$

Phase Matching & Efficiency for KTA

Bill Cooley
Appendix C

Constants & Units:

$h := 6.63 \cdot 10^{-34} \cdot J \cdot s$ $c := 2.9979 \cdot 10^{8} \cdot m \cdot s^{-1}$ $m_e := 9.1091 \cdot 10^{-31} \cdot kg$ $\varepsilon_o := 8.85 \cdot 10^{-12} \cdot C^2 \cdot N^{-1} \cdot m^{-2}$

$k := 1.38 \cdot 10^{-23} \cdot J \cdot K^{-1}$ $e := 1.602 \cdot 10^{-19} \cdot C$ $m_p := 1.6725 \cdot 10^{-27} \cdot kg$ $\mu_o := 4 \cdot \pi \cdot 10^{-7} \cdot \left(T \cdot m \cdot A^{-1} \right)$

$h_{bar} := h \cdot (2 \cdot \pi)^{-1}$ $ns := 10^{-9} \cdot s$ $\mu V := 10^{-6} \cdot V$ $\mu m := 10^{-6} \cdot m$ $fs := 10^{-15} \cdot s$

$eV := 1.602 \cdot 10^{-19} \cdot J$ $\mu s := 10^{-6} \cdot s$ $pm := 10^{-12} \cdot m$ $nm := 10^{-9} \cdot m$

$meV := 10^{-3} \cdot eV$ $ps := 10^{-12} \cdot s$ $mW := 10^{-3} \cdot W$ $Ang := 10^{-10} \cdot m$ $\mu W := 10^{-6} \cdot W$

Type II Phase Matching (oeo)

Pump => $\lambda_p := 800 \cdot nm$ $P_p := 400 \cdot mW$ $\tau_p := 130 \cdot fs$

Luminescence => $N := 20$ $i := 0 .. N$ $\lambda_{min} := 2.0 \cdot \mu m$ $\lambda_{max} := 4.0 \cdot \mu m$
subscript "s" for signal

$$\lambda_{s_i} := \frac{\lambda_{max} - \lambda_{min}}{N} \cdot (i) + \lambda_{min}$$ Sample Wavelength => $\lambda_{s_{15}} = 3.5 \, \mu m$

Angle of "non-collinearity" => $\psi := 16 \cdot deg$ **Radius of Spot Beam**

Crystal thickness   => $L_c := 1 \cdot mm$ Spot Size on Crystal => $\omega_p := 25 \cdot \mu m$

Rep Rate of Ti:Sapphire => $RR := 76 \cdot MHz$ Spot Size on Sample => $\omega_s := 35 \cdot \mu m$

Luminescence and Upconverted wavelenths and wave-vectors:

Pump => $k_p := 2 \cdot \pi \cdot \lambda_p^{-1}$ $\lambda_p = 800 \, nm$

Luminescence => $\vec{k_s} := 2 \cdot \pi \cdot \lambda_s^{-1}$ $\lambda_{s_{10}} = 3 \, \mu m$

Mixed Signal => $\vec{k_{up}} := k_p + k_s$ $\lambda_{up} := 2 \cdot \pi \cdot k_{up}^{-1}$ $\lambda_{up_{10}} = 0.632 \, \mu m$

Sellmeier Equations for KTA (from Fenimore, 1995)   As a function of λ

$$n_x(k) := \sqrt{1.90713 + \frac{1.23522}{1 - \left[0.19692 \cdot \mu m \cdot \left(\frac{2 \cdot \pi}{k} \right)^{-1} \right]^2} - \frac{0.01025}{\mu m^2} \cdot \left(\frac{2 \cdot \pi}{k} \right)^2}$$

$n_{x\lambda}(\lambda) := n_x \left(2 \cdot \pi \cdot \lambda^{-1} \right)$

$$n_y(k) := \sqrt{2.15912 + \frac{1.00099}{1 - \left[0.21844 \cdot \mu m \cdot \left(\frac{2 \cdot \pi}{k} \right)^{-1} \right]^2} - \frac{0.01096}{\mu m^2} \cdot \left(\frac{2 \cdot \pi}{k} \right)^2}$$

$n_{y\lambda}(\lambda) := n_y \left(2 \cdot \pi \cdot \lambda^{-1} \right)$

$$n_z(k) := \sqrt{2.14786 + \frac{1.29559}{1 - \left[0.22719 \cdot \mu m \cdot \left(\frac{2 \cdot \pi}{k} \right)^{-1} \right]^2} - \frac{0.01436}{\mu m^2} \cdot \left(\frac{2 \cdot \pi}{k} \right)^2}$$

$n_{z\lambda}(\lambda) := n_z \left(2 \cdot \pi \cdot \lambda^{-1} \right)$

Defining Ordinary index and Extraordinary Index of refraction

Index for XZ Cut => $n_o(k) := n_y(k)$ $n_{\lambda o}(\lambda) := n_o\left(2 \cdot \pi \cdot \lambda^{-1}\right)$

$$n_e(k,\theta) := \frac{n_x(k) \cdot n_z(k)}{\sqrt{n_z(k)^2 \cdot \cos(\theta)^2 + n_x(k)^2 \cdot \sin(\theta)^2}} \qquad n_{\lambda e}(\lambda,\theta) := n_e\left(2 \cdot \pi \cdot \lambda^{-1}, \theta\right)$$

Wavevectors in Crystal => $K_o(k) := n_o(k) \cdot k$ $K_e(k,\theta) := n_e(k,\theta) \cdot k$

Phase Matching Condition for Non-Collinear Geometry

$$PM\left(k_p, k_s, \Psi, \theta\right) := root\left[\mu m \cdot \left(K_o\left(k_s + k_p\right)^2 - K_e\left(k_p, \theta\right)^2 - K_o\left(k_s\right)^2 + 2 \cdot K_e\left(k_p, \theta\right) \cdot K_o\left(k_s\right) \cdot \cos(\pi - \Psi)\right), \theta\right]$$

       numerical tolerance and Initial guess => $TOL := 0.7$ $\Theta_0 := 40 \cdot deg$

Phase Matched Angle as a function of Angle between K_p and K_s => $\Theta_{pm}(\Psi) := \overrightarrow{PM\left(k_p, k_s, \Psi, \Theta_0\right)}$

     External Angle between k_p and k_s => $\psi := 16.0 \cdot deg$

     Nonlinear crystal cut angle   => $\Omega_x := 43.0 \cdot deg$

     Ψ (internal non-collinear angle) => $\Psi(\Phi) := \overrightarrow{asin\left(\frac{\sin(\Phi)}{n_o\left(k_s\right)}\right) - asin\left(\frac{\sin(\Phi - \psi)}{n_e\left(k_p, \Theta_0\right)}\right)}$

     Assume Ψ is constant so that $\Psi = \Psi_o$ => $\Psi_o := \Psi(0)$ $\Psi_o = 8.668 \cdot deg$

     Angle Between Z and K_{up} => $\Theta_{pm}\left(\Psi_o\right)$

     Angle between Z and K_p => $\Theta_p(\Phi, \psi) := \Omega_x - asin\left(\frac{\sin(\Phi - \psi)}{n_e\left(k_p, \Theta_0\right)}\right)$

     Angle between Z and K_{lum} => $\Theta_s(\Phi) := \Omega_x - asin\left(\frac{\sin(\Phi)}{n_o\left(k_{s_0}\right)}\right)$

     Angle Between
     Z & K_{lum}=> $PM\Theta_s\left(\Psi_o\right) := \Theta_{pm}\left(\Psi_o\right) - \overrightarrow{acos\left(\frac{K_o\left(k_s\right)^2 + K_o\left(k_s + k_p\right)^2 - K_e\left(k_p, \Theta_{pm}\left(\Psi_o\right)\right)^2}{2 \cdot K_o\left(k_s\right) \cdot K_o\left(k_s + k_p\right)}\right)}$

     Calculation of Crystal Angle Setting => $\Phi := \overrightarrow{asin\left(n_o\left(k_s\right) \cdot \sin\left(\Omega_x - PM\Theta_s\left(\Psi_o\right)\right)\right)}$

     Angle of Exit => $\theta_{out} := \overrightarrow{\Phi + asin\left(n_o\left(k_{up}\right) \cdot \sin\left(\Theta_{pm}\left(\Psi_o\right) - \Omega_x\right)\right)}$

The Numerical Values Calculated for input wavelengths between 2 and 4 μm

$$\lambda_s = \begin{bmatrix} 2 \\ 2.1 \\ 2.2 \\ 2.3 \\ 2.4 \\ 2.5 \\ 2.6 \\ 2.7 \\ 2.8 \\ 2.9 \\ 3 \\ 3.1 \\ 3.2 \\ 3.3 \\ 3.4 \\ 3.5 \\ 3.6 \\ 3.7 \\ 3.8 \\ 3.9 \\ 4 \end{bmatrix} \circ\mu m \quad \lambda_{up} = \begin{bmatrix} 571.429 \\ 579.31 \\ 586.667 \\ 593.548 \\ 600 \\ 606.061 \\ 611.765 \\ 617.143 \\ 622.222 \\ 627.027 \\ 631.579 \\ 635.897 \\ 640 \\ 643.902 \\ 647.619 \\ 651.163 \\ 654.545 \\ 657.778 \\ 660.87 \\ 663.83 \\ 666.667 \end{bmatrix} \circ nm \quad \Theta_{pm}(\Psi_o) = \begin{bmatrix} 54.967 \\ 53.176 \\ 51.628 \\ 50.274 \\ 49.081 \\ 48.023 \\ 47.078 \\ 46.232 \\ 45.471 \\ 44.785 \\ 44.164 \\ 43.601 \\ 43.09 \\ 42.625 \\ 42.202 \\ 41.817 \\ 41.467 \\ 41.148 \\ 40.858 \\ 40.593 \\ 40.353 \end{bmatrix} \circ deg \quad \Phi = \begin{bmatrix} -10.102 \\ -6.758 \\ -3.873 \\ -1.351 \\ 0.873 \\ 2.849 \\ 4.616 \\ 6.204 \\ 7.635 \\ 8.93 \\ 10.104 \\ 11.171 \\ 12.141 \\ 13.025 \\ 13.831 \\ 14.565 \\ 15.234 \\ 15.844 \\ 16.398 \\ 16.902 \\ 17.36 \end{bmatrix} \circ deg \quad \theta_{out} = \begin{bmatrix} 12.123 \\ 12.028 \\ 11.984 \\ 11.973 \\ 11.984 \\ 12.008 \\ 12.042 \\ 12.082 \\ 12.125 \\ 12.17 \\ 12.216 \\ 12.26 \\ 12.304 \\ 12.346 \\ 12.385 \\ 12.422 \\ 12.457 \\ 12.488 \\ 12.517 \\ 12.543 \\ 12.566 \end{bmatrix} \circ deg$$

Now for some Useful Plots

$$\lambda := 0.5 \cdot \mu m, 0.55 \cdot \mu m .. 4 \cdot \mu m$$
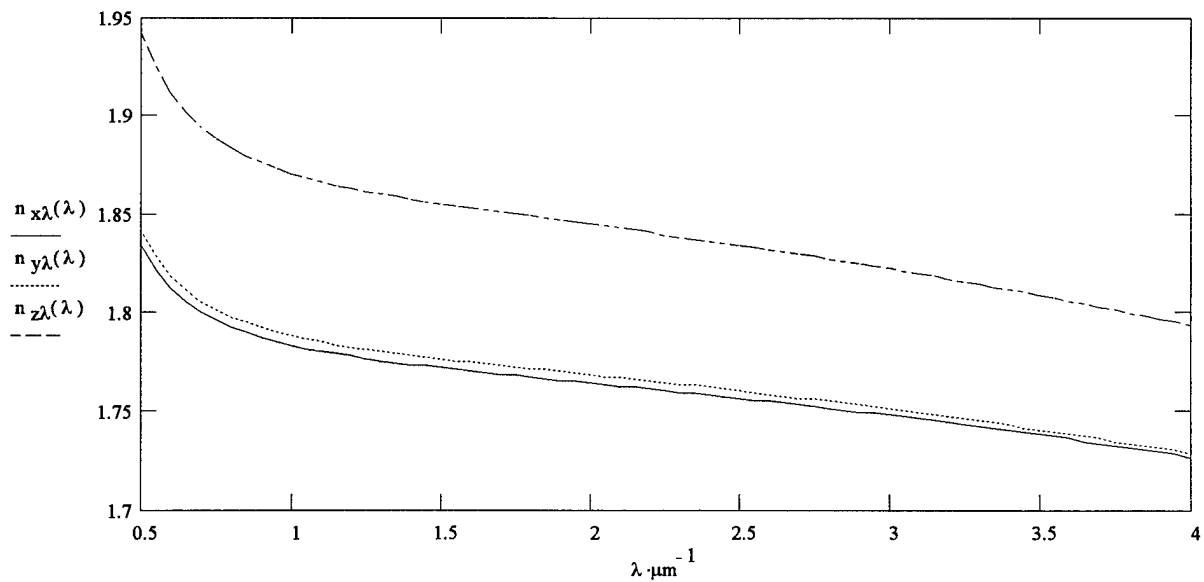
How Good is our Approximation the Ψ is constant? $\Phi_{plot} := -15 \cdot deg, -14.5 \cdot deg.. \ 15 \cdot deg$

$\dfrac{\Psi\left(\Phi_{plot}\right)_{12}}{deg}$

$\Psi_o \cdot deg^{-1}$ ....

$\Phi_{plot} \cdot deg^{-1}$
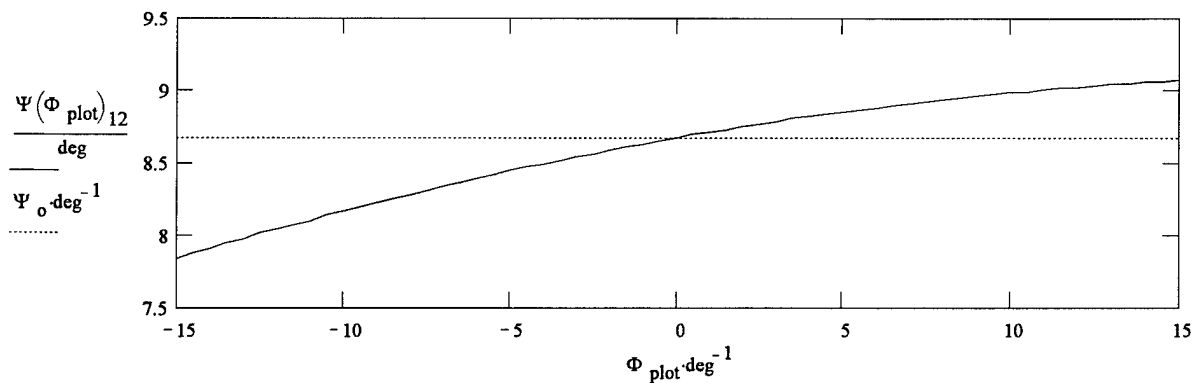
Plot of the Phase Matching Angle vs λ_s:

$\dfrac{\Theta_{pm}\left(\Psi_o\right)_i}{deg}$

$\lambda_{s_i} \cdot \mu m^{-1}$
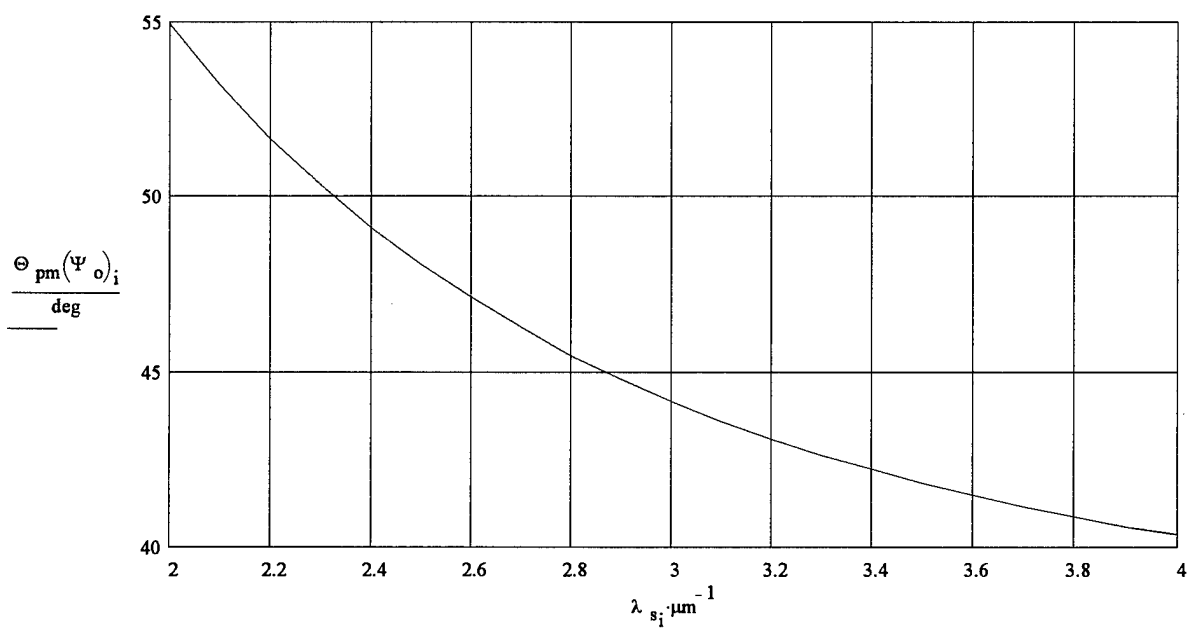
Plot of the Rotation Stage Angle vs λ_s:

$\dfrac{\Phi_i}{deg}$

$\lambda_{s_i} \cdot \mu m^{-1}$
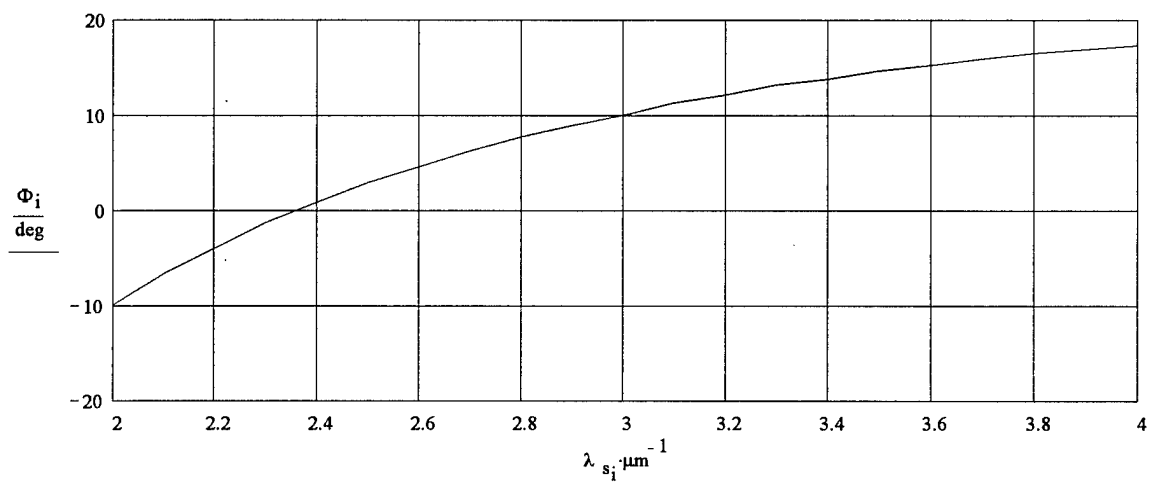
Calculations for Walkoff angle, Spatial and Temporal Effective Length

From Springer-Verlag
Walk-off Angle given by =>
for a *positive* crystal

$$\rho := -\operatorname{atan}\left(\frac{n_o(k_p)^2}{n_z(k_p)^2}\cdot\tan\left(\Theta_{pm}(\Psi_o)\right)\right) + \Theta_{pm}(\Psi_o)$$

$$\rho_{12} = 2.638 \circ\text{deg}$$

Spatial Effective Length:
Assuming Gaussian Beam

$$\omega_p = 25 \circ\mu m \qquad \omega_s = 35 \circ\mu m \qquad \beta := \sqrt{\frac{1}{\omega_p^2} + \frac{1}{\omega_s^2}}$$

$$L_s := \frac{\sqrt{\pi}}{2}\cdot\left[\left[\Psi_o^2\cdot\beta^2 + \frac{(\rho-\Psi_o)^2}{\omega_p^2}\right] - \frac{\left(\Psi_o\cdot\beta^2 + \frac{\rho-\Psi_o}{\omega_p^2}\right)^2}{2\cdot\beta^2}\right]^{-\frac{1}{2}}$$

$$L_{s_{15}} = 109.832 \circ\mu m$$

Group Velocities and Inverse Group Velocity Mismatch (GVM): Temporal Walk-Off

GVM between pump & Lum

$$v_{go}(k) := \left(\frac{n_o(k)}{c} + \frac{k}{c}\frac{d}{dk}n_o(k)\right)^{-1}$$

$$v_{plum} := \frac{1}{v_{go}(k_p)} - \frac{1}{v_{go}(k_s)}$$

$$v_{plum_{20}} = 63.11 \circ\frac{fs}{mm}$$

GVM between pump & mixed signal

$$v_{ge}(k,\theta) := \left(\frac{n_e(k,\theta)}{c} + \frac{k}{c}\cdot\frac{d}{dk}n_e(k,\theta)\right)^{-1}$$

$$v_{pup} := \frac{1}{v_{go}(k_p)} - \frac{1}{v_{ge}(k_{up},\Theta_{pm}(\Psi_o))}$$

$$v_{pup_{20}} = {}^-259.456 \circ\frac{fs}{mm}$$

Temporal Effective Lengths: Recall => $\tau_p = 130 \circ fs$ Assume => $\tau_s := 1\cdot ns$ $\gamma := \sqrt{\frac{1}{\tau_p^2} + \frac{1}{\tau_s^2}}$

$$L_t := \frac{\sqrt{\pi}}{2}\cdot\left[\left(v_{pup}^2\cdot\gamma^2 + \frac{v_{plum}^2}{\tau_p^2}\right) - \frac{\left(v_{pup}\cdot\gamma^2 + \frac{v_{plum}}{\tau_p^2}\right)^2}{2\cdot\gamma^2}\right]^{-\frac{1}{2}}$$

$$L_{t_{15}} = 412.629 \circ\mu m$$

Effective Length Combined   Thickness of Crystal => $L_c := 1\cdot mm$

$$L_w := \left[\left(\frac{1}{L_s^2} + \frac{1}{L_t^2}\right)^{-0.5}\right]$$

$$L_{eff} := L_w\cdot\operatorname{erf}\left(\frac{\sqrt{\pi}}{2}\cdot\frac{L_c}{L_w}\right)$$

Spatial => $L_{s_{15}} = 109.832 \circ\mu m$

Temporal => $L_{t_{15}} = 412.629 \circ\mu m$

Combined => $L_{eff_{15}} = 106.137 \circ\mu m$

Efficiency Calculation of SFG

KTA Nonlinear Coefficients: $d_{31} := 2.8 \cdot pm \cdot V^{-1}$ $d_{32} := 4.2 \cdot pm \cdot V^{-1}$ $d_{33} := 16.2 \cdot pm \cdot V^{-1}$

Effective Coefficient => $d_{oeo}(\theta) := d_{32} \cdot \sin(\theta)$ $d_{oeo}\left(\Theta_{pm}(\Psi_o)_{15}\right) = 2.8 \circ \dfrac{pm}{volt}$
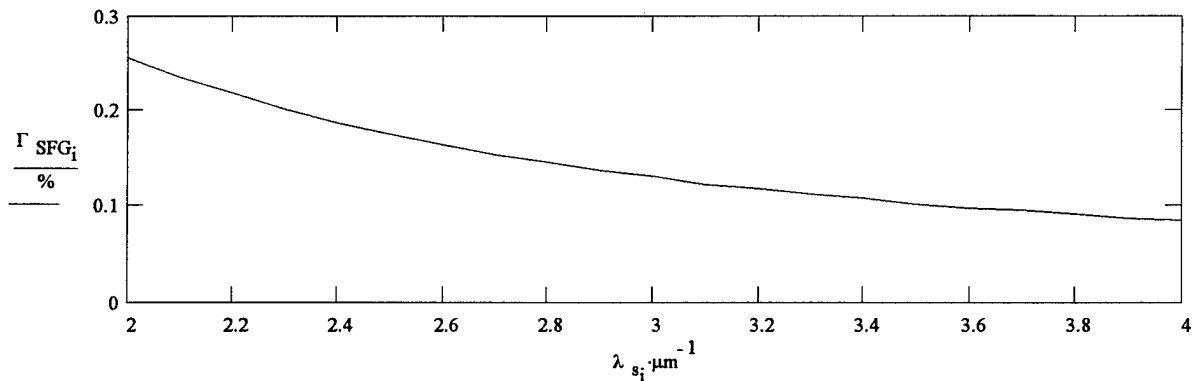
Average Laser Power => $P_p = 400 \text{ °mW}$ **Energy per pulse =>** $E_p := P_p \cdot RR^{-1}$ $E_p = 5.263 \cdot 10^{-9} \text{ °J}$

Peak Intensity => $I_p := \dfrac{E_p}{2 \cdot \pi \cdot \tau_p \cdot \omega_p^{~2}}$ $I_p = 1.031 \cdot 10^9 \circ \dfrac{W}{cm^2}$ **Assume =>** $\Delta k := 0 \cdot cm^{-1}$

Conversion Efficiency for Sum Frequency Generation (SFG):

$$\dfrac{P_{up}}{P_p} = \quad \Gamma_{SFG} := \dfrac{\overrightarrow{(2 \cdot \pi)^2 \cdot d_{oeo}\left(\Theta_{pm}(\Psi_o)\right)^2 \cdot L_{eff}^{~2} \cdot I_p}}{\varepsilon_o \cdot c \cdot n_o(k_{up}) \cdot n_o(k_s) \cdot n_e\left(k_p, \Theta_{pm}(\Psi_o)\right) \cdot \lambda_{up} \cdot \lambda_s}$$

$\Gamma_{SFG_{15}} = 0.10294223 \text{ °%}$

Estimate for Counts per Second from Upconversion Experiment

From InSb detector -- time integrated PL => $S_{pl} := 10 \cdot \mu V$

Quantum Efficiency => $QE := \dfrac{2.97 \cdot A \cdot W^{-1} \cdot h \cdot c}{e \cdot (4.51 \cdot \mu m)}$ $QE = 81.705 \text{ °%}$ **InSb Reisistor =>** $R_{InSb} := 23.18 \cdot 10^3 \cdot ohm$

Optics Efficiency => $\eta_{optic} := \left(\dfrac{150 \cdot mm}{250 \cdot mm}\right)^2$ $\eta_{optic} = 36 \text{ °%}$

Luminescence Pulse Width => $\tau_{pl} := 1 \cdot ns$

Number of mid-IR Photons/pulse = $\dfrac{S_{pl}}{e \cdot QE \cdot RR \cdot R_{InSb} \cdot \eta_{optic}} = 120.465$

Estimate for cps $cps := \left(\dfrac{S_{pl} \cdot RR}{e \cdot QE \cdot RR \cdot R_{InSb} \cdot \eta_{optic}}\right) \cdot \left(\dfrac{\tau_p}{\tau_{pl}}\right) \cdot \Gamma_{SFG_{15}}$ $cps = 1225.21 \cdot s^{-1}$

Analysis of Δk effect on Upconversion Efficiency

From "Handbook of Nonlinear Optical Crystals" by Dmitriev et al. we have the following relations:

$$\eta(\Delta k) = \eta(0) \cdot \frac{\sin\left(0.5 \cdot L_{eff} \Delta k\right)^2}{\left(0.5 \cdot L_{eff} \Delta k\right)^2} = \eta(0) \cdot \text{sinc}\left(0.5 \cdot L_{eff} \Delta k\right)^2 \quad \text{Thus} => \eta(\Delta k) = \frac{\eta(0)}{2} \quad \text{when} => L_{eff} \Delta k = 0.886 \cdot \pi$$

$$\theta_{pm} := \Theta_{pm}\left(\Psi_o\right)$$

Recognizing that => $\quad \Delta k = \dfrac{d(\Delta k)}{dT} \cdot \Delta T + \dfrac{d(\Delta k)}{d\theta} \cdot \Delta\theta + \dfrac{d(\Delta k)}{dv} \cdot \Delta v$

$$\Delta T = 2 \cdot \frac{(0.886 \cdot \pi)}{L_{eff}} \cdot \left(\frac{d(\Delta k)}{dT}\right)^{-1} \qquad \Delta\Theta = 2 \cdot \frac{(0.886 \cdot \pi)}{L_{eff}} \cdot \left(\frac{d(\Delta k)}{d\theta}\right)^{-1} \qquad \Delta v = 2 \cdot \frac{(0.886 \cdot \pi)}{L_{eff}} \cdot \left(\frac{d(\Delta k)}{dv}\right)^{-1}$$

Ignoring ΔT we can solve for $\Delta\Theta$ and Δv for SFG in KTA oeo interaction:

$\Delta\Theta$ FWHM relation for efficiency conversion:

OEO => $\quad \Delta\Theta := \dfrac{0.886 \cdot \lambda_{up} \cdot \left[1 + \left(\dfrac{n_{\lambda o}\left(\lambda_p\right)}{n_{z\lambda}\left(\lambda_p\right)}\right)^2 \cdot \tan\left(\theta_{pm}\right)^2\right]}{L_{eff} \tan\left(\theta_{pm}\right) \cdot \left|1 - \left(\dfrac{n_{\lambda o}\left(\lambda_p\right)}{n_{z\lambda}\left(\lambda_p\right)}\right)^2\right| \cdot n_{\lambda e}\left(\lambda_p, \theta_{pm}\right)}$
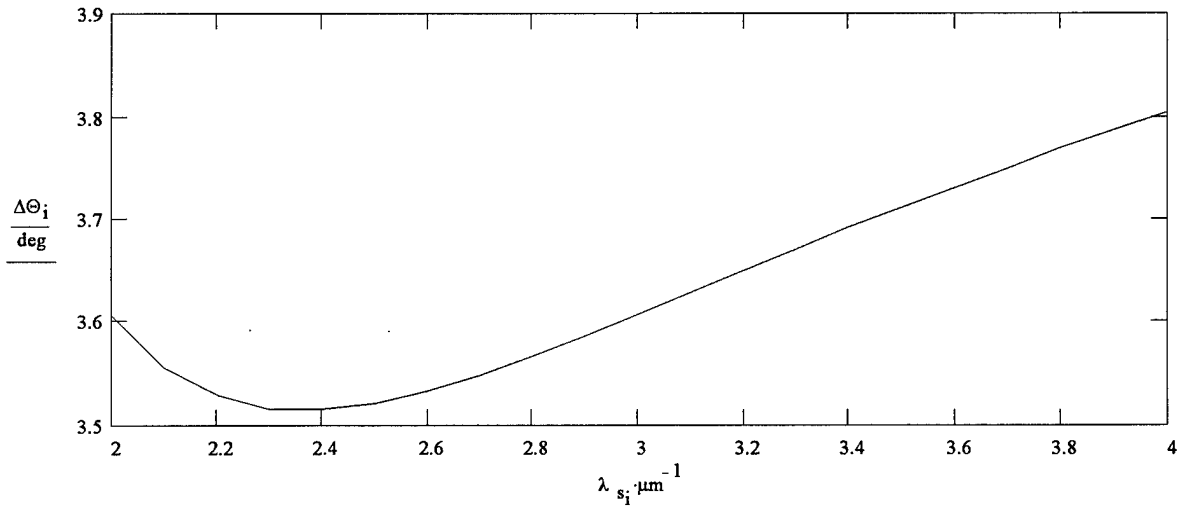
For $\Delta h\nu$ we need the following relations: $D_o(\lambda) := \dfrac{d}{d\lambda} n_{\lambda o}(\lambda)$ $D_e(\lambda,\theta) := \dfrac{d}{d\lambda} n_{\lambda e}(\lambda,\theta)$

SFG spectral bandwidth when the lower frequency interacting wave has a wid-band spectra:

$$\text{OEO} => \quad \Delta h\nu := \frac{0.886 \cdot h \cdot c}{L_{eff}\left| n_{\lambda o}\left(\lambda_s\right) - n_{\lambda o}\left(\lambda_{up}\right) - \lambda_s \cdot D_o\left(\lambda_s\right) + \lambda_{up} \cdot D_o\left(\lambda_{up}\right) \right|}$$
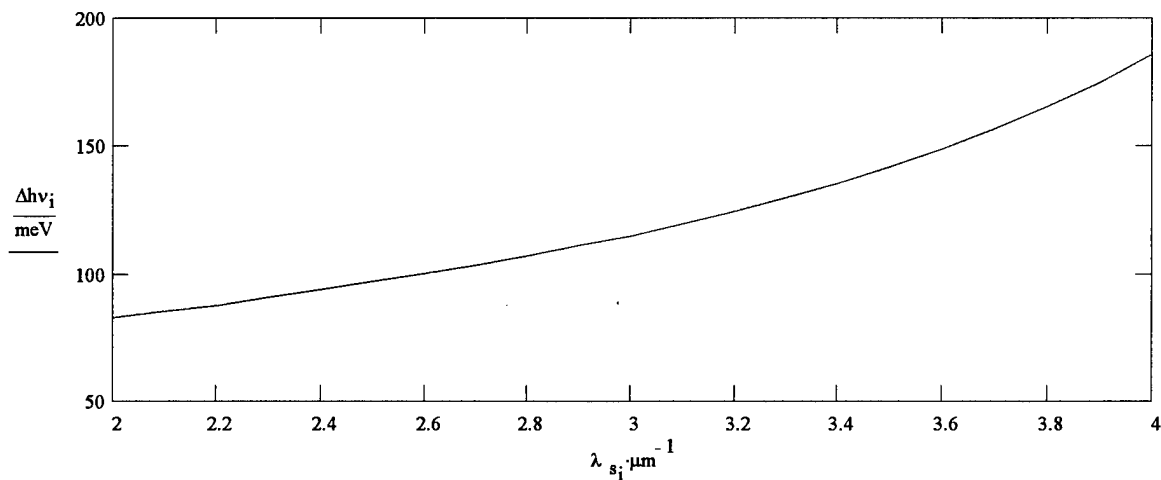
SFG spectral bandwidth when the higher frequency interacting wave has a wid-band spectra:

$$\text{OEO} => \quad \Delta h\nu := \frac{0.886 \cdot h \cdot c}{L_{eff}\left| n_{\lambda e}\left(\lambda_p, \theta_{pm}\right) - n_{\lambda o}\left(\lambda_{up}\right) - \lambda_p \cdot D_e\left(\lambda_p, \theta_{pm}\right) + \lambda_{up} \cdot D_o\left(\lambda_{up}\right) \right|}$$

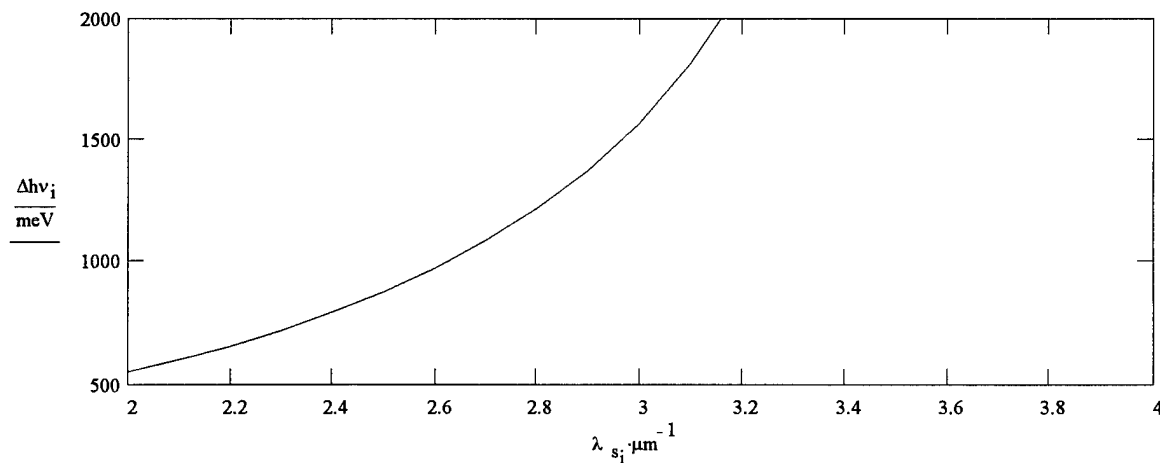# Bibliography

Abram, R.A and R.W. Kelsall and R.I. Taylor, "Auger Recombination in Low-Dimensional Structures" *J. Phys. Chem. Solids, 49(6):* 607-613, 1988

Adachi, S. "Band Gaps and Refractive Indices of AlGaAsSb, GaInAsSb, and InPAsSb: Key Properties for a Variety of the 2-4 μm Optoelectronic Device Applications, " *J. Appl. Phys., 61(10):* 4869-4876 (1987).

Adams, A.R., "Band-Structure Engineering for Low-Threshold High-Efficiency Semiconductor Lasers," *Electron Lett.,* 22:249-250 (January, 1986).

Agrawal, G.P. and N.K. Dutta, *Semiconductor Lasers,* 2nd edition, ITP Van Nostrand Reinhold, 115 Fifth Avenue, New York NY 10003.(1993).

Akimova, I.V. and A.E. Bochkarev and L.M. Dolginov and A.E. Drakin and L.V. Druzhinina and P.G. Eliseev and B.N. Sverdlov and V.A. Skipkin, "Room Temperature 2.0-2.4 μm Injection Lasers," *Sov. Phys. Tech. Phys, 33(4):* 429 (April 1988).

Anderson, E.E. "Modern Physics and Quantum Mechanics," W.B. Saunders Company, Independence Square West, Philadelphia, PA 19106 (1971).

Auston, D.H. and C.V. Shank and P. Lefur, "Picosecond Optical Measurements of Band-to-Band Auger Recombination of High-Density Plasmas in Germanium, " *Physical Review Letters, 35(15):*1022-1025 (October, 1975).

Aydaraliev, M. and N.V. Zotova and S.A Karandashov and B.A. Matveev and N.M. Stus and G.N. Talalakin, "Low-Threshold Long Wave Lasers (λ=3.0-3.6μm) Based on III-V Alloys," *Semicond. Sci. Technol, 8:* 1575-1580 (May, 1993).

Basov, N.G. and A.V. Dudenkova and A.I. Krasilnikov and V.V. Nikitin and K.P. Fedoseev, "Semiconductor P-N Junctions Lasers in the $InAs_{1-x}Sb_x$ System," *Soviet Physics -- Solid State, 8(4):* 847-849 (October, 1966).

Bauerle, R.J. and R. Klann and T. Elsaesser and W. Kaiser, "Observation of Hot Phonon Distributions in Polar Semiconductors Via Picosecond Free Carrier Absorption, " *20th Int. Conf. on The Physics of Semiconductors,* Thessaloniki, Greece, p. 2507 (August, 1990).

Beattie, A.R. and P.T. Landsberg, "Auger Effect in Semiconductors, " *Proc. Royal Soc. A., 249:* 16-29 (1958).

Benz, B. and R. Conradt, "Auger Recombination in GaAs and GaSb, " *Phys. Rev. B, 16(2):* 843 (July, 1976).

Bergman, J.P. and Q.X Zhao and P.O. Holtz and B. Monemar and M. Sundaram and J.L. Merz and A.C Gossard, "Time-Resolved Measurements of the Radiative Recombination in GaAs/AlGaAs Heterostrucures," *Phys. Rev. B, 43(6):* 4771-4776 (February 1991).

Bethea, C.B. and M.Y. Yen and B.F. Levine and K.K. Choi and A.Y. Cho, "Long Wavelength $InAs_{1-x}Sb_x$/GaAs Detectors Prepared by Molecular Beam Epitaxy," *Appl. Phys. Lett., 51:*1431-1432 (1987).

Bethea, C.B. and B.F. Levine and M.Y. Yen and A.Y. Cho, "Photoconductance Measurements on $InAs_{0.22}Sb_{0.78}$/GaAs Grown by Molecular Beam Epitaxy," *Appl. Phys. Lett., 53:* 291-292 (1988).

Blakemore, J.S., *Semiconductor Statistics*, Dover, 1986.

Blinov, L.M. and E.A. Bobrova and V.S. Vavilov and B.N. Galkin, *Sov. Phys Solid State, 9:* 2537 (1968).

Block, D. and J. Shah and A.C. Gossard, "Femtosecond Luminescence Measurements in GaAs," *Solid State Communications*, 59(8):527-531 (1986).

Bransden, B.H. and C.J. Joachain, *Physics of Atoms and Molocules*, Longman Scientific and Technical, (1983).

Brar, B. and J. Ibbetson and G. Kroemer and J.H. English, "Effects of the Interface Bonding Type on the Optical and Structural Porperties of InAs-AlSb Quantum Wells," *Appl. Phys. Lett., 64(25):*3392 (June, 1994).

Brosson, P. and J. Benoit and A. Joullie and B. Sermage, "Analysis of Threshold Current Density in 2.2µm GaInAsSb/GaAlAsSb/GaSb DH Lasers," *Electronics Letters*, 23(8): 417-419 (April, 1987).

Burt, M.B. and R.I. Taylor, "Radiative Efficiency in Low-Dimensional Semiconductor Structures," *Electron. Lett.*, 21: 733-734 (1985).

Campbell, I.H. and I. Sela and B. K. Laurich and D.L. Smith and C.R. Bolognesi and L.A. Samoska and A.C. Gossard and H. Kroemer, "Far-Infrared Photoresponse of the InAs / GaInSb Superlattice," *Appl. Phys. Lett., 59(7):*846 (August, 1991).

Caneau, C. and A.K. Srivastava and J.L. Zyskind and J.W. Sulhoff and A.G. Dentai and M.A. Pollack, "CW Operation of GaInAsSb/AlGaAsSb Lasers up to 190 K," *Appl. Phys. Lett., 49(2):*55 (July, 1986).

Caneau, C. and A.K. Srivastava and J.L. Zyskind and C.A. Burrus and A.G. Dentai and M.A. Pollack, "Reduction of Threshold Current Density of 2.2 µm GaInAsSb/AlGaAsSb Injection Lasers," *Electronics Letters, 22(19):*992-993 (September, 1986).

Caneau, C. and J.L. Zyskind and J.L. Sulhoff and T.E. Glover and J.Centanni and C.A. Burrus and A.G. Dentai and M.A. Pollack, "2.2 μm GaInAsSb/AlGaAsSb Injection Lasers with Low Threshold Current Density," *Appl. Phys Lett., 51(10):*764 (September, 1987).

Capasso, F. and J. Faist, "The Quantum-Cascade Laser," *APS News*, 4(4):S12 (April 1995).

Casey, H.C. and M.B. Panish, *Heterostructure Lasers*, New York: Academic, (1978).

Casey, H.C. "Temperature dependence of the Threshold Current Density in InP-$Ga_{0.28}In_{0.72}As._{0.6}$ (λ = 1.3 μm) double heterostructure lasers," *J. Appl. Phys, 56:*1959 (1984).

Cherng, Y.T. and K.Y. Ma and G.B. Stringfellow, "Raman Scattering in $InAs_{1-x}Sb_x$ Grown by Organometallic Vapor Phase Epitaxy," *Appl. Phys. Lett., 53:*886 (1988).

Chiang, P.K. and S.M. Bedair, "P-N Junction Formation in InSb and $InAs_{1-x}Sb_x$ by Metalorganic Chemical Vapor Deposition," *Appl. Phys. Lett., 46:*383 (1985).

Chiu, T.H. and W.T. Tsang and J.A. Ditzenberger and J.P. van der Ziel, "Room-Temperature Operation of InGaAsSb/AlGaSb Double Heterostructure Lasers near 2.2 μm Prepared by Molecular Beam Epitaxy," *Appl. Phys. Lett., 49(17):*1051 (October, 1986).

Chiu, T.H. and W.T. Tsang and J.A. Ditzenberger, "Summary Abstract: Molecular Beam Epitaxial Growth of Abrupt InAsSb / GaSb Heterostructures and Superlattices Lattice Matched to GaSb (100)," *J. Vac. Soc. Technol. B*, 4:600 (1986)

Choi, H.K. and S.J. Eglash, "High-Efficiency High-Power GaInAsSb/AlGaAsSb Double Heterostructure Lasers Emitting at 2.3μm," *IEEE Jour Quantum Electronics*, QE-27(6):1555-1559 (June, 1991).

Choi, H.K. and S.J. Eglash, "Room Temperature CW Operation at 2.2 μm of GaInAsSb / AlGaAsSb Diode Lasers Grown by Molecular Beam Epitaxy," *Appl. Phys. Lett., 59(10):*1165 (September, 1991).

Choi, H.K. and S.J. Eglash, "High-Power Multiple Quantum Well GaInAsSb / AlGaAsSb Diode Lasers Emitting at 2.1 μm with Low Threshold Current Density," *Appl. Phys. Lett., 61(10):*1154 (September, 1992).

Choi, H.K. and J.N. Walpole and G.W. Turner and S.J. Eglash and L.J. Missaggia and M.K. Connors, "GaInAsSb-AlGaAsSb Tapered Lasers Emitting at 2μm," *IEEE Photoincs Technology Lett., 5(10):*1117-1119 (October, 1993).

Choi, H.K. and G.W. Turner and Z.L. Liau, "2.2 μm of GaInAsSb / AlGaAsSb," *Appl. Phys. Lett., 65:* 2251-2253 (1994).

Chow, W.W., S.W. Koch, and M. Sargent III, *Semiconductor-Laser Physics*, Springer-Verlag, Berlin Heidelberg, 1994.

Christanell, R. and R.A. Hopfel, "Time-Resolved Luminescence from the AlGaAs Layer of AlGaAs / GaAs Heterostructures," *J. Appl. Phys., 66(10):*4827-4831·(November, 1989).

Christianen, P.C.M. and P.J. van Hall and H.J.A. Bluyssen and J.H. Wolter, "Ultrafast Carrier Dynamics at a Metal-Semiconductor interface Studied by Femtosecond Luminscence Spectroscopy," *Semicond. Sci. Technol.,* 9: 707-709 (1994).

Dalal, V.L. and W.A. Hicinbothem Jr. and H. Kressel, "Carrier Lifetimes in Epitaxial InAs," *Appl. Phys Lett., 24(4):*184-185 (February, 1974).

Dawson, L.R. "MBE Growth of Strained Layer Superlattices and Quantum Wells," *Jour. Crystal Growth*, 98: 220-225 (1989).

Dawson, M.D. and D.P. Norwood and H.E. Swoboda and T. F. Boggess and D.S. McCallum and A.L. Smirl and T.C. Hasenberg, "Optical Measurement of Tunneling and Overbarrier Hopping in GaAs / AlGaAs Multiple Quantum Wells at Room Temperature," *20th Int. Conf. on The Physics of Semiconductors*, Thessaloniki, Greece, p. 1661, (August, 1990).

Deveaud, B. and J. Shah and T.C. Damen and B. Lambert and A. Regreny, "Bloch Transport of Electrons and Holes in Superlattice Minibands: Direct Measurement by Subpicosecond Luminescence Spectroscopy," *Phys Rev. Lett., 58(24):*2582-2585 (June, 1987).

Deveaud, B. and T.C. Damen and Jagdeep Shah and C.W. Tu, "Dynamics of Exciton Transfer Between Monolayer-Flat Islands in Single Quantum Wells," *Appl. Phys. Lett, 51(11):*828 (September, 1987).

Deveaud, Benoit "Subpicosecond Luminescence of Quantum Wells," *20th Int. Conf. on The Physics of Semiconductors*, Thessaloniki, Greece, p. 1021-1028 (1990).

Deveaud, B. and D. Morris and A. Regreny and M.R.X. Barros and P. Becker and J.M. Gerard, "Quantum-Mechanical versus Semiclassical Capture and Transport Porperties in Quantum Well Laser Structures," *Optical and Quantum Electronics*, 26: S679-S689, (1994).

Deveaud, B. and D. Morris and A. Regreny and R. Planel and J.M. Gerard M.R.X. Barros and P. Becker, "Ultrafast Relaxation of Photoexcited Carriers in Quantum Wells and Superlattices," *Semicond. Sci. Technol.,* 9: 722-726 (1994).

Dmitriev, V.G., G.G. Gurzadyan, and D.N. Nikogosyan, *Handbook of Nonlinear Optical Crystals*, Springer-Verlag, Berlin Heidelberg, 1991.

Edelstein, Daniel C. *New Sources and Techniques for Ultrafast Laser Spectroscopy*, Dissertation, Cornell University (January 1990).

Egan, R.J. and V.W.L. Chin and T.L. Tansley, "Dislocation Scattering effects on Electron Mobility in InAsSb," *Jour. Appl. Phys., 75(5):*2473-2476 (March 1994).

Eglash, S.J. and H.K. Choi, "Efficient GaInAsSb/AlGaAsSb Diode Lasers Emitting at 2.29μm," *Appl. Phys. Lett., 57(13):*1292 (September 1990).

Eglash, S.J. and H.K. Choi, "{InAsSb / AlAsSb Double Heterostructure Diode Lasers Emitting at 4 μm," *Appl. Phys. Lett., 64(7):*833 (February 1994).

Elies, S. and A. Krier and I.R. Cleverley and K. Singer, "Photoluminescence of MBE-Grown $InAs_{1-x}Sb_x$ Lattice Matched to GaSb," *Jour. Phys. D: Appl. Phys*, 26: 159-162 (1993).

Elsaesser, T. and J. Shah and L. rota and P. Lugli, "Initial Thermalization of Photoexcited Carriers in GaAs Studied by Femtosecond Luminescence Spectroscopy," *Phys. Rev. Lett., 66(13):*1757 (April 1991).

Elsaesser, T. and J. Shah and L. Rota and P. Lugli, "Carrier thermalization in GaAs and InP studied by Femtosecond Luminescence Spectroscopy," *Int. Symp on Ultrafast Processes in Spectroscopy*, Bayreuth, 126: 313-316 (1992).

Esina, N.P. and N.V. Sotova, A.A. Rogachev and N.M Stus' and G.N. Talalakin, "Carrier Recombination in $InAs_{1-x}Sb_x$ Solid Solutions," *Soviet Phys. Semiconductors*, 12: 342-343 (1978).

Fenimore, D.L. and K.L. Schepler, and U.B. Ramabadran and S.R. McPherson, "Infrared corrected Sellmeier coefficients for potassium titanyl arsenate," *J. Opt. Soc. Am. B*, 12(5):794 (May 1995).

Ferguson, I.T. and A.G. Norman and B.A. Joyce and T-Y. Seong and G.R. Booker and R.H. Thomas and C.C. Phillips and R.A. Stradling, "Molecular Beam Epitaxial Growth of InAsSb Strained layer Superlattices. Can Nature Do It Better?" *Appl. Phys. Lett., 59(25):*3324 (December 1991).

Flatte, M.E. and C.H. Grein and H. Ehrenreich and R.H. Miles and H. Cruz, "Theoretical Performance Limits of 2.1 - 4.1 μm InAs/InGaSb, HgCdTe, and InGaAsSb Lasers," *J. Appl. Phys., 78(7):*4552-4559 (October 1995).

Fowles, Grant R., *Introduction to Modern Optics*, (Dover, 1989).

Fox, A.M. and R. J Manning and A Miller, "Picosecond Relaxation mechanisms in Highly Excited GaInAsP," *J. Appl. Phys., 65(11):*4287-4298 (June 1989).

Freeman, M.R. and D.D. Awschalom and J.M. Hong and L.L. Chang, "Femtosecond Spin-Polarization Spectroscopy in Diluted-Magnetic Semiconductor Quantum Wells," *Phys Rev. Lett., 64(20):*2430-2433 (May 1990).

Freeman, M.R. and D.D. Awschalom and J.M. Hong and L.L. Chang and K. Ploog, "Ultrafast Spin-Polarization Spectroscopy in GaAs/ AlGaAs Quantum Wells," *20th Int. Conf on The Physics of Semiconductors,*" p. 1129 (August 1990).

Fuchs, G. and S. Hauber and A. Hangleiter, "Recombination in GaSb / AlSb Multiple QWS Under High Excitation Conditions," *Superlattices and Microstructures,* 10(3):361-364 (1991).

Gale, B.M. and A. Chebira and E. Fazio and J. Chesnoy, "Femtosecond Relaxation of Photoexcited Single-Species Carriers in Bulk Doped Semiconductors," *Int. Symp. on Ultrafast Processes in Spectroscopy,* Bayreuth, 126:333 (1992).

Grein, C.H. and P.M. Young and H. Ehrenreich, "Minority Carrier Lifetimes in Ideal InGaSb / InAs Superlattices," *Appl. Phys Lett., 61(24):*2905 (December 1992).

Grein, C.H. and P.M. Young and H. Ehrenreich and T.C. McGill, "Auger Lifetimes in Ideal InGaSb / InAs Superlattices," *J. of Electronic Materials,* 22(8):1093-1096 (1993).

Hangleiter, Andreas "Coulomb Enhancement of Radiative and Non-Radiative Recombination Processes in Semiconductors," *20th Int. Conf. on The Physics of Semiconductors,* Thessaloniki, Greece, p.2566-2569 (August 1990).

Harle, V. and H. Bolay and E. Lux and P. Michler and A. Mortz and T. Forner and A. Hangleiter and F. Scholz, "Indirect Band-Gap Transition in Strained GaInAs / InP Quantum Well Structures," *J. Appl. Phys., 75(10):*5067 (May 1994).

Haug, A. and D. Kerkhoff and W. Lochmann, "Calculations of Auger Coefficients for III-V Semiconductors with Emphasis on GaSb," *Phys. Status Solidi (b),* 89:357-365, (1978).

Haug, A. "Temperature dependence of Auger Recombination in Gallium Antimonide," *J. Phys. C: Solid State Phys., 17:*6191-6197, (1984).

Haug, A. "Band-To-Band Auger Recombination in Semiconductors," *J. Phys Cem. Solids,* 49(6):599-605 (1988).

Huang, X.R. and D.S. McCallum and M.D. Dawson and A.L. Smirl and T.F. Boggess and T.C. Hasenberg and R.L. Tober, "Ambipolar Diffusion and Carrier Lifetime

Measurements in All-Binary (InAs)2(GaAs)5 Strained Quantum Wells Grown on GaAs," *J. Appl. Phys., 74(3):*1868-1873 (August 1993).

Hausser, S. and G. Fuchs and A. Hangleiter and K. Streubel and W.T. Tsang, "Auger Recombination in Bulk and Quantum Well InGaAs," *Appl. Phys. Lett., 56(10):*913-915 (March 1990).

Henry, C.H. and B.F. Levine and R.A. Logan and C.G. Bethea, "Minority Carrier Lifetime and Luminescence Efficiency of 1.3 μm InGaAsP / InP Double Heterostructure Layers," *IEEE J. of Quantum Electronics*, QE-19(6):905-912 (June 1983).

Heyen, E.T. and M. Hagerott and A.V. Nurmikko and D.L. Partin, "Radiative recombination in PbTe Quantum Wells," *Appl. Phys. Lett, 54(7):*653-655 (February 1989).

Hulin, D. and A. Migus and A Antonetti and I. Ledoux and J. Badan and J.L. Oudar and J. Zyss, "Parametric Amplification Sampling Spectroscopy of Luminescence at the Subpicosecond time scale in the 1 - 1.6 μm spectral range," *Appl. Phys. Lett., 49(13):*761-763 (September 1986).

Jang, D.J., J.T. Olesberg, M.E. Flatte, T.F. Boggess, and T.C. Hasenberg, "Hot carrier dynamics in a (GaInSb/InAs)/GaInAlAsSb superlattice multiple quantum well measured with mid-wave infrared, subpicosecond photoluminescence upconversion," *Appl. Phys. Lett., 70(9):1125*-1127 (March 1997).

Johnstone, D.K. and M.A. Marciniak and Y.K. Yeo and R.L. Hengehold and G.W. Turner, "Electrical and optical characterization of GaSb based diode laser material for 2-4 μm applications," *Proceedings of the 22nd International Symposium of Compound Semiconductors* (September 1995).

Jen H.R. and K.Y. Ma and G.B. Stringfellow, "Long Range Order in InAs_{1-x}Sb_x," Appl. Phys. Lett., 54:1154-1156 (1989).

Joullie, A. and C. Alibert and H. Mani and F. Pitard and E. Tournie and G. Boissier, "Characteristic Temperature T_o of $Ga_{0.83}In_{0.17}As_{0.15}Sb_{0.85}/Al_{0.27}Ga_{0.73}As_{0.02}Sb_{0.98}$ Injection Lasers," *Electronics Letters, 24(17):*1076-1077 (August 1988).

Kane, E.O. *Semiconductors and Semimetals*, Academic Press, Vol. 1, Ch. 3 (1966).

Kash, Kathleen and Jagdeep Shah, "Carrier Energy Relaxation in $In_{0.53}Ga_{0.47}As$ Determined from Picosecond Luminescence Studies," *Appl. Phys. Lett., 45(4):*401-403 (August 1984).

Kaspi, R., W.T. Cooley, and K.R. Evans, "In situ composition control of III-$As_{1-x}Sb_x$ alloys during molecular beam epitaxy using line-of-sight mass spectrometry," *J. of Crystal Growth*, 173:5-13 (April, 1997).

Kersting, R. and A. Kohl and T. Voss and K. Leo and H. Kurz, "Ultrafast Carrier Dynamics in Strained InGaAs/InP Heterostructures," *Appl. Physics A*, 55:596-598 (1992).

Kersting, R. and R. Schwedler and K. Leo and H. Kurz, "Ultrafast Carrier Transport and Capture in InGaAs/InP Heterostructures," *IEEE 4th International Conference on Indium Phosphide and related Materials*, p.565 (April 1992).

Kersting, R. and R. Schwedler and K. Wolter and K. Leo and and H. Kurz, "Dynamics of carrier transport and carrier capture in InGaAs/InP heterostructures," *Phsical Review B*, 46:1639-1648 (July 1992).

Kersting, R. and J. Pletner and K. Leo and S. Averin and H. Kurz, "Time-Resolved Luminescence study of Ultrafast Carrier Transport in GaAs Metal-Semiconductor-Metal Devices," *Appl. Phys. Lett.*, 62(7):732 (February 1993).

Kersting, R. and R. Schwedler and A. Kohl and K. Leo and H. Kurz, "Ultrafast Carrier Dynamics in InGaAs/InP Heterostructures," *Optical and Quantum Electronics*, 26:S705 (1994).

Kohl, M. and D. Heitmann and W.W. Ruhle and P. Grambow and K. Ploog, "Time-Resolved Photoluminescence of 1D Excitions in GaAs / AlGaAs Quantum Well Wires," *20th Int. Conf. on The Physics of Semiconductors*, Thessaloniki, Greece, p.2399-2402 (August 1990).

Krotkus, A. and S. Marcinkevicius and V. Pasiskevicius and U Olin, "Ultrafast Photoluminescence Decay in Low Temperature MOCVD Grown InGaAs," *Semicond. Sci. Technol.*, 9:1382-1386 (1994).

Kurtz, S.R. and G.C. Osbourne and R.M. Biefeld and S.R. Lee, "Photoluminescence and Band Structure of InAsSb Strained Layer Superlattices," *Appl. Phys. Lett.*, 53:216-218 (1988).

Lambert, B. and B. Sermage and B. Deveaud and F. Clerot and A. Chomette and A. Regreny, "Radiative and Non-Radiative Recombination in GaAs / AlGaAs Superlattices," *Survace Science*, 228:210-212 (1990).

Landsberg, P.T. and M.J. Adams, "Recombination Coefficients in Low-Dimensional Systems, with Special Reference to Long-Wavlength Quaternary Lasers," *IEE Proceedings*, 133(2):118-120 (April 1986).

Le, H.Q. and W.D. Goodhue and P.A. Maki and S. Di Cecca, "Diode Laser Pumped InGaAs/GaAs / AlGaAs Heterostructure Lasers with Low Internal Loss and 4-W Average Power," *Appl. Phys. Lett.*, 63(11):1465 (September 1993).

Le, H.Q. and G.W. Turner and S.J. Eglash and H.K. Choi and D.A. Coppeta, "High-Power Diode Laser Pumped InAsSb/GaSb and GaInAsSb/GaSb Lasers Emitting from 3 to 4 µm," *Appl. Phys. Lett., 64(2):*152 (January 1994).

Liau, Z.L. and H.K. Choi, "$InAs_{1-x}Sb_x/In_{1-y}Ga_yAs$ multiple-quantum-well heterostructure design for improved 4-5µm lasers," *Appl. Phys. Lett., 64(24):*3219 (June 1994).

Loehr, John P. "*Physics of Strained Quantum Well Lasers,*" Kluwer Academic Publishers, Boston (1997).

Loehr, John P. *Theoretical Studies of Pseudomorphic Quantum Well Optoelectronic Devices,*" Dissertation, University of Michigan (1991).

Loehr, John P. and M.O. Manasreh, "*Theoretical Modeling of the Intersubband Transitions in III-V Semiconductor Multiple Quantum Wells,*" Artech House Publisher, Ch.2 (1993).

Loehr, John P. "Improved Effective-Bond-Orbital Model for Superlattices," *Phys. Rev. B, 50(8):*5429-5434 (August 1994).

Madelung, O. *Data in Science and Technology: Semiconductors, Group IV Elements and III-V Compounds*, Springer-Verlag (1991).

Mahr, H. and M.D. Hirsch, "An Optical Up-Conversion Light Gate with Picosecond Resolution," *Optical Communications*, 13(2):96 (February 1975).

Manasreh, M.O., "*Semiconductor Quantum Wells and Wuperlattices for Long-Wavelength Infrared Detectors,*" Artech House, Inc. 685 Canton St., Norwood MA 02062 (1993).

Mani, H. and A. Joullie and G. Boissier and E. Tournie and F. Pitard and A.M. Joullie and C. Alibert, "New III-V Double Heterojunction Laser Emitting Near 3.2µm," *Electronics Letters*, 24:1542-1543 (October 1988).

Mao, Y. and A. Krier, "Liquid Phase Epitaxial Growth and Photoluminescence of InAsSb Grown on GaSb Substrates from Antimony Solution," *Jour. Crystal Growth*, 113:108-116 (1993).

Marciniak, Michael A. *Optical Characterization of MBE-Grown $InAs_{1-x}Sb_x$ Semiconductors on GaSb Substrate*, Dissertation, Air Force Institue of Technology (August 1995).

McCallum, D.S. and X.R. Haung and M.D. Dawson and T.F. Boggess and A.L. Smirl and T.C. Hasenberg and A. Kost, "Optical Nonlinearities and Ultrafast Charge Transport in All-Binary InAs / GaAs strained Hetero n-i-p-i's," *J. Appl. Phys.*, 70(11):6891-6897 (December 1991).

McKelvey, J.P. *Solid State and Semiconductor Physics*, Robert E. Krieger Publishing Company, Malabar, Florida (1966).

Midwinter, J.E. and J. Warner, "Up-Conversin of Near Infrared to Visible Radiation in Lithium-meta-Niobate," Jour. Appl. Phys., 38(2):519-523 (February 1967).
K. Mohammed and F. Capasso and R.A. Logan and J.P. VanDer Ziel and A.L. Hutchinson, "= {High Detectivity $InAs_{0.85}Sb_{0.15}$ / InAs Infra-Red (1.8-4.8 μm Detectors," *Electron. Lett.*, 22:215-216 (1986).

Mollay, B. and U. Lemmer and R. Kersting and R.F. Mahrt and H. Kurz and H.F. Kauffmann and H. Bassler, "Dynamics of Singlet Excitation in Conjugated Polymers: Poly(phenylenevinylene) and poly(phenylphenylenevinylene)," *Phys. Rev. B*, 50(15):10769-10779 (October 1994).

Morosini, M.B.Z. and J.L. Herrera-Perez and M.S.S. Loural and A.A.G. VonZuben and A.C.F. da Siveira and N.B. Patel, "Low-Threshold GaInAsSb/GaAsSbSb Double Heterostructure Lasers Grown by LPE," *IEEE Jour. Quantum Electronics*, QE-29(6):2103-2108 (June 1993).

Mozer, A. and K.M. Romanek and O. Hilderbrand and W. Schmid and M.H. Pilkuhn, "Losses in GaInAsP/InP and GaAlSbAs / GaSb Lasers - The Influence of the Split-Off Valence Band," *IEEE J. of Quantum Electronics*, QE-19(6):913-916 (June 1983).

Nilsson, N.G. and K.G. Svantesson, "The Spectrum and Decay of the Recombination Radiation from Strongly Excited Silicon," *Solid State Communications*, 11:155-159 (1972).

Norwood, D.P. and H.E. Swoboda and M.D. Dawson and A.L. Smirl and D.R. Andersen and T.C. Hasenberg, "Room-Temperature Short-Period Transient Grating Measurement of Perpendicular Transport in GaAs / AlGaAs Multiple Quantum Wells," *Appl. Phys. Lett., 59(2):*219-221 (July 1991).

Oberli, D.Y. and J. Shah and T.C. Damen and R.F. Kopf and J.M. Kuo and J.e. Henry, "Optical Phonon-Assisted Tunneling in Double Quantum-Well Structures," *OSA Proceedings on Picosecond Electronics and Optoelectronics*, 4:111-114 (March 1989).

Oberli, D.Y. and J. Shah and B. Deveaud and T.C. Damen, "Ultrafast Optical Studies of Tunneling and Perpendicular Transport in Semiconductor Microstructures," *OSA Proceedings on Picosecond Electronics and Optoelectronics*, 4:94-100 (March 1989).

Ockman, N. and W. Wang and R.R. Alfano, "Applications of Ultrafast Laser Spectroscopy to the Study of Semiconductor Pysics," *International Journal of Modern Physics B*, 5(20):3165-32334 (September 1991).

Ongstad, A.P., D.J. Gallant, and G.C. Dente, "Carrier lifetime saturation in InGaAs single quantum wells," *Appl. Phys. Lett., 66(20):2730* (May 1995).

Ongstad, A.P., M.L. Tilton, E.J. Bochove, and G.C. Dente, "Carrier spillover at 300, 195, and 77 K in InGaAs and GaAs single quantum wells," *J. Appl. Phys., 80(5):2866* (September 1996).

O'Reilly, E.P. and K.C. Heasman and A.R. Adams and G.P. Witchlow, "Calculations of the Threshold Current and Temperature Sensitivity of a GaInAs Strained Quantum Well Laser Operating at 1.55 μm," *Superlattices and Microstructures*, 3(2):99-102 (1987).

Pankove, Jacques I. *Optical Processes in Semiconductors*, Dover Publishing, 180 Varick St, New York, NY 10014, (1971).

Poole, P.J. and S. Charbonneau and M. Fritze and A.V. Nurmikko, "Time-Resolved Photoluminescence of Spacially Direct and Indirect Transitions in Shallow Etched Quantum-Well Wires," *Phys. Rev. B*, 49(16):11504-11507 (April 1994).

Prise, M.E. and M.R. Taghizadeh and S.D. Smith and B.S. Wherrett, "Picosecond Measurement of Auger Recombination Rates in InGaAs," *Appl. Phys. Lett., 45(6):652* (September 1984).

Qian, S. and J. Song and Y. Li and W. Peng and Z. Yu, "Nonradiative, radiative recombination and trapping processes in the InGaAs / GaAs Single Quantum Wells," Ultrafast Pulse Generation and Spectroscopy, *SPIE Vol. 1861*:363-369 (1993).

Ridley, B.K. *Quantum Processes in Semiconductors*, 3rd ed., Clarendon Press, Oxford 1993.

Ridley, B.K. "Kinetics of radiative recombination in quantum wells," Phys. Rev. B. 41(17): 12190, (June, 1990).

Rosenwaks, Y. and Y. Shapira and D. Huppert, "Metal Reactivity Effects on the Surface Recombination Velocity at InP Interfaces," *Appl. Phys. Lett., 57(24):2552-2554* (December 1990).

Rota, L. and P. Lugli and T. Elsaesser and J. Shah, "Ultrafast Thermalization of Photoexcited carriers in Polar Semiconductors," *Phys. Rev. B, 47(8):4226-4237* (February 1993).

Salman, E.G. and A.N. Korshunov and V.N. Vertoprakhov, "A DLTS Study of InAs MIS Structures," *Phys. Stat. Sol. (a),* 117:509-514 (1990).

Sermage, B. and H.J. Eichler and J.P. Heritage and R.J. Nelson and N.K. Dutta, "Photoexcited Carrier Lifetime and Auger Recombination in 1.3 micron InGaAsP," *Appl. Phys. Lett, 42(3):259-261* (February 1983).

Sermage, B. and J.L. Benchimol and J.P. Heritage, "Subnanosecond Carriers Lifetime Measurement in 1.3 μm InGaAsP," *J. of Luminescence*, 31:500-502 (1984).

Sermage, B. and J.P. Heritage and N.K. Dutta, "Temperature Dependence of Carrier Lifetime and Auger Recombination in 1.3 μm InGaAsP," *J. Appl. Phys., 57(12):*5443-5449 (June 1985).

Sermage, B. and D.S. Chemla and D. Sivco and A.Y. Cho, "Comparison of Auger Recombination in GaInAs-AlInAs Multiple Quantum Well Structure and in Bulk GaInAs," *IEEE Journal of Quantum Electronics*, QE-22(6):774-780 (June 1986).

Shah, Jagdeep and T.C. Damen and B. Deveaud and Dominique Block, "Subpicosecond Luminescence Spectroscopy Using Sum Frequency Generation," *Appl. Phys. Lett, 50(19):*1307-1309 (May 1987).

Shah, Jagdeep and B. Deveaud and T.C. Damen and W.T. Tsang and A.C. Gossard and P. Lugli, "Determination of Intervalley Scattering Rates in GaAs by Subpicosecond Luminescence Spectroscopy," *Phys. Rev. B, 59(19):*2222-2225 (November 1987).

Shah, Jagdeep "Ultrafast Luminescence Spectroscopy Using Sum Frequency Generation," *IEEE Journal of Quantum Electronics*, QE-24(2):276-288 (February 1988).

Shah, Jagdeep "Ultrafast Studies of Carrier Relaxation in Semiconductors and their Microstructures," *Superlattices and Microstructures*, 6(3):293-302 (1989).

Shah, Jagdeep and K. Leo and D.Y. Oberli and T.C. Damen and D.A.B. Miller and J.P. Gordon, "Ultrafast Studies of Electron and hole Tunneling in Quantum Well Structures," *20th Int. Conf on The Physics of Semiconductors*, Thessaloniki, Greece, p.1122 (August 1990).

Shah, Jagdeep *Hot Carriers In Semiconductor Nanostructures*, Academic Press, Inc., (1992).

Shah, Jagdeep, *Ultrafast Spectroscopy of Semiconductors and Semiconductor Nanostructures*, Springer-Verlag, (1996).

Snow, P.A., and P. Maly, D.J. Westland, and J.F. Ryan, "Picosecond Photoluminescence Measurements of Hot Carrier Relaxation and Auger Recombination in GaSb," *Solid-State Electronics* 32(12):1485-1489 (1989).

Srivastava, A.K. and J.L. Zyskind and R.M. Lum and B.V. Dutt and J.K. Klingert, "Electrical Characteristics of InAsSb / GaSb Heterojunctions," *Appl. Phys. Lett.,* 49:41-43, (1986).

Stradling, R.A. "InSb-Based Materials for Detectors," *Semicond. Sci. Technol.*, 6:C52-C58 (1991).

Stringfellow, G.B. "Ordered Structures and Metastable Alloys Grown by OMVPE," *Jour. Crystal Growth*, 98:108-117 (1989).

Strobel, R. and R. Eccleston and J. Kuhl and K. Kohler, "Tunneling versus Exciton Formation of Photo-Induced Carriers in Asymmetric Double Quantum Wells," *Int. Symp on Ultrafast Processes in Spectroscopy*, 126:415-418 (1991).

Sugimura, Akira, "Band-to-Band Auger Recombination Effect on InGaAsP Laser Threshold," *IEEE Journal of Quantum Electronics*, QE-17(5):627-653 (May 1981).

Sugimura, Akira, "Band-to-Band Auger effect in Long Wavelength Multinary III-V Alloy Semiconductor Lasers," *IEEE Journal of Quantum Electronics*, QE-18(3):352-363 (March 1982).

Sze, S.M. "Physics of Semiconductor Devices," Wiley InterScience (1981).

Takeshima, Masumi "Disorder-Enhanced Auger Recombination in III-V Alloys," *J. Appl. Phys., 49(12):*6118-6124 (December 1978).

Takeshima, M. "Effect of Anisotropic Band Parameters on Band-to-Band Auger Recombination in $In_{0.72}Ga_{0.28}As_{0.6}P_{0.4}$," *Phys. Rev. B, 29(4):*1993 (February 1984).

Taylor, R.I. and R.A. Abram and M.B. Burt and C. Smith, "Auger Recombination in a Quantum Well Heterostructure Laser," *IEE Proceedings, 132(6):*364-370 (December 1985).

Titkov, A.N. and G.V. Benemanskaya and B.L. Gelmont and G.N. Iluridthe and Z.N. Sokolova, "Auger Recombination in P-Type GaSb," *Jour. Lumin*, 24/25:697-700 (1981).

Tsang, W.T. and T.H. Chiu and D.W. Kisker and J.A Ditzenberger, "Molecular Beam Epitaxial Growth of $In_{1-x}Ga_xAs_{1-y}Sb_y$ lattice matched to GaSb," *Appl. Phys. Lett., 46:*283-285 (1985).

Tsou, Y. and A. Ichii and E.M. Garmire, "Improving InAs Double Heterostructure Lasers with Better Confinement," *IEEE J. of Quantum Electronics*, QE-28(5):1261-1268 (May 1992).

Turner, G.W. and H.K. Choi and K.R. Calawa and J.V. Pantano and J.W. Chludzinski, "Molecular Beam Epitaxy Growth of High-Performance Midinfrared Diode Lasers," *Journal of Vacuum Science and Technology B*, 12(2):1266-1268 (March 1994).

Turner, G.W. and H.K. Choi and H.Q. Le, "Growth of InAs$_{1-x}$Sb$_x$ Quantum Wells for Long Wavelength (4 μm) Lasers," *Journal of Vacuum Science and Technology B*, 13(2):699-701 (March 1995).

van der Ziel, J.P. and T.H. Chiu and W.T. Tsang, "Optically Pumped Laser Oscillation at 3.82 μm from InAs$_{1-x}$Sb$_x$ Grown by Molecular Beam Epitaxy on GaSb," *Appl. Phys. Lett.*, *47*:1139 (1985).

van der Ziel, J.P. and T.H. Chiu and W.T. Tsang, "Optically Pumped Laser Oscillation at 3.9 μm from Al$_{0.5}$Ga$_{0.5}$Sb / InAs$_{0.91}$Sb$_{0.09}$ / Al$_{0.5}$Ga$_{0.5}$Sb double heterostructures grown by molecular beam epitaxy on GaSb," *Appl. Phys. Lett., 48(5):*315 (February 1985).

van der Ziel, J.P. and R.A. Logan and R.M. Mikulyak and A.A. Ballman, "Laser Oscillation at 3-4μm from Optically Pumped InAs$_{1-x-y}$Sb$_x$P$_y$," *IEEE J. Quantum Electron*, QE-21(11):1827-1832 (November 1985).

Van Vechten, J.A. and T.K. Bergstresser, "Electronic Structures of Semiconductor Alloys," *Physical Review B*, 1(8):3351-3358 (April 1970).

Van Vechten, J.A. and O. Berolo and J.C. Woolley, "Spin-Orbit Splitting in Compositionally Dissordered Semiconductors," *Physical Review Letters*, 29(20):1400-1403 (November 1972).

Vengurlekar, A.S. and S.S. Prabhu and S.K. Roy and Jagdeep Shah, "Large Reduction in Hot-Carrier Energy-Loss Rates in CdSe Caused by Nonequilibrium Optical Phonons," *Physical Review B, 50*(20):15461-15464 (November 1994).

Verdeyen, Joseph T. *Laser Electronics*, ed. 2 Prentice Hall, Englewood Cliffs, New Jersey 07632 (1989).

Vishnubhatla, S.S. and B. Euglunent and J.C. Woolley, "Electroreflectance Measurements in Mixed III-V Alloys," *Canadian Jour. of Physics*, 47:1661-1670 (1969).

Walpole, J.N. and T.C. Harman and S.H. Groves and R.C. Williamson and A.J. Strauss, *Materials Systems for 2 to 5 μm Wavelength Diode Lasers*, Massachusetts Institute of Technology, Lincoln Laboratory, Lexington MA (August 1990).

Wintner, E. and E.P. Ippen, "Nonlinear Carrier Dynamics in GaInAsP Compounds," *Appl. Phys. Lett., 44*(10):999-1001 (1984).

Wise, F.W. and C.L. Tang, "Subpicosecond Luminescence Study of Hot-Electron Relaxation in GaAs Quantum Wells," *Solid State Communications*, 69(8):821-826 (1989).

Yablonovitch, E. and E.O. Kane, "Reduction of Lasing Threshold Current Density by the Lowreing of Valence Band Effective Mass," *J. of Lightwave Tech.*, LT-4(5):504-506 (May 1986)

Yariv, Amnon and Pochi Yeh, *Optical Waves in Crystals*, Wiley Interscience, New York (1984).

Yen, M.Y. and B.F. Levine and C.G. Bethea and K.K. Choi and A.Y. Cho, "Molecular Beam Epitaxial Growth and Optical Properties of $InAs_{1-x}Sb_x$ in 8-12 μm Wavelength Range," *Appl. Phys. Lett.*, 50:927-929 (1987).

Yen, M.Y. and R. People and K.W. Wecht and A.Y. Cho, "Long Wavelength Photoluminescence of $InAs_{1-x}Sb_x$ (0<x<1) Grown by Molecular Beam Epitaxy on (100) InAs," *Appl. Phys. Lett.*, 52:489-491 (1988).

Yen, M.Y. "Molecular Beam Epitaxial Growth and Electrical Properties of Lattice Mismatched $InAs_{1-x}Sb_x$ on (100) GaAs," Jour. Appl. Phys., 64:3306-3309 (1988).

Yen, M.Y. and R. People and K.W. Wecht, "Long Wavelength (3-5 and 8-12 μm) Photoluminescence of $InAs_{1-x}Sb_x$ Grown on (100) GaAs by Molecular Beam Epitaxy," *Jour. Appl. Phys.*, 64:952-955 (1988).

Young, P.M. and C.H. Grein and H. Ehrenreich and R.H. Miles, "Temperature Limits on Infrared Detectivities of InAs/InGaSb Superlattices and Bulk HgCdTe," *J. of Appl. Phys.*, *74(7):*4774-4776 (October 1993).

Youngdale, E.R. and J.R. Meyer and C.A. Hoffman and F.J. Bartoli and W.I. Wang, "Type-II Superlattices and Variable Overlap Superlattices in Total Internal Reflection Switches for the Longwave Infrared," *Int. J. of Nonlinear Optical Physics*, 2(3):415-436 (March 1993).

Youngdale, E.R. and J.R. Meyer and C.A. Hoffman and F.J. Bartoli and R.H. Miles and D.H. Chow, "Recombination Lifetime in $InAs/Ga_{1-x}In_xSb$ Superlattices," J. of *Vacuum Science and Technology B.*, 12(2):1129-1132 (March 1994).

Youngdale, E.R. and J.R. Meyer and C.A. Hoffman and F.F. Bartoli and C.H. Grein and P.M. Young and H. Ehrenreich and R.H. Miles and D.H. Chow, "Auger Lifetime Enhancement in InA/GaInSb Superlattices," *Appl. Phys. Lett.*, *64(23):*3160-3162 (June 1994).

Yu, P.Y. and Manuel Cardona, *Fundamentals of Semiconductors*, Springer-Verlag, (1996).

Zegrya, G.G., and V.A. Kharchenko, "New mechanism of Auger recombination of nonequilibrium current carriers in semiconductor heterostructures," *Sov. Phys.* JETP 74(1):173 (January 1992).

Zegrya, G.G. and A.D. Andreev, "Nechanism of suppression of Auger recombination processes in type-II heterostructures," *Appl. Phys. Lett., 67(18):2681* (October 1995).

Zhou, X.Q. and U. Lemmer and K. Seibert and G.C. Cho and W. Kutt and K. Wolter and H. Kurz, "Subpicosecond Dynamics of Hot Carrier Relaxation in InP and GaAs," *20th Int. Conf. on The Physics of Semicoductors*, Thessaloniki, Greece, p. 2522-2525 (August 1990).

Zhou, X.Q. and H. Kurz, "Hot Carrier Relaxation in Doped III-V Compounds Studied by Femtosecond Luminescence," *Int. Symp. on Ultrafast Processes in Spectroscopy*, Bayreuth, 126:339-342 (1991).

Zielinski, E. and H. Schweizer and S. Hausser and R. Stuber and M.H. Pilkuhn and G. Weimann, "Systematics of Laser Operation in GaAs/AlGaAs Multiquantum Well Heterostructures," *IEEE J. of Quantum Electronics*, QE-23(6):969-976 (June 1987).

Zyskind, J.L. and J.C. Dewinter and C.A. Burrus and J.C. Centanni and A.G. Dentai and M.A. Pollack, "Highly Uniform, High Quantum Efficiency GaInAsSb/AlGaAsSb Double Heterostructurese Lasers Emitting at 2.2μm," *Electronics Letters*, 25(9):568-569 (April 1989).

Zielinski, E. and F. Keppler and S. Hausser and R. Stuber and M.H. Pilkuhn and W.T. Tsang, "Optical Gain and Loss Processes in GaInAs/InP Multiquantum Well Laser Structures," *IEEE J. of Quantum Electronics*, QE-25(6):1407-1416 (June 1989)

Vita

Captain William T. Cooley was born on 4 February 1966 in Fort Worth, Texas. He graduated from Highland High School in Albuquerque, New Mexico in 1984. He graduated from Rensselear Polytechnic Institute with a Bachelor of Science in Mechanical Engineering in May 1988, obtaining a commission in the Air Force, through R.O.T.C. at the same time. From July 1988 through February 1990 he worked at Sandia National Laboratory while attending the University of New Mexico in pursuit of a Masters of Science in Mechanical Engineering, which was completed in January 1990. He worked at the Air Force Wright Laboratory at Wright-Patterson AFB in Dayton OH, from February 1990 through June 1993 where he was a project engineer for photovoltaic solar cells and later a crystal grower of III-V compounds using molecular beam epitaxy. In July 1993 he entered the Graduate School of Engineering at the Air Force Institute of Technology. Since leaving AFIT in December 1996, he has been working at the Air Force Phillips Laboratory at Kirtland AFB in Albuquerque New Mexico as chief of the laser applications group.

        Permanent Address: 608 Valverde Dr. SE
                                     Albuquerque, NM 87108

REPORT DOCUMENTATION PAGE

Public reporting burden for this collection of information is estimated to average 1 hour per response, including the time for reviewing instructions, searching existing data sources, gathering and maintaining the data needed, and completing and reviewing the collection of information. Send comments regarding this burden estimate or any other aspect of this collection of information, including suggestions for reducing this burden, to Washington Headquarters Services, Directorate for Information Operations and Reports, 1215 Jefferson Davis Highway, Suite 1204, Arlington, VA 22202-4302, and to the Office of Management and Budget, Paperwork Reduction Project (0704-0188), Washington, DC 20503.

1. AGENCY USE ONLY *(Leave blank)*	2. REPORT DATE 2 Dec 97	3. REPORT TYPE AND DATES COVERED Dissertation

4. TITLE AND SUBTITLE

Measurement of Ultrafast Carrier Recombination Dynamics
In Mid-Infrared Semiconductor Laser Material

5. FUNDING NUMBERS

6. AUTHOR(S)

William T. Cooley, Captain, USAF

7. PERFORMING ORGANIZATION NAME(S) AND ADDRESS(ES)

Air Force Institute of Technology
Engineering Physics Department
WPAFB, OH 45433-6583

8. PERFORMING ORGANIZATION REPORT NUMBER

AFIT/DS/ENP/97-10

9. SPONSORING / MONITORING AGENCY NAME(S) AND ADDRESS(ES)

AFRL/DELS (Major Greg Vansuch)
3550 Aberdeen Ave. SE
Kirtland AFB NM 87117

10. SPONSORING / MONITORING AGENCY REPORT NUMBER

11. SUPPLEMENTARY NOTES

Distribution unlimited; Approved for public release

12a. DISTRIBUTION / AVAILABILITY STATEMENT

12b. DISTRIBUTION CODE

13. ABSTRACT *(Maximum 200 words)*

Shockley-Read-Hall, radiative, and Auger recombination rates in mid-infrared laser structures are measured and reported using time resolved photoluminescence (TRPL) frequency upconversion. The mid-IR lasers studied were actual InAsSb / InAlAsSb multiple-quantum-well (MQW) diode lasers emitting near 3.3 μm which were previously characterized for laser performance. This effort extends the initial studies and reports on the carrier recombination dynamics. Shockley-Read-Hall, radiative and Auger recombination rates at low temperature (77 K) were measured and found to be $A_{SRH} \approx 10 \times 10^7 sec^{-1}$, $B_{rad} \approx 2 \times 10^{-10} cm^3 sec^{-1}$ and $C_{Auger} < 10^{-29} cm^6 s^{-1}$ respectively, for each sample measured. At higher temperatures (150 K), the recombination rates were measured to be $A_{SRH} \approx 40 \times 10^7 sec^{-1}$, $B_{rad} \approx 0.78 \times 10^{-10} cm^3 sec^{-1}$ and $C_{Auger} < 7.0 \times 10^{-28} cm^6 s^{-1}$ respectively. The Auger coefficient reported here is significantly lower than previous reports on similar material from both theoretical and experimental investigations. This has significant implications for mid-IR laser research, in that Auger may not be the limiting problem.

14. SUBJECT TERMS

Indium Arsenide Antimonide, Mid-infrared quantum well laser, Photoluminescence, Semiconductors, Non Linear Optics,

15. NUMBER OF PAGES
208

16. PRICE CODE

17. SECURITY CLASSIFICATION OF REPORT UNCLASSIFIED	18. SECURITY CLASSIFICATION OF THIS PAGE UNCLASSIFIED	19. SECURITY CLASSIFICATION OF ABSTRACT UNCLASSIFIED	20. LIMITATION OF ABSTRACT UL